



**This electronic thesis or dissertation has been
downloaded from Explore Bristol Research,
<http://research-information.bristol.ac.uk>**

Author:

Stanmore, Elizabeth A

Title:

Water – Rock Interaction in the Eocene and Upper Paleocene Formations, State of Qatar

General rights

Access to the thesis is subject to the Creative Commons Attribution - NonCommercial-No Derivatives 4.0 International Public License. A copy of this may be found at <https://creativecommons.org/licenses/by-nc-nd/4.0/legalcode>. This license sets out your rights and the restrictions that apply to your access to the thesis so it is important you read this before proceeding.

Take down policy

Some pages of this thesis may have been removed for copyright restrictions prior to having it been deposited in Explore Bristol Research. However, if you have discovered material within the thesis that you consider to be unlawful e.g. breaches of copyright (either yours or that of a third party) or any other law, including but not limited to those relating to patent, trademark, confidentiality, data protection, obscenity, defamation, libel, then please contact collections-metadata@bristol.ac.uk and include the following information in your message:

- Your contact details
- Bibliographic details for the item, including a URL
- An outline nature of the complaint

Your claim will be investigated and, where appropriate, the item in question will be removed from public view as soon as possible.



**This electronic thesis or dissertation has been
downloaded from Explore Bristol Research,
<http://research-information.bristol.ac.uk>**

Author:

Stanmore, Elizabeth A

Title:

Water – Rock Interaction in the Eocene and Upper Paleocene Formations, State of Qatar

General rights

Access to the thesis is subject to the Creative Commons Attribution - NonCommercial-No Derivatives 4.0 International Public License. A copy of this may be found at <https://creativecommons.org/licenses/by-nc-nd/4.0/legalcode>. This license sets out your rights and the restrictions that apply to your access to the thesis so it is important you read this before proceeding.

Take down policy

Some pages of this thesis may have been removed for copyright restrictions prior to having it been deposited in Explore Bristol Research. However, if you have discovered material within the thesis that you consider to be unlawful e.g. breaches of copyright (either yours or that of a third party) or any other law, including but not limited to those relating to patent, trademark, confidentiality, data protection, obscenity, defamation, libel, then please contact collections-metadata@bristol.ac.uk and include the following information in your message:

- Your contact details
- Bibliographic details for the item, including a URL
- An outline nature of the complaint

Your claim will be investigated and, where appropriate, the item in question will be removed from public view as soon as possible.

Water – Rock Interaction in the
Eocene and Upper Paleocene Formations,
State of Qatar

August 2019

By Elizabeth Anne Stanmore

A thesis submitted to the University of Bristol in accordance with
the requirements for award of the degree of Masters of Science
(Research) in Faculty of Science

School of Earth Sciences

August 2019



Masters Thesis
29,779 words

Abstract

Inter-bedded limestone, dolostone and evaporite sequences are typical of shallow carbonate deposits in arid climates such as Qatar. Their chemical reactivity makes them prone to diagenetic alteration and dependent on groundwater chemistry and flow patterns at a range of scales.

Continuous core recovered from ~130m depth at three locations along a North-South transect on the crest of the Qatar Arch defined four hydrostratigraphic units: 1) crystalline calcite and dolomite of the Dammam Formation (upper aquifer), 2) Rus Formation, a carbonate and clay deposit (middle aquifer), 3) crystalline gypsum/anhydrite Rus Evaporite (aquiclude – absent in the north of the country) and 4) the dolomitic Upper Um Er Radhuma (UER) (lower aquifer).

Nested piezometers suggested a vertical hydraulic gradient governing flow within and between each aquifer system. In the south, an upward hydraulic gradient is due to a substantial thickness of crystalline Rus Evaporite confining the underlying saline UER. In the north, the absence of the Rus Evaporite means the different aquifers are in hydraulic continuity with a downward flow driven by meteoric recharge.

Groundwater analyses indicate differences between northern, central and southern Qatar within similar rock types in the same aquifers. In the south, concentrations of Ca^{2+} , Mg^{2+} and SO_4^{2-} in excess of predictions from linear mixing show sulfate enrichment. These southern waters were also depleted in Mg^{2+} relative to local seawater. As these waters ascend, they become less depleted in Mg^{2+} and less enriched in Ca^{2+} relative to SO_4^{2-} enrichment. This vertical contrast suggests de-dolomitisation or recrystallization from less Ca-rich to more stoichiometric well-ordered (Ca=Mg) dolomites with Mg-rich clays. This trend is considered ongoing in centre and northern UER aquifers, although to a lesser degree.

Assessing these modern shallow groundwaters contribute to a better understanding of the deeper reservoirs, which have similar depositional and diagenetic environments, and provide effective management of a crucial resource.



Authors Declaration

I declare that the work in this dissertation was carried out in accordance with the requirements of the University's *Regulations and Code of Practice for Research Degree Programmes* and that it has not been submitted for any other academic award. Except where indicated by specific reference in the text, the work is the candidate's own work. Work done in collaboration with, or with the assistance of, others, is indicated as such. Any views expressed in the dissertation are those of the author.

SIGNED:  DATE:.....15.12.19.....

“Water scarcity is a fundamental challenge to sustainable development in arid and semi-arid regions, where renewable freshwater resources at the national level are insufficient to satisfy growing needs. Shared water resources often provide essential freshwater, and management of these can have important implications for regional stability, socio-economic development and environmental protection, as well as peace and security.”
(UN- ESCWA and BGR, 2013).

Acknowledgements

I am truly humbled and forever grateful to a lot of people. Specifically, Professor Fiona Whitaker my supervisor at the University of Bristol and Dr John Rivers from ExxonMobil Research Qatar. I also thank Andy Slate, Sallie Vest and Dr. Jeremy Jameson for starting this whole process.

At university, I was grateful to be surrounded by smart, friendly and very helpful fellow students including Didi, Tan, Rattana, Tom, Hazel and James.

I am also very grateful for the people whom housed me including my parents, siblings, Karen and Mike, and Tim and Donna. And of course my extraordinary friends from across the world including Victoria, Maria Ruth and Elise.

I am also thankful, always, to God.

TABLE OF CONTENTS

1.0	INTRODUCTION AND RATIONALE	1
1.1	Rationale.....	1
1.2	Main Goal and Objectives	1
2.0	STUDY AREA.....	4
2.1	Introduction	4
2.2	Location	4
2.3	Climate	5
2.4	Topography.....	5
2.5	Geology	6
2.6	Lithological Descriptions	9
2.7	Dolines – Karsts and Surface Depressions	16
2.8	Rock and Clay Mineralogy	17
2.9	Regional Configuration of Aquifers and Aquitards	18
2.10	Anthropogenic influences.....	26
2.11	Key water-rock reactions.....	28
3.0	METHODS.....	36
3.1	Introduction	36
3.2	Drilling of cored boreholes and monitoring wells	36
3.2	Groundwater monitoring standpipes.....	38
3.3	Packer (or Lugeon) Tests.....	45
3.4	Flow Meter Logging	44
3.5	Borehole Profiles including Temperature, pH and Conductivity Logging	44
3.6	Groundwater Monitoring and Sampling	45
3.7	Laboratory Testing	47
3.8	Chemical modelling (PHREEQC).....	47
3.9	Logging	48
4.0	AQUIFER PROPERTIES AND GROUNDWATER FLOW	50
4.1	Introduction	50
4.2	Location	50
4.3	Hydraulic Head Analysis	55
4.4	Packer hydraulic conductivity (K) results	62
4.5	Borehole Profiles.....	62

4.6	Scale-dependence of permeability characteristics of Qatar bedrock	69
5.0	GROUNDWATER CHEMSITY.....	75
5.1	Introduction	75
5.2	Field Results	78
5.2	Major elements	85
5.3	Excess	100
6.0	DISCUSSION AND CONCLUSION	110
6.1	Introduction	110
6.2	The Upper Domain.....	110
6.3	The Middle Domain.....	114
6.4	The Lower Domain.....	116
6.5	Conceptual Model.....	120
6.6	Conclusion	121

References	123
-------------------------	------------

Appendices	130
-------------------------	------------

Appendix A1 Drilling of cored boreholes and monitoring wells

Appendix A2 Packers

Appendix A3 Groundwater Monitoring

Appendix A4 Laboratory Testing

Appendix A5 Logging

Appendix A6 Darcy Conversion

Appendix B1 Field Results

Appendix B2 Laboratory Results

Appendix B3 Scale Permeability Results

Appendix C Geotechnical Logs RR and AG

Appendix D Composite Geology Logs South, Central and North Wells (Rivers et al., 2019a)

Table of Figures

Figure 2-1	Location of Qatar (Google Earth, 2019)	4
Figure 2-2	Map of Qatar showing karst features in Abu Al Dhalouf, northern coastline of Qatar, approximately 1km inland (Google Earth, 2019) and personal photo.....	6

Figure 2-3	Tectonic map of the Middle East, with Qatar circled in red (Perotti et al., 2012).	7
Figure 2-4	Geological traverse X-X' showing the sedimentary successions above the Hormuz salt in relation to Qatar (Al-Fahmi, 2016).	7
Figure 2-5	Late Paleocene (56Ma) depositional environment of the UER Formation (Rivers, 2019a).	8
Figure 2-6	Location map of the South Pars-North Dome super giant gas field (Rahimpour-Bonab et al, 2009).	8
Figure 2-7	Previously and recent vertical geological interpretation across the Qatar peninsula, Figure 8 from Rivers & Larson (2018)	9
Figure 2-8	Surface geological map of Qatar including descriptions of surface and underlying geology (to ~600m depth) (Rivers & Larson, 2018)	8
Figure 2-9	Chert / siliceous horizon in the UER Formation (Eccleston et al., 1981)	12
Figure 2-10	Rus Formation facies and province delineation (Eccleston et al., 1981)	12
Figure 2-11	Depositional Environment of Middle Eocene ~38Ma (Rivers et al., 2019a) Dammam Formation	16
Figure 2-12	Conceptual hydrogeological model of the eastern Arabian Peninsula (Alsharhan et al., 2001)	19
Figure 2-13	Groundwater flow of the Tertiary aquifers (Alsharhan et al., 2001)	20
Figure 2-14	Natural groundwater conditions in northern Qatar, and the effects of groundwater pumping (Alsharhan et al., 2001)	24
Figure 2-15	Regional piezometric surface (m QNHD) of the UER aquifer in 1981 (Eccleston et al., 1981)	25
Figure 2-16	Groundwater head for Rus Formation in 1981 (Lloyd et al., 1987 based on Eccleston et al., 1981)	25
Figure 2-17	Depth to groundwater 1981 from surface (Eccleston et al., 1981)	25
Figure 2-18	Qatar's population over the last 10years < http://www.mdps.gov.qa/en/ >	26
Figure 2-19	Groundwater inflow versus outflow (Ministry of Development Planning and Statistics, 2017)	27
Figure 2-20	Salinity classifications of Qatar Government groundwater monitoring wells, from April 1998 to September 2014 (Ministry of Development Planning and Statistics, 2017)	28
Figure 2-21 A.	The non-linear relationship between equilibrium PCO ₂ and dissolved CaCO ₃ ; B. Calcite saturation in the mixing zone of seawater and meteoric water (Jones & James, 2016)	31

Figure 3-1	Drilling of RR (southern) wells and surrounds, monitoring, and wells on completion	37
Figure 3-2	Well locations in Qatar	39
Figure 3-3	Southern Well (RR-1, RR-2, RR-3 and RR-4) installations	39
Figure 3-4	Central Wells (AS-1, AS-2) installations	40
Figure 3-5	Northern Wells (AG-1, AG-2, AG-3) installations.....	41
Figure 3-6	Northern (AG) well surrounds, site crew during drilling and geophysics down-the-hole temperature and EC probe attached to tripod winch.....	42
Figure 3-7	Farm 2- RR in the south.....	43
Figure 3-8	Physical and geological logging, and the team.....	46
Figure 4-1	Umm Er Radhuma rock core samples in the southern well (RR)	51
Figure 4-2	Umm Er Radhuma rock core samples in the central well (AS)	51
Figure 4-3	Rock core samples from the Rus in the southern wells	54
Figure 4-4	Umm Bab Member from the Dammam Formation, AG from 7.85m to 3.9m QNHD (1.25m to 5.2mbgl).....	55
Figure 4-5	Location of wells and monitoring points for piezometric head analyses (Google Earth, 2019)	56
Figure 4-6	Depth to groundwater (m QNHD) and SEC (mS cm ⁻¹) with time	58
Figure 4-7	From 1982 to present day, Salinity (SEC mS cm ⁻¹) with depth to groundwater (m QNHD).....	58
Figure 4-8	Groundwater head (manual dips) in southern (RR), central (AS) and northern (AG) set of wells from manual dipping.....	60
Figure 4-9	Mean northern, central and southern piezometric head with depth (m QNHD) .	61
Figure 4-10	Piezometric head (m QNHD) from north to south including Doha coast.....	61
Figure 4-11	Southern (RR) and Central (AS) wells borehole profile for temperature and conductivity SEC (mS cm ⁻¹). Individual results are the average SEC (mS cm ⁻¹) during field monitoring.....	66
Figure 4-12	Well P22a (Eccleston et al., 1981).....	67
Figure 4-13	Permeability (D) vs frequency for all test types (n=392).....	70
Figure 4-14	Permeability (D) vs cumulative frequency for all test types (n=392).....	70
Figure 4-15	Permeability (D) and frequency with each test type (n=392)	71
Figure 4-16	Permeability to formation (n=392)	71

Figure 4-17	Boxplots of permeabilities (D) for each formation, split as core and packer results (n=323), and slug and pump test results (n=69).....	71
Figure 4-18	Permeability and boxplot relative to mineralogy (core only, n=254)	72
Figure 4-19	Permeability (D) with depth (m QNHD) by Formation (core only, n=317) and by mineralogy (core only, n=254).....	72
Figure 4-20	Porosity (%) with frequency and cumulative frequency (core only, n=317)	73
Figure 4-21	Porosity (%) with depth (core only, n=317)	73
Figure 4-22	Porosity with formation (core only, n=318) and mineralogy (core only, n= 260)	73
Figure 4-23	Permeability with porosity (n=317)	74
Figure 5-1	Initial conceptual model.....	77
Figure 5-2	Field temperature	80
Figure 5-3	Field pH (± 0.01) compared to laboratory pH (± 0.01)	81
Figure 5-4	Laboratory pH	81
Figure 5-5	$\bar{x} \pm 1\sigma$ Laboratory pH with depth (m QNHD) for each well	81
Figure 5-6	Turbidity (NTU) with time	82
Figure 5-7	DO (± 0.01 mg l-1) with time	83
Figure 5-8	Box plot of Field SEC for 2017 and Laboratory SEC for 2018.	84
Figure 5-9	SEC with time for each well during monitoring, outliers identified by O	85
Figure 5-10	$\bar{x} \pm 1\sigma$ SEC (mS cm-1) with depth (m QNHD) for each well.....	85
Figure 5-11	Cl- for each well during monitoring, outliers identified by O	86
Figure 5-12	$\bar{x} \pm 1\sigma$ Cl- with depth	86
Figure 5-13	A. The ratios of Na vs Cl including 1:1, and B. Na/Cl vs Cl.....	86
Figure 5-14	$\bar{x} \pm 1\sigma$ of SO ₄ ²⁻ , Ca ²⁺ , Mg ²⁺ for each well with depth	88
Figure 5-15	Cl- with SO ₄ ²⁻	89
Figure 5-16	Ca ²⁺ with Cl-.....	90
Figure 5-17	Mg ²⁺ for each well during monitoring.....	91
Figure 5-18	A. Mg ²⁺ with Cl- and B. Mg/Cl vs Cl..	92
Figure 5-19	K ⁺ for each well during monitoring	93
Figure 5-20	$\bar{x} \pm 1\sigma$ K ⁺ for each well with depth..	94
Figure 5-21	$\bar{x} \pm 1\sigma$ SiO ₄ ²⁺ for each well with depth	95
Figure 5-22	Alkalinity (HCO ₃ ⁻) for each well during monitoring, outliers identified by O	96
Figure 5-23	$\bar{x} \pm 1\sigma$ Alkalinity (HCO ₃ ⁻) with depth	96
Figure 5-24	A. Ratio of Alkalinity (HCO ₃ ⁻) vs Cl-.....	97
Figure 5-25	TOC (mmol l-1) and TN (mmol l-1) with depth.....	99

Figure 5-26	Variation in Ca _{XS} with SO _{4XS} as a result of water-rock interaction process.....	101
Figure 5-27	A. Variation Δ Ca _{XS} with Cl ⁻ (mmol ⁻¹). B. Mg _{XS} with Cl.....	104
Figure 5-28	Variation of Δ Ca _{XS} with Mg _{XS} for all groundwater samples	105
Figure 5-29	SO _{4XS} with alkalinity (HCO ₃ ⁻)	105
Figure 5-30	$\bar{x} \pm 1\sigma$ for SI calcite, dolomite and gypsum with depth.....	106
Figure 5-31	$\bar{x} \pm 1\sigma$ CO ₂ with depth.	107
Figure 5-32	Phase diagramme showing the stability of calcite, dolomite and gypsum.	108
Figure 6-1	Box plot of the main geochemical characteristics for each Domain including pH, SEC, alkalinity (as HCO ₃), TOC, Ca _{XS} , Mg _{XS} , SO _{4XS} and Δ Ca _{XS}	112
Figure 6-2	Schematic drawing showing pathways for sulfate-reduced mixing zone fluids and resulting dissolution in the mixing zone (from Stoessell, 1992).....	115
Figure 6-3	Mineralogy of the southern well showing dolomite, crystal size and palygorskite content relative to geochemical groundwater excess	117
Figure 6-4	Possible dedolomitization trends comparing SO _{4XS} with Ca _{XS} , Mg _{XS} , pH, PCO ₂ and alkalinity.	119
Figure 6-5	The Conceptual Groundwater Model.....	120

Table of Tables

Table 2-1	Total monthly rainfall.....	5
Table 2-2	The five informal units of the UER from the Dukhan area (defined by Al-Saad and Hewaidy (n.d), and three members as defined in Boukhary et al., 2011....	11
Table 3-1	Southern well (RR) packer test depths.....	44
Table 3-2	Borehole location, elevation, base depths, installations, formation and mineralogy details	46
Table 3-3	Timeline of dates for which measure of piezometric head (G), piezometric head and groundwater sampling (W) were undertaken at the various sites. * indicates water sample in absence of piezometric head measurement.	49
Table 4- 1	Southern well (EMRQ_RR_BH001) packer permeability results	62
Table 4- 2	Flow summary.....	68
Table 4- 3	Range of effective permeability (D)	70
Table 5- 1	End member for each well, indicating the source and mixing solutes	76

1.0 INTRODUCTION AND RATIONALE

1.1 Rationale

The motivation for this research is to improve our understanding of both the evolution and character of the near-surface aquifers of Qatar. These aquifers are hosted in inter-bedded limestone, dolostone and evaporite sequences typical of shallow carbonate deposits in arid climates. Their chemical reactivity makes them prone to diagenetic alteration, particularly by groundwater flow during periods of subaerial exposure.

Qatar relies on desalination to meet its growing needs, as it has little rainfall and the only surface water is ephemeral surface retention after rare heavy rainfall events. Groundwater from the shallow aquifers are a major groundwater resource and the only natural source of fresh water (Baalousha, 2016a). Over-exploitation of groundwater is evident from a decrease in the water table level, and also the deterioration of water quality resulting from seawater intrusion (Ministry of Development Planning and Statistics, 2017). Effective management of available resources is essential in a political environment where there are currently no regional or cross-boundary agreements regarding groundwater (Alsharhan et al., 2001).

These same shallow inter-bedded carbonate deposits are reported to have similar depositional and diagenetic environments with the deeper hydrocarbon reservoirs of the region. As Qatar holds the third largest gas reserves in the world, hosting the largest (non-associated) gasfield (Hydrocarbons Technology, 2019), assessing the modern shallow environment can contribute to a better understanding of the deeper reservoirs.

1.2 Main Goal and Objectives

The shallow aquifers in Qatar are hosted in the Dammam – Rus – Umm Er Radhuma aquifer systems, which extend from the southern coast of the Arabian Peninsula in Saudi Arabia to northern Iraq, covering a total area of more than 1,220,000 km². Qatar covers about 1% of this area (UNESCWA and BGR, 2013) and is the distal end of the UER aquifer system which is recharged in Saudi Arabia. The shallow aquifers are an important supply for public, irrigation and industry water. Little is

known about the reaction between groundwater and the shallow carbonate, dolomitic and evaporitic sequences which dominate the upper lithologies of Qatar.

A number of major hydrological studies have been conducted on the groundwaters of Qatar. In the early 1970s', the Government of Qatar with technical assistance of the Food and Agricultural Organization of the United Nations (FAO) (Kimrey, 1985) , follow up work by Eccleston et al. (1981), United Nations programmes UN ESCWA (2013) and under various government-funded projects including The Qatar General Electricity and Water Corporation (Kahramaa) ASR (aquifer, storage, recovery) investigation, and Qatar's Public Works Authority country-wide shallow groundwater monitoring exercise, with monitoring wells related to deep injection systems (extending to depths ~400m). As is often the case, data from these reports are unavailable, and the core drilling and subsequent logging are lacking or insufficiently detailed and/or analysed. In addition, chemical analysis of the rock and groundwater is limited, as the chemistry of groundwater has been restricted to untargeted samples, i.e. those drawn from lengthy response zones which often span multiple aquifers.

This project integrates high quality, drilled rock core with detailed research-grade logging, focussing on geochemical analyses of both the rock and groundwater, and targeting groundwater from specific zones in aquifers which encounter different lithologies. The focus is to provide an understanding of the interactions between carbonate, dolomitic and evaporite aquifers and aquitards of Eocene-aged bedrock of Qatar (upper 130mbgl). This study will profile the shallow aquifers, identifying the local lithological characteristics such mineralogy and permeability, and how these affect groundwater flow and chemistry, given the nature and rate of water-rock interactions. It will identify flow units and barriers within the shallow aquifer systems, monitor the hydraulic head and understand the distribution of groundwater and interaction with the host rock based groundwater geochemistry.

The project will:

- further understand the scale-dependent permeability of the aquifer, including permeability extremes and barriers within the Dam/Dammam, Rus Formation and Upper Umm Er Radhuma aquifers (extending down to 130m bgl),
- extend our knowledge of the mineralogy of the shallow aquifers of Qatar

- understand the vertical and lateral chemical composition of these groundwater bodies, including major and trace elements, and
- identify the interdependency between aquifer quality and rock-water interactions by comparing groundwater flow, chemistry and bedrock permeability and mineralogy in Qatar and comparing it with the region.

The research is part of a large-scale ExxonMobil project, which is endeavouring to understand the broader geological stratigraphic framework of Qatar, specifically regarding diagenesis, evaporitic dissolution, dedolomisation and karstification. The School of Earth Sciences at Bristol University has been given access to the analyses of multiple borehole, rock core and groundwater samples which provide the basis of this research.

2.0 STUDY AREA

2.1 Introduction

Qatar is uniquely placed in the center of the Middle East, where rainfall is low, temperatures are very high and relatively low topography resulting in the absence of a continuous source of freshwater. Groundwater is the only natural water available which has lead an increasing pressure on this resource. This chapter provides an overview of region and Qatar, the climate, geology, the various shallow aquifers and their geochemical nature, and its population, to provide an understanding on groundwater.

2.2 Location

Qatar is an arid peninsula covering 11,610 km² and protruding northward from Saudi Arabia into the central zone of the Arabian Gulf. The peninsular is approximately 180km along its north-south axis, extending between latitudes 24°30'N and 26°10'N, and is 85km east-west between longitudes 50°40'E to 51°36'E. Saudi Arabia to the south is its only land neighbour and the shallow waters of the Arabian Gulf surround it to the north, east and west.

Figure 2-1 Location of Qatar (Google Earth, 2019)



2.3 Climate

Mean monthly temperatures range from a low of 18°C in winter up to a high of 35.1°C in summer, although much higher daily temperatures during summer (July to September) are common (>50°C) (Ministry of Development Planning and Statistics, 2014b).

Qatar is surrounded by sea apart from to the south, which significantly influences the overall climate. Humidity is high and averages 70% while average rainfall for a year is between 70mm to 80mm, but can significantly vary from year to year (Shamrukh, 2012, Baalousha, 2016a). Most of the rainfall occurs within in rare but heavy events for a few days during the winter months, with records indicating averages between 60mm and 105mm (October 2018) for a single month (Weatheronline, 2019).

Table 2-1 presents monthly rainfall totals during the period of this study. Drilling commenced on the first borehole on 4th October 2016 and the last monitoring round took place on 7th October 2018. Rates of potential evaporation are high throughout the country, especially during summer when high solar insolation and surface temperatures, sparse rainfall and moderate humidity give totals of about 1750mm/yr (Eccleston, 1981).

Table 2-1 Total monthly rainfall

Year	Jan	Feb	Mar	Apr	May	Jun	July	Aug	Sep	Oct	Nov	Dec
2016	0	0	36.0	15.4	0	0	0	0	0	0	41	0
2017	0	40.4	0.5	0	1.1	0	0	0.2	0	0	0.1	4.7
2018	0.2	36.3	0.9	3.3	0.3	0	0	0	0	105.0	87	0

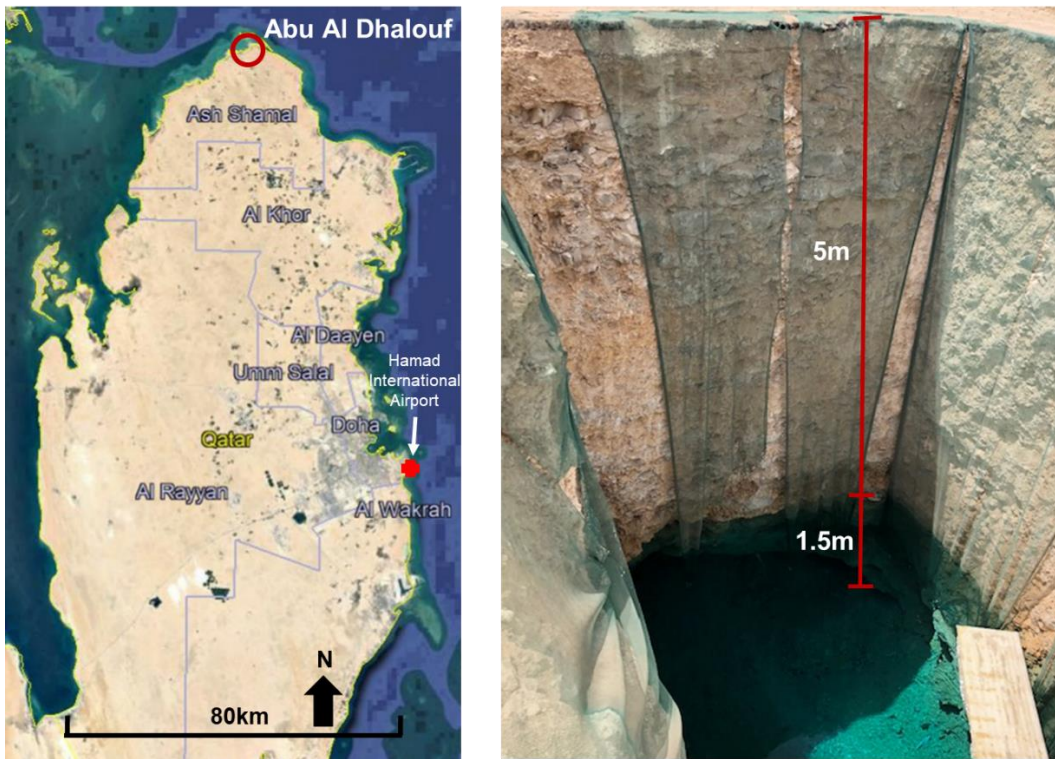
Note: Data from the weather station at Hamad International Airport on the south east coast of Qatar (location marked in Figure 2-2) from <www.weatheronline.com> and <www.weatheronline.co.uk>.

2.4 Topography

Qatar is a relatively flat arid country, sparsely vegetated with no permanent rivers or streams. The coastline has numerous inlets, tidal lagoons, mangroves and extensive areas of sabkha. Elevations up to 46m above sea level delineate the Qatar Arch, a north-south oriented anticline, through the center of the country. In the south west, erosional escarpments and relic mesa hills of the Dukhan Anticline record the highest permanent elevation of ~103m above sea level (Eccleston et al., 1981). A salty inland sea is located in the southeast, surrounded by mobile aeolian sand dunes reaching ~110m high, which extend into Saudi Arabia (Sadiq, 2002).

Sadiq and Nasir (2002) identified more than 9700 large and small depressions across the surface of the country representing subsurface collapse due to dolomite dissolution and karstification. They are often circular in shape with diameters ranging from a few hundred meters up to more than five kilometers and can become internal surface water catchments infilled with colluvium (Eccleston et al., 1981). Many caves are known to be present across the country, the best known being Dahl Al Misfir Cave or Musfer Sinkhole, which is at least 100m deep (Sadiq et al., 2002), although it is known to have recently collapsed. Other sinkholes and caves are present, particularly around the northern coastline at sea level.

Figure 2-2 Map of Qatar showing karst features in Abu Al Dhalouf, northern coastline of Qatar, approximately 1km inland (Google Earth, 2019) and personal photo



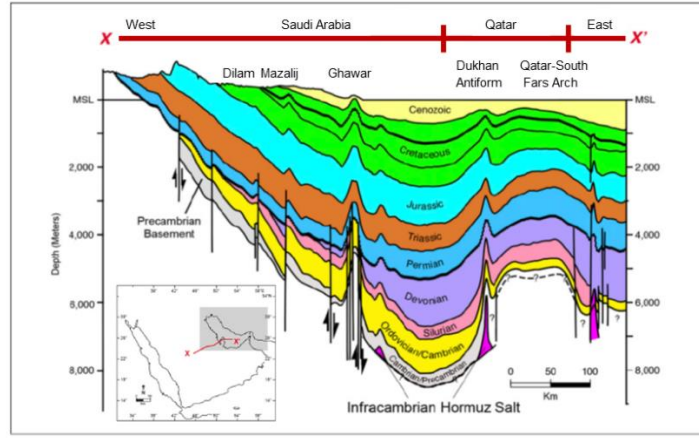
2.5 Geology

Qatar is located in the central northern area of the Arabian Shelf, which originated 25M years ago when rifting formed the Gulf of Aden and Red Sea, and the Arabian Plate split from the African continent (Le Blanc, 2017a) (Figure 2-3).

Figure 2-3 Tectonic map of the Middle East, with Qatar circled in red (Perotti et al., 2012).



Figure 2-4 Geological traverse X-X' showing the sedimentary successions above the Hormuz salt in relation to Qatar (Al-Fahmi, 2016).



The evolutionary history of the Arabian Platform is summarised as accumulation within a vast sedimentary basin from the Late Proterozoic through to the Holocene (Perotti et al., 2012). A Late Proterozoic extensional phase involving uplift of N-S orientated basement blocks, consolidated the Arabian Plate, creating major structural features including the Qatar Arch. The sequence comprised up to 6km thickness of interbedded carbonates and thick evaporites between the uplifted N-S basement blocks cut by further basement faults, delineating salt diapirism as the major structure-forming mechanisms (Le Blanc, 2017a) (Figure 2-4).

During the Palaeozoic, the area continued to accrete uniformly by continental and shallow-marine sedimentation followed by aggressive and prolonged mountain building to form Pangaea. This caused widespread erosion, regional uplift and basement movement along the inherited previous N-S uplifts.

From the Permian through to the end of the Oligocene, the region developed as an extensive, stable platform allowing the deposition of shallow water carbonates and associated facies including evaporites and shales. In the late Tertiary, the Arabian Plate split from Africa and moved northward, undergoing shortening and subsequent flexure, due to the collision with the Laurasia in the north. This “created a wedge-shaped low angle foreland basin” and with a marine transgression followed by several transgressive and regressive cycles and shallow-marine sedimentation (Mukhopadhyay et al., 2002, Sharland et al., 2001). Frequent episodes of “very shallow brackish water, evaporitic periods and

exposed continental conditions” combined with erosion and redeposition (Pike, 1985) resulted in the accumulation of mixed evaporitic, carbonate and clastic sediments (Figure 2-5).

Figure 2-5 Late Paleocene (56Ma) depositional environment of the UER Formation (Rivers, 2019a).

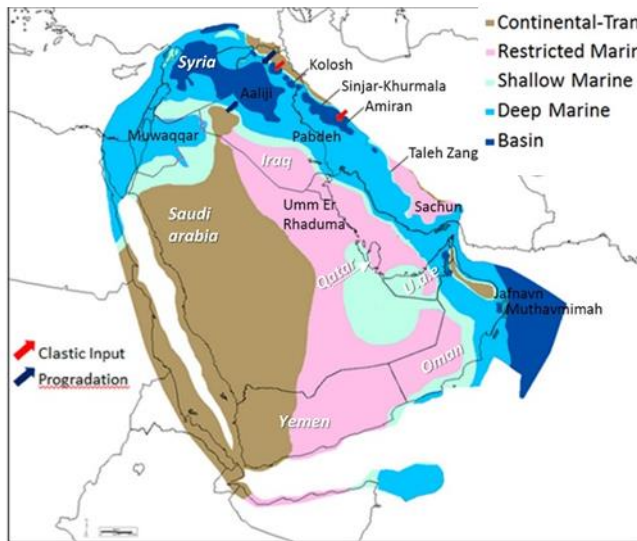
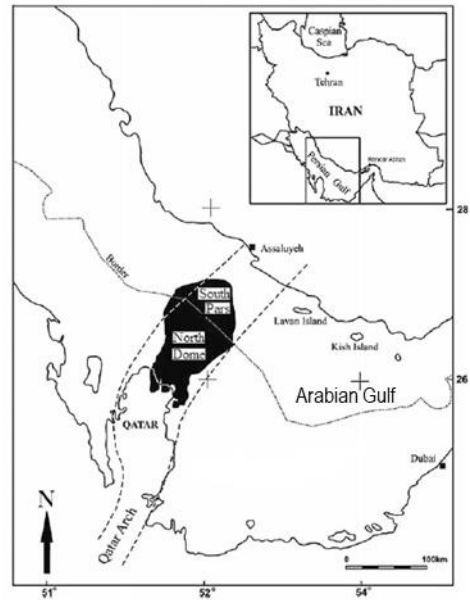


Figure 2-6 Location map of the South Pars-North Dome super giant gas field (Rahimpour-Bonab et al, 2009).



From the Oligocene, the region experienced submarine sedimentation, punctuated by a number of hiatuses which appear as a series of unconformities. Qatar peninsula’s final emergence occurred towards the end of the Miocene (Perotti et al., 2012, Sharland et al., 2001, Lloyd et al., 1987). The current land surface represents the recent rise in sea level 7000+ years ago (Puls, 2016).

The most prominent structural feature in Qatar is the north plunging Qatar-South Fars Arch, a north-south anticline extending through the center of Qatar into the Arabian Gulf to the north, which became sharply defined during the Upper Eocene and Oligocene period (Cavelier et al., 1970) (Figure 2-6). The Qatar Fars Arch is part an important hydrocarbon reserve, and is an extension of the North Dome (or North Field) in Qatar and the South Pars which is part of Iran (Rahimpour-Bonab, 2009). Smaller, gentler longitudinal folds of the Dukhan Anticline and Simsima Dome are situated in the west and north east of Qatar, respectively (Dill, 2003) and host oil and gas producing reservoirs (Al Siddiqi, 1998).

Recent evidence suggests that the anticlinal systems including the Qatar Arch and Dukhan Anticline, are separate antiformal structures, controlled by re-activation of basement faults as opposed to regional folding (Rivers, 2018) (Figure 2-7). Similar faulting has been recorded in Saudi Arabia, where basement-controlled faults define the lateral extent of the Ghawar anticlinal structure, Saudi's largest oil field (Afifi & ExxonMobil, 2004). The flat-lying stratigraphy of rock exposures at different elevations in and around Dukhan's 'anticline' or antiform further suggest that the structures are either upthrown fault blocks or horsts with faults defining the perimeter (Rivers et al., 2018).

Figure 2-7 East-west cross section showing previous and recent geological interpretation, Figure 8 from Rivers & Larson (2018)

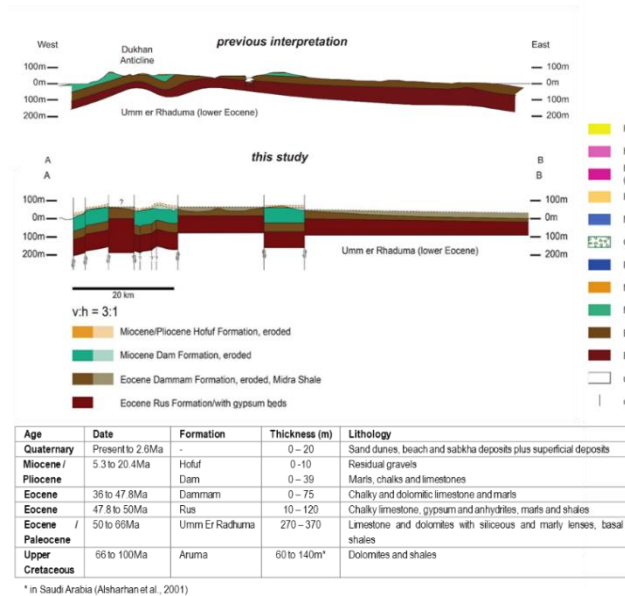
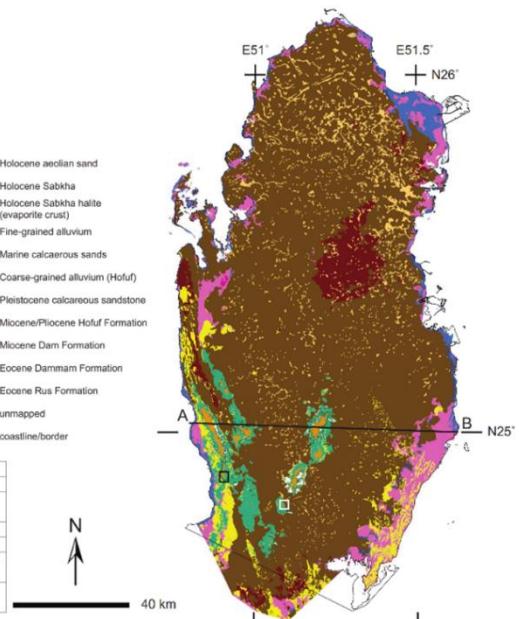


Figure 2-8 Surface geological map of Qatar including descriptions of surface and underlying geology (to ~600m depth) (Rivers & Larson, 2018)



2.6 Lithological Descriptions

For the purpose of this study, three lithologies comprise the top ~400m of Qatar. There are other younger geologies, however they have a restricted distribution and are only in the far west of the country. Relative to this project area, they are of no hydrogeological significance and therefore not discussed.

In vertical sequence from the bottom (based on Lloyd et al., 1987), the geological formations are:

- 1) Umm Er Radhuma Formation
- 2) Rus Formation
- 3) Dammam Formation.

2.6.1 Umm Er Radhuma Formation (UER)

The UER Formation is an extensive, thick, gently dipping and generally homogenous unit covering vast areas of Arabia including Qatar, Bahrain, Iraq, Kuwait, Oman and the UAE (Al-Hajari, 1990). Based on microfaunal evidence, the lower part of the UER is Paleocene with the upper part being of Lower Eocene (Cavelier C., Salatt A., Heuze, 1970). It sits conformably over the underlying Aruma Formation.

The UER was deposited in a transgressive marine environment (Rivers et al., 2019a) which was part of a large-scale HST (Highstand Systems Tract) prompting extensive carbonate production on a ramp margin of a semi-restricted basin (Dill, Nasir and Al-Saad, 2003, Boukhary et al., 2011, Ryan et al, 2018). The region was located at the equator and experienced warm climates with long episodes of open-marine conditions (Sharland et al., 2001). Alternating shallower, possibly sheltered lagoon and tropical settings during the Ypresian period built the Upper UER ramp (Dill, Nasir and Al-Saad, 2003, Boukhary et al., 2011).

Regionally, the UER thickens eastward, however folding during and after accumulation of the formation leads to a range of thicknesses from 300m to possibly 1000m (Eccleston et al., 1981). Within Qatar the UER ranges from 270m to 370m thick (Lloyd et al., 1987) compared with 300m to 800m further south in Saudi Arabia and 115m to >300m in Bahrain to the west (Eccleston et al., 1981). In Qatar, the top of the UER varies significantly, from up to 5-10m above sea level in higher elevations of Dukhan, to close to or slightly above sea level near the Qatar Arch, and approximately 120m below sea level in the very south of the country (Al-Hajari, 1990).

The UER is typically a repetitious series of light brown marly, dolomitic and calcarenitic limestones with occasional evaporitic intercalations. Rock core evidence from Dukhan (refer Table 2-2), the base of the UER is a pyritic to calcareous shale widely distributed over the Arabian plate and was formerly referred to as the 'Shammar Shale' (Boukhary et al., 2011).

This is overlain by a grey argillaceous limestone changing to a grey marly limestone, and subsequently overlaid by limestone and dolomitic limestone with white anhydrite nodules at the top, which is overlain by a dark grey richly fossiliferous compact limestone succeeded by the top-most member which is a chert-bearing white chalky and anhydritic limestone (Al-Saad et al., n.d.).

Table 2-2 The five informal units of the UER from the Dukhan area (defined by Al-Saad and Hewaidy (n.d), and three members as defined in Boukhary et al., 2011.

~Thickness (m)	Member 1	Member 2	Informal member name	Description
41m	E	C	Chalky	White chalky and anhydritic limestone
79m	D		Fossiliferous	Dark grey fossiliferous compact limestone
50 to 62m, locally 125m	C		Grey Unit	Light brown dolomite and light grey dolomitic limestone with white anhydrite nodules at top
7.5m to 66m	B	B	Limestone	Slightly dolomitic foraminiferal limestone over grey marly limestone over grey argillaceous limestone
9m to 14m	A	A	Shammar Shale	Dark blue pyritic shale to calcareous shale over blue grey pyritic marl with thin beds of black carbonaceous matter

The UER has undergone dolomitization (Rivers et al., 2019a) with distinguishable albeit thin siliceous zones. The upper beds, the stratigraphical unit relevant to this study, comprises light brown or light grey porous dolomite, sometimes chalky, where “dolomitized subtidal and peritidal carbonate cycles are capped by centimeter-scale beds rich in palygorskite” (Ryan, 2019). In the south of Qatar, gypsum or anhydrite nodules, sometimes as large as footballs, are found in the top 20 to 30m of the UER, immediately beneath the Rus sulphates.

A siliceous horizon, up to 200mm thick, is widely present comprising gravel to cobble-sized nodules of chert or silicified limestone or dolomite, in boreholes between 18-20m below the top of the formation (Lloyd et al., 1987, Eccleston et al., 1981) (Figure 2-9).

Figure 2-9 Chert / siliceous horizon in the UER Formation (Eccleston et al., 1981)

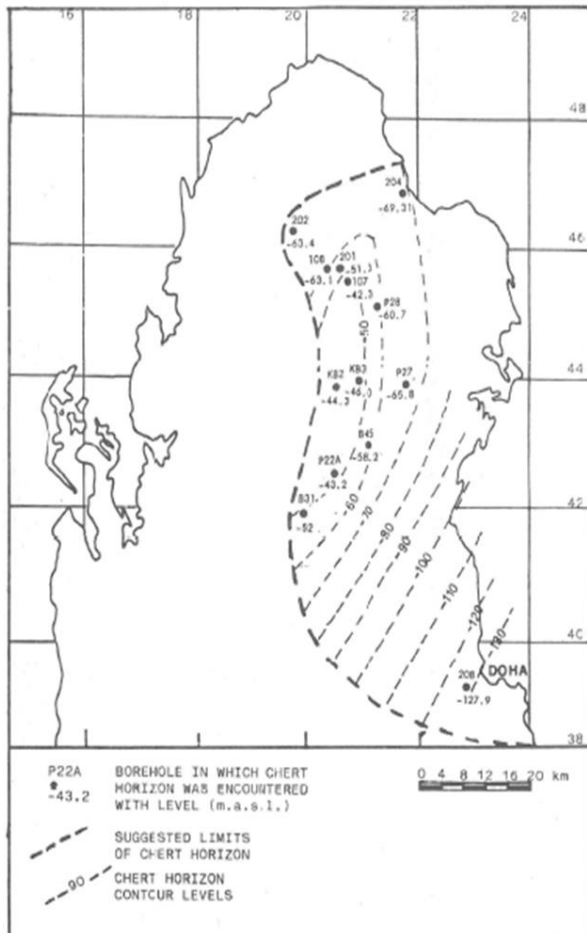


Figure 2-10 Rus Formation facies and province delineation (Eccleston et al., 1981)



2.6.2 Rus Formation

The Eocene-aged Rus Formation conformably overlies the UER Formation (Abu-Zeid & Boukhary, 1984) where the contact at the base of the Rus is characterized by a facies change suggesting a possible pause in sedimentary deposition of the UER (Lloyd et al., 1987, LeBlanc, 2017b) and the disappearance of deep open marine fauna (Le Blanc, 2017a). The following lowstand exposed a sabkha-salina setting, leading to the deposition of the Rus (Rivers et al., 2019a) although the overall depositional environment was variable across the country (Lloyd et al., 1987).

The Rus Formation is contiguous with the Rus Formation of Saudi Arabia and Bahrain and is exposed in Qatar only in a small area in northern central part of the country. Within Qatar

the Rus is recorded between 30 and up to 150m thick, extending to a maximum depth of 50m to 180m below ground level (Eccleston et al., 1981, Al-Saad, 2003).

Initially (Cavelier et al., 1970, Eccleston et al., 1981) the Rus Formation was broadly classified by depositional mode into two facies; Depositional Carbonate facies (or 'Rus Carbonate') composed of primarily carbonate sediment and the Depositional Sulphate facies (or 'Rus Sulphate') dominated by beds of gypsum and anhydrite formed by evaporation, and interbedded with argillaceous clays and white limestone (Figure 2-10). The Depositional Sulphate facies was thought to be absent in the north and an additional facies – the Residual Sulphate Facies - was included to describe the supposed transition to the northern area where deposition was entirely carbonate facies (Eccleston et al., 1981).

A recent re-evaluation by Rivers et al (2019a) further characterises the Rus by defining “a V-shaped escarpment apparent in satellite imagery” which segregates the depositional facies in the north and south. Fossil evidence of a shallow marine environment in Saudi Arabia indicates the basal Rus Formation was deposited in much shallower waters than the underlying UER (Lloyd et al, 1987, Le Blanc, 2017a). The lower Rus, or Traina Member, comprising m-scale dolomite-gypsum-clay cycles in the south, was deposited in an environment restricted from marine circulation. Argillaceous materials interbedded within the evaporitic thicknesses towards the top of the basal sequence suggest shallow water depositional environments and possible periods of freshwater flooding (Eccleston et al., 1981). This member is considered to extend across the country, though to the north of the escarpment, dolomitic limestones dominate and the thick gypsum beds are absent (Rivers et al., 2019a). Authigenic quartz and chalcedony have been recorded in the area of Fhailhil near Dukhan within the Traina Member (Abu-Zeid & Boukhary, 1984, Le Blanc, 2017b).

The upper Rus identified as the Al Khor Member (Al-Saad, 2003, Rivers et al., 2019a) comprises chalky dolomite and limestone with minor gypsum, marl and clay intercalations, and extends over the entire country. It was likely deposited in an open marine transgressive setting with possible shoals and some beaches (Le Blanc, 2017a). Siliceous sediments, such as chert and quartz crystal geodes, are recorded at the base of Al Khor member (Le Blanc, 2017b) with thicknesses of the argillaceous clay, both smectite and palygorskite (Ryan et al., 2019).

Faults resulting from compressional deformational folding are present within the Rus and cut through the younger overlying Dammam (Umm Bab) (Le Blanc, 2017a). Silicified tubular

conduit remains of paleo-freshwater springs with high sulphide content are found locally within the Rus around the Dukhan area approximately 4 to 14m above sea level, and were most likely active in the Miocene (LeBlanc, 2017b).

2.6.3 Dammam Formation

The Dammam Formation spans the middle Eocene to the lower Miocene and is separated from the overlying Dam Formation by a disconformity (Sharland et al., 2001). The Dammam Formation is exposed, forming the land surface over 80% of the country. The Formation can be subdivided it into five stratigraphic members, from bottom to top.

Fhahil Velates

This member, formerly identified as part of the Rus Formation, has recently been (re)included in the Dammam Formation (Rivers et al., 2019a, Seltrust Engineering Ltd, 1980) and comprises a distinct whitish, crystalline, compact, hard and fossiliferous limestone (Abu-Zeid & Boukhary, 1984). It represents the base of the Dammam Formation, however it is sometimes absent.

Midra Shale

This distinctive dark brown sometimes massive greenish layer comprises generally brown palygorskite clays, both mottled and very thinly to thickly laminated, within intercalations of discontinuous hard crystalline sometimes chalky limestones (LeBlanc, 2017a, Seltrust Engineering Ltd, 1980) . It sits below the overlying Alveolina, or Umm Bab if the Alveolina is not present, with a maximum known thickness of 10m. In places in the north of the country, the Midra Shale is absent.

Alveolina

White to yellowish brown argillaceous compact limestone, identified as the Alveolina Member, conformably underlies the carbonate muds at the base of the Umm Bab Limestone (LeBlanc, 2017a). The member is discontinuous across Qatar, rarely exceeding one meter thick (Seltrust Engineering Ltd, 1980). The extreme abundance of *Alveolina elliptica* fossils distinguishes it from other members (Abu-Zeid & Boukhary, 1984)

Umm Bab

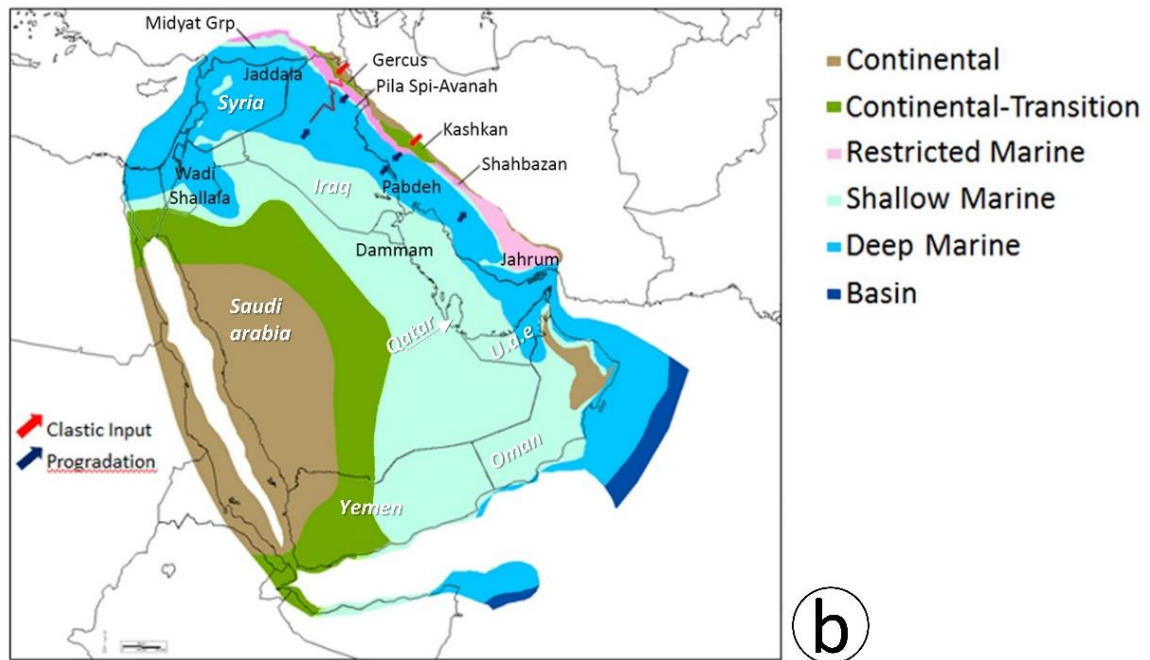
The Umm Bab Member covers most of the surface of Qatar and is characterized by a hard, crystalline white limestone, dolomitic limestone with small intermittent layers of chert, and noticeable red and sometimes green attapulgite clay (LeBlanc, 2017a). It is lithologically variable, both laterally and vertically, varying in strength from crystalline to very weak calcareous siltstone, and is often brecciated and vuggy. Paleo-fluid escape structures are also found within the Umm Bab in the west of the country, near Dukhan (LeBlanc, 2017a).

Abaruq

The Abaruq Member is a dolomitic limestone and generally of small thickness and is understood to outcrop in western Qatar only (Rivers et al., 2019a, Seltrust Engineering Ltd, 1980). The Abaruq was not identified during the project and is of no hydrogeological significance.

The Dammam Formation is a marine environment during a late transgressive to highstand event (Rivers et al., 2019a) (Figure 2-11). The Fhail Velates represents a transitional environment from the Rus into a compressed marine transgression and the deposition of the Midra Shale in a shallow back-bank setting near a continental supply (Le Blanc, 2017b). Fossil evidence of the discontinuous Alveolina member indicates the environment became very shallow marine and restricted in a protected shelf and reef shoal setting (Al-Saad et al., n.d.). A second highstand event deposited the remaining Upper Dammam Formation over the entire Arabian Shelf, as an open marine carbonate ramp progressively shallowing upwards (Dill et al., 2003, Boukhary et al., 2011).

Figure 2-11 Depositional Environment of Middle Eocene ~38Ma (Rivers et al., 2019a) Dammam Formation



2.7 Dolines – Karsts and Surface Depressions

Karstic features including depressions, sinkholes, caves and vugs are widespread across Qatar in the Rus and Dammam Formations. Sadiq and Nasir (2002) observed that the surface expression of the joint and fracture systems across the country are predominantly NE-SW and NW-SE and this is reflected in the orientation of the surface karst features. Their development can be related to isostatic and eustatic events, resulting in direct exposure or periods of direct influence of meteoric waters (Rivers, pers com) and flows through joints leading to dissolution, particularly of sulphates. These periods were most likely during the general uplift of Qatar from the end of the UER to the Lower Dammam transgression, during a potential hiatus of the Upper Eocene, and then again following the final emergence of the peninsula (Rivers et al., 2019a).

Analysis of aerial photographs by Sadiq and Nasir (2002) identified more than 9,700 large and small depressions, or dolines, covering 16% of the total land surface area of Qatar. These depressions can penetrate the Dammam into the Rus Formation, and can possibly extend into the UER, often accompanied with localised fractures and partings on bedding planes. There are strong feedbacks between karstification resulting in subsurface collapse and focusing of flow (Harmon, 2006).

2.8 Rock and Clay Mineralogy

The shallow geology of the Arabian peninsula is dominated by limestone (calcite - CaCO_3) and dolostone (dolomite $\text{CaMg}(\text{CO}_3)_2$). Sediments deposited in shallow water, often with trace elements Sr, Mn, Fe and Mg, are affected by early dissolution and cementation on and just below the seafloor. Primary dolomites are formed by direct nucleation of the crystals during deposition and are generally considered of minor importance. Most dolomites are thought to form from the transformation of calcite to dolomite after deposition (secondary dolomitization).

Evaporite sequences dominated by gypsum ($\text{CaSO}_4 \cdot 2\text{H}_2\text{O}$) with subsidiary anhydrite (CaSO_4), are found primarily in the Rus, although gypsum has been recorded in all formations.

Terrestrial sequences are found in porous detrital limestones of the Upper UER and Rus, and the clays smectite including illite, and palygorskite including minor sepiolite, have been identified UER, Rus and Dammam Formations (Ryan et al., 2019, Rivers et al., 2019a). Kaolinite and chlorite have also been identified in chemical analyses however the amounts are very small. Characteristics of various types of clays recorded are summarized below (after Tucker et al., 2009 and Drever, 1997):

- Smectites are a family of three-layered structured minerals which an alumina layer is sandwiched between two silica layers (2:1 group of sheet silicates). Montmorillonite is the most common. $\text{Al}_4(\text{Si}_4\text{O}_{10})_2(\text{OH})_4 \cdot n\text{H}_2\text{O}$. Smectites have an exchangeable interlayer such that substitution of the Al^{3+} by Fe^{2+} , Mg^{2+} and Zn^{2+} can take place. A net negative charge resulting from substitutions is balanced by other cations, especially Ca^{2+} and Na^+ , which are contained in interlayer positions which typically contains water. Smectites are known as an expandable clay a typical basal spacing of 14 Å, however basal spacing may vary from 9.6 Å (with no adsorbed water) to 21.4 Å (adsorbed water molecules).
- Illite, part of the mica group, have a mixed-layer structure and similar in construction to the smectites. It is the most common mineral in sediments is $(\text{K}, \text{H}_3\text{O})(\text{Al}, \text{Mg}, \text{Fe})_2(\text{Si}, \text{Al})_4\text{O}_{10}[(\text{OH})_2, (\text{H}_2\text{O})]$ resulting in an overall negative charge which is balanced by K^+ in the central layer however it may also contain Fe^{+2} and Mg^{+2} .

- Palygorskite and sepiolite are magnesium-rich fibrous clay minerals, where palygorskite $(\text{Mg,Al})_2\text{Si}_4\text{O}_{10}(\text{OH})\cdot 4(\text{H}_2\text{O})$ (Ryan et al., 2019) is a monoclinic and orthorhombic clay mineral, and usually contains some exchangeable cations. Sepiolite is hydrous magnesium silicate $\text{Mg}_4\text{Si}_6\text{O}_{15}(\text{OH})_2\cdot 6\text{H}_2\text{O}$ white clay.

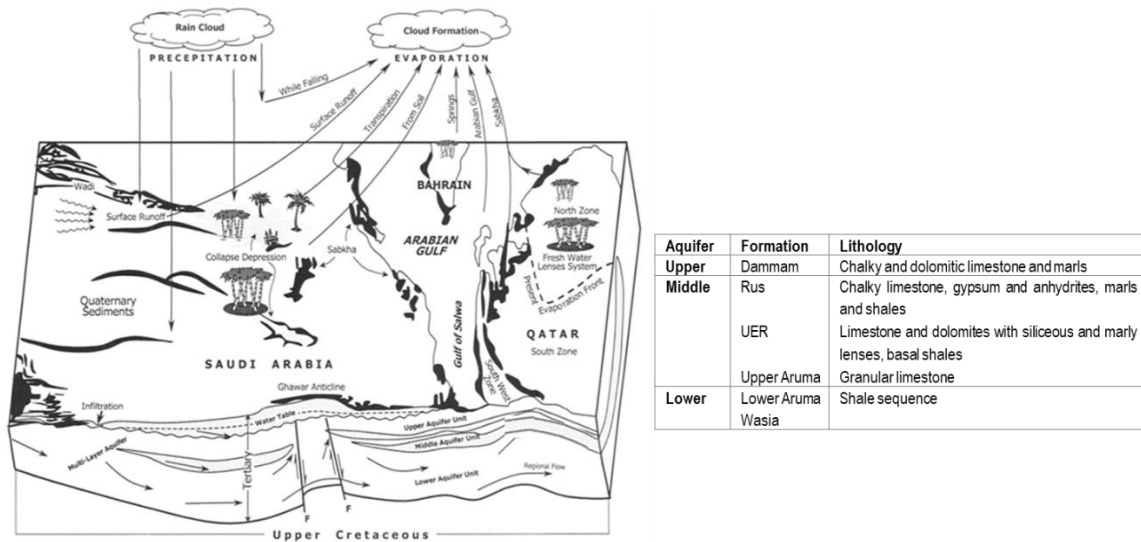
2.9 Regional Configuration of Aquifers and Aquitards

Based on piezometric head, the Food and Agricultural Organization of the United Nations (Alsharhan et al., 2001, FAO, 1979 in Al-Hajari, 1990) define three aquifer systems within the larger regional setting of the Arabian Peninsula. The Lower Wasia-Biyadh Aquifer Complex, which includes the deep Wasia and Lower Aruma Formations, is a low gradient, high hydraulic head aquifer. This is overlain by the Middle Aquifer, comprising the upper permeable section of the Aruma Formation, and the entire UER and Rus.

The Upper Aquifer of the region comprises the more recently deposited formations which overlie the Rus, including the Dammam, and is unconfined. It is considered a discontinuous freshwater lens, the lateral and vertical extent of which changes over a range of timescales due to rainfall and abstraction rates (Ministry of Development Planning and Statistics, 2017, Eccleston, B.L., Harhash, 1982, Eccleston et al., 1981,). Surface springs used as sources of freshwater were documented along the north western coastline in 1836 (Macumber, 2015), and offshore springs were known in the north west (Alsharhan et al., 2001), but with abstractions for industry and farming, these are no longer naturally discharging.

The regional aquifers have been defined by key aquicludes including the Midra Shale at the base of the Dammam that separates the Middle and Upper Aquifers, and the shales (formerly known as the Shammar Shale) at the base of the Aruma, which separates the Lower and Middle Aquifers. The evaporitic layer within the Traina Member of the Rus Formation in some areas, subdivides the Middle Aquifer (Figure 2-12).

Figure 2-12 Conceptual hydrogeological model of the eastern Arabian Peninsula (Alsharhan et al., 2001)



2.9.1 Characterising the Shallow Aquifers of Qatar

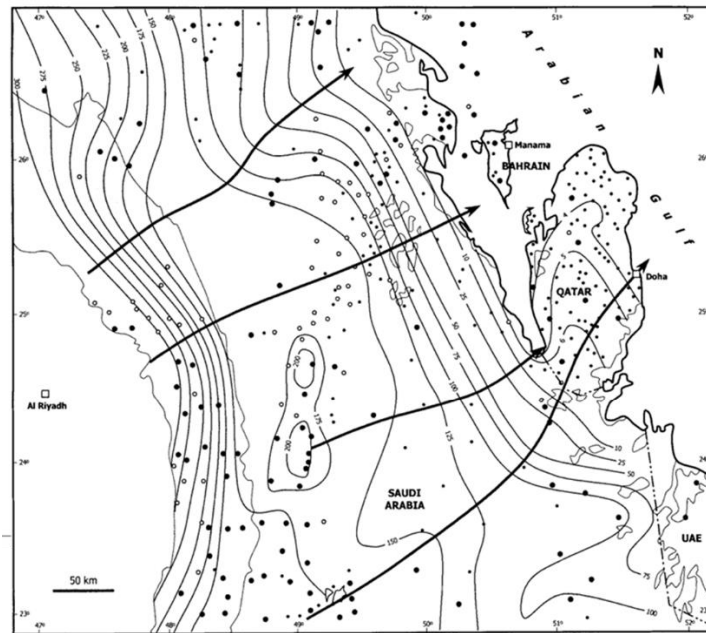
Within Qatar, three water-bearing layers relevant to this study are the Dammam (Upper Aquifer), Rus and Umm Er Radhuma formations (Middle Aquifer). Across the country, shallow groundwater fed from surface recharge flows radially outwards and discharges into coastal sabkhas and into the Gulf, and the geological structure of the Dukhan antiform in the southwest creates a physical barrier to groundwater movement (UN-ESCWA and BGR, 2013). In addition, anomalies to this general radial groundwater flow pattern are encountered where heads are affected by abstraction of water for irrigation.

Current recharge of the aquifers within the country are thought to include:

- lateral flow through confined portions of the UER and Rus from Saudi to the south and west
- meteoric recharge to the Dammam and Rus either by direct infiltration through outcrops or through unconfined portions
- upward leakage from underlying UER and Rus (northern province) and Dammam (although limited)
- lateral inflow of seawater into both the Dammam and Rus, and
- anthropogenic injection into the UER, Rus and Dammam.

Most of the recharge of the Eastern Arabia aquifer systems occurred during the pluvial periods over the past 50ky (Eccleston & Harhash, 1982), and present rates of recharge are considered to be minimal in comparison to lateral groundwater flow from Saudi Arabia (Cavelier *et al.*, 1970). The latter is estimated to be 2.2million m³/year (Baalousha, 2016a). The UER's only meteoric recharge is a large elongated outcrop in Saudi Arabia, extending from southern central area of Saudi Arabia up to the Iraqi-Saudi border (Al Bassam *et al.*, 1997) (Figure 2-13). The slow moving confined aquifer water has been modified by mixing with subsurface brines or surface waters, evaporation, hyperfiltration, and water rock interaction (Al-Hajari, 1990). The very saline waters of the UER are brines of ancient meteoric, connate and marine origin (Eccleston *et al.*, 1987, Al Bassam *et al.*, 1997).

Figure 2-13 Groundwater flow of the Tertiary aquifers (Alsharhan *et al.*, 2001)



The semi-arid to arid climate of the region limits the regularity of freshwater and rainfall related recharge occurs intermittently due to erratic rainfall. Direct recharge occurs for the soils and bare outcrops of the Dammam Formation which covers over 80% of the country, and the small exposed outcrop of the Rus Formation in the central area of the country. However, meteoric recharge to the Dammam and Rus, and possibly UER in Qatar, is primarily via natural karst depressions where surface runoff accumulates and ponds, and percolates down into the aquifers (Baalousha, 2016b, Al-Saad, 2005, Eccleston & Harhash, 1982). Small localized slightly saline waters have been recorded in the southern and south-

western areas of Qatar, indicating recharge dominates through these natural depressions (Eccleston et al., 1981).

Estimates of natural recharge in Qatar vary from 20.9M m³/year to 66M m³/year (from Table 1 from Baalousha, 2016a). The aridity of the Qatar and the region is a result of low rainfall, however high evaporation rates also significantly reduce the availability of any remaining water such as surface runoff or groundwater recharge (UNESCWA and BGR, 2013).

Subsurface flow of groundwater between aquifers is controlled by a combination of head differences and the permeability of confining units. In the south of the country, due to the presence of the low permeability Rus Sulfate and Midra Shale, groundwater leaks upward from the UER. Within the UER Formation itself, a lithological change eastward of shales and clays towards Qatar, results in a decline in groundwater circulation (Eccleston et al., 1981). The latter proposed that vertical flow to stratigraphically higher aquifers is dominantly via lithological 'windows' with eventual discharge to the Gulf.

In the north of Qatar, the Rus sulphate layer and the Midra Shale are either absent or of minimal thickness, and all three aquifers are in hydraulic continuity, allowing flow to occur between them. Therefore, in the south the aquifers remain distinct hydraulic entities, but in the north the UER, Rus and Dammam are all considered to behave as one aquifer (Lloyd et al., 1987). Seawater intrusion is prolific around the coast (Ministry of Development Planning and Statistics, 2014a) and the mixing zone thickens as well as oscillates laterally across different stratigraphies due to cyclical movement of the interface following pressure variations (Eccleston et al., 1981).

Eccleston et al. (1981) established groundwater ages using environmental isotopes including deuterium and oxygen stable isotopes, the radioactive isotope of hydrogen (tritium), and carbon isotopes. The age of groundwaters in Qatar have been dated to between 16ky to 28ky for the UER and 6.3ky years for the Rus. Younger ages were also recorded, however they are thought to represent the effect of dilution via boreholes associated with irrigation (Eccleston et al., 1981).

2.9.2 UER Aquifer

The UER, the deepest aquifer of this study, represents the principal aquifer of Qatar. It is confined by the evaporitic unit of the Rus and the Midra Shale of the Dammam, dips to the east and is 270m to 370m thick in Qatar (UNESCWA and BGR, 2013, Alsharhan et al.,

2001). The UER Formation is dominated by dolostone (Rivers et al., 2019a) and characterised as a karstified fractured bedrock aquifer with well-developed secondary intergranular porosity and low intergranular permeability (Al Bassam et al., 1997). Kalbus et al. (2011), Sadiq et al., (2002) and Sharaf (2001) agree with Eccleston et al., (1981) that “groundwater movement in the UER is primarily through secondary openings such as joints, fissures and bedding-plane openings which are often enlarged by solution processes”. This leads to the development a multi-layered aquifer system, with groundwater flow occurring across layers in the absence of confining layers, or vertical flow where there are significant fractures (Al Bassam et al., 1997).

The UER is a leaky aquifer as it occurs under semi-confined to rather fully-confined conditions (Sharaf, 2001, Kalbus et al., 2011). Therefore only the uniform upper part of the formation is of hydro-geological significance and will be considered in this study. The confined/semi confined nature of the aquifer leads to a piezometric head of above sea-level (Lloyd et al., 1987). In Qatar a shallow groundwater gradient between the north and the south indicates a very high horizontal permeability in the upper zone (Eccleston et al., 1981). Based on environmental isotopes from Eccleston et al. (1981) and Sharaf (2001) modern sea water intrusion is impeding the easterly flow of the UER into and through Qatar.

2.9.3 Rus Aquifer

The Rus Aquifer is of low yield relative to the underlying UER, and is between 30 to 150m thick, extending to a maximum depth of 50m to 180m below ground level (Eccleston *et al.*, 1981, Al-Saad, 2003). In the central and northern areas, where sulphates interbedded with clays are absent, the Rus Formation is in hydraulic continuity with the upper section of the Umm Er Radhuma aquifer (Kalbus et al, 2011). In the south, the presence of sulphates and basal clays in the Rus develops progressively more distinct and multiple hydraulic entities within the Rus itself (Eccleston et al., 1981).

The Rus aquifer is considered semi-confined in the southern area as the overlying Midra Shale acts as an aquitard. As such, the piezometric head recorded in Eccleston et al., (1981) is above sea-level and further elevated in the higher central areas of the country, reflecting the topographic gradient. In the north where the Midra Shale is absent, the Rus piezometric head is fed only by local meteoric recharge and is determined to sea-level.

Within the calcareous facies, flow is both intergranular and through secondary porosity such as fissures and karsts. The sulphate layers display limited secondary porosity localised around karstic features.

2.9.4 Dammam Aquifer

The Dammam Formation occurs over numerous surrounding countries but is it only locally important as an aquifer in the north of Qatar. Although the Dammam outcrops almost all of Qatar, in the southern and central areas it lies entirely within the vadose zones.

The Dammam acts as a near surface reservoir for the temporary storage of fresh recharge rainwater (Eccelston et al., 1981). The Umm Bab member, the most laterally and vertically dominant member of the Dammam Formation for this study, has high matrix porosity and karstic features such as vugs, cavities, sinkholes and dolines, with secondary fissures and karst dominating (Sharaf, 2001). Intergranular flow also occurs, but the dominantly calcitic rocks typically show low porosity and permeability. However vuggy limestones that are not filled with clay have elevated permeabilities but still low porosities (Rivers et al., 2019a). Observation of dolomite crystal size and subsequent comparison with laboratory permeability and porosity results indicate crystal size has limited significance in determining the aquifer quality of these rocks (Rivers et al., 2019a).

Historic depth to groundwater for each aquifer in m QNHD (Qatar National Height Data) is found in Figure 2-15 for the UER, Figure 2-16 for the Rus, and Figure 2-15 for depth to groundwater from surface.

2.9.5 Freshwater Lens

A complex freshwater lens extends through the central and northern areas of the country, constrained by underlying saline groundwaters controlled by the hydraulic head in mountains of eastern Saudi Arabia and by the sea water level of the Arabian Gulf (Lloyd et al., 1987). The lens is floating on the deeper more saline water. In 1980, FOA mapped the freshwater lens and found the base to be approximately 100m below sea-level in the central northern area of the country (Eccleston et al., 1981). Freshwater was also within the Rus and Upper UER at a few groundwater fields situated along the V-shaped structure through the center of Qatar (Al-Hajari, 1990), although only in the areas where it was suggested the Rus sulphate was not present (Eccleston et al., 1981). The historic freshwater lens was larger in the north, and presumed to be the result of local recharge in combination with

variable lithology and subsequent permeability/impermeability under the hydrostatic head-salinity Ghyben-Herzberg relationship.

Due to current aggressive abstraction rates, the freshwater lens is being invaded laterally by modern seawater intrusion and vertically by brackish to saline groundwater from the UER (Alsharhan et al., 2001, Eccleston et al., 1981) (Figure 2-14). There is no known replenishment of fresh or brackish water from Saudi Arabia into Qatar, either past or present. Some minor water bearing lenses are found within the Rus, however due to lack of hydraulic continuity between the Rus aquifer layers and any recharge area in Saudi, this precludes any lateral supply of freshwater.

Figure 2-14 Natural groundwater conditions in northern Qatar, and the effects of groundwater pumping (Alsharhan et al., 2001).

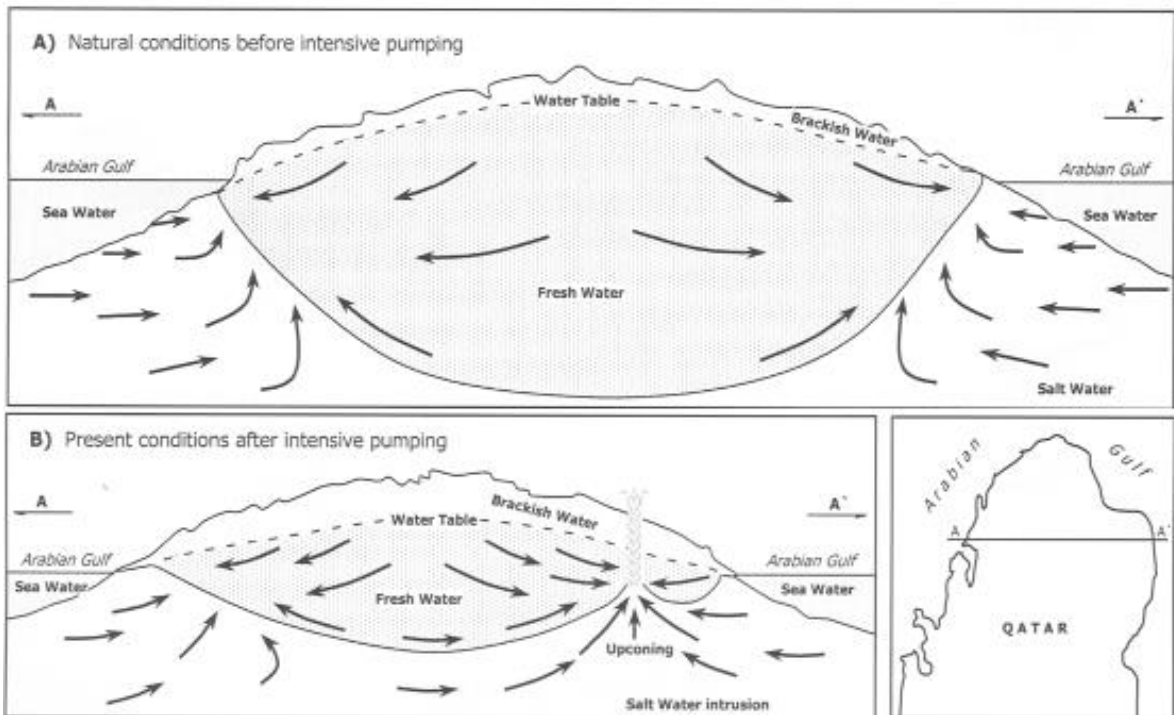


Figure 2-15 Regional piezometric surface (m QNHD) of the UER aquifer in 1981 (Eccleston et al., 1981).

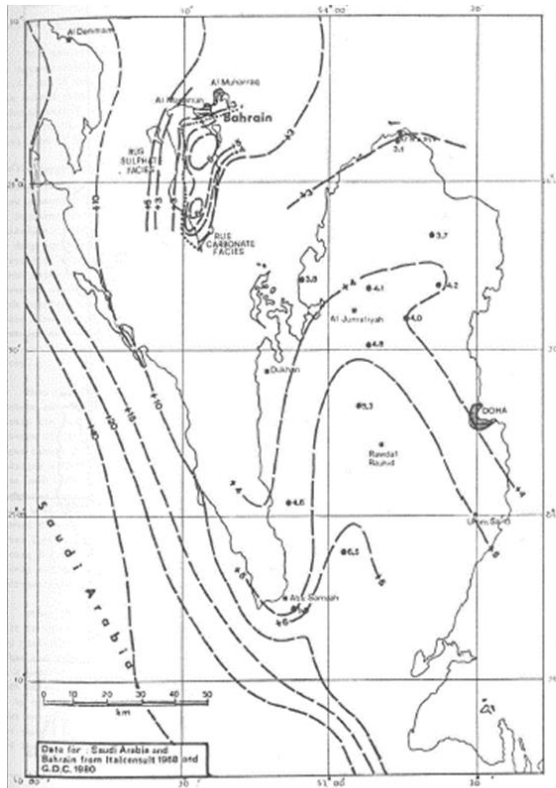


Figure 2-16 Groundwater head for Rus Formation in 1981 (Lloyd et al., 1987 based on Eccleston et al., 1981)

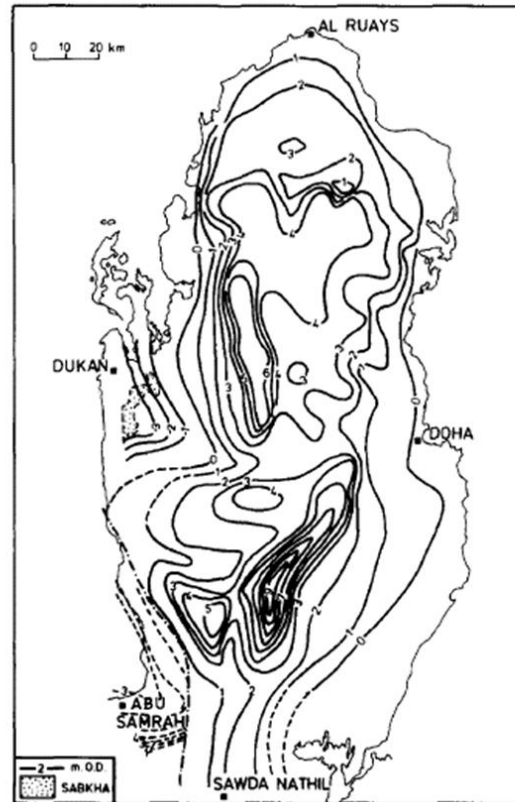
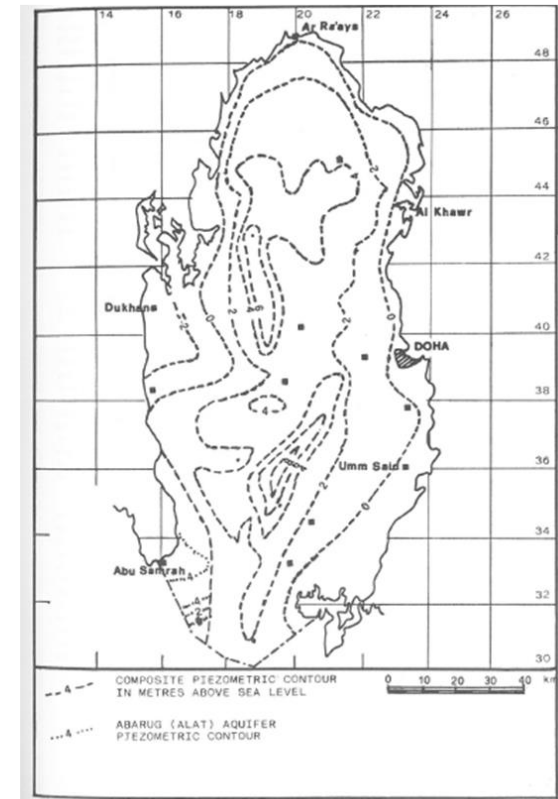


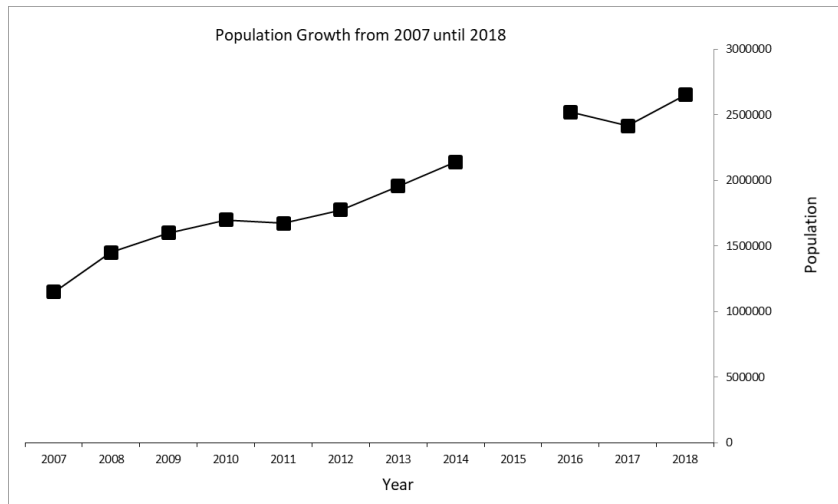
Figure 2-17 Depth to groundwater 1981 from surface (Eccleston et al., 1981)



2.10 Anthropogenic influences

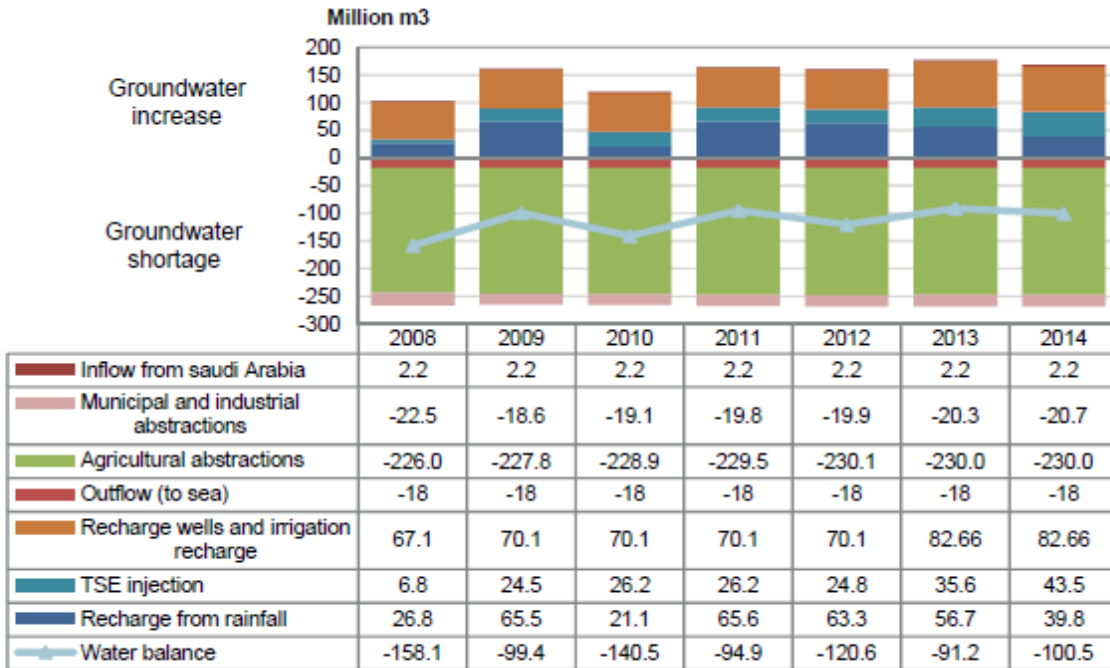
The total population of Qatar has more than doubled over the last 10 years (Figure 2-18) and was 2.77M in February 2019 <<https://www.mdps.gov.qa/en/statistics1-/StatisticsSite/Pages/Population.aspx>, 2019> (Figure 2-18). Approximately 33% of these people live within the capital city Doha (estimated 2015), <https://www.indexmundi.com/-qatar/demographics_profile.html, 2019> which is located on the east coast. Also in coastal areas are three large industrial zones - Ras Laffan, Masaieed and Dukhan – that have developed largely to support the oil industry with accompanying residential townships. The remainder of the country is open desert, military space, farms and occasional small towns.

Figure 2-18 Qatar’s population over the last 10years <<http://www.mdps.gov.qa/en/Statistics1/StatisticsSite/Pages/Population.aspx>, 2019>



Qatar’s government has encouraged rapid urbanisation and aggressive expansion of its agricultural and industrial sectors to provide economic security for its future. The expanding population and requirements for food self-sufficiency and water security have increased demands on suitable water for agricultural, domestic and municipal requirements, including demands on potable water. This has created a significant demand on groundwater in an aquifer system where supply is greater than demand (Figure 2-19).

Figure 2-19 Groundwater inflow versus outflow (Ministry of Development Planning and Statistics, 2017)



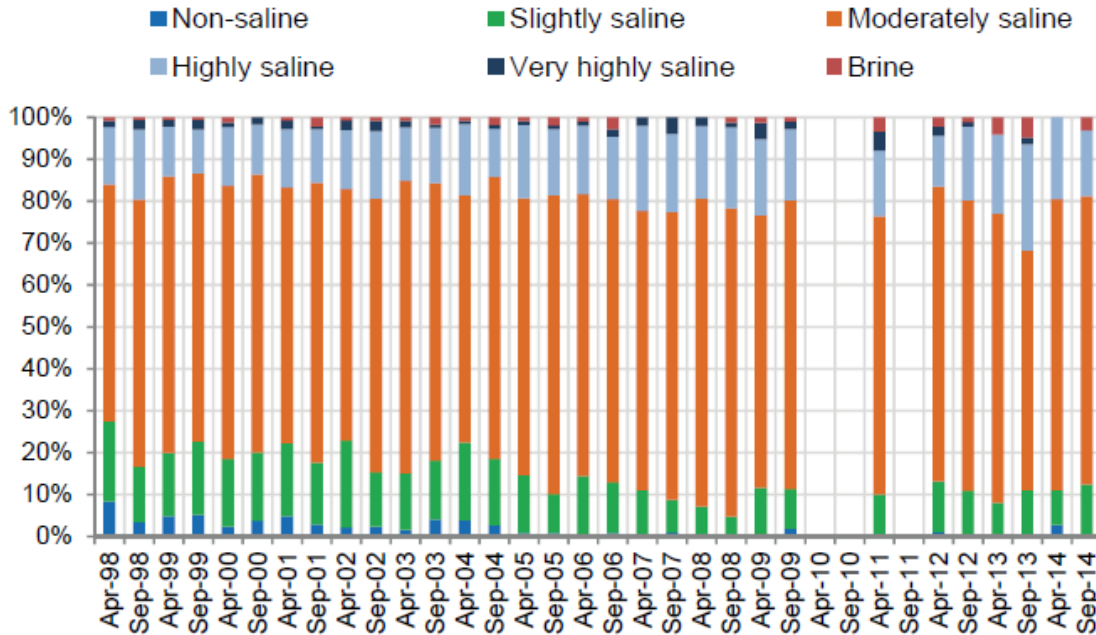
Water production, by artificial means, has grown significantly from 220M m³ in 1990 to 841M m³ in 2014, through the injection of treated industry, domestic effluent (TSE - treated sewage effluent) and irrigation returns. Desalination has also increased and represents 59% of water produced in country for 2014 (Ministry of Development Planning and Statistics, 2017), which is typical for the region.

Combining all sources of available water including desalination, abstracted groundwater, treated TSE and waste water discharge, the total quantity of water available for use in 2014 was 926M m³. The government's calculated quantity of water consumed by farming, industry, households, or discharged into the sea or lost during the same time period was recorded at 926M m³, giving a zero net overall (Ministry of Development Planning and Statistics, 2017).

Current population and expansion trends are envisaged to continue, albeit not as fast as over the last decade. Issues of both water quantity and quality associated with depletion of the aquifers are of considerable concern. Salinity (generally expressed as TDS) has increased in abstracted groundwaters, and since April 2014 all groundwater wells have

recorded *slightly saline* and higher (Figure 2-20) as based on categories first defined by FAO in 1981 (Ministry of Development Planning and Statistics, 2017).

Figure 2-20 Salinity classifications of Qatar Government groundwater monitoring wells, from April 1998 to September 2014 (Ministry of Development Planning and Statistics, 2017)



Salinity Classifications	Electrical Conductivity (dS/m)	Total Dissolved Solids (mg/l)	Water quality
Drinking and irrigation water	<0.7	<500	Non saline
Irrigation water	0.7 – 2	500 – 1,500	Slightly saline
Primary drainage water and groundwater	2 – 10	1,500 – 7,00	Moderately saline
Secondary drainage water and groundwater	10 – 25	7,000 – 15,000	Highly saline
Very saline water	25 – 45	15,000 – 35,000	Very highly saline
Seawater	>45	>45,000	Brine

2.11 Key water-rock reactions

Most carbonate sediments were formed when seawater became supersaturated with respect to calcium carbonate (CaCO₃) typically through evaporation without any loss of dissolved solids (James & Jones, 2016). High magnesium calcite (HMC) and aragonite, although less stable, are more likely to initially precipitate than pure calcite. Carbonates are

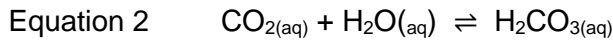
often extensively modified during diagenesis by recrystallization, replacement, dissolution or cementation. They undergo dolomitization ($\text{CaMg}(\text{CO}_3)_2$), and are commonly found in association with gypsum ($\text{CaSO}_4 \cdot 2\text{H}_2\text{O}$) and anhydrite (CaSO_4). The most common water - rock interactions are discussed briefly below;

a) Carbonate precipitation and dissolution

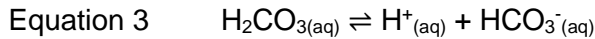
The carbonate precipitation and dissolution processes are the product of five equilibria reactions, Equation 1 to 6 (James & Jones, 2016, Drever, 1997) which are primarily dependent on the addition or removal of CO_2 . When CO_2 gas is exposed and in contact with water, it dissolves;



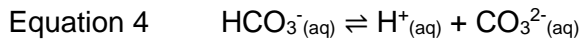
This is followed by the hydration of CO_2 by H_2O to form a weak carbonic acid;



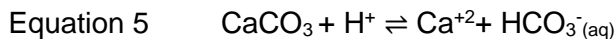
The carbonic acid molecule is an acid and almost instantaneous dissociation into hydrogen and bicarbonate ions, forming a weakly acid solution;



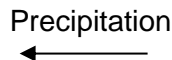
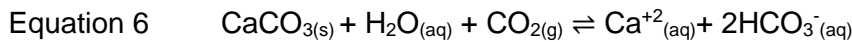
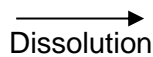
Some bicarbonate dissociates further into a hydrogen ion and carbonate ion;



The overall reaction between carbonic acid solution and solid calcium carbonate is;



Or alternatively;



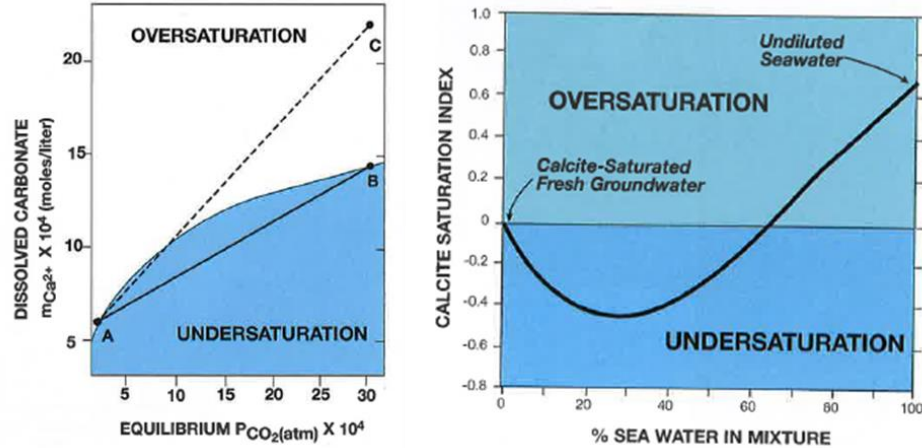
Removing carbon dioxide from solution will lower the acidity and causing precipitation of solid calcium carbonate (drive the reaction in Equation 6 to the left) while conversely adding CO_2 to a fluid at equilibrium will cause dissolution (Drever, 1997). Favourable conditions for dissolution are falling temperatures with increasing hydrostatic pressure, conversely

precipitation occurs with increasing temperature and decreasing hydrostatic pressure. Sources of CO₂, most commonly, are biogenic from root respiratory and microbial oxidation of organic matter.

Precipitation can range in scale from intraparticle to larger, where cement precipitation and resulting lithification in and between particles are the most important (James & Jones, 2016). Carbonate dissolution can occur in a variety of places and scales, including the seafloor, throughout the meteoric zone, at the mixing zone of fresh and saline water, and during deep burial, as carbonates often dissolve when pore waters become undersaturated (James & Jones, 2016).

Mixing zones are particularly relevant in Qatar due to the close proximity of the sea and the relic freshwater lens which sits as a near-surface aquifer under the country. This zone is found at the top of the water table and at the brackish zone of mixing at the base of the freshwater lens. At the interface of the vadose zone and water table, mixing of fresh meteoric water with a different CO₂ content to the resident groundwaters at the water table and therefore different concentrations of dissolved carbonate, result in undersaturation and often dissolution, until equilibrium is reached (Morse, 1990) (Figure 2-21). Within the brackish phreatic zone, where seawater mixes with carbonate saturated fresher water, initially the fluid becomes more undersaturated with respect to calcite. However, as mixing continues and increasing seawater oversaturates the fluid, precipitation is prevented by various kinetic and other factors which result in dissolution (Stoessell, 1992, Morse & Mackenzie, 1990) (Figure 2-21).

Figure 2-21 A. The non-linear relationship between equilibrium P_{CO_2} and dissolved $CaCO_3$; B. Calcite saturation in the mixing zone of seawater and meteoric water (Jones & James, 2016)



b) Dolomitization

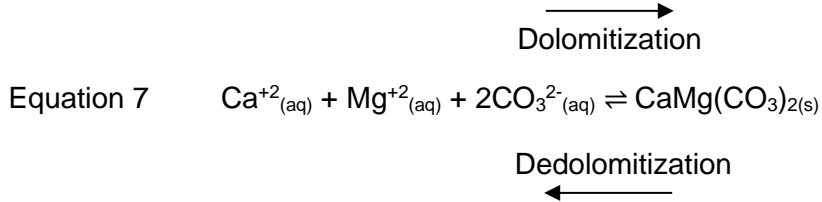
Dolomite $CaMg(CO_3)_2$ has an ordered structure of alternating layers $Ca^{+2} - CO_3^{2-} - Mg^{2+} - CO_3^{2-} - Ca^{+2}$ (James & Jones, 2016). However, natural dolomite often does not display ideal ordering, with surplus of Ca (a few percent) with an associated Mg deficit (Machel, 2004). Diagenetic settings of dolomite include 1) syndimentary (authigenic), 2) early diagenetic where dolomites form in the shallow subsurface and 3) late diagenetic dolomites which usually form in the deep subsurface, generally as cement overgrowths on pre-existing crystals (James & Jones, 2016).

Machel (2004) suggests dolomites that originally form close the surface, often from evaporitic brines, tend to recrystallize with time and during burial, while those formed at depths greater than several hundred down to a few thousand meters, exhibit little evidence of recrystallization

Primary dolomitization originates by direct precipitation from an aqueous solution forming dolomite, usually involving microbes or penecontemporaneous replacement of carbonate sediment, and driven by CO_3^{2-} (Ooi, 2018). This process is rare (Tucker et al., 2009), and commonly forms only a few percent of microcrystalline dolomite, 1-3 μm long, with a mineral content of Ca-to locally Mg-rich and generally non-stoichiometric (Machel, 2004, James & Jones, 2016). Although primary dolomitization does not form massive dolostones, this process can take place in range of environments including muddy tidal flats, lakes, and

organic-rich carbonate sediments beneath sites of active ocean upwelling (James & Jones, 2016), and can provide ‘seeds’ for later dolomitization.

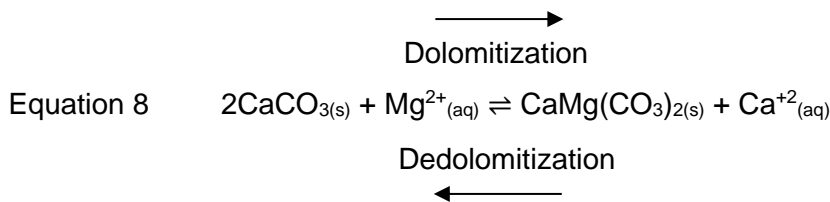
Primary dolomitization:



The most common form of dolomitization is secondary dolomitization, which is either by replacement (replacing CaCO_3) or cementation (precipitation) (Machel, 2004, Tucker *et al.*, 2009). Replacement dolomitization involves the direct replacement of previously deposited calcium carbonate (CaCO_3) by dolomite ($\text{CaMg}(\text{CO}_3)_2$), preferentially with the more soluble metastable aragonite and HMC which inherently contains more Mg^{+2} , and releases Ca^{+2} ion (James & Jones, 2016). Replacement can range from fabric destructive, selective to persuasive, or retentive (Tucker *et al.*, 2009) where replacement is predominantly matrix-selective favouring matrices initially comprising aragonite or HMC (which are more soluble) and having larger reaction surfaces due to smaller grain sizes (Machel, 2004).

Dolomite cementation involves the precipitation of dolomite from supersaturated solutions as a cement into primary or secondary pore space, often as overgrowths on pre-existing crystals of dolomite, between dolomitized grains and voids left from dissolution (Machel, 2004, Tucker *et al.*, 2009). The concentration of calcium and carbonate in solution will determine the outcome of dolomitization, as dolomite replacement requires undersaturation with respect to calcium carbonate, otherwise dolomite cementation will take place (Machel, 2004).

Replacement dolomitization:



All mechanisms for dolomitization require fluid flow (advection) to move reactants to and products from sites of mineral formation, ensuring a long-lasting efficient source of Mg^{2+} (and CO_3^{2-}) (Tucker *et al.*, 2009). Forces driving fluid flow include hydrostatic head (either

meteoric or seawater), temperature or salinity creating fluid density gradients, sedimentology or tectonic processes although there is often a combination of all (Whitaker et al., 2008). Given these flux requirements, and an abundance of available calcium carbonate for replacement, chemical conditions favourable for large scale dolomitization are documented by James & Jones (2016), Tucker et al., (2009) and Machel (2004) include:

- Low Ca/Mg ratios, such as result from increasing absolute concentration of ions in seawater by evaporation
- Decreasing Ca/Mg ratios due to the precipitation of gypsum/anhydrite
- High temperatures, which are both thermodynamically important (reducing the requirement for low Ca/Mg) and critically to reduce kinetic barriers to dolomitization
- Limited ion pair formation such that significant increases in Mg concentrations overcome the thermodynamic barrier leading to more available Mg ions for dolomitization. This could favour dolomitization by dilute solutions, if Ca/Mg ratios are sufficiently low
- Reduction of hydration barrier whereby OH ions surrounding Mg^{2+} effectively create a hydration sheath, such that CO_3^{2-} will bond before Mg, particularly where fluids have $<pH\ 9$ (James & Jones, 2016)
- A release of CO_2 (degassing) by increasing temperature
- Low sulfate concentrations as high concentrations inhibit dolomitization
- Sufficient time to exceed the induction period and/or the presence of dolomite 'seeds', as dolomitization occurs at a very slow rate.

Further, vugs and moulds resulting from dissolution often form during the advanced stages of dolomitization. Voids of various sizes are often observed in dolomites and are interpreted to be formed by dissolution of allochems/biochems which were originally calcite, aragonite or HMC. Dissolution extends into the un-replaced allochems and biochems moulds, proceeding beyond the existing mould margin into the already dolomitized matrix (Machel, 2004). These features are often self-propelling and can develop into larger scale karsts.

c) Dedolomitization

Dedolomitization (or calcitization), in this instance, involves the partial or full precipitation of calcite cement in a dissolved dolomite crystal core (James & Jones, 2016). This type of dedolomitization creates a distinctive rhomb-shaped crystal with a thin outer zone or rim of

unclouded crystal dolomite surrounded by a calcite core, although in some cases the rim is destroyed and all trace of the original dolomite crystal vanishes (James & Jones, 2016).

Dedolomite has also been proposed to occur by dissolution of dolomite followed by the immediate precipitation of calcite, similar to the dissolution-precipitation process associated with the transformation of aragonite to calcite (James & Jones, 2016). Irrespective of process, calcite surrounded by a dolomite rim, or precipitated between crystals, is referred to dedolomitization (Equation 8).

Dedolomitization can take place in groundwater waters (25-50°C) with high Ca^{+2} and low Mg^{2+} concentrations, often leading to a decrease in porosity due to formation of calcite crystals in and between particles (Escorcia, 2013). The rate of dedolomitization can be enhanced by the presence of calcium-bearing minerals such as anhydrite whose kinetics of dissolution are faster. Results from numerical modelling (Escorcia et al., 2013) suggests that dedolomitization is enhanced when the fluid fluxes are in balance with reaction kinetics, not too slow or fast (ideal flow rate of 10 m year^{-1}).

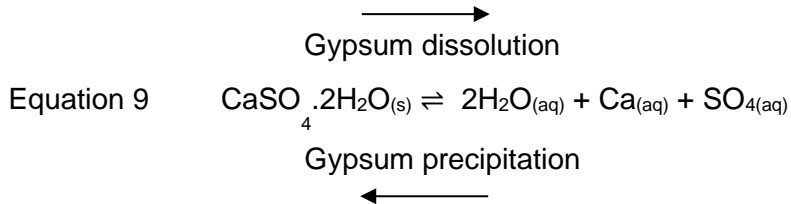
d) Dolomite dissolution

Dissolution of dolomite crystals and matrix creates oversized pores, dissolution pits and voids which are noticeably coarsely crystalline, porous and more permeable than original dolomite (Machel, 2004). Solubility of dolomite is dependent on the % of Ca in the crystal, as metastable crystals of HCD with growth defects and inclusions of non-dolomitized calcite, aragonite and apatite, are vulnerable to dissolution (Jones & James, 2016). Increased flow rate and lower pH of the surrounding fluid lead to faster reaction rates and higher levels of dissolution (Singurindy, 2003).

e) Evaporite precipitation and dissolution

The evaporites gypsum and anhydrite are precipitated / dissolved at different scales. Deposition of evaporites commonly occur in hot and arid climates on exposed or shallow carbonate platforms or in lagoons, peritidal zones, local salinas and marginal marine lakes. During periods of lower sea level, restricted circulation of seawater or brines lead to the precipitation of sulphates and halitic evaporates (James & Jones, 2016). When seawater begins to evaporate, calcite is first to precipitate, usually as aragonite, after the loss of 40 to 60‰ seawater. Gypsum precipitates after seawater concentrations are 130 to 160‰, although other influences such as microbes and algae affect rates of precipitation (Warren,

1999). Large scale precipitation of evaporites, or salt giants, can also form in deep restricted basins. Based on microscopic texture, gypsum appears to be precipitated first and during burial is dehydrated to anhydrite (Machel, 2004).



f) Calcite cementation and dissolution

Calcite precipitation between particles, and the resulting lithification, is a primary function of diagenesis of both limestone and dolostones, affecting the rocks porosity and permeability. Calcites precipitate or dissolve in various environments, depending on water quality. Calcite and aragonite precipitate more readily than dolomite as they are stoichiometrically less ordered requiring less levels of energy to precipitate (James & Jones, 2016). Conversely, calcite dissolution is a function of Mg content, as increasing amounts of Mg in the calcite lattice deform the crystal making it progressively unstable, such that HMC and aragonite are more soluble than calcite (Tucker et al., 2009).

3.0 METHODS

3.1 Introduction

Traditional drilling and monitoring methods were employed to obtain rock core and groundwater samples at the various well locations across Qatar, and all works were undertaken in accordance with the *Code of practice for ground investigations* (British Standards Institution, 2015). At each location, the following sequence of site works included:

1. Drilling of cored borehole; RR (south) from 04th to 26th October 2016, AG (north) from 11th May 2017 to 21st June 2017, and AS (central) from 14th to 27th December 2017
2. In-situ testing including geophysics (all cored boreholes), borehole profiles and flow logging (southern and central boreholes), and packers (southern borehole only)
3. Drilling of adjacent sister monitoring wells
4. Installation and well development of monitoring wells
5. Groundwater monitoring and sampling

Following site works, and after the retrieval of groundwater samples:

6. Laboratory testing on groundwater samples
7. Logging of cored borehole, and
8. Interpretation and analyses.

3.2 Drilling of cored boreholes and monitoring wells

Rotary cored boreholes to retrieve rock samples were drilled to depths between 120m and 134m bgl (Figure 3-1) at three different locations along the crest of the Qatar Arch, away from marine groundwater influence (Figure 3-2). The locations had already been selected for a detailed study by ExxonMobil (Rivers et al., 2019a), as each location gave access to one of the three separate depositional facies in the Rus as proposed in Eccleston *et al.* (1981); the Depositional Sulphate (RR southern wells), Depositional Carbonate (AG northern wells) and Residual Sulphate (AS central wells) (refer Section 2.6.2).

The borehole locations formed a transect from the southern groundwater zone, where the Rus contains a substantial thickness of gypsum, to the north where the evaporitic layer was

absent. The locations captured important diagenetic features, including the transition from evaporitic to carbonate-dominated Rus, and associations with the development of karstic features which are found across the country. The rotary core drilling of three boreholes were:

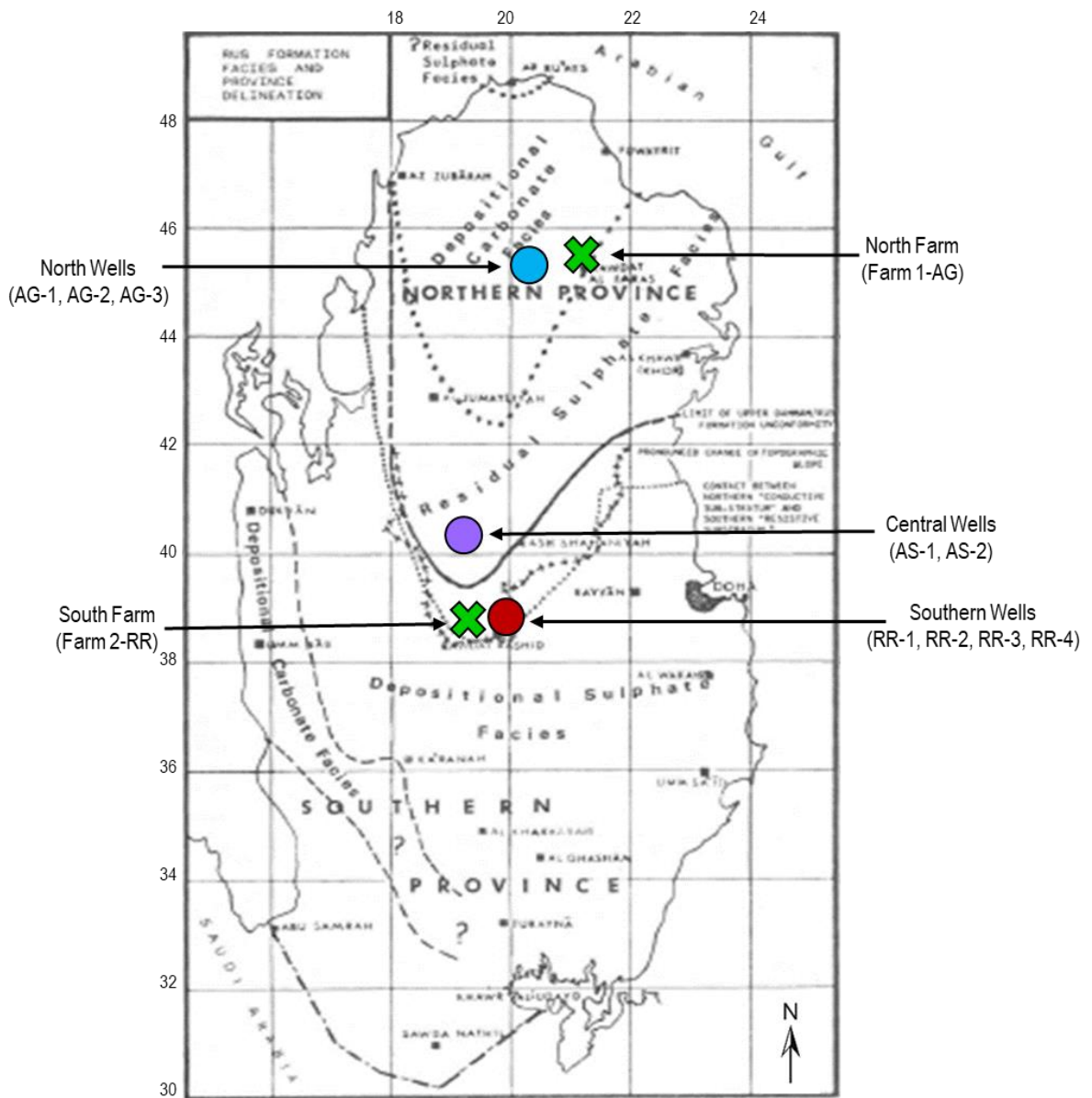
- RR (EMRQ_RR_BH001), the southern well located near Rawdat Rasid and completed at the end of 2016,
- AS (EMRQ_AS_BH001), the central well is situated near Ash-Shahaniyah and completed December 2017,
- AG (EMRQ_AG_BH001), the northern well near Al-Ghuwayriyah, completed at the end of June 2017 (Figure 3-6).

At each location, and immediately adjacent to the main rotary cored borehole (<10m), a set of additional boreholes were drilled specifically for groundwater monitoring purposes, to target the different shallow aquifers (Appendix A1). This allowed a comparison of the same aquifers at three different locations within the country. Response zones were based on flow zones determined during site works and are further explained in Chapter 4. Design details of the well cluster and intercepted lithologies are shown in Figure 3-3, Figure 3-4, Figure 3-5. The monitoring wells were numbered from the deepest monitoring pipe upwards, as the deepest well is always drilled first (Table 3-2).

Figure 3-1 Drilling of RR (southern) wells and surrounds, monitoring, and wells on completion



Figure 3-2 Well locations in Qatar



3.2 Groundwater monitoring standpipes

Groundwater monitoring standpipes (uPVC) of 50mm diameter were installed in the cored boreholes and adjacent monitoring wells for long term groundwater monitoring. Full details on depth and response zone of each well are shown in Table 3-2. Two nearby established farm water wells were also included as part of the monitoring and the location of these wells was established using a hand-held GPS with an accuracy of +/-3m.

Figure 3-3 Southern Well (RR-1, RR-2, RR-3 and RR-4) installations

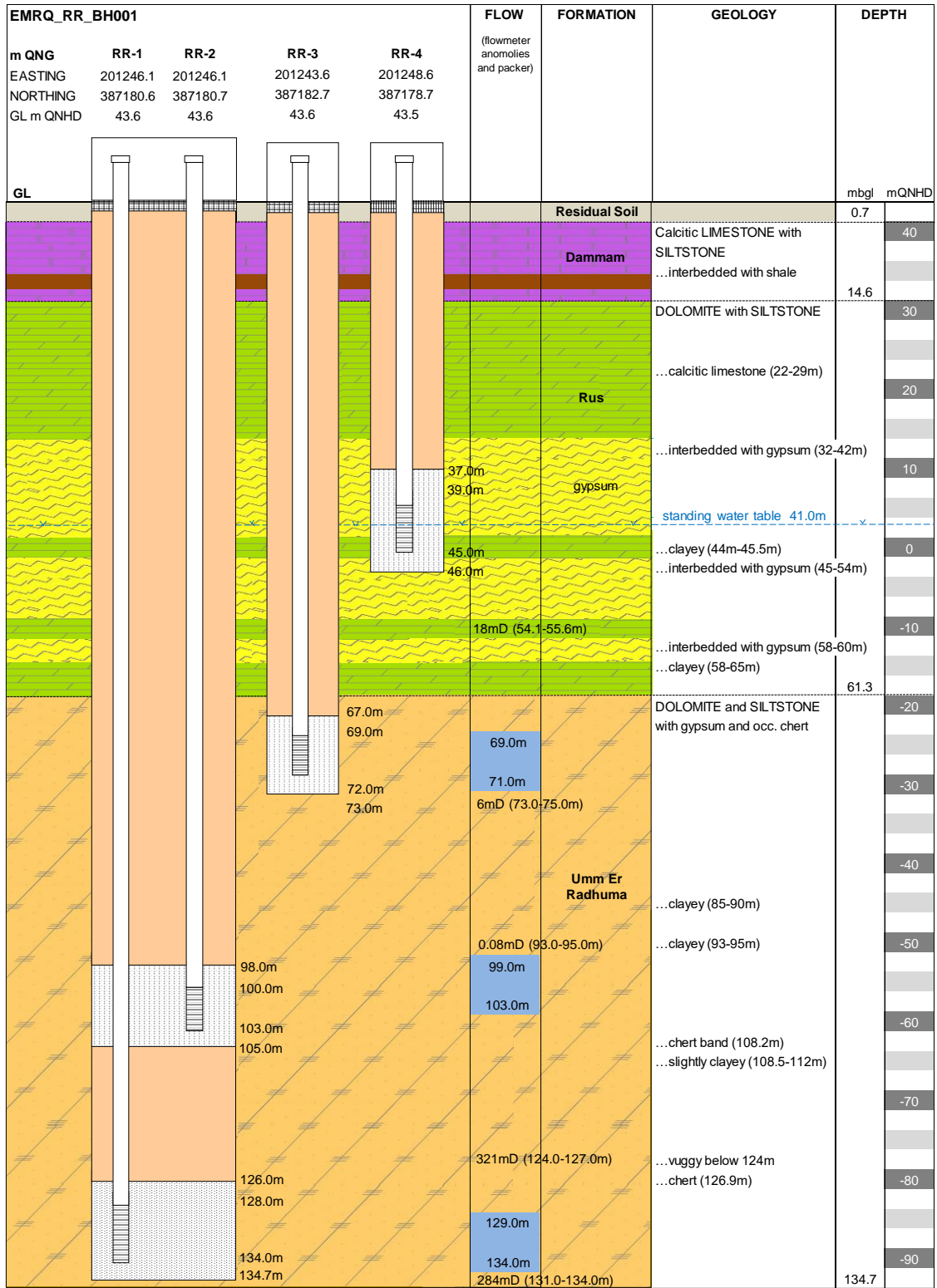


Figure 3-4 Central Wells (AS-1, AS-2) installations

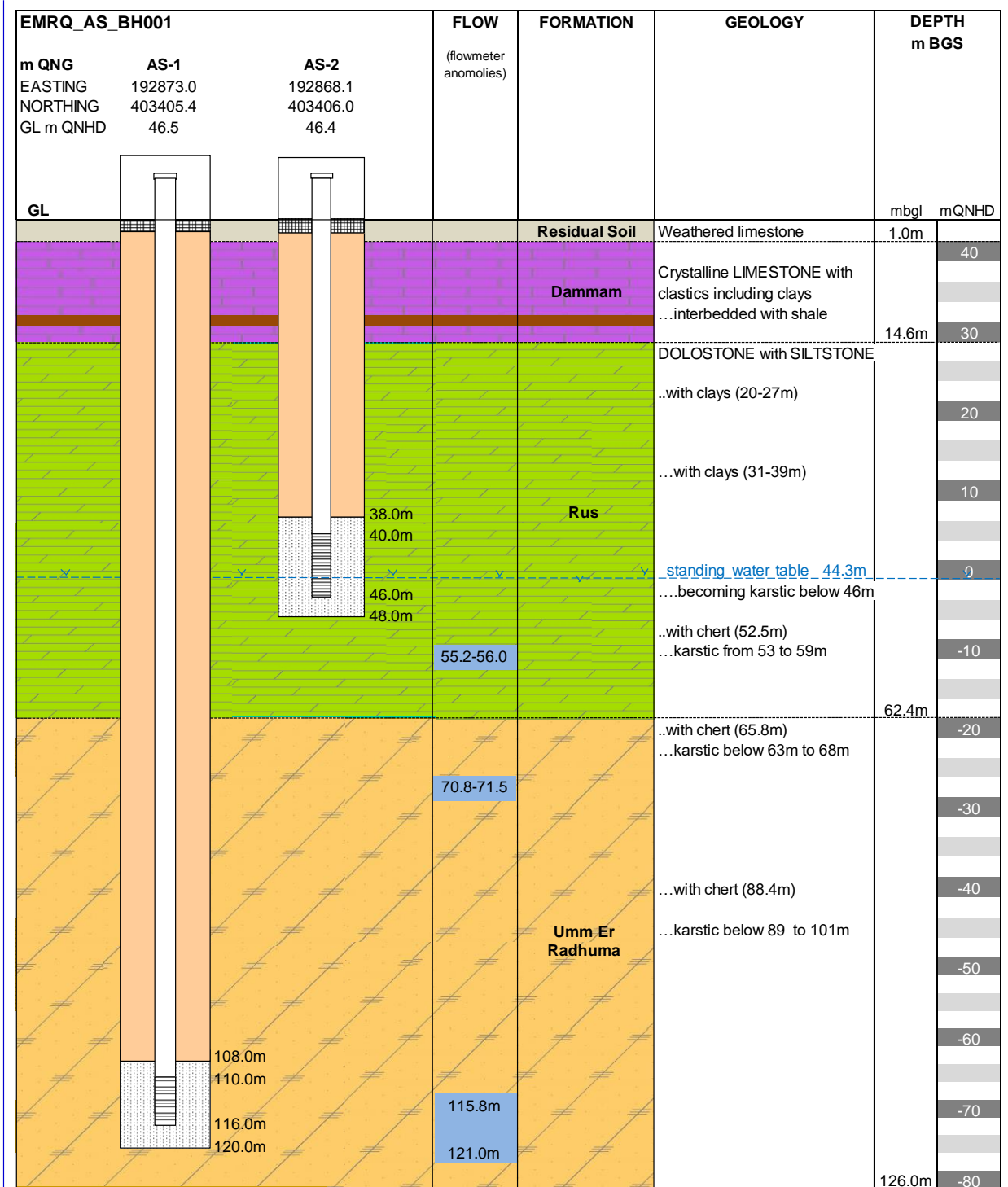


Figure 3-6 Northern (AG) well surrounds, site crew during drilling and geophysics down-the-hole temperature and EC probe attached to tripod winch



Specific details of the farm wells were not known, however these types of wells are typically cased with galvanized steel in the top 5m with the remaining borehole left open and uncased down to base depth, usually ~100m bgl. A 6" outlet submersible pump is placed between 60-80m bgl, at least 20m below the local area's static groundwater level. The northern farm provided water to both the local farm and surrounding area (by tanker) and the pump remained continuously on unless there was significant rainfall. The southern farm provided water to a nearby concrete tank which was kept full and fed the farm through a network of pipes as well as the occasional tanker. It was understood the pump was turned on for 12 hours a day only, seven days a week (Figure 3-7).

After completion of each installation and prior to sampling, each well was developed by purging five well volumes using a submersible pump or compressed air in combination with regular field tests of temperature, pH and EC to ensure the borehole was stabilised i.e. three

consecutive readings for each parameter are within 2%. The boreholes were then left to recover for at least a week prior to the first monitoring event.

Figure 3-7 Farm 2- RR in the south.

A: top of well covered by concrete plinth, with 6" black riser main (arrow) and pipe connecting the well to tank. B: the tank fed by the well (from black pipe), which then distributes water through the network using gravity. C & D: the network comprising black plastic 4" diameter irrigation pipes laid in square grid type formation (~5m x 5m), covered with dirt with an outlet for each square.



3.3 Packer (or Lugeon) Tests

Packer hydraulic conductivity tests were undertaken to understand the hydraulic properties of a rock mass, particularly in regard to the degree to which they are governed by discontinuities (BS EN ISO, 2012). Packer test were only performed in the southern (RR) at interval depths shown in Table 3-1. No packers were able to be undertaken in the northern and central boreholes due to the unstable and karstic nature of the bedrock as the

success of a packer test relies on sealing off the test section. Further details on methodology are found in Appendix A2.

Table 3-1 Southern well (RR) packer test depths

Borehole ID	Test Depth (m bgl)	Test Depth (m QNHDI)
EMRQ_RR_BH001	54.1 – 55.6	-10.5 to -12.0
EMRQ_RR_BH001	60.0 – 61.8	-16.4 to -18.4
EMRQ_RR_BH001	73.0 – 75.0	-29.4 to -31.4
EMRQ_RR_BH001	93.0 – 95.0	-49.4 to -51.4
EMRQ_RR_BH001	124.0 – 127.0	-80.4 to -83.4
EMRQ_RR_BH001	131.0 – 134.0	-87.4 to -90.4

3.4 Flow Meter Logging

Flow meter logging was undertaken by a geophysical specialist contractor in both the southern (RR) and central (AS) boreholes, to interpret the horizontal and vertical movement of groundwater within and between aquifers (Driscoll, 1986). Recording the movement of water in or out of a fracture or discontinuity, or ‘in’ and ‘out’ flow anomalies, in a borehole using an impeller flowmeter (FLOW) meter provides information about the differences in hydraulic head between two transmissive units, and the movement of water in/out of discontinuities (U.S. Department of Interior & U.S. Geological Survey, 2016).

During testing, the aquifers were ‘stressed’ by inducing a flow at the top of the borehole using a submersible pump abstracting groundwater at an average flow rate between 4 and 5.6 l s⁻¹. A continuous flow log of the impellor was lowered and raised at a constant logging speed (between 4 and 12.5 m s⁻¹) and recorded on a log which is found and discussed in Section 4.0. Flow anomalies were determined onsite by the geophysical specialist, with reference to Keys (1990) and U.S. Department of Interior/U.S. Geological Survey (2016).

3.5 Borehole Profiles including Temperature, pH and Conductivity Logging

Downhole field parameters temperature ($\pm 0.005^\circ\text{C}$), pH (± 0.001 pH) and conductivity (± 0.007 mS cm⁻¹) were profiled by a specialist geophysical contractor. The logs were obtained by lowering the sensors at a slow but constant rate (between 4 to 10 m s⁻¹) from the top of the water table to the base of the borehole. These profiles give an indication of salinity as well as an understanding of vertical flow caused by differences in effective head,

net product of pressure head, temperature, salt-controlled density and temperature (Driscoll, 1986).

An Ocean Seven 302 water quality probe (southern and central borehole) and YSI multiparameter (southern borehole) were deployed for the borehole profiles and results can be found in Section 4.0. Due to borehole instability, a borehole profile was unable to be completed in the northern well. Borehole profiles were done on the completion of drilling and well development.

3.6 Groundwater Monitoring and Sampling

Groundwater monitoring was undertaken in all wells at the three locations for over a year. Monitoring comprised regular manual measurement of piezometric heads and retrieval of groundwater samples for field and laboratory testing. Onsite measurements of temperature (± 0.5 °C), pH (± 0.01), conductivity EC (± 0.001 mS cm⁻¹), TDS (± 1 mg l⁻¹), dissolved oxygen (± 0.01 mg l⁻¹) and turbidity ($\pm 2\%$ repeatability of reading) where possible, were taken using a portable multiprobe (Aqua Read AP-800). The multiprobe was calibrated prior to use using a manufacturer's calibration solution, which simultaneously calibrated all parameters. Two agricultural wells of nearby farms, one in the north ~1km north-east from the cored borehole (AG-1) and ~2km due west from the southern cored borehole (RR-1), were also intermittently included as part of a monitoring event. Detailed methodology are found in Appendix A3 and the field results are found in Appendix B1.

Groundwater monitoring began on each of the wells after they have been drilled and developed and left to stabilise (at least a month), the first being the southern wells in mid February 2017. The last monitoring round for all boreholes and farms was in early October 2018.

Table 3-2 Borehole location, elevation, base depths, installations, formation and mineralogy details

Formal BH No.	Well ID	Easting (m QNG)	Northing (m QNG)	Ground Level Elevation (m QNHD)	Base Depths (m bgl)	Details	Response Zone (m bgl)	Slotted Zone (m bgl)	Response Zone Depth (m QNHD)	Formation	Mineralogy
EMRQ-AG-BH001 (northern)	AG-1	204618.949	456320.034	9.11	122.2	RC + SP	115 - 122	117 – 120	-109.4	UER	Calcite
	AG-2	204615.985	456326.217	9.08	43.0	SP	35 - 43	37 - 40	-29.4	Rus-Al Khor	Impure Dol.
	AG-3	204622.148	456313.561	9.12	14.0	SP	3 - 14	4 - 13	0.6	Dammam	Dolomite
EMRQ-AS-BH001 (central)	AS-1	192872.956	403405.382	46.50	126.0	RC + SP	108 - 120	110 - 116	-66.5	UER	Impure Dol.
	AS-2	192868.112	403406.033	46.44	46.0	SP	38 - 48	40 - 46	3.4	Rus - Traina	Dolomite
EMRQ-RR-BH001 (Southern)	RR-1	201246.066	387180.577	43.55	134.7	RC + two SP	126 - 134.7	128 - 134	-87.4	UER	Gypsum
	RR-2	201246.080	387180.653	43.55	105.0	As above	98 - 105	100 – 103	-57.9	UER	Dolomite
	RR-3	201243.608	387182.671	43.61	72.0	SP	67 - 73	69 – 72	-26.9	UER	Dolomite
	RR-4	201248.566	387178.719	43.50	46.0	SP	37 - 46	39 – 45	1.5	Rus - Traina	Dolomite
Farm 1 - AG		205329.200	456859.010	13	~100	Agricultural	5 – 100	~13*	~ -40	Rus / UER	Unknown
Farm 2 - RR		199220.680	387081.440	32	~100	Agricultural	5 - 100	~43*	~ -20	Rus / UER	Unknown

* approximate depth of submersible pump

RC – rotary core to take rock core sample

SP – groundwater monitoring standpipe

Impure dolomite (Impure Dol.) includes clastics and clays



Figure 3-8 Physical and geological logging, and the team

In total, and as shown in Table 3-3, groundwater monitoring included:

- Northern Wells (AG): 11 groundwater level measurements and 8 chemical analyses spanning 15 months
- Central Wells (AS): 4 groundwater level measurements and 4 chemical analyses over 7 months
- Southern Wells (RR): 14 groundwater level measurements and 11 chemical analyses over 19 months
- Two water samples (Farm 1 – AG) from a nearby farm well c. 900m NE of the northern wells, over a 6 month interval
- One water sample (Farm 2 – RR) from a nearby farm well c.2100m W of the southern well taken at the final monitoring event in October 2018.

3.7 Laboratory Testing

Laboratory analysis of water samples included pH, EC, TDS, a conservative tracer (Cl^-) and the major cation (Na^+), anticipated water-rock interaction elements (Ca^{2+} , Mg^{2+} , SO_4^{2-}), HCO_3^{-2} a derivative of alkalinity (as CaCO_3^-), major element (K^+) and minor element (SiO_2^{4+}), and trace elements (Al^{3+} and Fe^{3+}). The laboratory testing was initially undertaken by Gulf Laboratories Co. WLL in Qatar until the end of 2017, and then by ExxonMobil Research Laboratories Qatar for 2018. Two rounds of groundwater monitoring and subsequent laboratory testing from the central wells (AS-1 and 2) were undertaken by Fugro Peninsula Services Co. Qatar.

A list of laboratory tests, together with standards used and standards of testing including detection limits, are detailed in Appendix A4. The techniques used, which varied depending on the laboratory, are also listed in Appendix A4. Laboratory results from all monitoring events and from all laboratories are in Appendix B2.

3.8 Chemical modelling (PHREEQC)

Aqueous geochemistry is a relatively sensitive indicator of diagenesis as distinctive geochemical signatures can identify certain processes which are currently ongoing (Whitaker & Smart, 2007a), whereas rock core provides information about the environment since deposition. Mixing processes can be understood by calculating proportions of end-

members within a sample to assist in identifying the geochemical processes influencing groundwater chemistry (Pelizardi, 2017). Quantifying water–rock interaction by calculating ‘excess’ relative to concentrations predicated from mixing with proposed source or end-members, using Cl⁻ as a conservative tracer provides detail on the mineral controlled reactions and subsequent chemical evolution of the water along its flow path (Whitaker & Smart, 2007a) (Equation 10).

Excess relative to concentrations expected from simple dilution between possible end members local rainwater and local seawater or UER groundwater from the Saudi Arabia and local seawater were calculated for the carbonate water-rock elements Ca²⁺, Mg²⁺, SO₄²⁻ using Equation 1 from (Whitaker & Smart, 2007a) where, in the instance of Ca²⁺;

$$\text{Equation 10} \quad Ca_{XS} = Ca_{SAMPLE} - (Ca_{ENDMEMBER} \times Cl_{SAMPLE} / Cl_{ENDMEMBER})$$

Ca_{SAMPLE} is the molar concentration of Ca in the sample, and Ca_{ENDMEMBER} the molar concentration of the respective end-member, and Cl_{SAMPLE} and Cl_{ENDMEMBER} give the Cl molar concentration ratio of chloride in the sample to the end-member. Positive excess indicates dissolution whereas conversely negative excess values indicate precipitation has occurred.

The geochemical aqueous speciation model PHREEQC has been used to derive the activities and saturation indices of waters with respect to key evaporite and carbonate minerals, indicating the thermodynamic status of the solution including the potential of a forward reaction (mineral precipitation), equilibrium, and backward reaction (mineral dissolution) (Moore, 2010) and P_{CO2} of waters. In addition, the potential for water – rock interaction (Parkhurst, 2013) and the effect of mixing can further explain the various diagenetic processes which may have and continue to take place.

3.9 Logging

Two methods of logging were employed to describe the core. The first utilised the British Standard BS5930:2015 to describe physical attributes of the rock specifically geotechnical rock properties such as rock strength, colour, rock core quality including core sample length and percent recovery, and rock mass characteristics of weathering and discontinuities (Appendix A5). The physical rock logs for RR (southern) and AG (northern) boreholes were compiled by myself and are also found in Appendix C. The central well physical log was not available, as it was undertaken by a different drilling contractor.

Table 3-3 Timeline of dates for which measure of piezometric head (G), piezometric head and groundwater sampling (W) were undertaken at the various sites. * indicates water sample in absence of piezometric head measurement.

Groundwater Monitoring Summary																								
Borehole ID	Response Zone		16.02.17	22.02.17	26.03.17	02.05.17	07.06.17	26-27.07.17	10.08.17	28.08.17	31.10.17	18.01.18	31.01.18	18-19.02.18	03.03.18	14.03.18	22-23.04.18	26-27.05.18	06.06.18	08.07.18	12.08.18	19-20.09.18	07.10.18	
	From (m bgl)	To (m bgl)																						
RR Boreholes (Southern)																								
RR-4	42.0	45.0	G	W	G	W	W	W		W	W	W	W	W			W	W					G, O	
RR-3	70.0	72.0	G	W	G	W	W	W		W	W	W	W	W			W	W					G, O	
RR-2	100.0	102.0	G	W	G	W	W	W		W	W	W	W	W			W	W					G, O	
RR-1	130.0	133.0	G	W	G	W	W	W		W	W	W	W	W			W	W					G, O	
AS Boreholes (Central)																								
AS-2	40.0	46.0														W*			W*	W	W		G, O	
AS-1	110.0	116.0														W*			W*	W	W		G, O	
AG Boreholes (Northern)																								
AG-3	4.0	13.0						G	W	W	W	W	W	W	G		W	W					G, O	
AG-2	37.0	40.0						G	W	W	W	W	W	W	G		W	W					G, O	
AG-1	117.0	120.0						G	W	W	W	W	W	W	G		W	W					G, O	
Nearby Farms																								
Farm 1 -	5	100															W	W					G, O	
Farm 2 -	5	100																						W, O

G = depth to groundwater only
 W = depth to groundwater and sample taken
 O = sample taken for organic analyses
 * no depth to groundwater

A composite geological log was compiled by a team of four geologist, including myself, supervised by ExxonMobil’s senior geologist, which described the mineralogy and composition, depositional and diagenetic features at hand sample and microscopic scale by observing the lithology, texture using Dunham texture scale (1962), visible biota, petrography using thin sections to ascertain grain or crystal size, porosity and pore type, and integrating the attributes with mineralogy from XRD results (Appendix A5). Composite logs for all three cored boreholes using the geology logging methodology is found in Appendix D, as published in Rivers et al., 2019a.

4.0 AQUIFER PROPERTIES AND GROUNDWATER FLOW

4.1 Introduction

Permeability characteristics of Qatar's bedrock can be established by observing lithology and groundwater physical properties of flow, temperature, salinity and scale-dependency, and are discussed in this chapter. The scope of the analyses is the top 135m bgl and limited to the immediate vicinity of the project wells. Therefore, only the Upper UER, Rus and Dammam has been assessed and any reference to the UER in subsequent chapters and discussion of this report implies to the upper UER only.

4.2 Location

Based on inspection and logging of the rock core using the methodology as described in Section 3.0, four hydrostratigraphic units were defined for the three shallow aquifers. From deep to shallow these were: 1) Paleocene Upper Um Er Radhuma (UER) dolomitised shallow-marine deposits formed in relatively restricted conditions overlying fining-upward cycles of open marine deposits with clay rich caps (lower aquifer) (Ryan et al., 2018), 2) crystalline gypsum/anhydrite Rus Evaporite deposited in a marginal marine environment (aquiclude – absent in the north of the country), 3) Early Eocene Rus Formation, a shallow marine deposit comprising impure dolomite and clay (middle aquifer) and 4) crystalline calcite and dolomite of the Middle Eocene Dammam Formation considered by Rivers et al., (2019a) to be deposited in an open marine environment (upper aquifer).

The following geological descriptions were based on personal logging of the cores, as part of the larger ExxonMobil project. On occasion, core recovery was reduced particularly in karstic zones which comprised incompetent bedrock. These sections were noted on the composite logs (Appendix D) that form part of a published paper which I co-authored, Rivers et al., (2019a).

4.2.1 UER

The UER formation from all three cores typically comprised fossil-obliterative dolomite. The UER was characterized by cycles of light brown dolomitic packstones and mud-lean packstones fining up to a darker dolomitic wackestone with occasional dolomite mudstone caps, often in association with palygorskite clay (Rivers et al., 2019a). All three boreholes terminated within this sequence; therefore the basal extent of these successions and the base depth of the UER was not proven. The full UER formation is proven to be up to 370m

thick, (Eccleston et al., 1981) extending to an estimated depth of 450m bgl (Shamrukh et al., 2012).

Figure 4-1 Umm Er Radhuma rock core samples in the southern well (RR)

A: Typical vuggy UER, RR at -81.5 to -82.5mQNHD (125.10m to 126.10m bgl). B: Siliceous band, RR at -64.4mQNHD (grey circle at 108.20m bgl). C: Gypsum nodule RR between -47.0 to -47.2m QNHD (90.60 to 90.75m bgl).

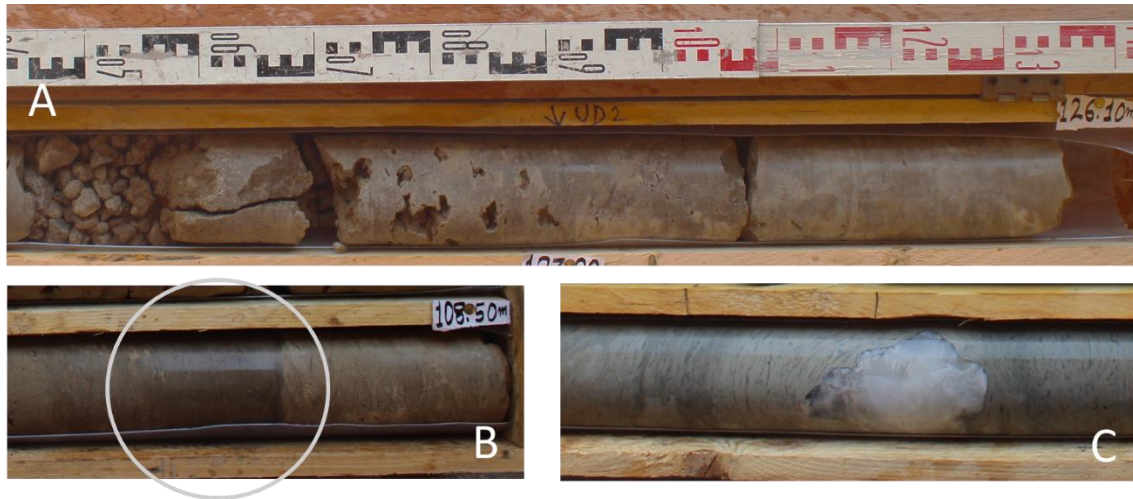
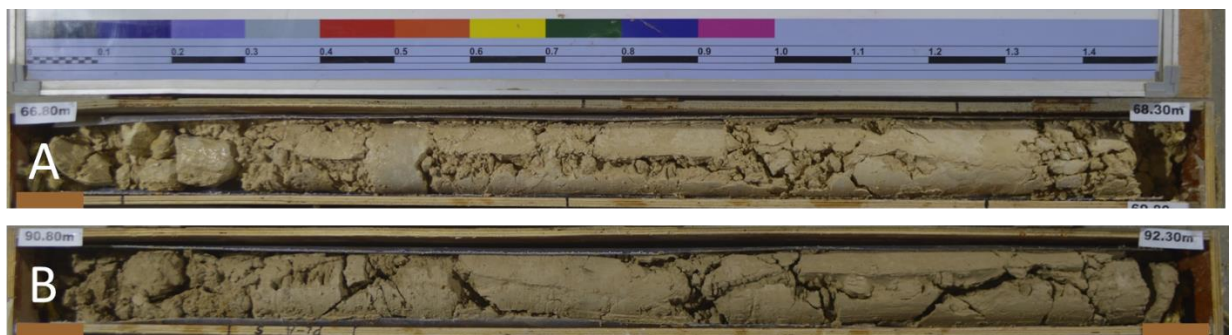


Figure 4-2 Umm Er Radhuma rock core samples in the central well (AS)

A: Subvertical discontinuity within karstic sediments, AS from -20.3 to -21.8mQNHD (66.8 to 68.3m bgl). B: Karstic dolomitic clays, silts and sands, AS from -44.3 to -45.1mQNHD (90.8 to 91.6m bgl).



Gypsum, in the form of large nodules >102mm diameter, was recorded in the top 30m of the UER in the southern borehole only. These nodules are considered to have developed in-situ prior to lithification, due to the deformed nature of the sediment surrounding them (Figure 4-1C)

A notably lighter in colour off-white dolomite was recorded at the very top ~10m of the UER in all three cores. In the south, this sequence was often laminated, fining from a packstone at the base to a wackestone, with an abundance of various sized replacive (or displacive) gypsum nodules (Rivers et al., 2019a). A similar lighter coloured packstone was recorded in the central and northern boreholes, but no gypsum was noted and the central borehole graded upward into a finer wackestone and mudstone.

Chert nodules or siliceous bands, often larger than the diameter of the core (>102mm), were present near the top of the UER in all three cores. In the southern well (RR), a 0.15m thick siliceous band was recorded at -83.3m QNHD (126.9m bgl) and again at -64.6m QNHD (108.2m bgl), in the central (AS) borehole a large nodule of chert >102mm at -41.9m QNHD (88.4m bgl), -19.3m QNHD (65.8m bgl) and -6.0m QNHD (52.5m bgl), and in the northern (AG) chert nodules >102mm were noted at -62.3m QNHD (71.4m bgl) and -62.9m QNHD (72.0m bgl) (Figure 4-1B). Isotopic evidence indicates that the cherts were formed in meteoric waters where the “continuous chert horizon was precipitated in association with the paleo-water table, and this occurred prior to dolomitization of UER” (Rivers et al., 2019a).

Small amounts of calcite (<1.02%) were present within the upper UER, as coarse crystalline calcite or calcite cement in the central borehole -32.5m to -42.5m QNHD (79.0m to 89.0m bgl), and as intermittent crystalline beds in the north from -51.9m to -61.4m QNHD (61.0m to 70.5m bgl). No calcite was recorded within the UER in the southern borehole. These diagenetic calcites are commonly associated with chert cements, and formed during meteoric exposure (Rivers et al., 2019a).

Vugs were recorded in the sequences, below -61.5m QNHD (105.0m bgl) in the UER of southern (RR) borehole, below -69.0m QNHD (115.5m bgl) in the UER of the central borehole (AS) and below -88.4m QNHD (97.6m bgl) in the UER of the northern borehole (AG) (Figure 4-1A). Vugs were intermittent and larger in the southern borehole (~5 up to ~60mm diameter) and rarely connected, becoming much smaller (2 to ~10mm diameter), infrequent and not connected in the central and northern boreholes.

In the central and northern boreholes, multiple karst intervals from 0.2m to ~13m thick and comprising a fine to coarse sometimes laminated sediment of dolomitic sand, silt and clays were recorded in the dolomitic mud-lean packstone bedrock. Karsts in the central borehole (AS) were between -54.5 to -16.5m QNHD (~101.0 to ~63.0m bgl) and similar karstic sediments in the northern well (AG) between -64.9 to -82.1m QNHD (~74.0 to 91.2m bgl).

These karst features are considered the result of in-situ karstification as the mineralogy was nearly 100% dolomite, with rare calcite and clastics. In some sections, sub-vertical to near-vertical fractures were noted in the sediments which match the adjacent core. No karst features were recorded in the southern borehole despite the occurrence of larger vugs.

The depositional environment of UER was considered to be a fluctuating shallow open inner-to-mid ramp, where a distinctive brecciated dolostone, sometimes fractured and overlain by an erosional surface, defined the contact between the UER and overlying Rus (Rivers et al., 2019a).

4.2.2 Rus

The base of the Rus Formation overlies the UER in the southern, central and northern boreholes at -17.7m -15.9m and -41.9m QNHD (61.3m , 62.4 and 51.0m bgl), respectively. The contact between the UER and Rus was marked in the southern borehole by a 30m thickness of interbedded gypsum/anhydrite, fine grained dolomite and green palygorskite clays, referred to as the Rus Evaporite (Rivers et al., 2019a) (Figure 4-3A and 3B). This was interpreted as the result of deposition in a shallow water salina setting (Rivers et al., 2019a).

The evaporite is part of the larger Traina Member, (refer Section 2.0) logged in the central and northern boreholes as a notable off-white or very light brown dolomite grading from packstone to wackestone, with more clay content in the north and dominated by intact mudstone in the central borehole. No significant thicknesses of gypsum or anhydrite were recorded in the Traina Member in the northern or central boreholes. Karstic features were recorded in the central borehole (AS) from 0.5 to -12.5m QNHD (~46.0 to ~59.0m bgl) and were not observed in the Rus in the north or south.

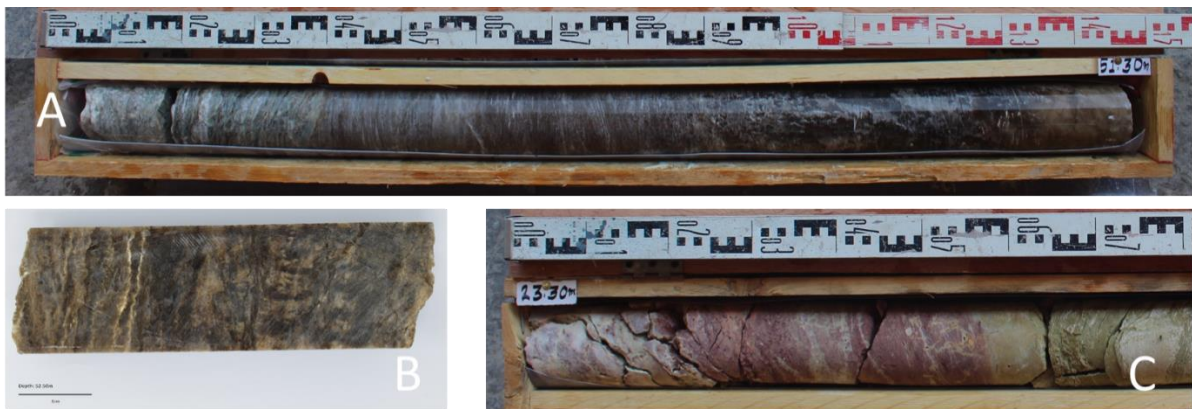
Calcite crystals and rare disseminated chert are commonly associated in the central borehole in the Traina Member and are interpreted to be related to meteoric exposure.

Overlying the Traina Member is an offwhite dolomitic mudstone, dominated by red (illite rich) and green (palygorskite) clays with intermittent crystalline limestone beds. These clay-rich soft dolostones make up the Al Khor Member, and are considered the result of deposition within a protected lagoon and mud-flat environment (River et al., 2019). In places, the Al Khor mudstones included thin beds of carbonate wackestone and some packstones with distinctive microcodium textures indicating former exposure surfaces with developed soil profiles (River et al., 2019a).

The top of the Rus Formation was defined at 29.0m, 31.9m and 0.5m QNHD (14.6mbgl, 14.6m and 8.6m) in the southern, central and northern boreholes respectively (Appendix D) due to unconformity features such as brecciation, erosion, recrystallization and cementation (Rivers et al., 2019a).

Figure 4-3 Rock core samples from the Rus in the southern wells

A: Gypsum and anhydrite in the Rus Traina Member, RR at -6.2m to -7.7m QNHD (49.8m to 51.3mbgl). B: Gypsum in Rus Traina Member with very thinly laminated terrestrial clays, RR at -8.9m QNHD (RR at 52.5mbgl). C: Clays of the Rus Al Khor Member, RR from 20.3m to 19.5m QNHD (23.3 to 24.1mbgl).



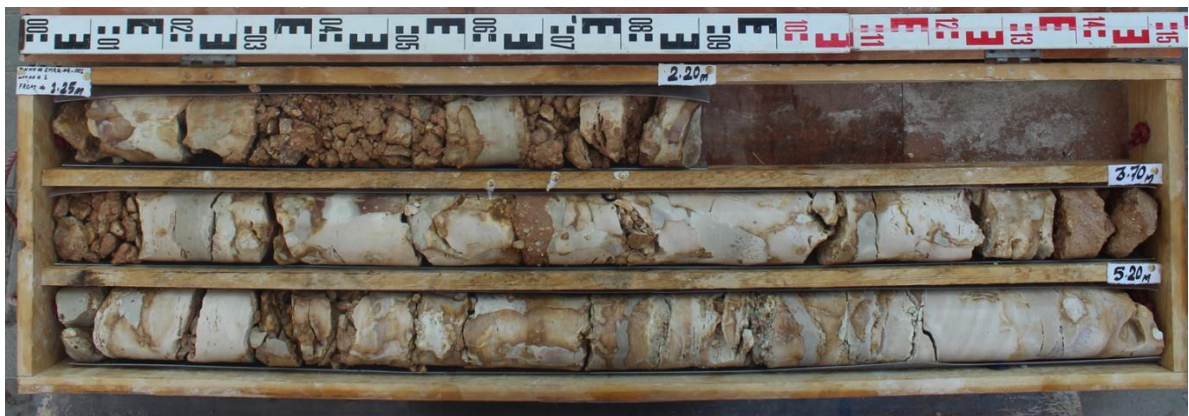
4.2.3 Dammam

The Dammam Formation was recorded in all three cores. At the base was thin (<1m) layer of fossiliferous limestone from the Fhailil Velates Member, however this member was only identified in the southern borehole at the contact with the Rus. Fossils previously identified within the member include nummulites and molluscs *Velates cf. schmiedli* (Abu-Zeid & Boukhary, 1984), plus small and large benthic foraminifera and bivalves (Rivers et al., 2019b)

The distinctive Midra Shale, a brown and white mottled carbonate primarily wackstone thinly interbedded with brown mudstone, was recorded at the base of the Dammam in the central core, and overlying the Fhailil Member in the south. A second fossiliferous limestone, the Alveolina Member, distinguishable by the abundance of *Alveolina elliptica nummulites* (Abu-Zeid & Boukhary, 1984), sat disconformably on the Midra Shale in the southern and central cores, and was <1m thick. Both the Midra Shale and Alveolina were absent in the northern borehole.

The Umm Bab Member was the thickest member of the Dammam recorded in the boreholes, and typically comprised recrystalline limestone, packstones grading in places to wackestone, with dolomitized intervals (<1m to ~4m) in the central and northern cores (Figure 4-4). Abundant large benthic foraminifera were visible in thin section, reflecting a depositional environment of open marine to mid-ramp with lower energy. Red, brown, green and white palygorskite clays dominated the matrix between the brecciated dolostone or limestone and infilled vugs.

Figure 4-4 Umm Bab Member from the Dammam Formation, AG from 7.85m to 3.9m QNHD (1.25m to 5.2mbgl).



4.3 Hydraulic Head Analysis

As outlined in Section 3.0, monitoring of the hydraulic head was undertaken at all three well locations with a number of piezometers, and results of the elevation of groundwater are shown in Figure 4-8. Groundwater elevations and samples were also undertaken at two nearby farms (Farm 1 AG in the north, and Farm 2 RR in the south). Historical well data has also been included in the analysis to provide perspective and understand trends within the data. Locations of the wells, including two historic wells (P22a and P27 from Eccleston et al., 1981) are shown in Figure 4-5. From the start of monitoring in mid-February 2017 until the last monitoring event in September 2018, the southern wells show only a subdued (<0.3 m) winter rise in groundwater levels, irrespective of depth. Head in the Rus aquifer is lower than in the underlying UER, indicating the UER is a confined aquifer with potential for upward flow.

Figure 4-5 Location of wells and monitoring points for piezometric head analyses (Google Earth, 2019)



The 6m unexplained anomaly in groundwater head in Pipe 3, compared to the pipes 1 and 3 which are within the same UER aquifer, continued. This difference could be due to the fine nature of the cyclical clayey caps and large gypsum nodules in the top 30m of the UER in the southern borehole, which may retard the natural upward movement of groundwater. Other possibilities are nearby abstractions associated with farms, domestic use or construction, often where the latter is illegal. The well itself may be faulty, however during construction it was fully developed under supervision. The base of the well has been

repeatedly tagged to prove its depth, and the depth to groundwater has been consistent for the duration of monitoring.

The central well (AS) was the last well to be drilled and has been monitored over a couple of months only. Monitoring took place during the summer months, when there has been no rain, and therefore the head remained constant. The hydrostatic head for both the UER and Rus formations are similar to the southern UER wells, and ~1.5m above the northern well head.

In the north, groundwater head had remained constant from installation in July 2017, but rose c.0.7 m in all aquifers in January-February, 2018. Although rainfall was recorded during this time, it was in the form of intermittent light showers and therefore could not have contributed to such distinct and equal rises in hydraulic head of all three aquifers. The northern wells are surrounded by farms which abstract large volumes of groundwater for irrigation. The nearest irrigation well is 700m north east of the boreholes and there are many other large farms with pumps within 1.5km radius of the wells. We visited the farms and noted that their pumps had been switched off when it rained. Samples were taken from the nearest pumping well for field testing and laboratory analysis.

Comparisons were made between recent monitoring undertaken as part of this project and historical groundwater levels and conductivity values reported in Eccleston et al., (1980) (Figure 4-6). All the groundwaters considered classified fresh to brackish, therefore hydrostatic differences caused by densities were considered insignificant. Both groundwater levels and conductivity values were estimated from country-wide piezometric head and salinity maps. Groundwater readings were in meters above sea level, and conductivity was converted from TDS (ppm) salinity plots into EC mS cm^{-1} using conversion of values from USGS (Hem, 1985). For convenience, piezometric head of the agricultural wells at the farms monitored during this project were estimated as 0.00m QNHD.

Figure 4-6 Depth to groundwater (m QNHD) and SEC (mS cm^{-1}) with time

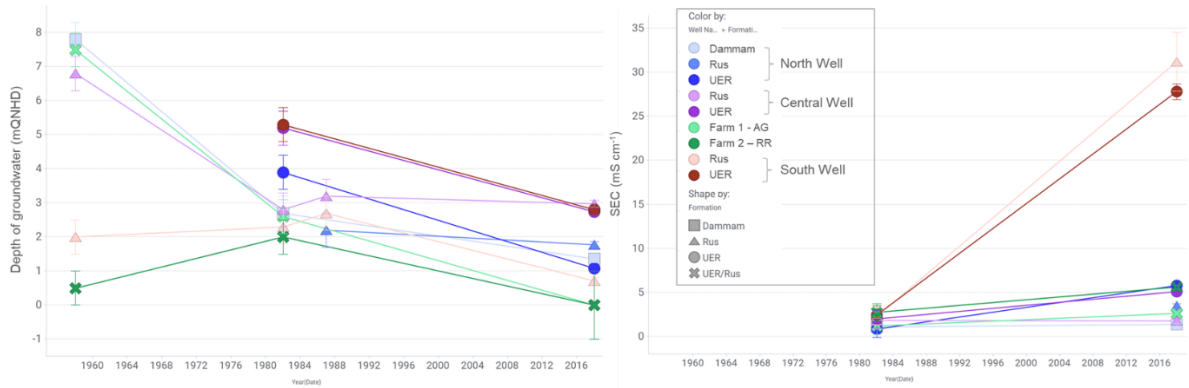
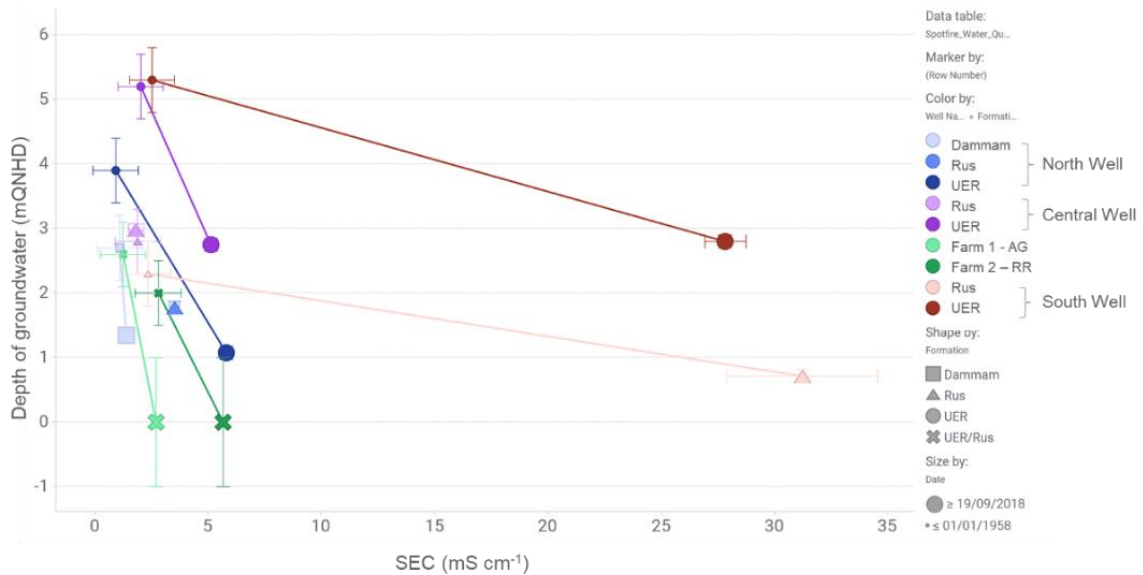


Figure 4-7 From 1982 to present day, Salinity (SEC mS cm^{-1}) with depth to groundwater (m QNHD)



From 1958 until the present, the Dammam aquifer in the north has seen a decrease in piezometric head (-6.5m) with a small increase in salinity ($+0.3\text{mS cm}^{-1}$) from 1982 (Figure 4-7). Records for the Rus and UER are not as comprehensive. Records from 1982 indicate the Rus has also experienced a drop in piezometric head (-0.4m) and the underlying UER (-2.8m) with increase in salinity ($+4.9\text{mS cm}^{-1}$).

In the central area, the Rus has decreased in piezometric head (-3.8m) and salinity remained about the same. The UER aquifer head has decreased (-2.5m) and salinity increased ($+3.1\text{mS cm}^{-1}$).

In the south, both the Rus and UER aquifers have decreased in piezometric head (-1.3m and -2.5m respectively), with a significant increase in salinity ($+28.9$ and $+25.3 \text{mS cm}^{-1}$).

The nearby farms both recorded decreases in hydrostatic head and increases in salinity over time.

Piezometric head gradients were calculated between aquifers at each location and for each aquifer between the locations (Figure 4-10). In the south (RR), the flow is upward in both the UER and Rus aquifers, however the gradient is steeper within the Rus as would be expected as its an aquitard. The central wells flow downwards as the aquifers are in hydraulic continuity.

The northern wells record a downward flow from Rus to UER, while there is noticeable upward flow from Rus to Dammam. This is unexpected, as all three aquifers are in hydraulic continuity, and lithology suggests that meteoric recharge in combination with irrigation recharge should produce a downward flow. This upward flow from the Rus into the Dammam indicates that more water is being removed from the system than is being recharged, and is most likely due to excessive abstraction by the surrounding farms and domestic residences.

Lateral flow is calculated to the north (-ve) as expected, from the central (AS) wells to the northern (AG) wells, and central and northern coastlines. A southerly lateral flow was calculated from the central (AS) wells to the southern (RR) wells, however this unlikely. A single reference point in each aquifer was used to calculate the gradient. The apparent gradient (+0.0789) between the wells in the UER aquifer represents a 0.13m vertical difference over 20km, and therefore considered negligible. In addition, the central UER well piezometer head reading plots on the gradient line of the UER southern wells (RR) (Figure 4-10). The Rus aquifer in the south is confined and could explain the unexpected southerly flow between central and southern Rus aquifers.

Figure 4-8 Groundwater head (manual dips) in southern (RR), central (AS) and northern (AG) set of wells from manual dipping

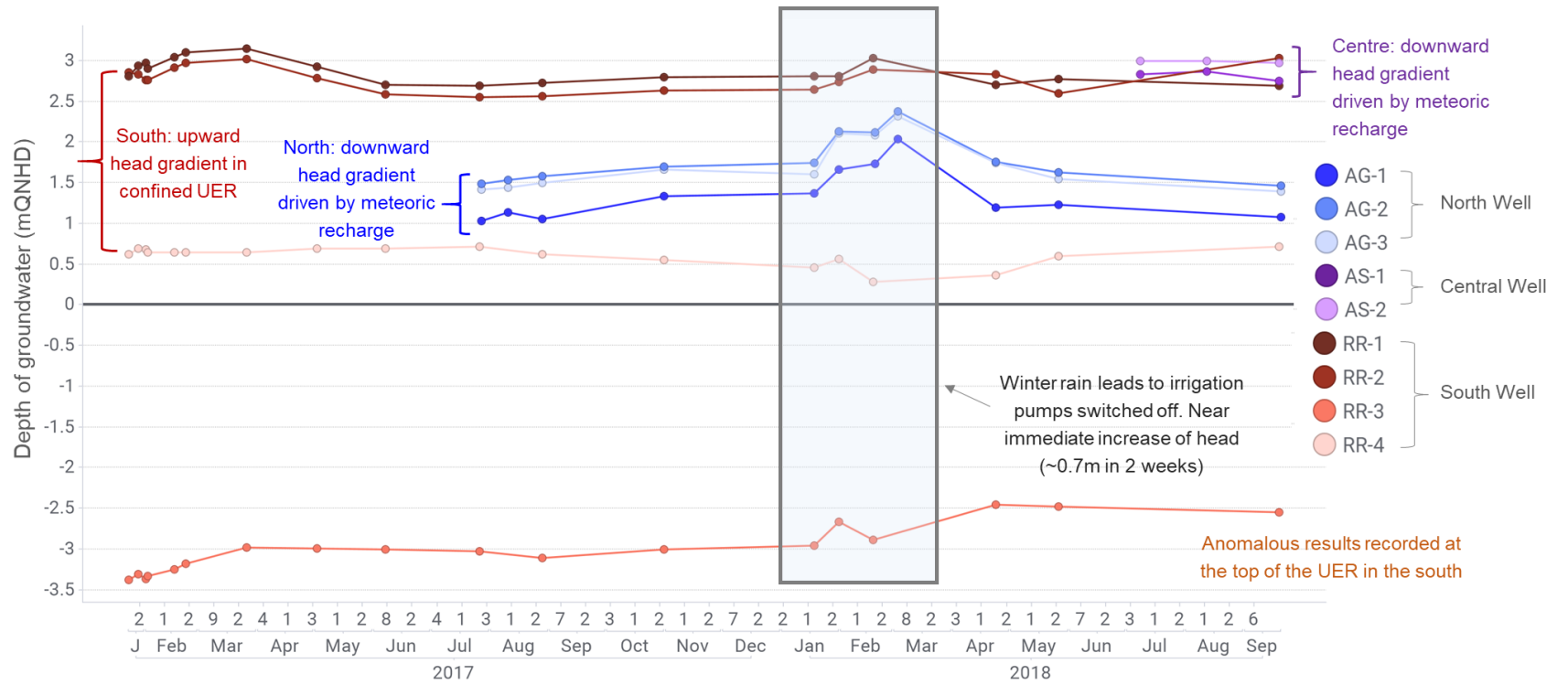


Figure 4-9 Mean northern, central and southern piezometric head with depth (m QNHD)

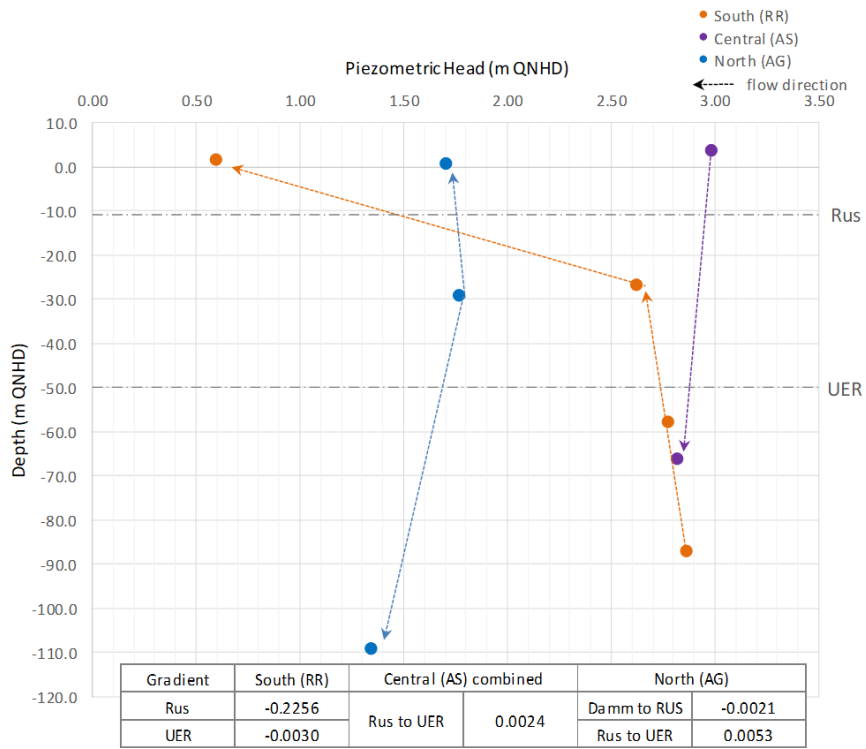
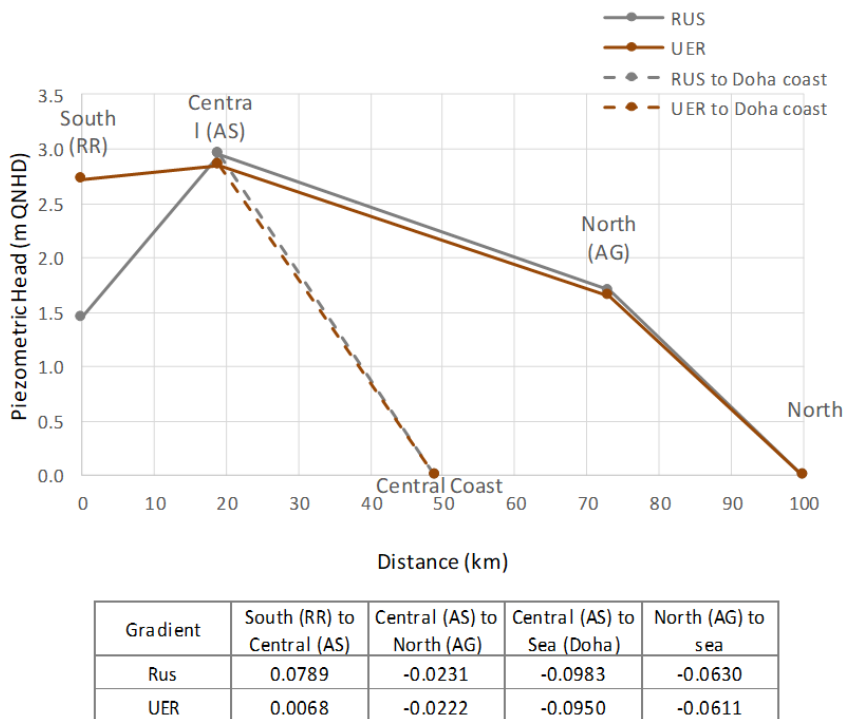


Figure 4-10 Piezometric head (m QNHD) from north to south including Doha coast



4.4 Packer hydraulic conductivity (K) results

Hydraulic conductivities of the packer tests undertaken in the southern borehole (RR) (Table 4- 1) show conductivities range over four orders of magnitude. These results could reflect the significant difference in conductivity associated with the UER, as intergranular permeability is low and secondary porosity dominates (Sharaf, 2001). However, it could indicate a deficiency in the test type, as packer testing at depth is often difficult to stabilise below 60m.

Table 4- 1 Southern well (EMRQ_RR_BH001) packer permeability results

EMRQ_RR_BH001	Test Depth (m bgl)	Test Depth (m QNHDI)	Packer Permeability - Using Hamm et al. (2007) approach m/sec	Packer Permeability - Using Hamm et al. (2007) approach D
Rus	54.1 – 55.6	-10.5 to -12.0	1.73E-07	1.79E-02
Rus/UER	60.0 – 61.8	-16.4 to -18.4	4.76E-07	49.52E-02
UER	73.0 – 75.0	-29.4 to -31.4	6.01E-08	6.26E-03
UER	93.0 – 95.0	-49.4 to -51.4	7.35E-10	7.65E-05
UER	124.0 – 127.0	-80.4 to -83.4	3.08E-06	3.21E-01
UER	131.0 – 134.0	-87.4 to -90.4	2.73E-06	2.84E-01

4.5 Borehole Profiles

Permeability characteristics of the three aquifers were further examined using results from in-situ borehole profiles and fluid logs undertaken in the southern (RR) and central (AS) boreholes during site works. Borehole profiles comprised temperature ($\pm 0.005^{\circ}\text{C}$), pH (± 0.001 pH) and conductivity (± 0.007 mS/cm) measurements. Historical borehole profiles Figure 4-12 Well P22a (Eccleston et al., 1981) and salinity maps (Annexure v, Figure 10.11 from Eccleston et al., 1981) provide further insight into the nature and distribution of temperature and salinity in the shallow aquifers.

4.5.1 Temperature

Borehole temperature profiles (thermal gradients) can provide information on groundwater movement through a borehole to better understand permeability, the depth of intervals that “produce or accept water”, relative hydraulic head and response to seasonal recharge (USGS, 1990). The temperature gradient of groundwater in a borehole is reflective of climate which determines the temperature at the water table, and the geothermal heat flux combined with the resulting heat transport by conduction and/or advection (Domenico & Schwartz, 1999). The depth of the water table to ground level influences near-surface water

temperatures. However the water table temperature will approximate mean annual temperature unless the vadose zone is very thin or recharge is sufficiently rapid that it transports relatively warmer or colder water to the water table. The transport of heat from deeper formations depends on the thermal conductivity of the aquifer rock and its porosity, as well as any vertical flow from differences in hydrostatic head, water quality such as density from vertical contrasts in solute concentration, and/or differential temperatures between aquifers (Driscoll, 1986). Temperature logs can be used to determine lithological changes (USGS, 1990).

For groundwater in thermal equilibrium with the rock, temperatures within a borehole will typically reflect the geothermal gradient unless vertical movement by either head differences or differences in temperatures and density between discrete aquifers leading to circulation, tending to reduce the thermal gradient. Development of an open hole by drilling allows vertical flow, that maybe be driven by difference in hydrostatic head, by differences in temperature between aquifers, and by density. Rapid vertical flow eliminates the natural thermal gradient resulting in near-isothermal fluids between two connected more permeable intervals. Flow direction can be determined from the perturbation of temperature or conductivity (Driscoll, 1986).

The temperature profile of RR was measured three times, initially by the drilling subcontractor (Gulf Labs) four days after completion of drilling and prior to well development, and twice by the University of Bristol following well development. Analyses was undertaken on the final 'downward' profile as the well have been developed and had sufficient time to equilibrate as it had not disturbed.

Using the final 'down' profile (dated 11.12.18), the temperature gradient increased linearly with depth, with three distinguishable 'zones' (A to C) (Figure 4-11). Zone A extended from the water table down 18m in the groundwater column, from approximately +2.6m to -15.0m QNHD (40.9m to 58.5mbgl) at a gradient of 0.5 C°/10m. Temperature increased rapidly with depth, with the gradient reducing to 0.24 C°/10m in Zone B from -17.5 m to -40.0m QNHD (61.1m to 83.5m blg), to a near vertical gradient of 0.04C°/10m in Zone C below -45.0m QNHD (88.5mbgl) to the base of the borehole.

The gradient is steeper in Zone A at the top of the water column in the southern well (RR), which relates to the Rus evaporite. Evaporites limit flow due to low permeability, and therefore heat transfer is by conduction. Multiple temperature runs were undertaken, the earliest most likely reflecting the cooler introduced water which was used as drilling flush.

Temperature increased by 1° in 6 days (28.11.16) and by a further 0.2°C in the following 13 days and therefore the temperature gradient cannot just be the result of conduction. There must also be warmer water moving upwards, which is supported by EC, ambient and fluid flow logs.

Evaporites are thermal insulators as they have reduced porosity and therefore poor conductivity. Dolomite has low open pore porosity and therefore high effective thermal conductivity (avg. 4.68 Wm⁻¹ K⁻¹) relative to limestone (avg. 2.91 Wm⁻¹ K⁻¹) and gypsum (avg. 1.98 Wm⁻¹ K⁻¹) (Di Sipio et al., 2014).

The top 70m of the water column in the central (AS) well, from 3.4m down to -70m QNHD (43.1m to 116.5m bgl), exhibits a linear relationship of steadily increasing temperature with depth at a gradient of 0.17C°/10m. This is more reflective of typical geothermal gradients and conduction (Domenico & Schwartz, 1999). Below -70.0m QNHD (116.5mbgl), temperature drops immediately by half a degree and could be related to the near base of the borehole, however it could be reflective of other factors. At -70.5m QNHD (117mbgl) the calliper log indicates an increase in borehole diameter implying a fracture, which aligns with the temperature increase. The ambient flow log also significantly increases with ingress into the well (up to 2 l/min) at the same depth. However, as these deflections are also recorded near the base of the borehole.

A difference in temperature of 3.3 to 4.9°C was noted between the southern (RR) and central (AS) wells, with the southern well (RR) being warmer than the central well (Figure 4-11). It is typical for groundwater at the water table to be reflective of the mean annual temperature (28.7°C), although the vadose zones in both wells are greater than 40m. Therefore, the difference in temperature between the wells and the groundwater table temperature warmer is the south must be due to other factors.

It is likely that the warmer temperatures found in the south are related to the confined nature of the aquifers, which restricts mixing so that groundwater temperature are more likely to reflect the thermal conditions of the rock. Cooler temperatures in the central well indicate influence from cooler meteoric waters. The southern well temperature profile displays a minor deflection at the formation boundary between the Rus and UER, whereas the central well does not display any notable deflection or anomaly between formations, or at the formation boundaries themselves. Typical geothermal gradients show a temperature increase of between 0.47°C and 0.6°C for every 30.5m depth (USGS, 1990). Gradients in

the southern well do not exhibit this trend, probably because it is a confined aquifer which would have long established geothermal equilibrium.

Comparing temperature gradients with historic borehole profiles from Eccleston et al., (1980), Well P22a located approximately 23km inland from the coast in the centre of the country and 24km east of the central well (AS) exhibited temperatures ranging from 29°C and 30°C (Figure 4-12), with a linear increase in temperature with depth. A small deflection (reduction) in temperature was noted at the boundary of the Rus and UER at -28 (60mbgl) and a second deflection (also reduction) was noted at -53m QNHD (85mbgl), coinciding with a slight decrease in conductivity. Below -78.0m QNHD (110mbgl), approximately 15m above the sudden increase in salinity (conductivity), the temperature gradient decreased and can be considered to represent the base of fresh water into more saline waters.

Differential temperature within the wells can be attributed to rock type, which is influenced by mineralogy, density or salinity in conjunction with meteoric influence.

4.5.2 Conductivity

Chemical equilibrium can only be established over time when formation fluid and fluid in the borehole mix (USGS, 1990). Therefore, due to vertical or other flow, fluid-conductivity logs may not be representative of interstitial fluids in the formation itself (USGS, 1990). They can, however, provide information on seawater encroachment, as well as groundwater flow and recharge (USGS, 1990).

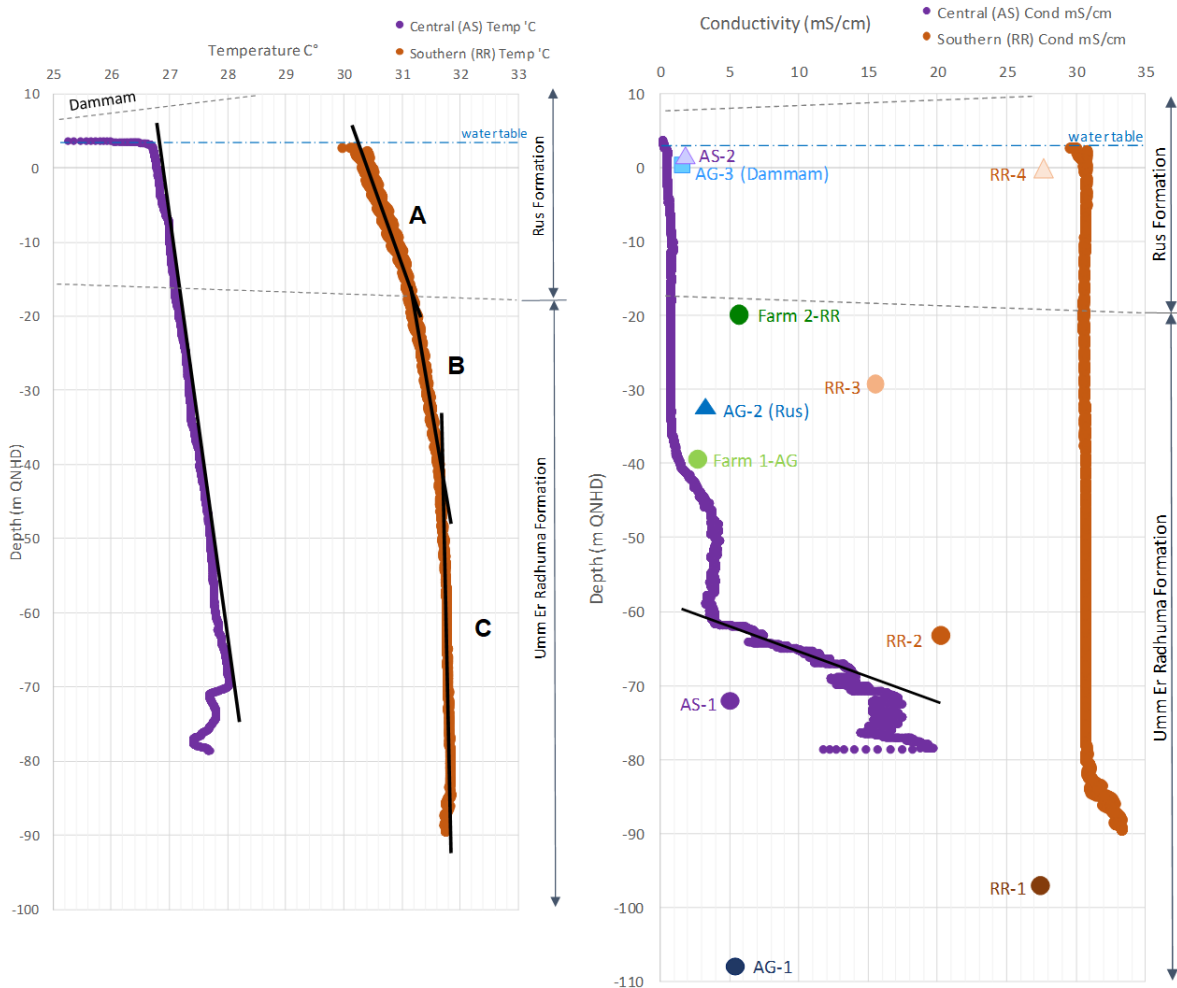
Three conductivity runs were undertaken on the southern (RR) well, and the final upward profile was considered the most reflective of real time conditions as the well had been developed and given time to equilibrate.

The southern (RR) well displayed high conductivity values of between 30.6 to 30.8mS/cm, with a shallow gradient in the top 80m of the water column, from the standing water table down to -78.5m QNHD (122.0mbgl). Below this depth -78.5m QNHD (122.0mbgl), conductivity rapidly increased with a steeper gradient of 2.9mS/cm/10m before reaching the highest value of 33.3 mS/cm at the base of the well -90.0m QNHD (133.1mbgl).

In the central borehole (AS), three 'zones' of different conductivity were noted in the profile. Conductivity of 1mS/cm was recorded from the top of the water table down to -35.5m QNHD (from 46.5 to 82mbgl) with a shallow gradient. At -38.0m QNHD (84.5m bgl) conductivity stepped up to ~4.1mS/cm and stabilised for the next 15m. This increase in SEC is at similar depths to karstified materials (dolomitic sands and clays) identified during logging. Below -

61.5m QNHD (108.0mbgl), conductivity rapidly increased with a gradient of 13.6 mS/cm/10m, increasing to a maximum conductivity of 17.6mS/cm at -72.2m QNHD (118.7mbgl). In the lowest six meters at the base of the well, below -72.2m QNHD (118.7mbgl), conductivity oscillated between 14.7 and 17.5mS/cm before peaking at 19.8mS/cm near the very base of the well at -78.6m QNHD (125mbgl).

Figure 4-11 Southern (RR) and Central (AS) wells borehole profile for temperature and conductivity SEC (mS cm⁻¹). Individual results are the average SEC (mS cm⁻¹) during field monitoring.

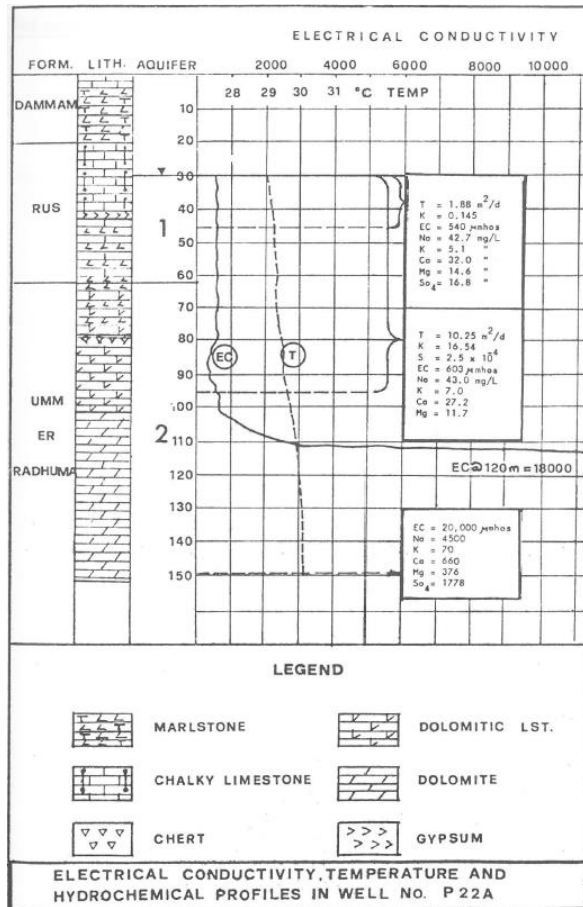


The historical conductivity profile of Well P22a in Eccleston et al., (1980) (Figure 4-12) recorded EC values of ~0.6mS/cm from the top of the water table extending down to -75m QNHD (109.8mbgl). Between -75.0m and -82.2m QNHD (109.8m and 117.0mbgl) was an increase in conductivity from 0.7mS/cm up to 3mS/cm followed by a marked increase to <18mS/cm below -82.2m QNHD (117.0mbgl), indicating the mixing zone and its base.

Another historic nearby well P27, situated closer to the coast and ~ 20km south west of the northern well (AG), recorded EC rising from 3mS/cm to 7mS/cm at -69m QNHD and up to 9 mS/cm at -96m QNHD (114m.0mbgl), representing the top and lower part of the mixing zone, respectively (Eccleston et al., 1981).

In all the wells, including the historic wells, EC remained relatively constant with a shallow gradient from the top of the water table to between 40m to 80m below the water table, at -38.0m QNHD (84.5mbgl) in the central (AS) well and -78.5m (122.0mbgl) in the southern well. At these depths, the central well EC increase represents the base of either the freshwater or brackish/semi saline lens, followed by a steady increase into moderately saline waters. A marked increase at -61.5m QNHD (108.0mbgl) indicates the top of highly saline waters. In the southern well, SEC values were already very highly saline and appears to be further increasing with depth. The freshwater / brackish lens decreases in thickness closer to the coast, whereas the mixing zone increases in thickness and becomes more diffuse (Eccleston et al., 1981).

Figure 4-12 Well P22a (Eccleston et al., 1981)



4.5.3 Flow

Impellor flow logs were recorded for the southern and central boreholes using methodology found in Section 3.0. In the southern (RR) well, flow logging was undertaken under 'stressed' (pumped) conditions, whereas in the central (AS) well, a log was taken both in ambient (non-pumped) and stressed (pump) conditions. A summary of the recorded flow anomalies are presented in Table 4-2. No flow log was available for the southern (RR) well.

Over the four runs (two up and two down), the southern (RR) well recorded flow 'anomalies' at the similar depths -25.4 to -27.4m QNHD (69 to 71mbgl), -55.4 to -59.4m QNHD (99 to 103mbgl) and at the base of the well below -85.4m QNHD (129mbgl). In the central well, flow rates were quantified including whether the flow was coming into, or out of the well. Flow was recorded flowing out of the well from the water table 2.5m QNHD (44.0m bgl) down to -9.5m QNHD (56.0mbgl), which is the approximate base of the Rus Formation. Flow then is into the borehole and a few anomalies ie reverse of the impellor, are local noted at depths shown in Table 4- 2 and possibly relate to karstic materials and minor fractures. At the base where the largest ingress of groundwater into the well was recorded, is a large fracture as recorded on the calliper log. Although it is near the base of the borehole, the ingress extends for over 10m, there was a distinctive drop in temperature and therefore most likely the result of a fractures.

Table 4- 2 Flow summary

Flow										
South (RR)										
Run 1	mbgl	m QNHD	Flow	Comment	mbgl	m QNHD	Flow	Comment		
	Impellor down					Impellor down				
	69 - 71	-25.4 to -27.4	flow anomaly		66 - 69	-22.4 to -25.4		impellor stopped		
	99-103	-55.4 to -59.4	flow anomaly	impellor stopped	99-103	-55.4 to -59.4		impellor stopped		
	129 - 133	-85.4 to -89.4	flow anomaly		129-133	-85.4 to -89.4	flow anomaly			
Run 2	Impellor down				Impellor up					
	69 - 74	-25.4 to -30.4	flow anomaly	impellor stopped	68 - 70	- 24.4 to -26.4	low flow anomaly			
	84-86	-40.4 to -42.4	low flow anomaly		92	-48.4	localised anomaly			
	93	-49.4		impellor stopped	97	-53.4	flow anomaly	impellor stopped		
	129-133	-85.4 to -89.4	flow anomaly		109 - 113	-65.4 to - 69.4	low flow anomaly			
	* impellor stopped usually due to suspended materials				129-133	-85.4 to -89.4	flow anomaly			
Central (AS)										
Run 1	mbgl	m QNHD	Flow	Comment						
	71 - 72	-24.5 to -25.5	flow anomaly	reverse of impellor						
	87 - 90	-40.5 to -43.5	minor anomaly	reverse of impellor						
	98 - 100	-51.5 to -53.5	flow anomaly	reverse of impellor						
	104 - 116	-87.5 to -69.5	increasing flow rate							
	118-121	-71.5 to -74.5	major flow anomaly							

Flow anomalies also coincide with increasing core porosity and permeability recorded on composite borehole logs in Rivers et al. (2019a) however it is unlikely that the impellers sensitivity could reflect these microscopic characteristics. In the central borehole (AS),

where laboratory porosity and permeabilities were unable to be determined most likely due to the fine material within the karstic zones, the flow anomalies often coincided at the similar depths to the karstic zones and minor fractures.

4.6 Scale-dependence of permeability characteristics of Qatar bedrock

Defining a representative elementary volume (REV) to adequately reflect the aquifers heterogeneity is important as permeability is the most significant control factor for subsurface flow. However, difficulties arose in statistically and spatially defining a REV for aquifers with significant secondary porosity and permeability (Whitaker & Smart, 2000).

Flow properties from a range of scales of observation for all three near-surface aquifers were combined from various sources to determine scale dependency. The sources included measurements of Klinkenberg permeability (D) and helium porosity from core plugs (34mm diameter x 50mm) subsampled from rock core retrieved during the drilling of the three (southern, central and northern) boreholes (Rivers et al., 2019a). Hydraulic conductivities (m/d) were established from a combination of site works and literature values. Packer tests were undertaken as part of this master's project in the RR (southern) borehole (refer Section 3). Slug and pumping tests were undertaken during a previous Bristol University master's project at various locations around the Qatar (Simmonds, 2014). Published data from the pumping tests provided a range in conductivities from each of the shallow aquifers (Al Bassam et al., 1997, Eccleston et al., 1981, Sharaf, 2001).

For convenience, results provided in hydraulic conductivity (m/d) were converted to effective permeability (k in Darcy) assuming the density and viscosity of seawater and are detailed in Appendix A6. A summary of the number of results per test type, the range of effective permeabilities (D) and formation type in which the test was undertaken, is found in Table 4-3 and full results in Appendix B3.

Core plug permeabilities (D) ranged over six orders of magnitude (10^{-6} to 10^0 D), and also encompassed all six packer results, ranging over five orders of magnitude. As expected, estimates from larger scale tests are generally higher, with a similar range of values for slug tests (10^{-2} – 10^{+2} D) and pump tests (10^{-2} – 10^{+3} D), and most tests recorded permeabilities 10^0 D and greater.

Table 4- 3 Range of effective permeability (D)

Formation		Core plug	Packer	Slug	Pump
Total	(n)	317	6	33	36
	median	0.03	0.03	43.28	7.76
	outliers	36	0	3	6
	min (D)	2.00E-06	8.00E-05	6.08E-02	1.53E-02
	max (D)	7.42E+00	3.21E-01	5.41E+02	1.62E+03
Dammam	(n)	40		32	9
	min (D)	1.00E-05		8.81E-01	2.56E-01
	max (D)	1.54E-01		5.41E+02	3.89E+01
Rus	(n)	112	2	1	15
	min (D)	2.00E-06	1.80E-02	6.08E-02	1.53E-02
	max (D)	2.24E+00	3.21E-01		8.10E+01
UER	(n)	165	4		12
	min (D)	1.00E-05	8.00E-05		4.50E+00
	max (D)	7.42E+00	3.21E-01		1.62E+03

After plotting permeabilities (D) against frequency for the three formations (dataset n = 392), seven modes of distribution (A-G) were identified, which were found to be log-normally distributed (Figure 4-13). The centers of distribution for the four lower permeability modes A (10^{-6} D - 10^{-4} D), B (10^{-3} D), C (10^{-2} D) and center D (10^{-1} D) were derived primarily from core and packer tests. Those for mode E (10^0 D) are a combination of core, slug and pump test data, whilst F and G (10^1 D and 10^2 D, respectively) are from the slug and pump test data, with two outliers $>10^3$ D from pump tests. The modes are apparent from the cumulative frequency chart shown in Figure 4-14.

Figure 4-13 Permeability (D) vs frequency for all test types (n=392)

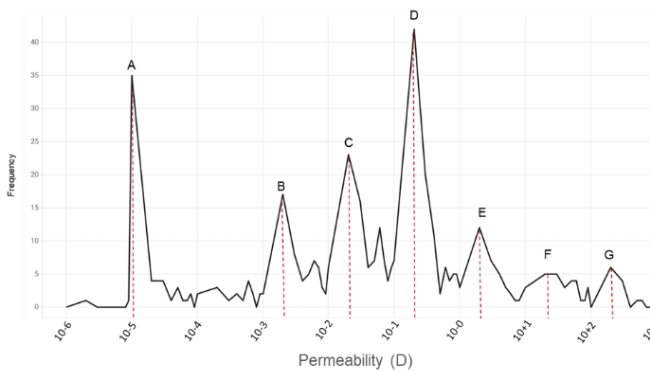
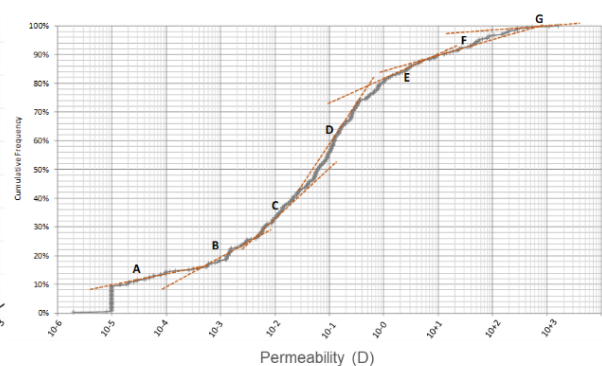


Figure 4-14 Permeability (D) vs cumulative frequency for all test types (n=392)



The most abundant permeability is peak D ($D 10^{-1}$) from core test data plus one packer and one pump test result. The magnitude of this peak can be attributed to the high number of core plug tests used in the analyses ($n=317$) relative to the number of results available from other test types (slug $n = 33$, pump = 36 and packer = 6). The range of permeabilities (D) relative to the type of test are shown in Figure 4-15. Permeabilities vary for the different formations and mineralogy, as shown in Figure 4-16, Figure 4-18 and the associated box plots Figure 4-17.

Figure 4-15 Permeability (D) and frequency with each test type (n=392)

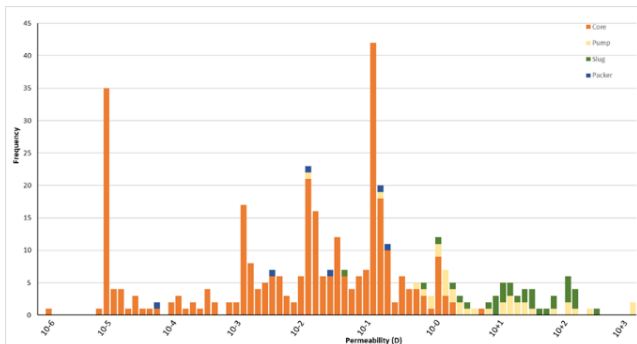


Figure 4-16 Permeability to formation (n=392)

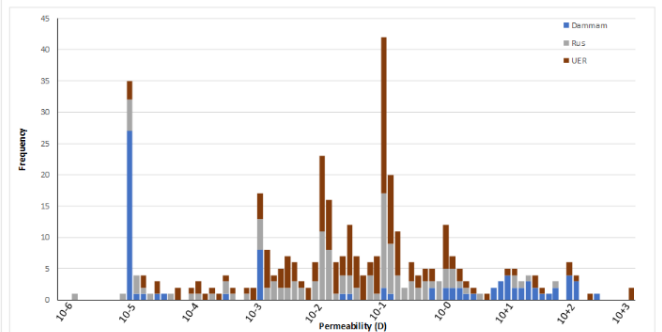
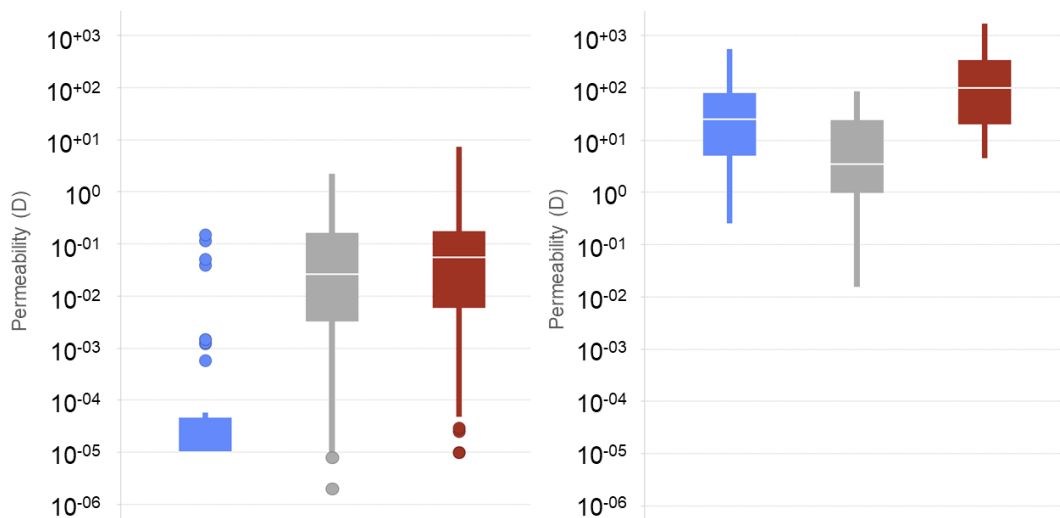


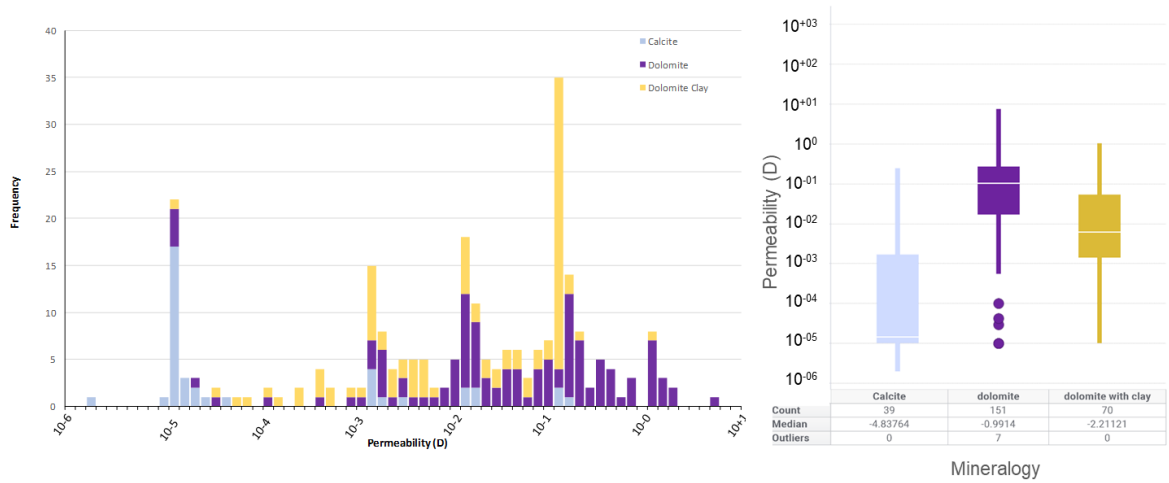
Figure 4-17 Boxplots of permeabilities (D) for each formation, split as core and packer results (n=323), and slug and pump test results (n=69)



Core & Packer	Dammam	Rus	UER
Count	40	114	169
Median	1.0×10^{-5}	0.03	0.06
Outliers	9	2	5

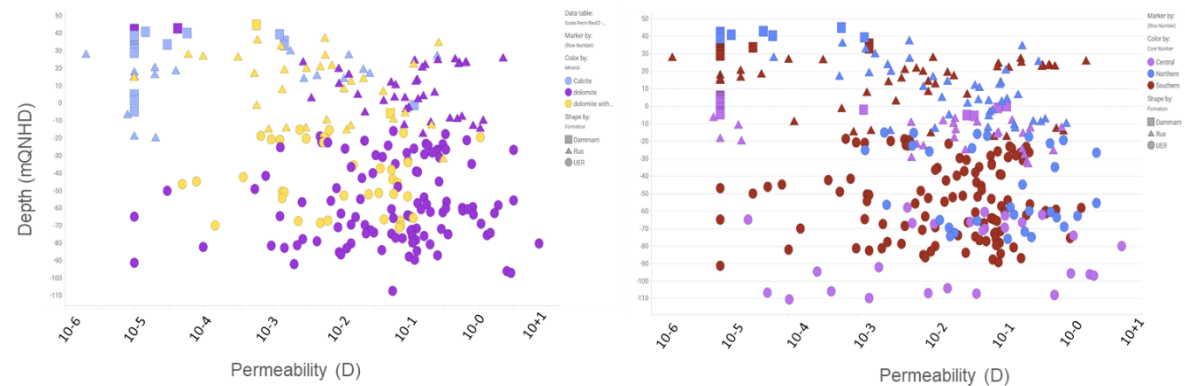
Slug & Pump	Dammam	Rus	UER
Count	41	16	12
Median	25.25	3.34	106.48
Outliers	0	0	0

Figure 4-18 Permeability and boxplot relative to mineralogy (core only, n=254)



Permeability with depth, by formation and mineralogy is shown in Figure 4-19. The Dammam Formation is noticeably less permeable than the underlying Rus and UER Formations and is most likely related to mineralogy (Figure 4-19). The UER displays the greatest range of permeabilities (1×10^{-5} to 1.72×10^3 D), as well as the highest absolute values. Therefore, geological formations are scale dependent although no specific REV can be assigned to a formation.

Figure 4-19 Permeability (D) with depth (m QNHd) by Formation (core only, n=317) and by mineralogy (core only, n=254)



Analyses of porosity ($\emptyset(\text{He})$ (%)) on core plugs in the laboratory (Rivers et al., 2019a), were initially classified by frequency with respect to frequency (Figure 4- 20), depth (Figure 4- 21) formation and mineralogy (Figure 4-22). Similar to conclusions drawn with regards to pore permeability, porosity decreases in the Dammam as it contains crystalline calcite. Both the Rus and UER have a wide spread of porosity results, as does dolomite and dolomite clays.

Figure 4- 20 Porosity (%) with frequency and cumulative frequency (core only, n=317)

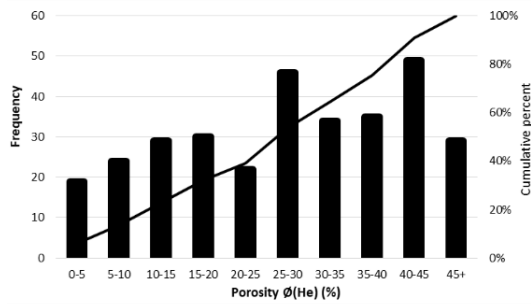


Figure 4- 21 Porosity (%) with depth (core only, n=317)

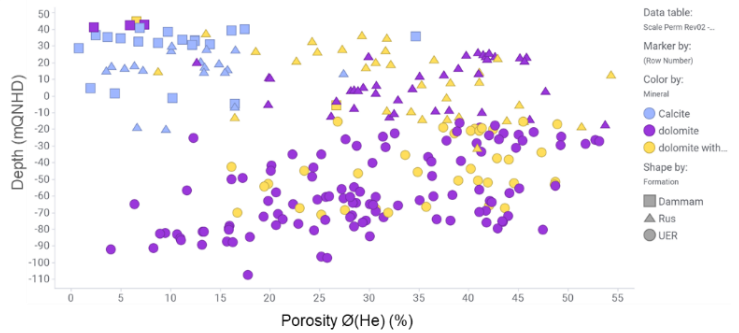
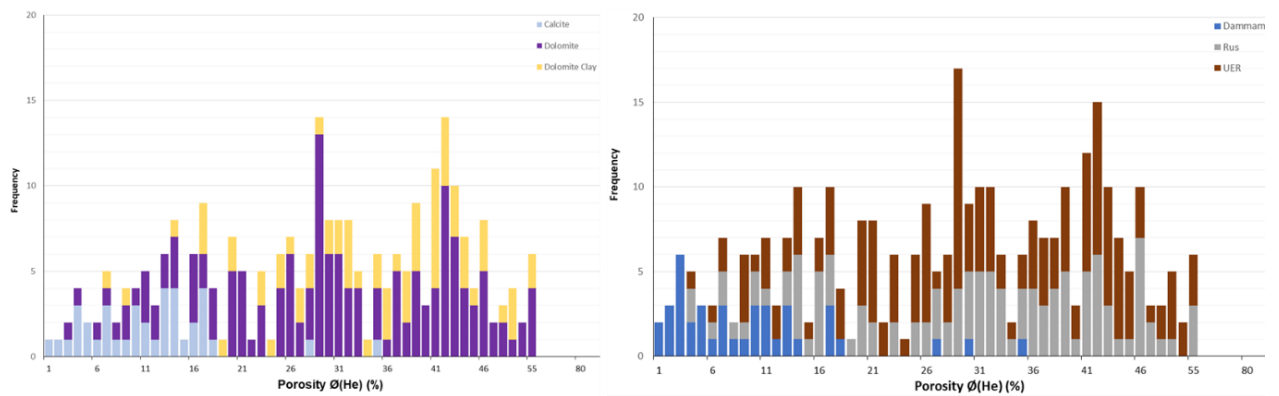
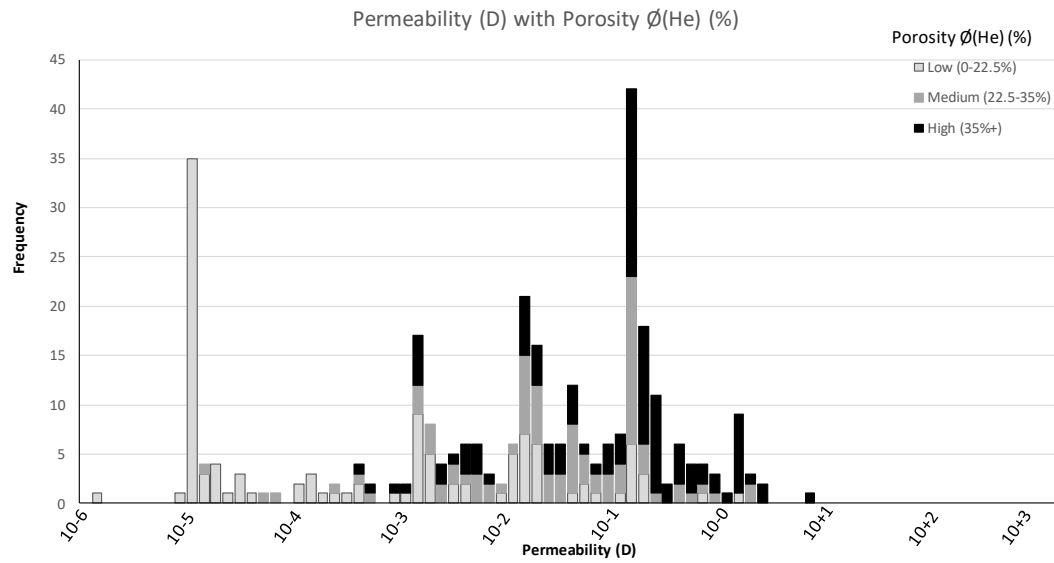


Figure 4-22 Porosity with formation (core only, n=318) and mineralogy (core only, n= 260)



Porosity frequency results were further grouped into low (0-22.5%), medium (22.5-35%) and high (35%+) porosity, and compared with permeability (Figure 4-23). As expected, higher porosities related to permeabilities (D) $>10^{-3}$ up to 10^{+1} . This highlights the dependence of scale, as no porosity has been recorded for permeabilities above (D) 10^{+1} . Therefore, the fifty plus permeability results above (D) 10^{+1} have not been captured in laboratory core analyses and must therefore relate to secondary permeability of fractures, discontinuities, vugs and karsts.

Figure 4-23 Permeability with porosity (n=317)



5.0 GROUNDWATER CHEMISTRY

5.1 Introduction

5.1.1 Geochemistry background

Groundwater chemistry is widely used for understanding the geological impact of groundwater flows, providing insight into water-rock interactions and to distinguish distinctive geochemical signatures associated with diagenesis (Baalousha 2016c, Whitaker et al., 2014, and Whitaker & Smart, 2007a and b, Plummer et al., 1976). Water-rock reactions can be understood by calculating the contribution of rock-derived solutes, differentiated from those derived from conservative mixing of waters (Stoessell, 1992) providing insight into regional groundwater geochemical processes (Whitaker & Smart, 2007a). Combining concentration of rock-derived solutes with groundwater flux can be used to derive estimated reaction rates and distribution (Whitaker & Smart, 2007b).

The geochemistry of groundwaters sampled in the wells varies both laterally and vertically, governed by factors including host rock mineralogy (Section 2.9), flow patterns (Section 4.3), and local and/or regional water-rock interactions, as groundwater tends to evolve chemically towards the composition of seawater (Alsharhan et al., 2001). This chapter intends to define and understand the dominant processes controlling groundwater by integrating prior data with recent groundwater monitoring results.

Groundwater from all wells and two farms were tested regularly, with samples retrieved during a monitoring event, establishing background levels and any allowing identification of any local, regional, or seasonal variations. Field and laboratory testing were undertaken as documented in Methods – Section 3.0. Field results are in Appendix B1 and laboratory results are given in millimoles per liter (mmol l^{-1}) and found in Appendix B2.

Water-rock interactions have been investigated using the chemical data processing techniques, which included observations of solute concentrations relative to mixing of hypothesized end members (or solute sources) and subsequent ratio analyses, referred to as excess (x_s) (Ooi, 2018, Pelizardi et al., 2017, Moore et al., 2009, Whitaker & Smart, 2007a), computation of mineral and CO_2 saturation indices (SI) to understand the mineral phases that dissolve or precipitate to reach chemical equilibrium within the aqueous phase (USGS, 2013), and activity phase diagrams (Moore et al., 2010).

Unravelling diagenesis using end members is often difficult due to the continual interaction of groundwaters with mineral surfaces and gasses, variations in residence time (Pelizardi et al., 2017), and flow regimes associated with karstic subsurface environments (Moore et al., 2010). Based on the hydrogeological and lithological understandings established in Chapter 2, and piezometric head and salinity concentrations from Chapter 4, in addition to chemical analyses detailed within this chapter, the wells have been separated into two groups with respect to suitable end members.

All of the southern wells (RR-1, 2, 3 and 4) plus the UER aquifer wells in the central (AS-1) and north (AG-1) and the southern farm (Farm 2 – RR) are primarily influenced by groundwater flow within the UER from Saudi Arabia and horizontal and some upward flow in Qatar. The central Rus (AS-2), upper northern wells (AG-2, 3) and northern Farm (Farm 1 – AG) have been proven to be primarily influenced by meteoric recharge. Both the UER and meteoric waters eventually discharge to the Gulf of Arabia (Eccleston et al., 1981) and experience a varying degree of mixing with seawater, depending on depth and flow patterns. Local seawater has been used as an end member for all wells (Table 5- 1) (Eccleston et al., 1981, Eccleston, B.L., Harhash, 1982, Lloyd et al., 1987)(Figure 5-1). The mixing line is distinguished on the graphs as brown for UER Saudi groundwater to seawater, whereas rainwater to seawater is blue.

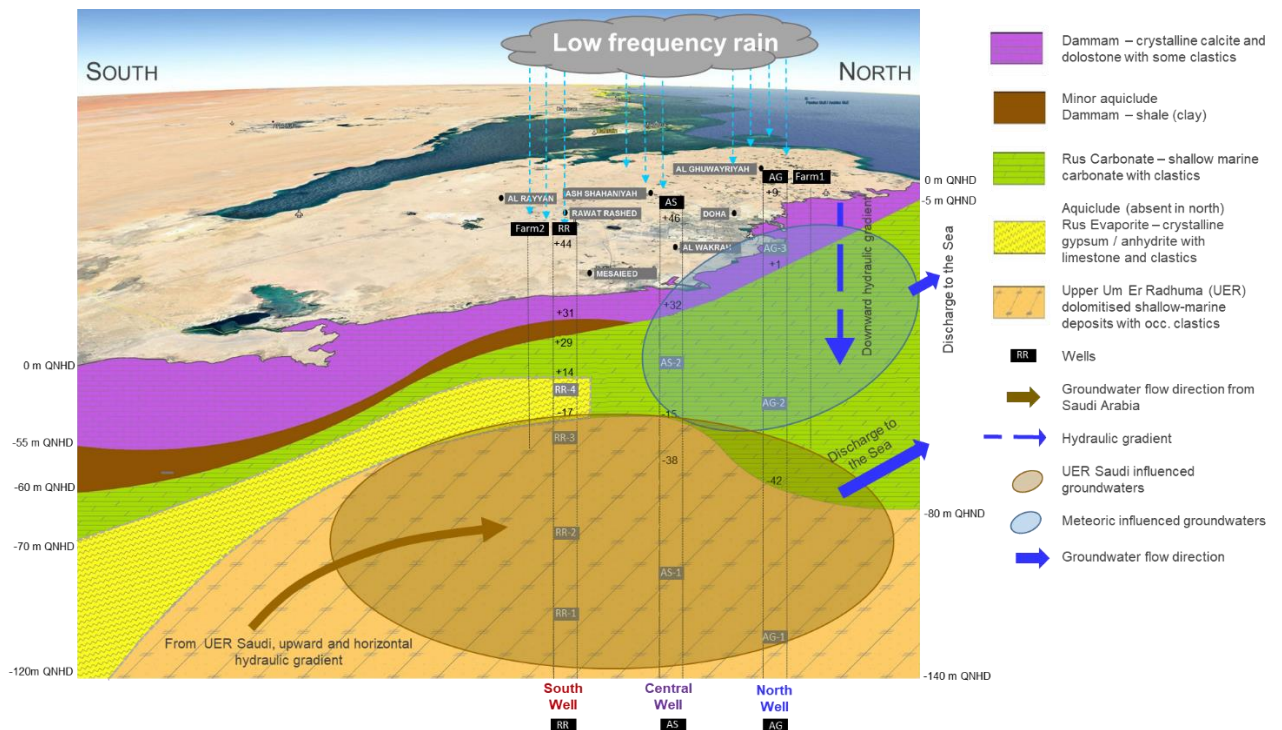
Seawater (n=5) geochemistry was obtained by combining data from ExxonMobil Research Qatar recent seawater analyses of local seawater (Rivers et al., 2019b) with that from a prior PhD study in Qatar (Ooi, 2018), which also provided the single rainwater analysis also from Qatar (n=1). UER Saudi groundwater results were taken from 150 wells across Saudi Arabia (Sharaf, 2001) and presented in terms of the average (\bar{x}), minimum (min), maximum (max) and standard deviation (σ). Groundwaters from Saudi Arabia were variable and most likely reflect spatial and lithological variability such as meteoric influence and gypsum content.

Table 5- 1 End member for each well, indicating the source and mixing solutes

Location	Well ID	Formation	Source	Mixing
South	RR-1	UER	UER Saudi	seawater
South	RR-2	UER	UER Saudi	seawater
South	RR-3	UER	UER Saudi	seawater
South	RR-4	Rus	UER Saudi	seawater

Location	Well ID	Formation	Source	Mixing
Central	AS-1	UER	UER Saudi	seawater
Central	AS-2	Rus	rainwater	seawater
North	AG-1	UER	UER Saudi	seawater
North	AG-2	Rus	rainwater	seawater
North	AG-3	Dammam	rainwater	seawater
North	Farm 1 – AG	UER/Rus	rainwater	seawater
South	Farm 2 - RR	UER/Rus	UER Saudi	seawater

Figure 5-1 Initial conceptual model showing end-members and groundwater flow direction. Groundwaters in all of the southern wells, and southern farm and UER wells in the center and north are influenced from groundwaters flowing from UER Saudi (brown arrow), whereas the central and northern Rus and Dammam wells, plus the northern farm are influenced by rainwater (blue arrow). All discharge into the gulf.



5.1.2 Uncertainty and limitations

It is expensive and sometimes difficult to obtain continuous, adequate and accurate subsurface data ie sufficient borehole coverage to provide an adequate understanding of the underlying stratigraphy, competent drilling subcontractors to give accurate samples of

the geology (Wang, 2019). Laboratory uncertainty and temporal variations of waters sampled in each well due to local or regional fluctuations or errors during sampling, all combine to lead to a level of uncertainty. To identify anomalous measurements, all laboratory results were examined to determine the extent to which they are representative of the average groundwater conditions. Fluctuations are anticipated, for example a shallow aquifers response to recharge, however the objective was to differentiate data that should be included in the analyses, as distinct from those which are likely to reflect errors.

Both field and laboratory parameters were plotted per well, for the duration of the monitoring period, to establish any legitimate local and seasonal trends, or whether the recorded differences were due to either faulty sampling equipment or techniques. Box and whisker plots were undertaken on each parameter for each individual well, and any outliers on the outlier removed from the dataset. Outliers were identified as point with values less than the first quartile less $1.5 \times$ the interquartile range, or greater than the third quartile plus $1.5 \times$ interquartile range. The count (n), mean (\bar{x}), minimum (min), maximum (max) and error of one standard deviation (1σ) were recalculated without the outliers and used in the subsequent analyses. Graphs showing parameter with respect to time included outliers which are identified with a grey circle, but they have not been included in the subsequent analyses.

Ion balance errors (IBE) were calculated during geochemical modelling using PHREEQC for all waters. A slight positive trend, with mean IBE of $+1.6\% \pm 4.5\%$ was noted despite five negative values of samples from the central wells.

5.2 Field Results

Field tests were undertaken as part of the groundwater monitoring sequence, as described in Section 3.8. Results from the field tests from all monitoring events are found in Appendix B1.

5.2.1 Colour and odour

During well development, waters was pumped from the UER aquifer wells were initially black in colour with a strong hydrogen sulfide odour. After approximately 20 minutes of abstraction at approximately $4\text{-}6 \text{ l s}^{-1}$, the groundwater became clear and the odour became milder.

During monitoring, groundwater samples retrieved from the UER and Rus wells (RR-1, 2, 3, AS-1 and 2, and AG-1 and 2) were typically clear. However a mild hydrogen sulfide odour was noted from these same wells during sampling which persisted when the monitoring cap was removed from the groundwater samples. No odour was recorded in southern Rus monitoring well (RR-4), although these waters were always noticeably cloudy and turbid. This well typically recorded a small volume of water within the monitoring pipe as the response zone was mostly within the gypsum and therefore of low yield, explaining the milky cloudy appearance.

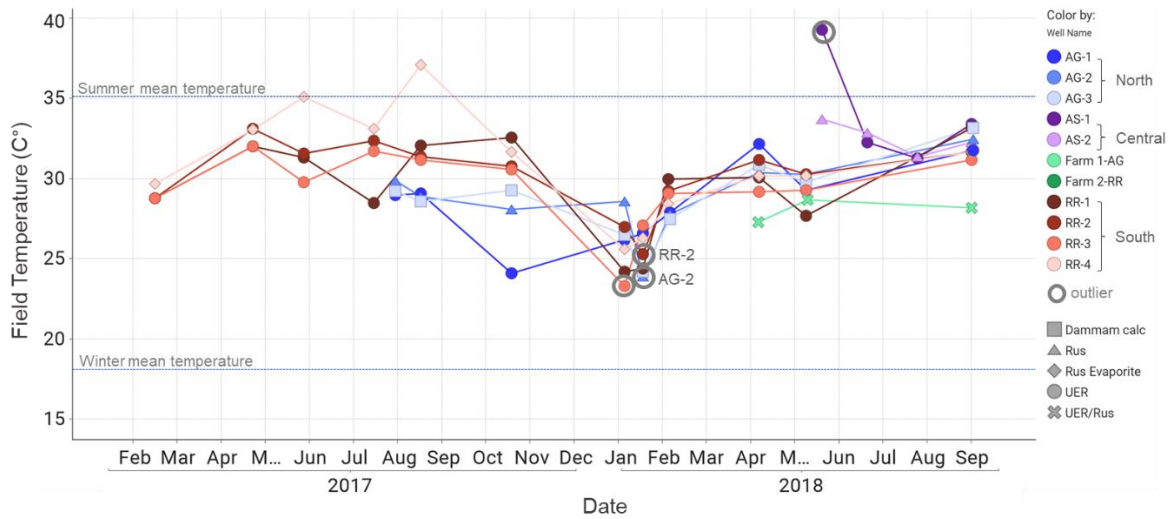
Groundwater samples retrieved from the only Dammam monitoring well in the north (AG-3), were slightly cloudy with no odour.

Samples taken from the adjacent farm in the north (Farm 1-AG) were clear with no odour. In the south (Farm 2-RR), the groundwater samples were clear but with a mild hydrogen sulfide odour.

5.1.2 Field Temperature

Temperatures (C°) were taken from groundwater samples brought to surface using a multiprobe by immediately submersing it in the sample. Given the thickness of the vadose zone, no seasonal variation in temperature was anticipated. Field temperatures from the wells display a typical seasonal trend of dropping in the winter months (October through to March ranging 23.3 to 32.6°C) and rising during the hotter summer months (April through to September ranging 27.3 to 39.3°C) (Figure 5-2). This is likely due to the sample being warmed to the ambient air temperature, exposure of the probe of sample to direct sunlight, particularly during the summer months when temperatures during sampling were often above 40°C. Specifically the deepest central pipe (AG-1) in July 2018 which records an extremely high temperature (39.3°C).

Figure 5-2 Field temperature ($\pm 0.5^{\circ}\text{C}$) of each well during monitoring, where outliers identified by \bigcirc .



5.1.3 pH

pH readings were taken in the field and laboratory, and a comparison between the two sets of results show 32% of the results ($n=70$) fall within the analytical uncertainty (± 0.01 pH) of the 1:1 line, with 47% results are higher for the field determination and 21% of the results higher for the laboratory determination (Figure 5-3). There is greater confidence using the laboratory results as all the laboratories were UKAS accredited, as such the laboratory results were used for all of the analyses (Figure 5-4).

The pH values for all samples from the wells (excluding outliers) over the monitoring period ranged significantly, from pH 6.5 to 8.0 with mean values for each site ranging from pH 6.7 to pH 7.4.

At each location, a trend of pH increasing with depth was noted, and values tend to be similar relative to the depth below ground level, irrespective of formation (Figure 5-5). Groundwater at the water table at each location, the Rus (RR-4 and AS-2) and Dammam (AG-3), recorded a lower pH (neutral to mildly acidic) than the underlying UER waters.

Figure 5-3 Field pH (± 0.01) compared to laboratory pH (± 0.01)

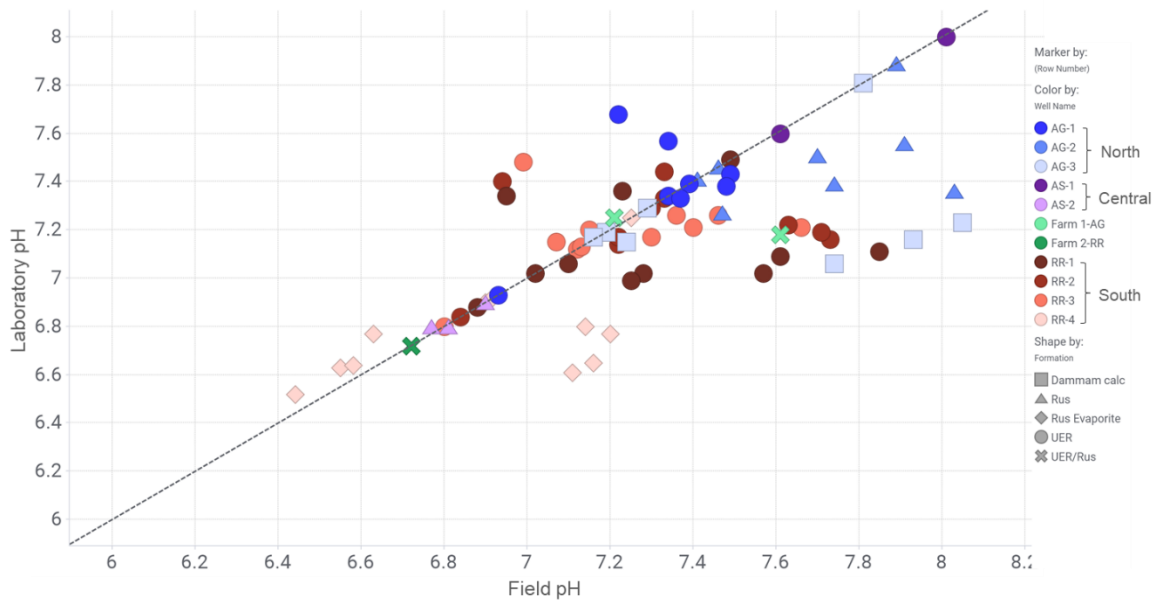


Figure 5-4 Laboratory pH (± 0.01) for each well during monitoring, outliers identified by \circ

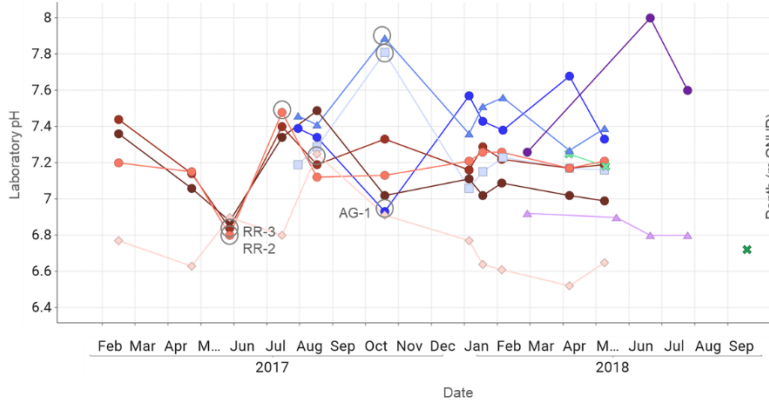
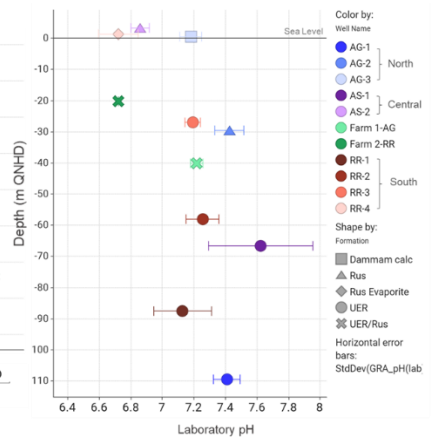


Figure 5-5 $\bar{x} \pm 1\sigma$ Laboratory pH with depth (m QNHD) for each well



The southern wells were typically neutral to locally acidic relative to the neutral to mildly alkaline northern wells. pH within the UER in the southern wells (RR1, 2 and 3) tended to follow similar monthly fluctuations, which is to be expected as these three pipes are within the same aquifer. The central wells (AS-1 and 2) exhibited the greatest range in pH (6.8 to 8.0) although these two wells were only sampled over a period of four months. The central deeper UER well (AS-1) had similar neutral mildly-alkaline values as the northern wells. The

central and northern wells appear to be more influenced by meteoric recharge and mixing between aquifers.

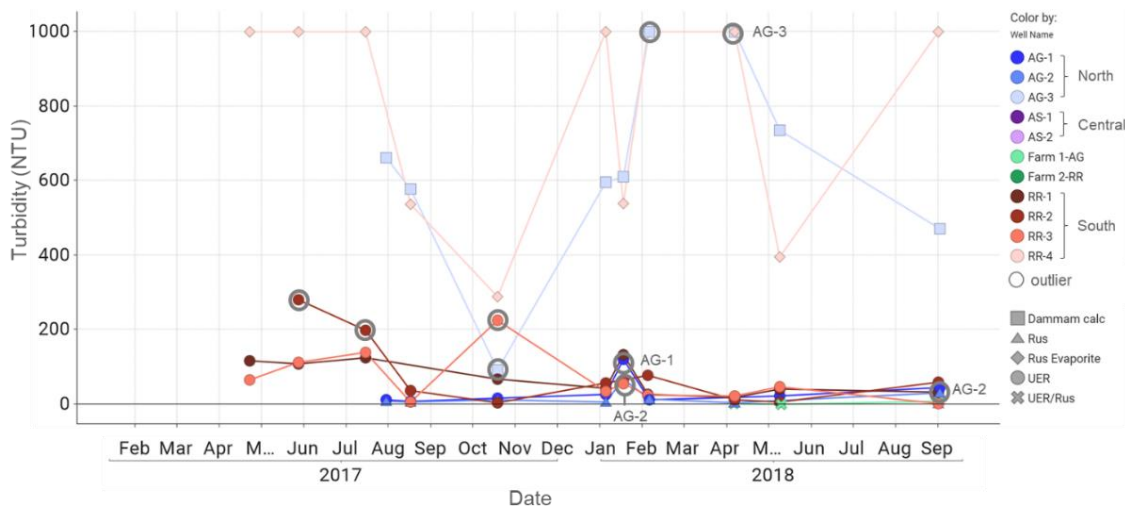
pH values from the farms (Farm 1-AG and Farm 2-RR) are similar to those from samples taken from the same depth in the aquifer in the nearby wells (AG-3 and RR-4 respectively).

5.1.4 Turbidity

Turbidity (NTU) recorded in the field (Figure 5-6), ranged from 0.8 to >1000NTU (above detection limit), and was often reflected the degree of discolouration observed during monitoring. The southern well (RR-4) was often milky in colour and had very high turbidity (289 to >1000 NTU) at all times, often exceeding the detection limit.

Higher turbidity readings (471 to 735 NTU) were also recoded at the water table in the northern well (AG-3) of the upper Dammam aquifer, and possibly reflect the minimum degree of filtration of turbid recharge waters by thin vadose zone, as the water table was between 7-8m bgl. Results for most other wells are much lower, and those from 2018 tend to be more consistent and lower than the 2017 results. This most likely reflects an improved sampling methodology and time since drilling allowing the well to settle.

Figure 5-6 Turbidity (NTU) with time



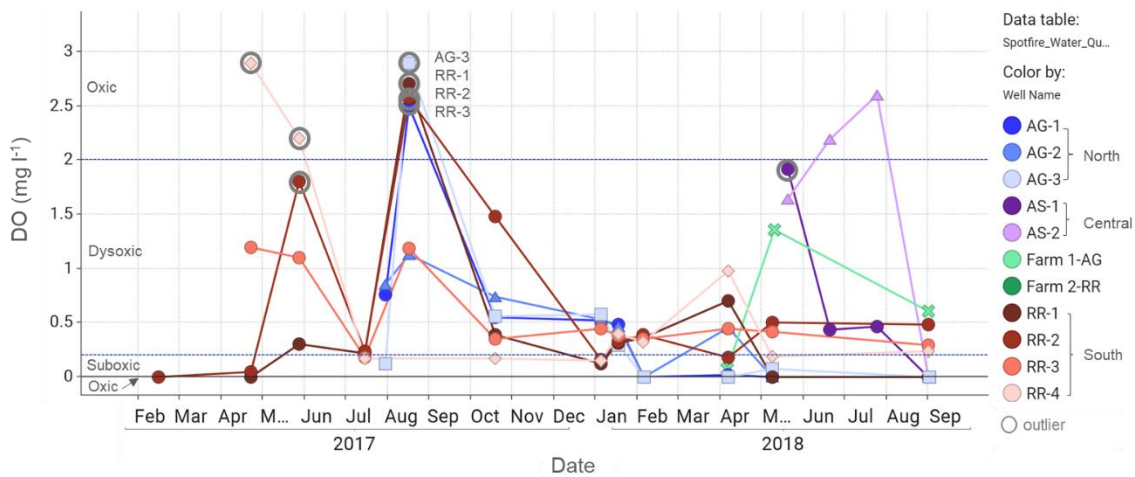
5.1.5 Dissolved Oxygen (DO)

DO (mg l⁻¹) readings were only taken in the field and due to the methodology of sampling such as exposure to the atmosphere, the recorded DO concentrations can be unreliable.

Based on dissolved oxygenation levels (Tyson & Pearson, 1991), groundwaters were mostly dysoxic (0.2 mg l^{-1} to 2.0 mg l^{-1}). Through the winter month, DO values were lower and $<1 \text{ mg l}^{-1}$, whereas in the summer value ranged from 0 to $<2 \text{ mg l}^{-1}$. The UER deeper wells appear to have lower DO levels than the upper shallower aquifers.

During well development and following monitoring, a hydrogen sulfide odour was noted in all the UER wells, and central and northern Rus wells indicating sulfate reduction and therefore DO levels will be reduced.

Figure 5-7 DO ($\pm 0.01 \text{ mg l}^{-1}$) with time



5.1.6 Specific Electrical Conductivity (SEC)

SEC (mS cm^{-1}) were taken in both the field and laboratory, with both sets of results were automatically corrected to standard temperature of 25°C and atmospheric pressure of 1 atm. All field SEC measurements were taken using the multiprobe (Aqua Read AP-800) but results in 2018 were noticeably erratic, possibly due to the heat or lack of on-site calibration. SEC was measured in the laboratory from 2018 for samples collected in 2018, however not during 2017. After calculating the mean and standard deviation of each data set, a single data set was created by combining field SEC from 2017 and laboratory SEC from 2018.

SEC values in each well remained relatively constant over time, and increased with depth, as expected within a density stratified aquifer (Figure 5-9 and 5-9). Although SEC values are similar between the central (AS) (1.81 to 5.72 mS cm^{-1}) and northern wells (AG) (1.08 to 5.99 mS cm^{-1}), they are much higher in all of the southern wells (RR-1 to RR-4) (12.97 to 32.16 mS cm^{-1}). These higher values are thought to be the consequence of long-term

residence in the confined UER aquifer in Qatar and Saudi Arabia, with known evaporites, such as gypsum and anhydrite. The northern and central wells experience a level of meteoric flushing. SEC is considered to be independent of formation, but varies with mineralogy, as well as the degree of mixing with either rainfall or underlying aquifers.

SEC values from the southern farm (Farm 2-RR) are slightly higher than those from the northern farm (Farm 1-AG), however the southern farm (Farm 2-RR) SEC values are still markedly low in comparison to the southern RR wells.

Figure 5-8 Box plot of Field SEC ($\pm 0.001 \text{ mS cm}^{-1}$) for 2017 and Laboratory SEC ($\pm 0.001 \text{ mS cm}^{-1}$) for 2018, where the boxes define the 25th (Q1) and 75th (Q3) percentiles and the white line within the box is the median (IQR = Q3 - Q1); the whiskers extend to data points not considered outliers; an outlier is defined as a data value greater than $Q3 + 1.5(Q3 - Q1)$ and less than $Q1 + 1.5(Q3 - Q1)$ (Tibco Spotfire, 2018).

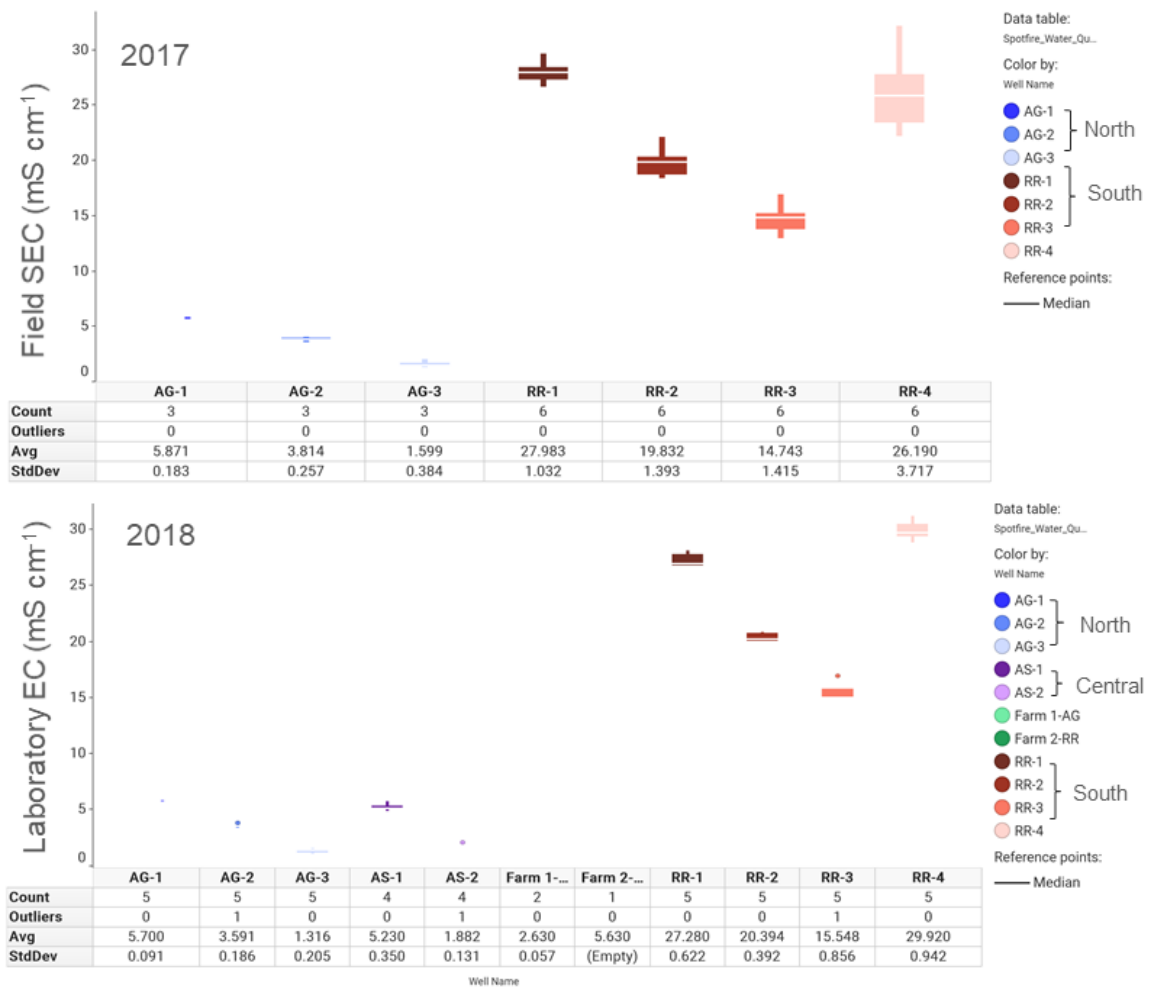


Figure 5-9 SEC ($\pm 0.001 \text{ mS cm}^{-1}$) with time for each well during monitoring, outliers identified by \bigcirc

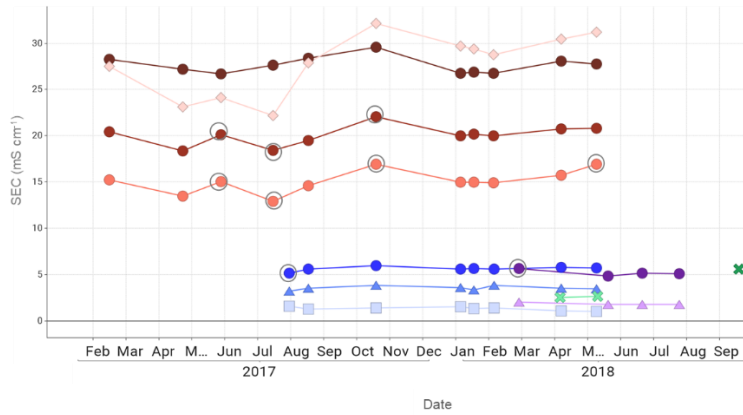
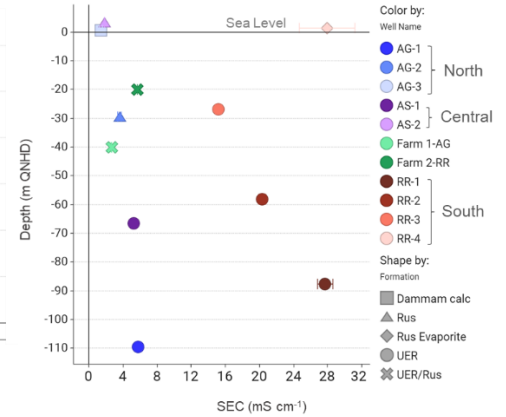


Figure 5-10 $\bar{x} \pm 1\sigma$ SEC (mS cm^{-1}) with depth (m QNHD) for each well



5.2 Major elements

5.2.1 Chloride and Sodium

The conservative tracer Cl^- both displayed limited variation over time, (Figure 5- 11), with no notable fluctuations in concentrations in response to recharge such as rainfall, or abstraction from pumping for the duration of monitoring. Cl^- concentrations are highest in the deeper sampling pipes and decrease linearly upwards at all well locations (Figure 5-12). Mean Cl^- concentrations within the central (AS) and northern (AG) wells are similar in range (2 to 25 mmol l^{-1}) but are an order of magnitude lower than the southern (RR) wells (116 to 269 mmol l^{-1}). Cl^- is also high in Rus evaporite well (RR-4) in the south and possible indicate the dissolution of halite in the Rus in either Saudi Arabia or Qatar or both, greater mixing with seawater which is known to recharge the Rus from the south west, or from over-abstraction.

Cl^- concentrations from both neighbouring farms (Farm 1-AG and 2-RR) are low, and within a similar range as the central and northern wells (13 to 26 mmol l^{-1}).

Figure 5- 11 Cl⁻ for each well during monitoring, outliers identified by ○

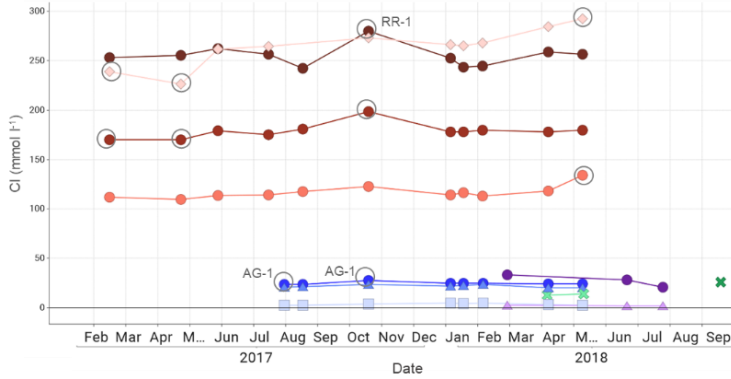
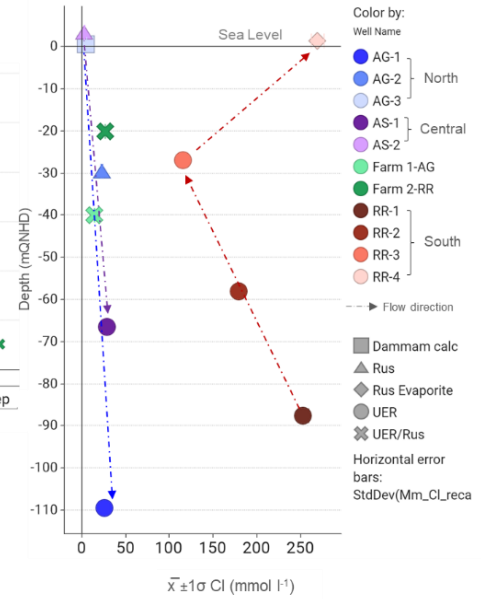
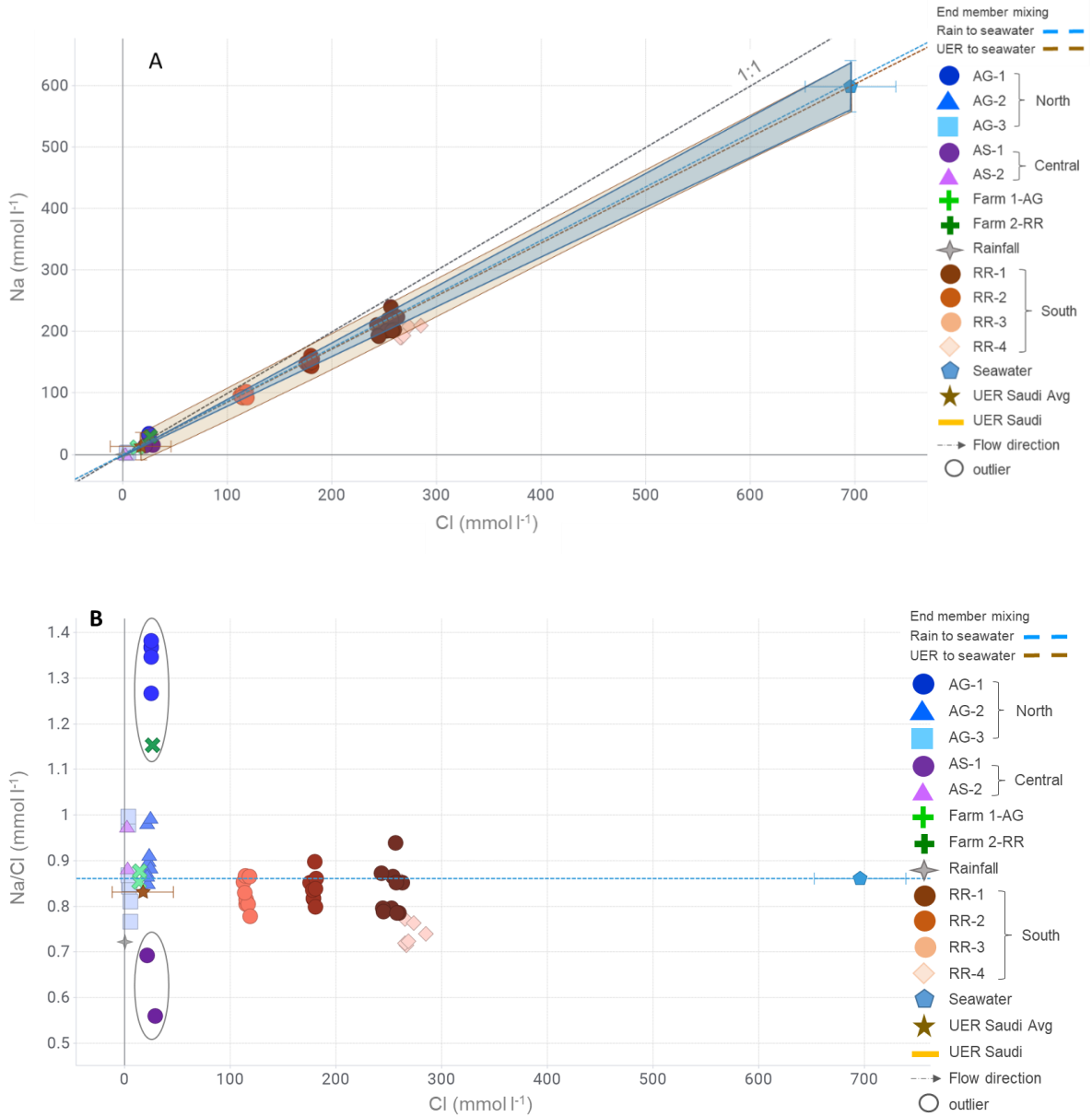


Figure 5- 12 $\bar{x} \pm 1\sigma$ Cl⁻ with depth



Sodium concentrations appear to reflect trends of Cl⁻, with Na⁺:Cl⁻ following the expected mixing trend between rainfall (blue dashed line) or UER Saudi groundwater (brown dashed line) with seawater. However, the central UER well (AS-1) has a lower ratio, and the UER/Rus southern Farm 2-RR and northern UER well (AG-1) wells both have higher Na/Cl ratios seen more clearly when comparing Na/Cl vs Cl ratios (Figure 5-13). These differences in Na/Cl and (Na/Cl)/Cl ratios are most likely influenced by the presence and subsequent interaction with various clays, as interlayer cations such as Na⁺ are exchangeable in clays (Plummer et al., 1990) such as smectites (Drever, 1997). Clays, including smectite, are present intermittently in the Rus and within the multiple clastic bands recorded throughout the UER, particularly in the central and northern wells (Rivers et al., 2019a).

Figure 5-13 A. The ratios of Na vs Cl including 1:1, and B. Na/Cl vs Cl. Mixing trends (dashed lines) including uncertainty (shaded) between end members rain to seawater (blue) and UER Saudi to seawater (brown). Circles highlight the central and northern UER wells and their proposed interaction with clays.



5.2.2 Sulfate

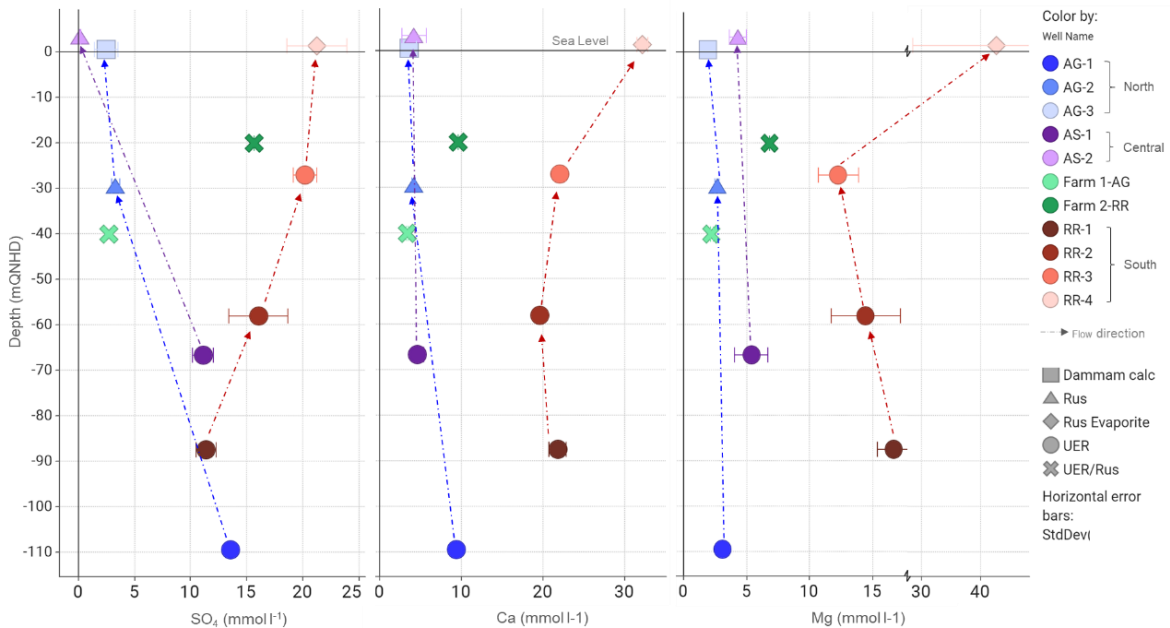
SO₄²⁻ concentrations remained relatively constant during monitoring, and are elevated in all of the UER aquifer wells, including the south (RR1, 2 and 3), central (AS-1) and north (AG-1), and the southern Farm 2-RR with means ranging from 11 to 21 mmol l⁻¹. SO₄²⁻ concentrations within the southern boreholes increase linearly upwards through the UER, and as expected are highest in the Rus sulfate evaporitic aquiclude (RR-4) (Figure 5-14). Values in the UER from the central and northern wells (AS-1 and AG-1) are similar in concentrations to those samples from the deepest southern UER well (RR-1).

Sulfate concentrations in upper aquifers (Dammam and Rus carbonate) of the central (AS-2) and northern wells (AG-2 and 3), including Farm1-AG, are lower by an order of magnitude (<1 to 3 mmol l⁻¹) relative to the underlying UER.

Comparing Cl⁻ with SO₄²⁻ molar concentrations (Figure 5-15) relative to values expected from with the respective end-members, SO₄²⁻ is enriched in the shallowest UER well of the south (RR) and central and north (AS-1 and AG1) and the southern Farm 2-RR.

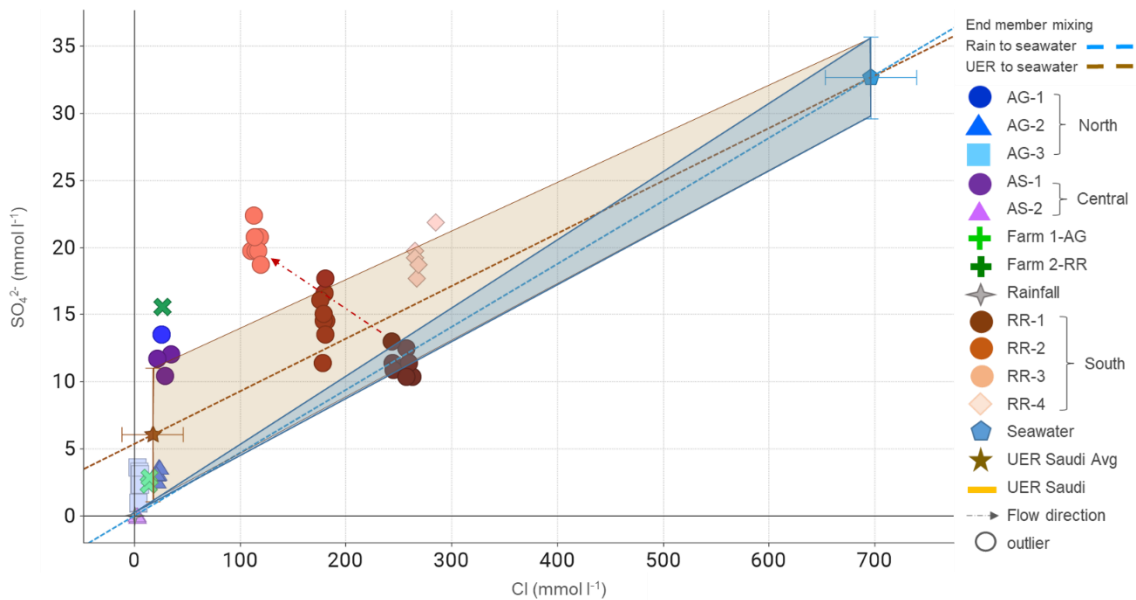
In the south, the UER wells display increasing SO₄²⁻ with decreasing depth and salinity (Cl⁻). The southern upper UER well (RR-3) has similar SO₄²⁻ concentrations to the overlying Rus evaporite well (RR-4) although Cl⁻ in this Rus well are higher. Elevated SO₄²⁻ in the southern Rus well (RR-4) is to be expected as the response zone is within beds of gypsum. The upper UER well (RR-3) has lower chloride concentrations than the overlying Rus evaporite (RR-4) and must be related to ongoing mixing and horizontal and some upward flow.

Figure 5-14 $\bar{x} \pm 1\sigma$ of SO₄²⁻, Ca²⁺, Mg²⁺ for each well with depth



SO₄²⁻ concentrations are similar at the southern upper UER well (RR-3) and southern farm well (Farm 2-RR), which are at similar depth. The shallow Damman and Rus aquifers in the north (AG-3 and AG-2) and central Rus well (AS-2) exhibit minor enrichment relative to rainwater.

Figure 5-15 Cl⁻ with SO₄²⁻. Mixing trends (dashed lines) including uncertainty (shaded) between end members rain to seawater (blue) and UER Saudi to seawater (brown).



Elevated sulfate levels from the dissolution of gypsum, as reported in the UER aquifers of Saudi Arabia and Qatar by Alsharhan et al., (2001) and Eccleston et al., (1981), are likely the result of the resident time in the UER aquifer and subsequent dissolution of any available sulfates. The enrichment of SO₄²⁻ in the central and northern wells (AS-1 and AG-1) suggests continued dissolution as waters flow north within the UER.

5.2.3 Calcium

Ca²⁺ concentrations remain relatively constant in all wells for the duration of the monitoring. Ca²⁺ concentrations are consistently higher in the southern wells (RR) (20 to 32 mmol l⁻¹) relative to the central (AS) and northern wells (AG), and both farms (3 to 10 mmol l⁻¹) (Figure 5-14). Ca²⁺ is significantly higher in the Rus evaporite well in the south (RR-4) and can most likely be attributed to the dissolution of Rus evaporites gypsum and anhydrite (refer Equation 9).

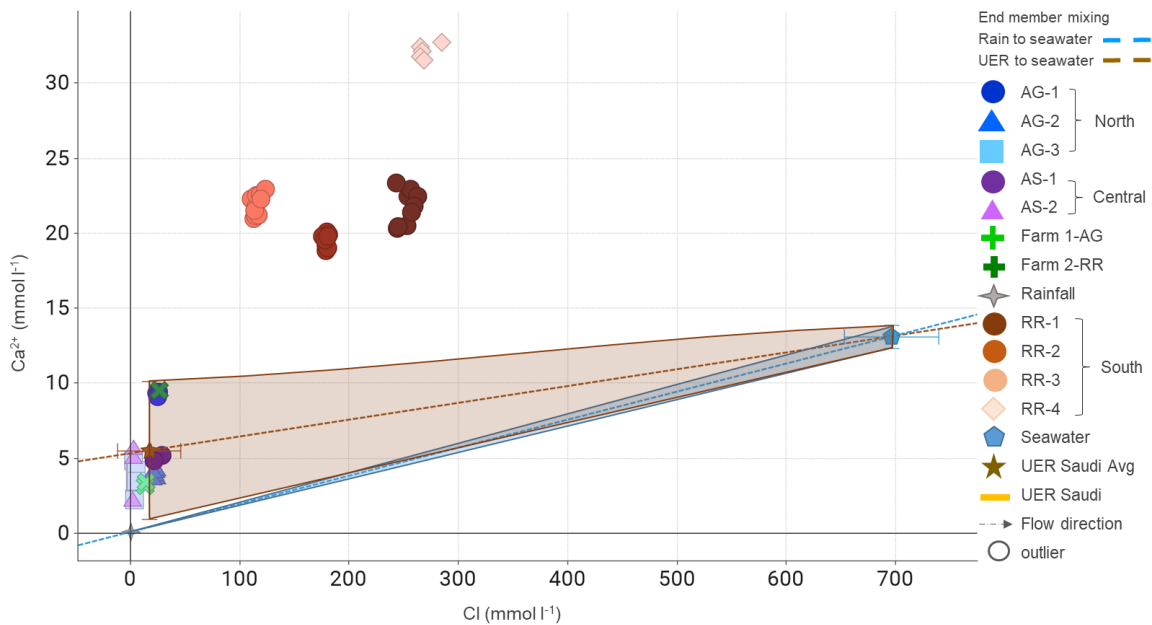
Ca²⁺ concentrations in deeper UER aquifer in the center of Qatar (AS-1) behave similarly to the predicted mixing of UER Saudi with seawater (Figure 5-15). The deeper UER and Rus aquifer wells in the south (RR-1 to 4) are significantly enriched in Ca²⁺. Ca²⁺ concentrations in the southern farm (Farm 2-RR) are lower than the nearby southern wells (RR's), but similar in values to the deeper wells of the center (AS-1) and north (AG-1). Although the

UER wells in the northern (AG-1) and southern Farm (Farm 2-RR) are above the UER Saudi-seawater mixing trend, they both lie just within the standard deviation of error (shaded brown box), resembling the most Ca²⁺ rich UER waters in Saudi Arabia. The UER well in the center of the country shows no such high Ca²⁺.

Ca²⁺ is slightly enriched relative to the predicted mixing of rainwater with seawater in the upper aquifers of the central (AS-2), north (AG-2 and AG-3) and northern farm wells (Farm1-AS). The northern farm concentrations (Farm 1-AG) are similar to values in the nearby northern well (AG-2), where samples were taken at a similar depth below ground level.

The source of Ca²⁺ is proposed to be from the dissolution of dolomite and gypsum. Stratification has occurred in the southern wells and somewhat in the northern wells, as concentrations increased with depth. There are various hypotheses regarding stratification including meteoric mixing in the north, and in the southern wells due to the influence from the overlying confining evaporitic layer. The effects of water-rock interaction as distinct from mixing with end members can be better distinguished using excess concentrations. This will be discussed in the subsequent sections.

Figure 5-16 Ca²⁺ with Cl⁻. Mixing trends (dashed lines) including uncertainty (shaded) between end members rain to seawater (blue) and UER Saudi to seawater (brown).

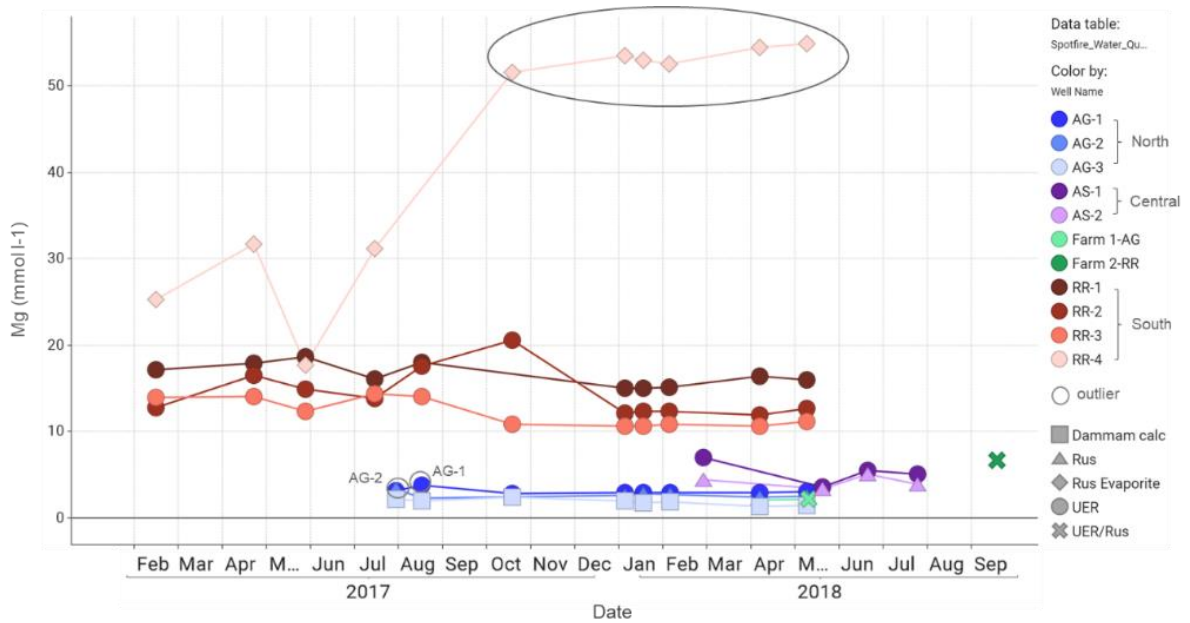


5.2.4 Magnesium

Absolute Mg^{2+} concentrations remained relative constant with time, apart from samples from the Rus in the southern well (RR-4) which increased in the later half of 2017 and then remained constant in 2018. Although this Rus evaporite well (RR-4) was continually of low yield and sometimes dry during sampling, it does not explain the significant increase in concentrations halfway through the monitoring period.

Samples from the southern boreholes have high Mg^{2+} concentrations, particularly in the Rus evaporite (RR-4), with a linear increase with depth through the UER (12 to 43 $mmol\ l^{-1}$). In the center (AS-1 and 2) and northern wells (AG-2 and 3), Mg^{2+} concentrations are relatively similar irrespective of depth (2 to 5 $mmol\ l^{-1}$) but are an order of magnitude less relative to the southern wells. The northern farm concentrations (Farm 1-AG of 2 $mmol\ l^{-1}$) are similar in readings to the nearby northern well (AG-2) at similar depth from ground level (3 $mmol\ l^{-1}$). The southern farm (Farm 2-RR) concentrations (7 $mmol\ l^{-1}$) are almost half the mean concentration recorded in the same aquifer from the nearby southern wells (RR-3) (12 $mmol\ l^{-1}$).

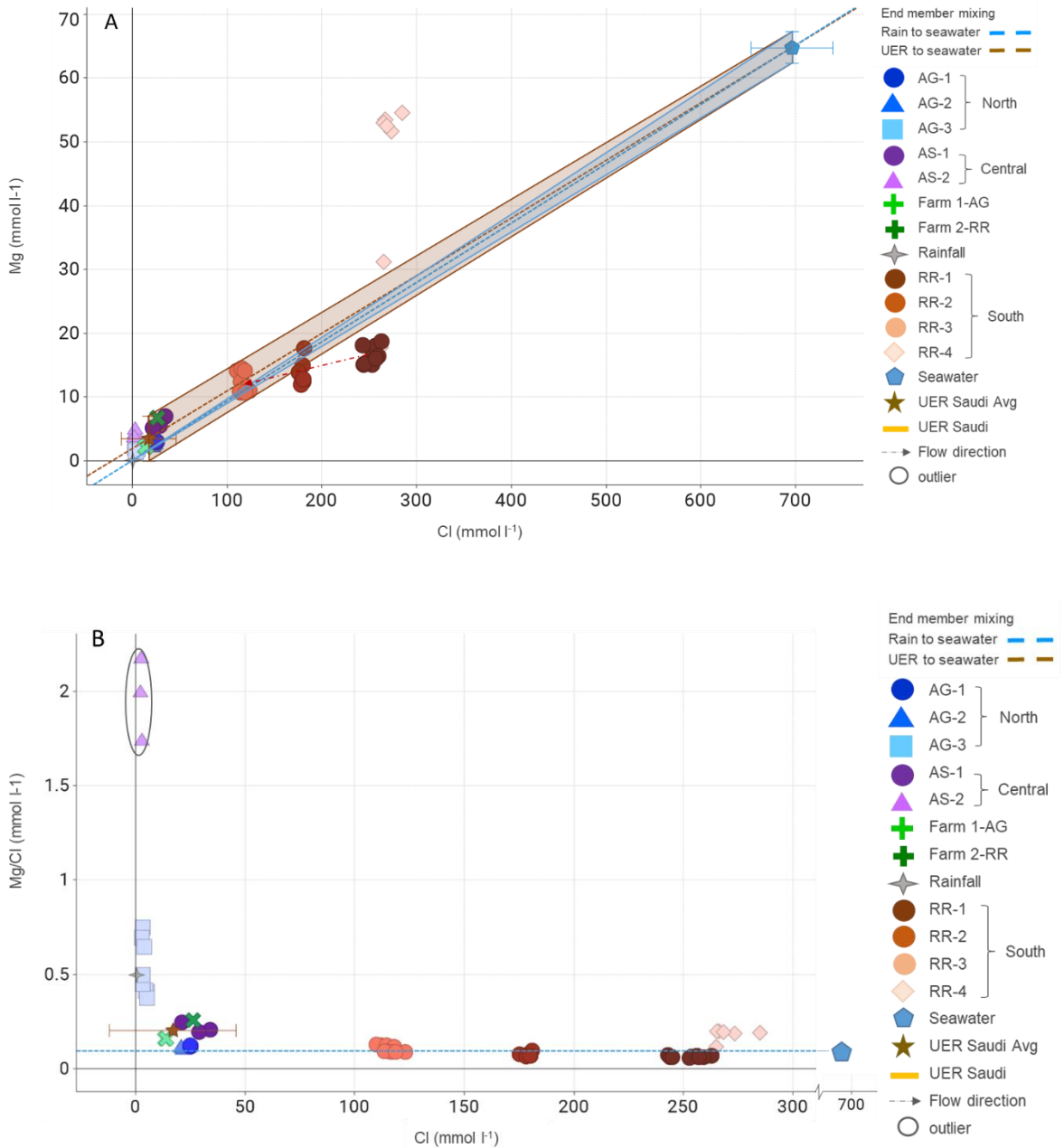
Figure 5-17 Mg^{2+} for each well during monitoring, outliers identified by ○. Circle indicating higher concentrations in 2018



Mg^{2+} concentrations in the southern Rus evaporite (RR-4) are significantly enriched based on molar ratios with Cl^- , as it is well above the mixing trend of UER Saudi groundwater and

seawater (Figure 5-18). The deepest UER well in the south (RR-1) is depleted with respect to Mg^{2+} whereas the middle southern UER wells (RR-2 and 3), the central and northern UER wells (AS-1 and AG-1, respectively), and southern farm (Farm 2-RR) are within the expected mixing of UER Saudi groundwaters and seawater.

Figure 5-18 A. Mg^{2+} with Cl^- and B. Mg/Cl vs Cl . Mixing trends (dashed lines) including uncertainty (shaded) between end members rain to seawater (blue) and UER Saudi to seawater (brown). Circle highlighting higher Mg/Cl ratio in the central Rus well (AG-3).



In the south, Mg^{2+} concentrations appear to decrease from deeper to shallower UER and Mg/Cl ratios increase. The upper aquifer of the Dammam in the north (AG-3) is enriched in Mg^{2+} concentrations relative to concentrations expected from rainwater mixing with seawater (Figure 5-18). The Rus in the central (AS-2) and northern well (AG-2) are within the expected range from mixing.

Overall, Mg^{2+} concentrations appear less dependent on formation alone, as absolute concentrations in the central and north are in the same order of magnitude irrespective of formation. Variations, such as a higher Mg/Cl ratio in the central Rus well (AS-2) and to a lesser degree the northern Dammam well (AG-3), indicate additional water-rock geochemical process are ongoing in addition to mixing. This is discussed in Section 5.3.

5.2.5 Potassium

K^+ concentrations are elevated in the deeper UER wells relative to the Rus and Dammam aquifers, and typically decrease when shallower (Figure 5-18 and 5-19). A trend of decreasing K^+ concentrations from the south to the north is observed in all wells including the farm wells. Over time, all four of the southern wells appear to display an increasing trend which could be related to exchange with interlayer cations in the clays.

Figure 5-19 K^+ for each well during monitoring, outliers identified by \circ . Dashed lines depicting an increase in concentration over time in the southern wells

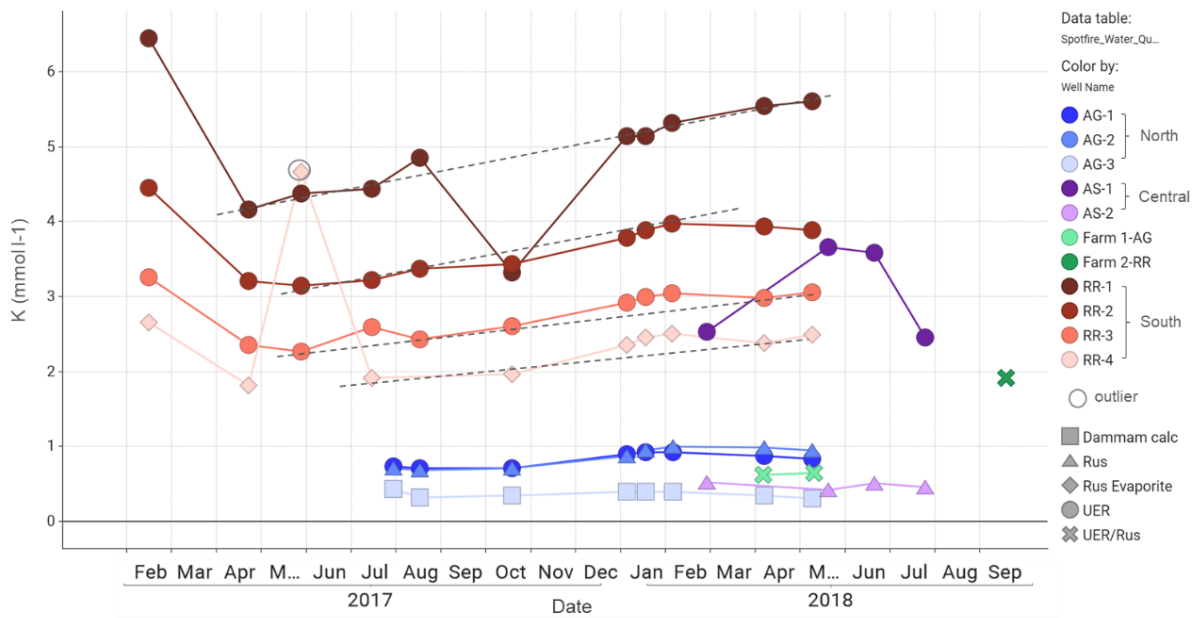
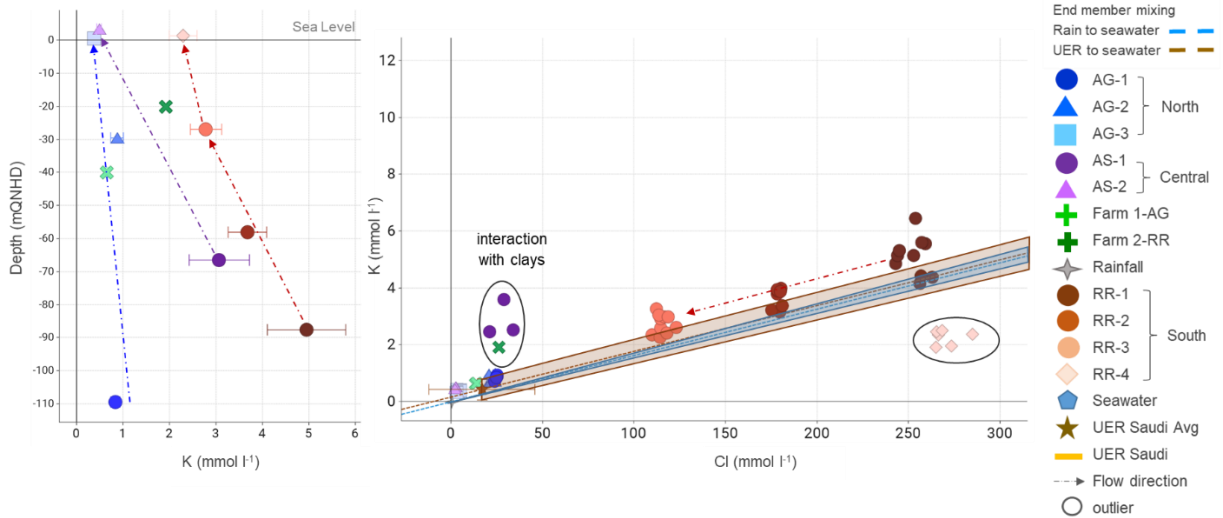


Figure 5-20 $\bar{x} \pm 1\sigma$ K⁺ for each well with depth. Ratio of K⁺ vs Cl⁻ with mixing trends (dashed lines) including uncertainty (shaded) between end members rain to seawater (blue) and UER Saudi to seawater (brown). Circles highlight the southern Rus, central UER and southern farm wells and their proposed interaction with clays.

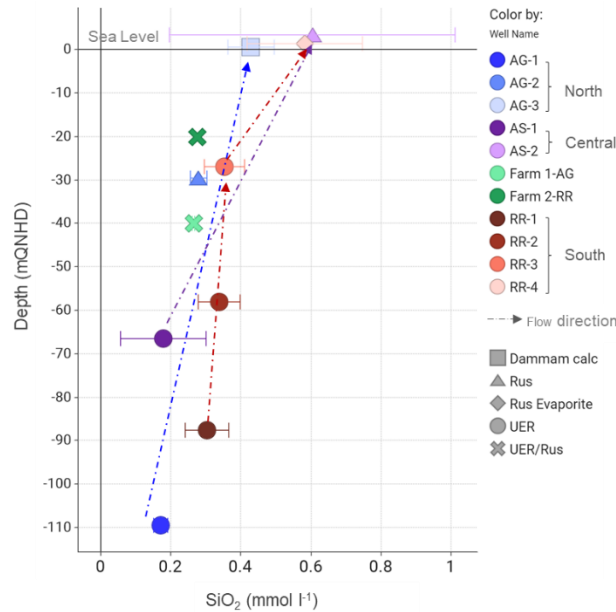


Relative to Cl⁻, K⁺ concentrations are enriched in the UER southern wells (RR-1 to 3), central well (AS-1) and southern farm (Farm 2-RR) but depleted in the southern Rus well (RR-4). Variations are likely due to interaction with 2:1 clays such as illite/mica and smectite (Drever, 1997) releasing Na⁺ and other cations.

5.3.6 Silicon

Dissolved SiO₂⁴⁺ concentrations are highest in the upper aquifers and decrease with depth. SiO₂⁴⁺ is higher in the southern wells, with no significant variation within the UER with increasing depth. Variations in SiO₂⁴⁺ concentrations can often be attributed to clay and clastics, which are prevalent in the Dammam, Rus and Rus evaporite (Rivers et al., 2019a).

Figure 5-21 $\bar{x} \pm 1\sigma$ SiO_2^{4+} for each well with depth



5.3.7 Trace Elements (Al and Fe)

Both Al and Fe have consistently exhibited very low concentrations, with 45% of the Al and 20% of the Fe concentrations of the samples below the detection limits of the laboratory. In both central wells (AS-1 and 2), concentrations for both Fe and Al were slightly more than the other wells (0.04mmol l⁻¹ and 0.05mmol l⁻¹ respectively), however they were still very low and considered insignificant, and not discussed further.

5.2.8 Alkalinity

Alkalinity was reported as CaCO₃, and subsequently converted to HCO₃⁻ as within the pH range of the waters samples, HCO₃⁻ is the dominant component of alkalinity (Domenico & Schwartz, 1999).

Alkalinity remained consistent with time (Figure 5-22), apart from the shallowest pipe in the southern wells in which temporal variations could be related due to sampling difficulties (as it was often dry or low yield) (Figure 5-23). Mean alkalinity in the central well in the Rus (AS-2) (20 mmol l⁻¹) was much higher the other project wells (2 to 6 mmol l⁻¹), including the underlying well in UER (AS-1) (5 mmol l⁻¹) at the same location.

Results from the central wells (AS-1 and 2) can be included with confidence, as both samples were tested in two different laboratories during the monitoring period and gave similar results.

The central UER well (AS-1) and all northern wells (AG-1,2 and 3) have similar mean ranges (5 to 6 mmol l⁻¹), while the southern UER wells (RR-1, 2 and 3) record lower alkalinity (2 to 3 mmol l⁻¹). The southern Rus well (RR-4) mean (6 mmol l⁻¹) has similar alkalinity values to all the northern wells (AG-1, 2 and 3) and the central UER well (AS-1). Both farm samples exhibit similar ranges to their respective nearby well at similar depths (Figure 5-23).

Figure 5-22 Alkalinity (HCO₃⁻) for each well during monitoring, outliers identified by ○

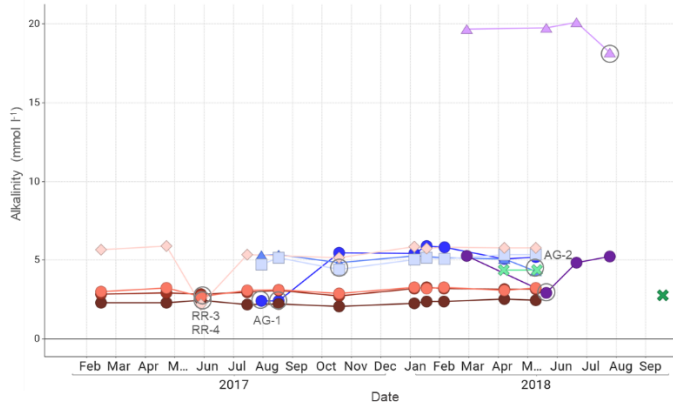
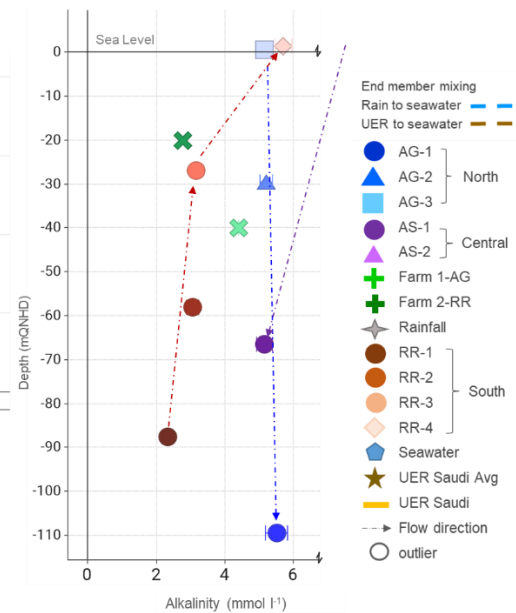


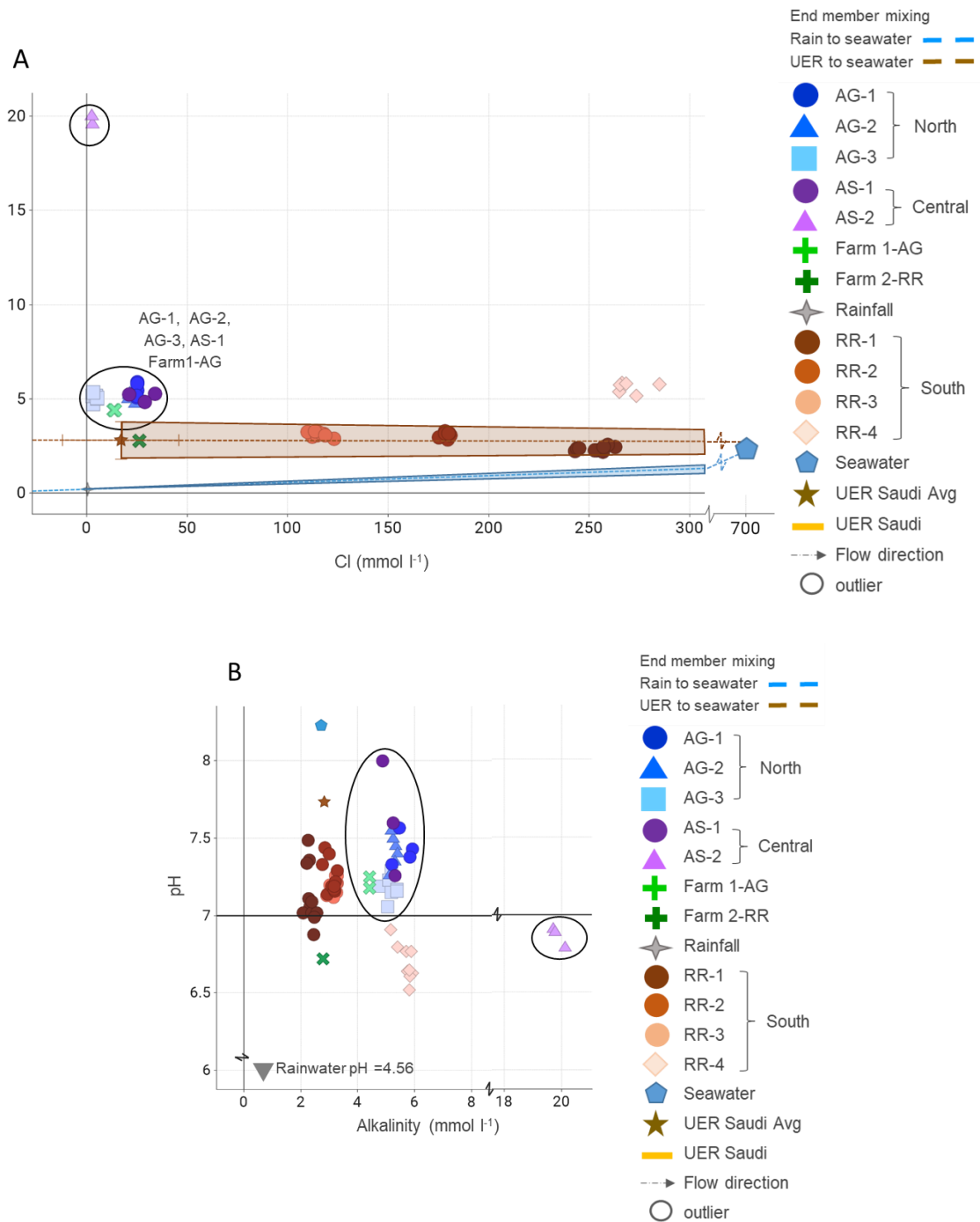
Figure 5-23 $\bar{x} \pm 1\sigma$ Alkalinity (HCO₃⁻) with depth



Comparing HCO₃⁻/Cl ratios (Figure 5-24), the central UER well (AS-1), all of the northern wells (AG-1, 2 and 3) plus the northern farm (Farm 1-AG) show higher ratio's than anticipated when mixing rainwater with seawater (blue dashed line and shaded area). This is in addition to the significantly elevated alkalinity value recorded in the central Rus well (AS-2).

Comparing pH with alkalinity (Figure 5-24), highlights the three groups with respect to alkalinity, although the pH varies within each group. Variations in alkalinity are due most likely to additional geochemical processes which are discussed in the following section.

Figure 5-24 A. Ratio of Alkalinity (HCO_3^-) vs Cl^- with mixing trends (dashed lines) including uncertainty (shaded) between end members rain to seawater (blue) and UER Saudi to seawater (brown) and B. Alkalinity (HCO_3^-) vs pH. Circles highlight the significantly elevated alkalinity in the central Rus well, and elevated alkalinity in the central UER well, all northern wells and northern farm.



5.2.9 Organics (TOC and TN)

Total organic carbon (TOC) measured as NPOC (non-purgeable organic carbon) and total nitrogen (TN) were tested at the University of Bristol School of Geography laboratory with the assistance of a fellow masters student. The samples were initially filtered through 22 μ m apertures, processed using a Shimadzu TOC-L, to quantify the amount of non-volatile organics within the groundwater. Uncertainty for the 39 samples was calculated for both TOC and TN as $\pm 2\%$.

TOC was very high in the central Rus carbonate well (AS-2) $2.3 \pm 0.1 \text{ mmol l}^{-1}$ ($27.7 \pm 0.6 \text{ mg l}^{-1}$) relative to all of the other wells. TOC was also elevated in the deepest UER wells in the south (RR-1), central (AS-1) and north (AG-1) from 0.5 to 1.0 mmol l^{-1} (6.1 to 12.5 mg l^{-1}), and in the following order such that $\text{RR-4} > \text{AG-2} > \text{RR-3} > \text{RR-2} > \text{AG-3}$ with values of 0.3 to 0.1 mmol l^{-1} (3.2 to 1.2 mg l^{-1}), and both farms $< 0.1 \text{ mmol l}^{-1}$ (1 mg l^{-1}).

A single TOC result of 0.98wt% was recorded on a rock sample from the central well at -67.2m QNHD (113.7mbgl). No other chemical analyses for TOC or TN was undertaken on the rock core. Very thin laminations or darker material, including darker clays, were visual noted in the UER central well at -38.9 and -41.0m QNHD (85.4 and 87.5mbgl) and the northern well between -62.9 and -63.9, and at 90.4m QNHD (72.0 to 73.0m and 99.5mbgl). These darker strands could contain organics. No such material was noted in the southern well and from personal and extensive logging experience, nor in the Dammam or Rus.

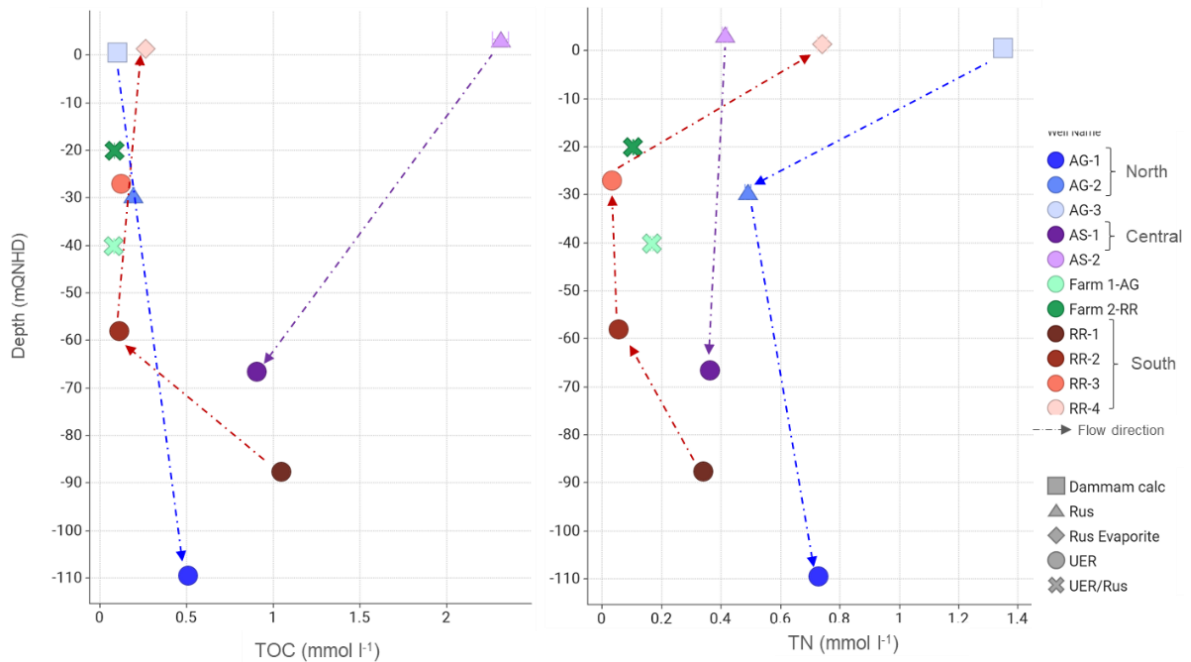
TOC content of seawater from multiple sites surrounding Qatar recorded concentrations from 0.04 to 0.3 mmol l^{-1} (0.5 to 3.6 ml l^{-1}) (Emara, 1998) indicating the central Rus well and all the UER wells exhibit higher TOC values than seawater. Typical DOC concentrations of natural groundwaters outside of Qatar have been documented to range between 0.04 mmol l^{-1} (0.5 mg l^{-1}) (Drever, 1997) and 0.1 mmol l^{-1} (1.2 mg l^{-1}) (Whitaker & Smart, 2007a). TOC values from a groundwater samples taken from 42 agricultural wells (between 40m and 80m depth) situated in the central and north east of Qatar by the Qatar Foundation (QEERI) in 2013, ranged from 0.1 to 2.4 mmol l^{-1} (1.5 to 28.9 mg l^{-1}) with a mean of 0.4 mmol l^{-1} (4.6 ml l^{-1}) (Kuiper et al., 2015). It appears that TOC is higher than seawater and regionally elevated above typical natural groundwaters, particularly in the north where farming is prevalent.

Sources of organic material within the groundwaters could be naturally occurring organic acids, bacteria or other biological means, which are already residing in the groundwaters.

These natural communities could be stimulated from artificially injected waters, such as TSE. Alternatively, high TOC concentrations could be the sole result of anthropogenic activities, and should be considered in future analyses.

The central Rus well (AS-2) has significantly elevated TOC values, as well as high alkalinity (\bar{x} 19.5 mmol l⁻¹), depleted sulphate and is mildly acidic (pH<7). High levels of organics in the groundwater usually lead to bacterial decomposition of the organic matter, such that the respired CO₂ in the groundwater decreases pH and potentially leads to dissolution of carbonate minerals (Morse & Mackenzie, 1990). During monitoring, all of the UER and Rus wells had mild to moderate H₂S odours, indicating sulphate reduction. Partial sulphate reduction during the early stages of reduction can lead to undersaturation of carbonate minerals and therefore carbonate dissolution (Morse & Mackenzie, 1990). Ongoing sulfate dissolution and undersaturation of gypsum/anhydrite can lead to carbonate saturation and subsequent precipitation (Section 2.11).

Figure 5-25 TOC (mmol l⁻¹) and TN (mmol l⁻¹) with depth



TN is noticeably elevated in the shallowest northern well (AG-3) and most likely related to fertilizer sourced from the surrounding farms. Farming could also explain the TN value recorded below in the northern Rus aquifer well (AG-2). However it is harder to use explanation for the higher TN value recorded deeper in the northern UER well (AG-1). It is

possible that due to head differences, as shown in Figure 4-9, Section 4.3, abstraction in the area has induced a slight upward flow from the Rus well (AG-2) into the Dammam well (AG-3), effectively diluting the nitrogen in the Rus aquifer.

TN is greater in the shallowest aquifers as well as increase with depth in the southern and northern wells. TN increases from south to north, which is to be expected as there are a greater number of farms in the north relative to the south. Possible sources of nitrogen in addition to fertilizer could be bacteria, artificially injected waters which can contain treated effluent, domestic effluent and surface run-off which are often injected below 80m bgl. However, these sources are unable to be quantified or qualified.

5.3 Excess

5.3.1 Ca_{XS} and $\text{SO}_{4\text{XS}}$

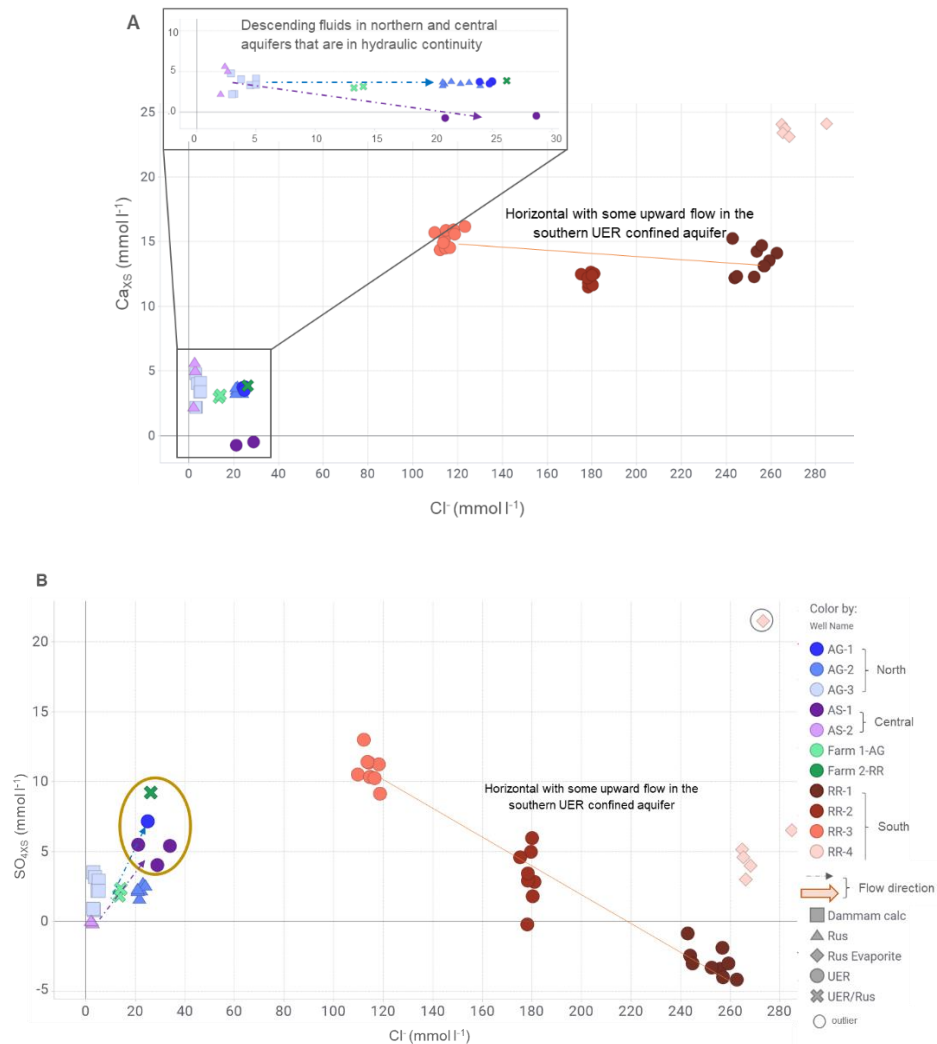
The southern wells (RR-1 to 4) show positive Ca_{XS} , with the Rus evaporite well (RR-4) recording significantly higher enrichment in Ca^{2+} and SO_4^{2+} (Figure 5-26). In the southern UER wells (RR1, 2 and 3) Ca_{XS} remains relatively constant, despite a progressive decrease in $\text{SO}_{4\text{XS}}$ with depth. Given the proximity of Rus Evaporites, the high $\text{SO}_{4\text{XS}}$ in all of the southern wells is most likely due to gypsum dissolution. A 1:1 $\text{Ca}_{\text{XS}}:\text{SO}_{4\text{XS}}$ molar ratio indicating gypsum dissolution trend is noted between the deep UER (RR-1) and the Rus evaporite (RR-4) wells. However, the two upper UER wells (RR-2 and 3) in the south lie below the gypsum dissolution 1:1 trend line suggesting an extra source of SO_4^{2+} or sink of Ca^{2+} .

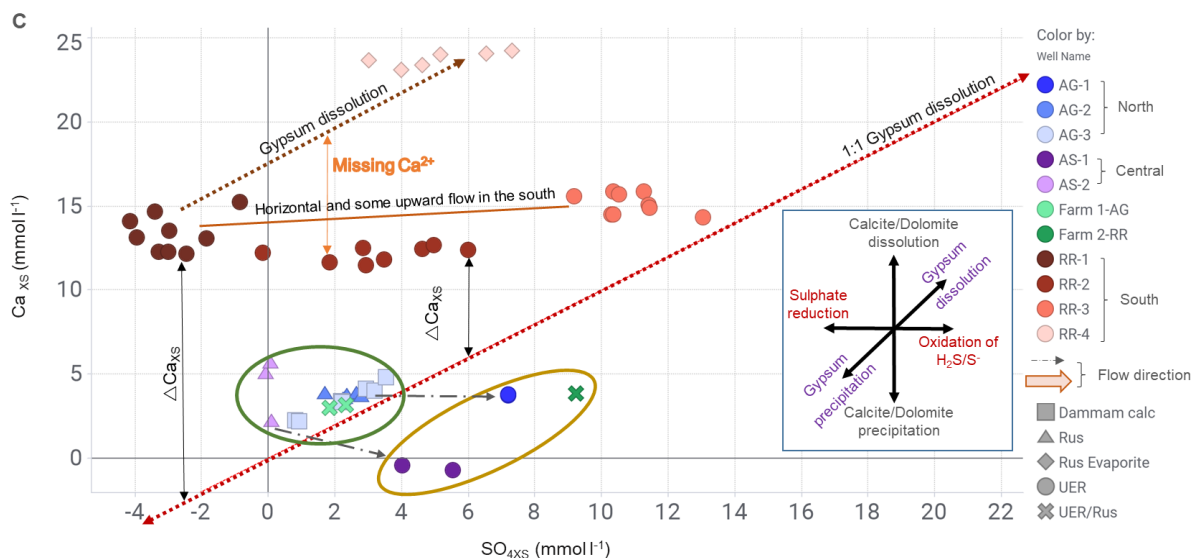
The shallow wells in the Dammam and Rus in the center (AS-2) and north (AG-2 and 3) record lower Ca_{XS} than the southern wells and SO_4 enrichment up to 4 mmol l^{-1} . The central (AS-1) and northern wells (AG-1) UER samples both have higher $\text{SO}_{4\text{XS}}$ and lower Ca_{XS} , with Ca_{XS} depletion in the central UER well (AS-1) (Figure 5-26A&B). The elevated sulfate concentrations could be due to longer residence time in the aquifer, where groundwater can interact with gypsum accumulating sulfate (Alsharhan, 2001).

Compared to the 1:1 molar ratio of $\text{SO}_{4\text{XS}}$ and Ca_{XS} (Figure 5-26C) expected for gypsum dissolution/precipitation, all the wells are enriched in Ca_{XS} relative to $\text{SO}_{4\text{XS}}$, apart from the deeper UER wells in the center (AS-1) and north (AG-1), and at the southern farm (Farm 2-RR). The southern wells recorded higher Ca_{XS} relative to the north, and Ca_{XS} decreases with depth in the center wells and marginally in the north. The southern wells display

horizontal stratification and could be attributed to horizontal flow dominating the general flow direction.

Figure 5-26 Variation in Ca_{XS} with SO_{4XS} as a result of water-rock interaction processes. Plot of Ca_{XS} and SO_{4XS} with Cl ($mmol\ l^{-1}$) (A and B), and Ca_{XS} with SO_{4XS} (C). Red dashed lines indicate gypsum dissolution / precipitation. ΔCa_{XS} is calculated as the difference between expected Ca_{XS} from 1:1 dissolution/precipitation of gypsum and the sample Ca_{XS} . In the southern wells, the missing Ca_{XS} relative to the dissolution trend is shown by the orange arrow. The green ellipse indicates the central and northern shallow aquifer wells and northern farm (AS-2, AG-2 and 3 and Farm 1-AG). The brown ellipse indicates the deep UER wells in the center and north, and the southern farm (AS-1, AG-1 and Farm 2-RR) recording higher SO_{4XS} . Arrows show descending waters in the central and northern aquifers that are in hydraulic continuity (blue/purple dashed arrow).





Positive or negative deviation in calcium excess beyond the 1:1 ratio indicates further geochemical processes are taking place, such as bacterially-controlled sulfate reduction (Stoessell, 1992). Other potential sources of enrichment could be from the dissolution of calcite, but there is no geochemical evidence of calcite allochems or cement within the UER dolomite. Limestone has been recorded in Dammam, but only in localised and intermittent lenses within the Rus and UER (Appendix D). Calcite dissolution cannot explain quantity of Ca_{XS} in the UER aquifers in the south, as most of the limestone is recorded above the water table and separated by the Rus evaporite. Limestone recorded above the water table including the very thin lenses in the UER (<1% maximum, Rivers et al, 2019a) within the southern core are most likely due to primary calcite precipitation.

5.3.2 Mg_{XS}

Further investigation was undertaken using $\Delta\text{Ca}_{\text{XS}}$ relative to Mg_{XS} , where $\Delta\text{Ca}_{\text{XS}}$ is the difference between the expected 1:1 gypsum precipitation/dissolution calculation, assuming $\text{SO}_{4\text{XS}}$ is a representative molar of gypsum precipitated (Ooi, 2018). Relative to the 1:1 molar ratio, the southern UER wells (RR-1 to RR-3) display Mg_{XS} enrichment relative to Saudi Arabia UER groundwaters, increasing in Mg_{XS} and a minor increase in $\Delta\text{Ca}_{\text{XS}}$ with shallower depth, indicating possible dedolomitization (Figure 5-27 and 5-27). The UER wells in the center (AS-1) and north (AG-1) record the lowest $\Delta\text{Ca}_{\text{XS}}$, rather lower than anticipated from both their Mg_{XS} and from $\Delta\text{Ca}_{\text{XS}}$ in the shallower wells at these sites. The central and northern upper aquifers of the Rus (AS-2, AG-2) and Dammam (AG-3) exhibit minor enrichment in both ΔCa and Mg_{XS} , possibly indicating minor dolomite dissolution

relative to the mixing line. The southern Rus well (RR-4) has been omitted from the trends as it sits in a thick of gypsum/anhydrite unit and is significantly enriched in both $\Delta\text{Ca}_{\text{XS}}$ and Mg_{XS} .

The central (AS-1 and 2) and northern wells (AG-1, 2 and 3) show positive to negative $\Delta\text{Ca}_{\text{XS}}$ values with depth, contrary to the trend exhibited in the south. Flow in the central and northern wells is downward, which is different to the southern wells which is considered to be dominated by horizontal flow with some upward movement due to the confined nature of the aquifer. Plotting $\Delta\text{Ca}_{\text{XS}}$ with the conservative tracer Cl^- , the dedolomitization trend of the southern wells is extrapolated to the central and northern UER wells that lie further along the proposed flow path (Figure 5-27A). It is possible that the two UER wells of the center and north initially followed a similar dedolomitization trend, but have lost Mg^{2+} . Lower Mg^{2+} concentrations relative to the expected concentrations associated with dedolomitization could be explained by the uptake of Mg^{2+} in the formation of magnesium-based clays such as palygorskite. The loss of Mg^{2+} cannot be attributed to primary dolomitization as there would also be a loss of Ca^{2+} . If magnesium was used in the creation of palygorskite/sepiolite, or exchanged with ions within the existing clays, the central and northern UER groundwaters could be following the dedolomitization trend and subsequently losing magnesium.

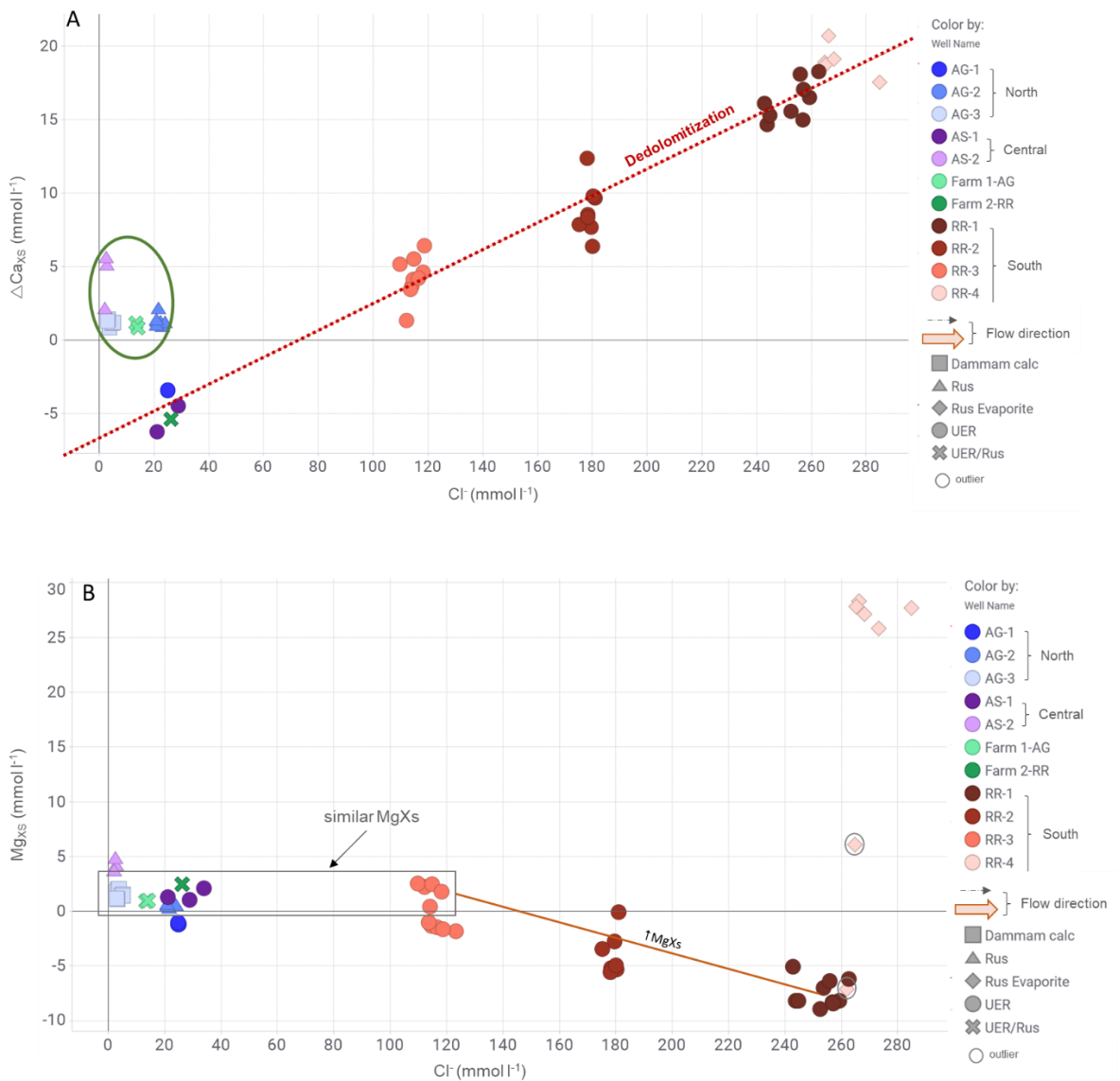
There is a source of Mg^{2+} causing the enrichment in Mg at the top of the UER in the south, as well as the Rus central well (AS-2), which also exhibited higher levels of Mg_{XS} (Figure 5-27). Given that $\Delta\text{Ca}_{\text{XS}}$ already accounts for dissolution of gypsum, the high Ca_{XS} at depth in the south could result from secondary dolomitization (replacement of calcite), calcite dissolution and/or exchange with Ca-rich clays. The decrease in Ca_{XS} moving shallower in the UER in the south could be due to dedolomitization, calcite precipitation, and/or primary dolomitization, although both the latter are considered unlikely.

Alternatively, if horizontal flow dominated with limited upward flow within the UER that was sampled at the various depths in the southern wells, the deeper waters may not be the source of the southern UER shallower waters. In this case, the deeper waters could be enriched in Ca^{2+} and depleted in Mg^{2+} as a result of less stoichiometric poorly ordered Ca-rich dolomites found in the southern core between 80 to 120m depth, recrystallizing to more stoichiometric well-ordered (Ca=Mg) dolomites with palygorskite (Ryan et al., 2019).

Another consideration is the possibility that $\Delta\text{Ca}_{\text{XS}}$ has been overestimated as this calculation does not include the effect of sulfate reduction process on $\text{SO}_{4\text{XS}}$. Hydrogen

sulfide odours was noted in all of the southern wells, and in the UER and Rus aquifer wells in the center and north. Low field DO levels in combination with hydrogen sulphide odours indicates the possibility of ongoing sulfate reduction.

Figure 5-27 A. Variation ΔCa_{XS} with Cl^- ($mmol\ l^{-1}$) highlighting the proposed dedolomitization trend. The green ellipse indicates the central and northern shallow aquifer wells and northern farm (AS-2, AG-2 and 3 and Farm 1-AG). B. Variation of Mg_{XS} with Cl^- ($mmol\ l^{-1}$) indicating similar Mg_{XS} values of the shallowest UER well in the south (RR-3), the central UER well (AS-1) and the northern wells of all three aquifers (AG1, 2 and 3) plus the two farms (Farm 1-AG, Farm 2-RR) (grey rectangular box).



Sulfate reduction in carbonates is common in aquifers (Domenico & Schwartz, 1999, Drever, 1997, Stoessell, 1992 and Morse & Mackenzie, 1990). Sulfate reduction is often associated with lower SO_4^{2+} concentrations, higher TOC, elevated alkalinity and lower pH. Such conditions are seen in the central Rus well (AS-2) (Figure 5-29), and could also occur, albeit at lower levels, in the other wells. Given the aridity of the climate, the input of organic matter into the aquifer would be expected to be limited.

Figure 5-28 Variation of $\Delta\text{Ca}_{\text{XS}}$ with Mg_{XS} for all groundwater samples with expected water-rock interactions. In the southern wells, the waters are depleted in Mg increasing with shallower depth, and vice versa for Ca which can lead to replacement of dolomite with calcite. This is similar to central and northern UER wells indicating possible dedolomitization. However, the deeper waters may simply just be enriched in Ca^{2+} and depleted in Mg^{2+} which could be due to Ca-rich less stoichiometric dolomites have been recrystallized to more stoichiometric ($\text{Ca}=\text{Mg}$) dolomites. The central and northern wells show minor Ca^{2+} and Mg^{2+} depletion possibly due to exchanging with Na in clays. The grey rectangular box are wells with similar Mg_{XS} values.

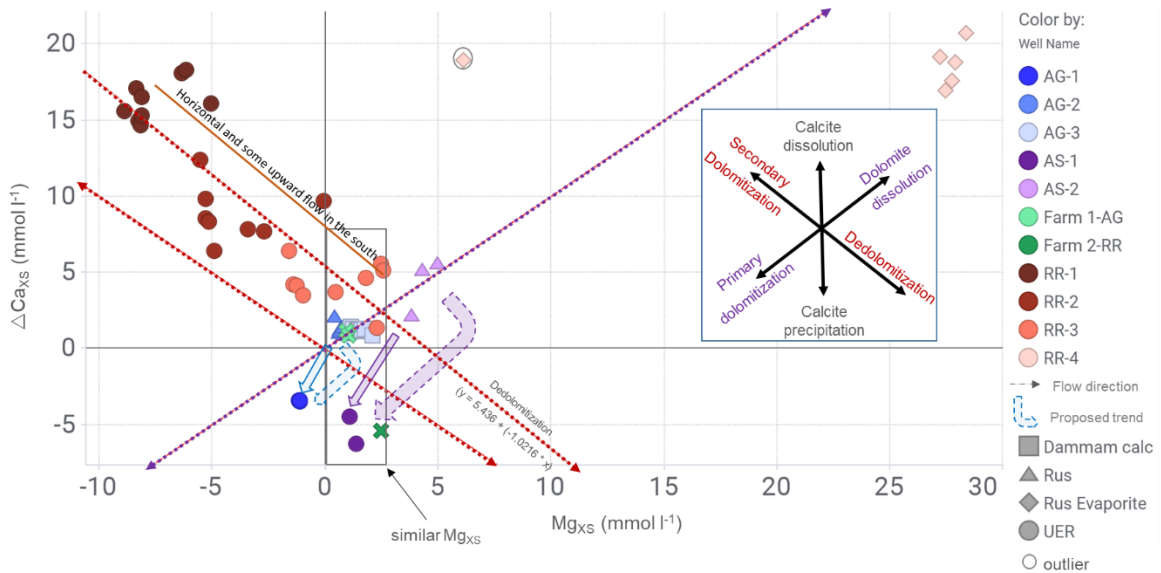
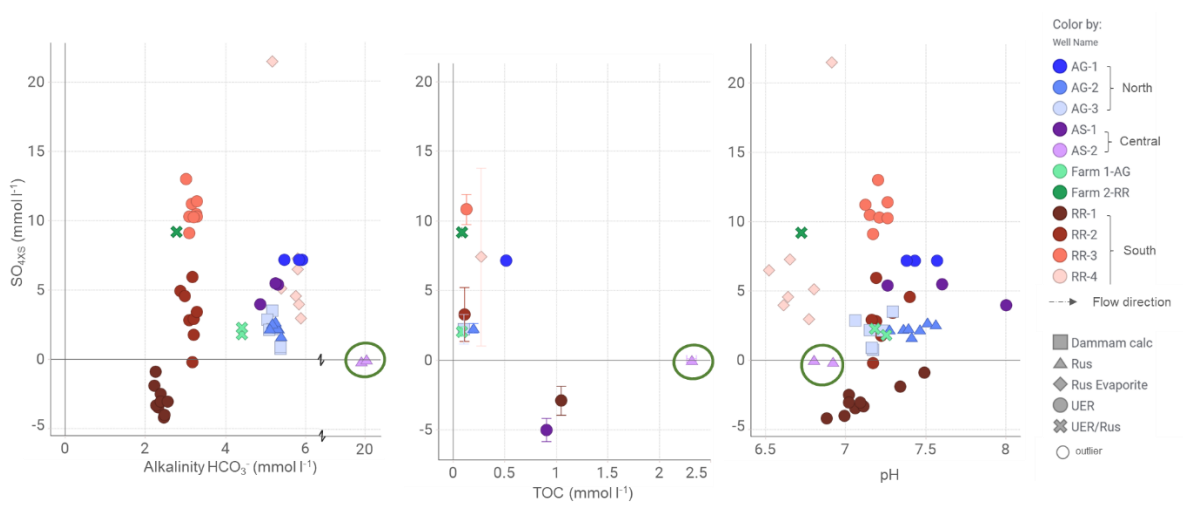


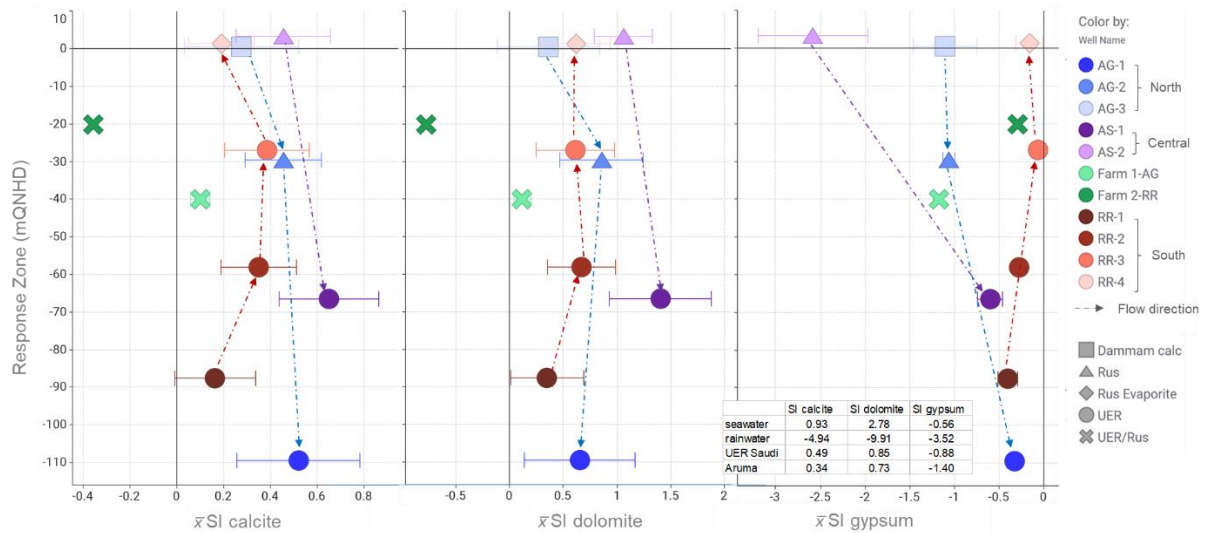
Figure 5-29 $\text{SO}_{4\text{XS}}$ with alkalinity (HCO_3^-) indicating lower SO_4 levels with respect to high alkalinity and TOC, and lower pH, specifically the central Rus aquifer (AS-2) (green circle)



5.4 Modelling (PHREEQC)

In all but one well groundwaters (Figure 5-30), were marginally saturated with respect to calcite and slightly more with respect to dolomite. Groundwaters were calcite and dolomite undersaturated in the southern farm (Farm 2-RR). Both SI for calcite and dolomite slightly increased with depth in the central and northern wells, but decreased with depth in the southern wells. All wells were undersaturated with respect to gypsum. The southern well waters were only marginally gypsum undersaturated approaching equilibrium at the top of the UER.

Figure 5-30 $\bar{x} \pm 1\sigma$ for SI calcite, dolomite and gypsum with depth



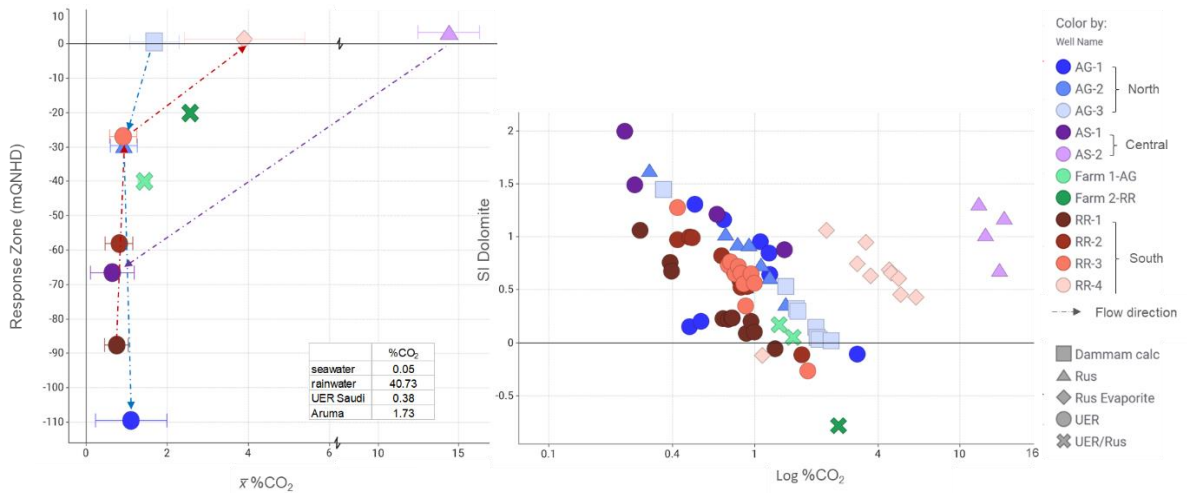
P_{CO2}

P_{CO_2} calculated in PHREEQC, was converted into %CO₂ for analyses (Figure 5-31). CO₂ was high (>1%) in the three wells at the water table (RR-4, AS-2 and AG-1), particularly the central well (AS-2) where concentrations were an order of magnitude higher. High CO₂ was also recorded in the both the southern and northern farm wells, while CO₂ in all of the UER wells was less than the overlying shallower aquifers. In the north, CO₂ of the Rus and UER waters were similar.

Elevated CO₂ values in the central Rus well (AS-2) are most likely the cause of the lower pH which drives dissolution of carbonates. Sources of CO₂ may include bacterial oxidation of natural organic materials, artificially injected TSE waters or recharge containing high levels of organic fertilizers. This organic matter oxidation leads to depletion of dissolved oxygen described earlier, followed by sulfate depletion once sulfate becomes the terminal electron acceptor.

With the addition of CO₂, saturation with respect to carbonate minerals decreases. Given the dolomitic nature of aquifers, groundwaters would be expected to be at equilibrium with dolomite. The dolomite supersaturation calculated for all waters suggests a degree of CO₂ degassing may have occurred once samples were brought to the surface during sampling. Variations noted within each well do not appear seasonal.

Figure 5-31 $\bar{x} \pm 1\sigma$ CO₂ with depth highlighting higher CO₂ in the groundwaters at the water table. SI Dolomite with log CO₂ indicating an increase in dolomite supersaturation as CO₂ levels decrease within the primarily dolomitic aquifers.

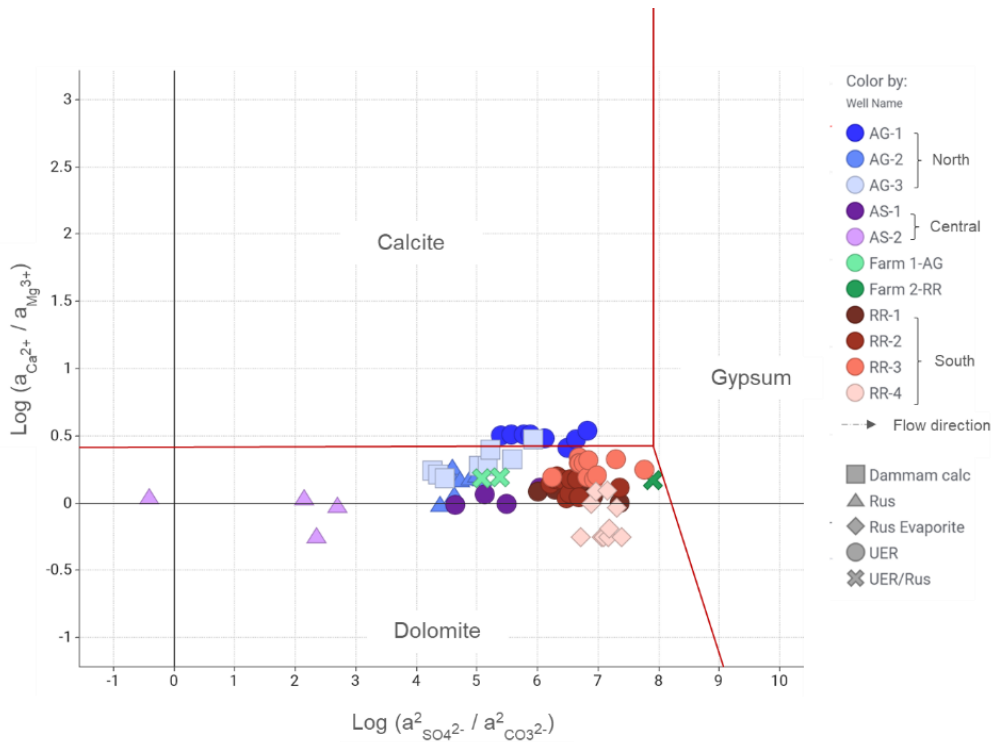


5.5 Phase diagrams

Activity ratios, calculated using activities calculated by PHREEQC were plotted in a phase diagram and relate to the stability of calcite, dolomite and gypsum to identify which minerals may have reacted with groundwater samples (Ooi, 2018, Moore et al, 2010). The phase boundaries, which are based on the log of equilibrium rate constants for the mineral reactions as defined in Table 2 of Moore et al. (2010), are considered representative of the reactions within Qatar’s shallow aquifers.

All of the project samples plot within the dolomite field (Figure 5-32) indicating the samples have interacted primarily with dolomite, apart from the northern UER well (AG-1). The UER well in the north sits on the boundary with calcite indicating this water has reacted with both minerals, and possibly the intermittent calcite lenses found in the Dammam. The upper UER in the southern well (RR-3) and southern farm (Farm 2-RR) plot towards the gypsum boundary indicating a level of interaction with gypsum. The Rus evaporite well (RR-4) is a distance from gypsum boundary and could suggest ongoing interaction with clays.

Figure 5-32 Phase diagramme showing the stability of calcite, dolomite and gypsum with respect to activity ratios in groundwater at 25°C and 1 atm pressure.



5.6 Conclusion

Groundwater composition in the wells remained relatively constant over the duration of the monitoring period (up to 18 months). Ca:SO₄ ratios indicate groundwaters in the south are actively dissolving gypsum, and to a lesser degree in the central and northern wells, although this may in part be inherited from sulfate-rich UER groundwaters moving north-easterly from Saudi Arabia.

Stratification of waters, based on differences in ion concentrations, occurred at all locations. In the north, meteoric recharge results in shallow groundwaters that are less evolved, and with increasing depth the waters become dominated by equilibration with the dolomite aquifer. In the south, stratification indicates limited mixing with the underlying saline groundwaters.

Gypsum dissolution appears to be the primary driver of the various groundwater signatures recorded. Sharaf (2001) recorded the UER groundwaters as saturated with respect to calcite and dolomite and under-saturated with respect to gypsum. Dedolomitization has been noted in the southern wells and also, to a lesser degree, in the central and northern UER wells. Due to the presence of sometimes thick lenses of clays (up to maximum 1m) within all formations, it is likely that groundwater chemistry has been influenced with ion exchange with the clays, giving atypical geochemical signatures. The central and northern upper aquifers of the Rus and Dammam exhibit minor enrichment in both $\Delta\text{Ca}_{\text{XS}}$ and Mg_{XS} relative to rainwater, possibly indicating minor dolomite dissolution and likely driven by high CO₂.

Total organic carbon levels are much higher than anticipated and CO₂ generated by organic matters could be driving the dissolution of carbonate minerals, specifically in the Rus aquifer in the centre of the country and to a lesser degree in the other wells.

Definitive linkage of evidence of rock-water interaction from water chemistry with diagenetic signatures seen in the rocks is difficult as the current regional and local groundwater flow systems governed by sea level and have only been operation in the last 7000+ years (Puls, 2016). This is in addition to karstified fractured bedrock, where groundwater movement is primarily through joints, fissures and bedding-plane openings (Kalbus et al., 2011, Sharaf, 2001, Al Bassam et al., 1997), and anthropogenic activities of abstraction and injection which further alter water-rock interactions.

6.0 DISCUSSION AND CONCLUSION

6.1 Introduction

Permeability characteristics of Qatar's bedrock can be established by observing lithology and groundwater carbonate sediments and the groundwaters hosted within them are susceptible to modification by water-rock interaction (Ahm, 2018). Lithology, secondary porosity and confined aquifer conditions, combined with ongoing seawater intrusion, natural and anthropogenic recharge and subsequent mixing dominate the evolution of the shallow aquifers groundwaters in Qatar (Al Bassam et al., 1997). Post-depositional diagenetic processes can be understood by analyzing rock and groundwater geochemistry, as aqueous solutions are relatively sensitive indicators of diagenesis (Whitaker & Smart, 2007a).

The shallow aquifers of Qatar have been categorized into three distinct groundwater 'Domains' on the basis of their geochemical characteristics, which are not simply related to geological formations that host the waters. The characterization and grouping into Groundwater Domains as per parameters ascertained during the project (Figure 6-1), relate to the key physical, water-rock and diagenetic processes operating at the present time within the shallow aquifers. The full extent the characteristics of Qatar's groundwaters cannot be determined from this project.

6.2 The Upper Domain

The Upper Domain is based on hydrogeological characteristics of the central and northern Dammam and Rus wells, including the northern farm (AS-2, AG-2 and 3, Farm 1-AG) and are heavily influenced by meteoric recharge (Section 2.9). Due to abstraction, increasing sea-water intrusion and ongoing dissolution of gypsum (Rahimpour-Bonab et al., 2009, Alsharhan et al., 2001, Eccleston et al., 1981), this Domain exhibits slightly saline conditions with SEC values ranging from 1.1 to 3.9 mS cm⁻¹. Localised differences may occur where depressions act as internal catchments directing meteoric recharge (Eccleston et al., 1981).

The Upper Domain is typically <3 mS/cm and extends from the water table in the central and north of the country down to where groundwater notably increases in SEC (> ~3 mS/cm)(Section 4.5.2). The increase was recorded at -38.0m QNHD (84.5mbgl) in the central well, and somewhere between the Rus (AG-2) and UER (AG-1) well in the north although a definitive boundary was unable to be determined in the north due to the potential

of the borehole collapse during site works. This increase in SEC is considered to represent the transition from fresh/slightly saline conditions into moderately saline groundwaters (SEC classifications are defined in Section 2.10).

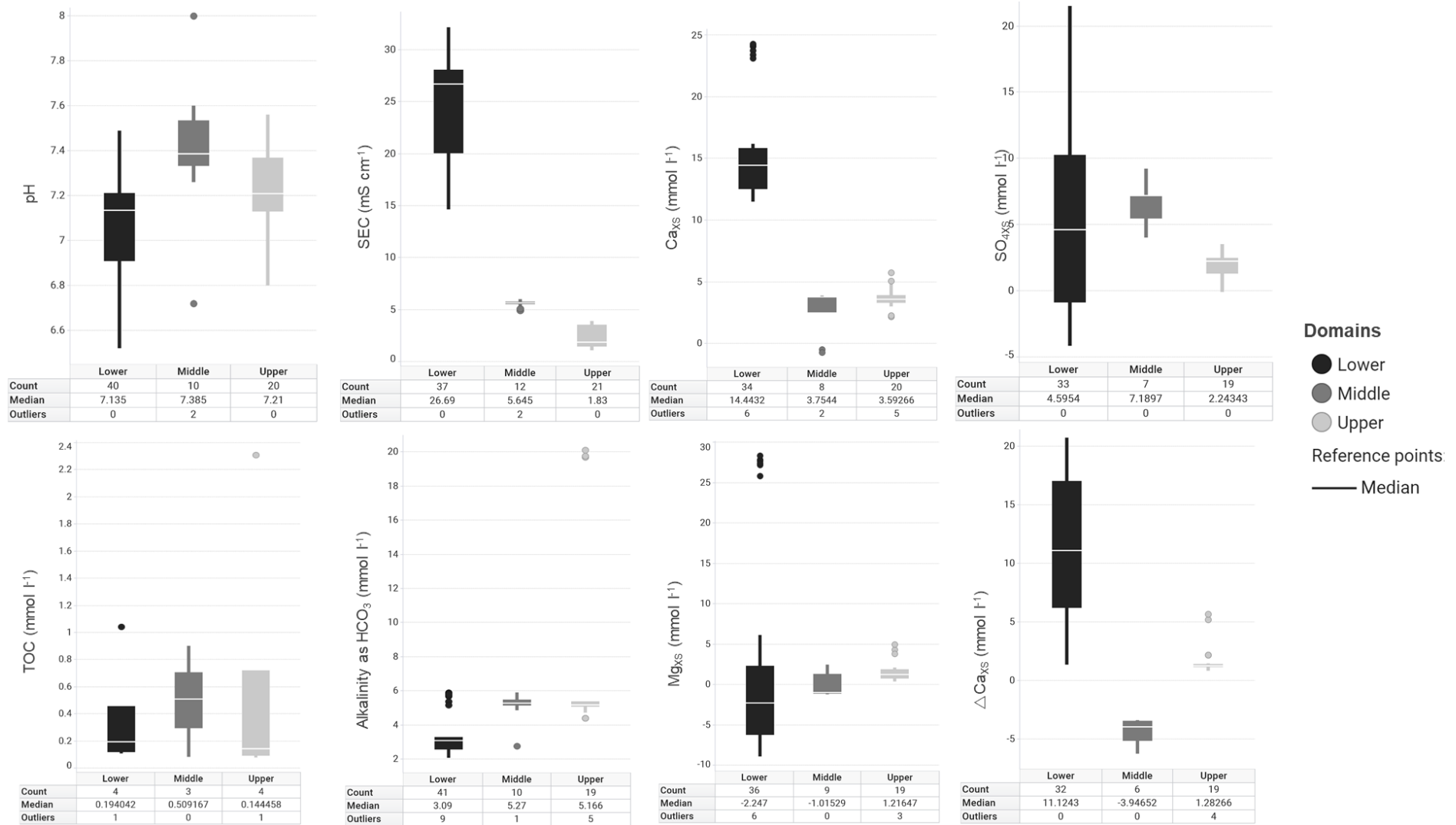
The depth and extent of the Upper Domain was not dependent on lithology, but primarily controlled by the higher saline underlying aquifers and intruding seawaters. It extends through the Dammam and Rus into the very top of the UER. It has shown to fluctuate vertically and laterally in response to hydrostatic pressures, such as the change of piezometric head following significant rains in early 2018 (Section 4.3). These groundwaters are most likely the historical potable fresh water lens, and have experienced a reduction in piezometric head of ~-6.5m since 1958 (Section 4.2).

Geologically, the Upper Domain contains the Dammam comprising both calcite and dolomite, becoming dolomite with varying quantities of clays in both the Rus and very uppermost UER. Analysis of scale-dependent permeability (Section 4.6) proved calcite was of low permeability ($<10^{-1}D$) and porosity ($<18\% \text{ ØHe\%}$) whereas dolomite and dolomites with clays had large ranges in both permeability (10^{-4} to $10^{+1}D$) and porosity (10 to 45+ ØHe\%).

Historically, the main hydrochemical process within this Domain has been identified as carbonate and sulfate dissolution (Alsharhan et al., 2001, Lloyd et al, 1987, Eccleston et al., 1981). This project records these groundwaters to be relatively fresh and though undersaturated with respect to gypsum, sulfate concentrations are considered to be inherited from the migrating more sulfate-rich waters from the south. Sulfate in the form of gypsum was not recorded in the rock core mineralogy in the north (Rivers, 2019a).

Carbonate dissolution is considered active in the central Rus well (AS-2) where anomalously high alkalinity ($\bar{x} = 19.9 \text{ mmol l}^{-1}$) and relatively low pH ($\bar{x} = 6.9$) readings were recorded, in addition to low SO_4 (0.1 mmol l^{-1}) and $\text{SO}_{4\text{XS}}$ (0.01 mmol l^{-1}). These deficiencies in sulfate concentrations may be due to bacterially controlled sulfate reduction which can lead to carbonate dissolution (Drever, 1997). High TOC ($2.3 \pm 0.1 \text{ mmol l}^{-1}$) and CO_2 (14.5%) values recorded in this well, in addition to a prominent hydrogen sulfide odour, are all signatures of anoxic conditions and sulfate reduction (Morse & Mackenzie, 1990).

Figure 6-1 Box plot of the main geochemical characteristics for each Domain including pH, SEC, alkalinity (as HCO₃), TOC, Ca_{XS}, Mg_{XS}, SO_{4XS} and ΔCa_{XS}



The process of bacterial decomposition leading to an increase in CO₂ levels and subsequently carbonic acid (Equation 1-6, Section 2.11), contributes to the alkalinity and is the prominent driver for carbonate dissolution (James, & Jones, 2016, Chidambaram et al., 2011). This phenomena has been reported within modern shoal-water carbonate sediments in the Bahamas (Morse & Mackenzie, 1990), the mixing of fresh and spring waters from late Pleistocene limestones in Barbados with adjacent Atlantic sea-waters (Stoessell, 1992) and mixing zones of cenotes in the Gulf of Mexico (Stoessell, 1993) which experience high inputs of organic matter and often associated with alkalinity excesses (Stoessell, 1992), deficiencies in sulfate and low pH, leading to carbonate dissolution (Morse & Mackenzie, 1990).

Elevated TOC values have also been recorded in various locations across the country (Kuiper, 2015) and elevated TOC levels could be the result of naturally occurring organic acids and bacteria. However, it is considered that injection and irrigation using TSE and other waste waters, may be a significant additional contribution. Exchange sites on clay minerals can also enhance the dissolution of carbonate minerals by the uptake of Ca²⁺ and Mg²⁺ and release of Na⁺ (Plummer, 1990).

An increase in alkalinity can lead to the precipitation of carbonate minerals, although during the early reduction stages, minor sulfate reduction can result in undersaturation of carbonate minerals and subsequent dissolution of carbonates (Alsharhan et al., 2001, Whitaker & Smart, 2007b). A lower pH can also have a greater impact than that of increased alkalinity (Morse & Mackenzie, 1990), leading to carbonate dissolution. It is therefore possible carbonate dissolution is ongoing in the Upper aquifer albeit to a lesser degree than the central Rus well.

The Upper Domain is enriched in Ca²⁺ and SO₄²⁻ which is most likely from gypsum dissolution, however this would have to have been inherited as there was no sulfate in the form of gypsum or anhydrite recorded in the rock core (Rivers et al., 2019a). Other sources of sulfate could include dry deposition followed by subsequent infiltration but recent analyses of dust in respect solar polar efficiency recorded calcite and dolomite to be the most abundant minerals (Javed, 2017). Water for irrigation and dust management could also contain elevated sulfates as often excess water from dewatering and desalinization is pumped across country and utilized elsewhere. Sulfate reduction and extent of any gypsum dissolution could be investigated by sulfur isotope analyses and is recommended for future work.

6.3 The Middle Domain

The Middle Domain is defined by the physical and hydrochemical properties of the central and northern UER wells (AS-1 and AG-1), and the southern Rus/UER farm well (Farm 2-RR). These groundwaters have slightly higher SEC values ($<4 \text{ mS cm}^{-1}$) than the Upper Domain, but are not considered saline as they contain limited seawater content as local seawater SEC ranges from 61.0 to 65.1 mS cm^{-1} (Rivers et al., 2019b, Ooi, 2018). Based on borehole profiles and monitoring salinity values (SEC), the Middle Domain represents moderately saline conditions (Section 2.10 and based on MDPS, 2017 and Eccleston et al., 1981) that are constrained by salinity concentrations from the underlying aquifers and encroaching sea.

The Middle Domain is hosted in the primarily dolomitic UER with intermittent small lenses of calcite ($<200\text{mm}$) in the central and northern wells. Karstic features were recorded at lower depths within the central borehole (AS) from -16 to -54 mQNHD (63 down to ~ 101 mbgl) and the northern borehole (AG) from -64.9 to -82 mQNHD (~ 74.0 to 91.2 mbgl).

Permeability and porosity characteristics of the geology of the Middle Domain do not appear to be dependent on formation, and whether or not clay is present. Both have wide ranges, for permeability from 10^{-3} to 10^{+1} D and porosity 5 to 45+ \%He . Laboratory core analyses for permeability and porosity did not capture the numerous results above 10^{+1} (D) in the UER, which must relate to secondary permeability of fractures, discontinuities, vugs and karsts.

The Middle Domain is distinctly gypsum undersaturated, implying the potential for ongoing sulfate dissolution. Nevertheless, sulfate excesses are elevated, which can be attributed to prior and continuing dissolution of the Rus evaporite and subsequent mixing with lower aquifers. The lower aquifer from the UER are themselves enriched in sulfate, as sulfate concentrations lie within the mixing boundary of Saudi Arabia UER source groundwaters waters and seawater (Section 5.2.4). Therefore the appearance of ongoing dissolution of sulfate can also be associated with long residence time within the aquifer, as contact between bedrock and groundwater over distance with sufficient time results in an increase of sulfate dissolution (Alsharhan et al., 2001).

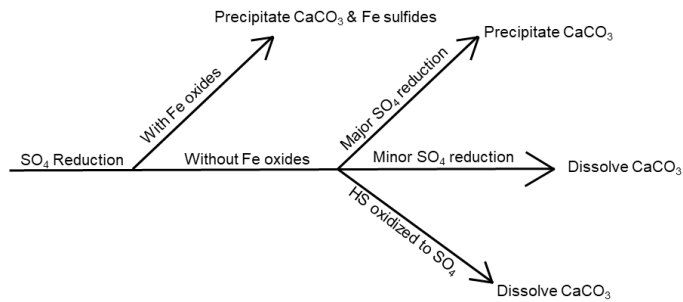
Continuing dissolution of gypsum leads to supersaturation of calcite and dolomite (Eccleston et al., 1981). The saturation indices for both calcite and dolomite were slightly positive in the Middle Domain, indicating saturation. The dissolution of gypsum could drive other processes

such as de-dolomitization (Section 5.3). The ratio of $\Delta\text{Ca}_{\text{XS}} : \text{Mg}_{\text{XS}}$ does not clearly indicate de-dolomitization but a de-dolomitization trend is present when extrapolating the expected de-dolomitization trend for $\Delta\text{Ca}_{\text{XS}}$ relative to a conservative tracer (Cl^-) from the southern wells through the central and northern UER wells (Figure 5-26). This apparent lower Mg^{2+} concentration of the Middle Domain could be explained by the uptake of Mg^{2+} by clays (Plummer et al., 1990), specifically for the creation of magnesium-based clays such as palygorskite which have been identified throughout the core samples (Ryan, 2019). De-dolomitization is also possibly ongoing in the Lower Domain, however there are other hydrochemical process to consider and they are further discussed in the Lower Domain.

Alternatively, the lower Mg^{2+} concentrations in the Middle Domain, relative to 1:1 dolomitization ratio (Figure 5.27) may be due to primary dolomitization, which is unlikely due to the level of obliterative dolomitization, subsequent recrystallization and karstification of the rock core recorded in the Middle Domain (Rivers et al., 2019a).

Salinity and TDS values of the Middle Domain are higher than fresh water, which in-turn increases the potential for calcium and magnesium ions to be exchanged for Na^+ and other ions such as K^+ and Si^{4+} , on the surface of clay minerals (Eccleston et al., 1981) and can cause dissolution of carbonate minerals (Plummer et al., 1990). Dissolution of carbonate minerals by anoxic sulfate reduction may also be ongoing due to the presence of hydrogen sulfide odours, slightly elevated alkalinity and higher TOC measurements and subsequent increase in CO_2 .

Figure 6-2 Schematic drawing showing pathways for sulfate-reduced mixing zone fluids and resulting dissolution in the mixing zone (from Stoessell, 1992)



The possibility of re-oxidation, or back-oxidation, of hydrogen sulfide which in turn effects sulfate reduction by lowering the pH producing carbonate dissolution (Stoessell, 1992) (Figure 6-2), must also be considered. There are strong hydrogen sulphide odours in the

waters samples from the Middle Domain and pyrite is almost non-existent in any of the rock cores (Rivers et al., 2019a). Re-oxidation can occur when waters become oxygenated if exposed to the atmosphere, either by natural processes such as moving through fractures or anthropogenic activities such as abstraction, dewatering or injection.

6.4 The Lower Domain

The Lower Domain is the most saline of the Domains, increasing in salinity with depth and representing groundwaters of the Upper UER and Rus Evaporite in the south of the country. The hydrochemical characteristics of the Lower Domain are derived from the southern UER wells (RR-1 to 4) and are summarized below. It must be noted that the groundwaters in Rus (RR-4) exhibit a different geochemical signature due to its position within an evaporitic aquiclude

The Lower Domain is hosted in the UER where permeability and porosity are varied. Permeability ranges (10^{-3} to 10^{+1} D) as does porosity (5 to 45+ ØHe%) for both pure dolomite and dolomite with clays of the UER. Characteristics of the Rus Evaporite gypsum/anhydrite component were unable to be tested in the laboratory, however it is known to be of very low permeability and porosity (Rivers et al., 2019a, Eccleston et al., 1981).

Groundwater flow of the Lower Domain is controlled by head in eastern Saudi Arabia and moves in a northeasterly direction in confined to semi-confined conditions, as there numerous localised depressions which penetrate the Rus connecting the UER (Section 2.4). Salinity increases eastwards from Saudi Arabia towards the Qatar peninsula (Al Bassam et al, 1997, Eccleston et al., 1981). Historical SEC values recorded in the upper UER in Qatar typically exceed 40 mS cm^{-1} , and localised higher salinity (SEC) concentrations at the top of the UER and Rus aquifer have been reported that can be attributed to the dissolution of the Rus evaporite (Eccleston et al., 1981).

Previous chemical analyses of UER groundwaters in Saudi Arabia record them to be dominated by sulfate, as gypsum dominated evaporite and argillaceous facies become prevalent and available for dissolution towards the east of Saudi (Lloyd et al, 1987). De-dolomitization with ion exchange was documented to be ongoing within the thin shale/clay horizons (Al Bassam et al, 1997) and dissolved hydrogen sulfide was recorded throughout the formation (Alsharhan et al., 2001). In Qatar, UER groundwaters are recorded as been saturated with respect to calcite and dolomite and under-saturated with respect to gypsum (Sharaf, 2001).

Within the Lower Domain, dissolution of gypsum is occurring as signified by groundwaters that are elevated in $\text{SO}_{4\text{XS}}$, particularly in the Rus Evaporite. They are undersaturated with respect to gypsum indicating the potential for continued dissolution. This source of sulfate and calcium could lead to precipitation of calcite, with the donation of a carbonate ion from possible dolomite dissolution, or bicarbonate from sulfate reduction (Plummer et al., 1990).

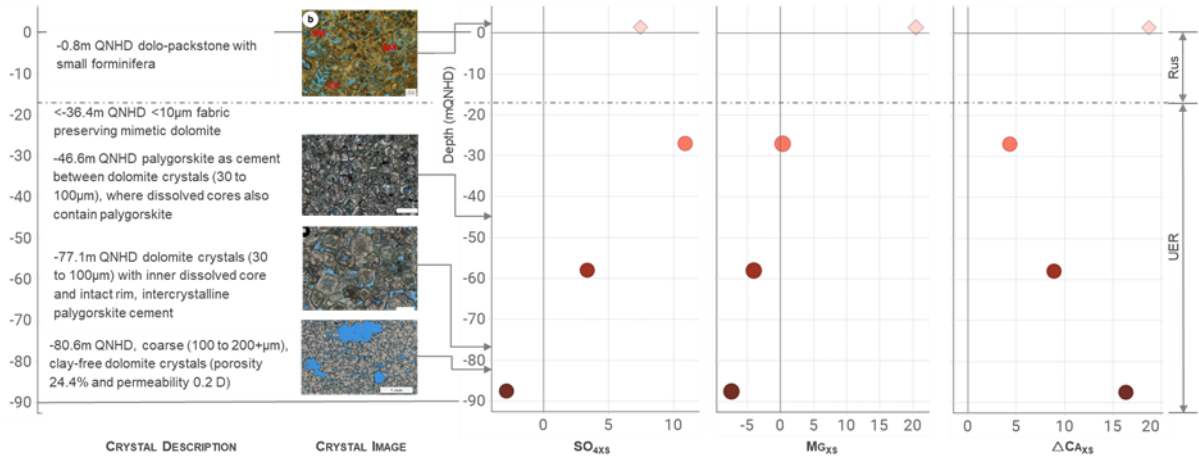
Ca_{XS} displays a very minor decrease with decreasing depth (as percentage of seawater increases) whereas $\Delta\text{Ca}_{\text{XS}}$ increases. Both Mg_{XS} and $\text{SO}_{4\text{XS}}$ increase moving up to the top of the UER (shallower depth,) and these trends reflect a number of water-rock interactions (Figure 6-3). Excess calculations indicate de-dolomitization (Figure 5-27) where calcium rich waters from the dissolution of gypsum hosted in the Rus evaporite move through dolomite removing Mg^{2+} from the rock matrix replacing it with Ca^{2+} (Al Bassam et al., 1997).

Signs of de-dolomitization include a systematic increase in both calcium and magnesium as sulfate increases, associated with a decrease in pH and increase in P_{CO_2} which is likely to be fueled by the higher TOC levels (also reported in the Madison of western USA in Plummer et al., 1990). These trends are highlighted using Ca_{XS} and Mg_{XS} relative to $\text{SO}_{4\text{XS}}$, as actual sulfate concentration changes are a function of the irreversible progress of gypsum dissolution (Figure 6-4) (Plummer et al., 1990). Although there are variations from the expected de-dolomitization 1:1 $\Delta\text{Ca}_{\text{XS}} : \text{Mg}_{\text{XS}}$ ratio, differences such as lower Mg^{2+} concentrations, may be attributed to various processes including the upflow and subsequent mixing with the lower more saline UER waters. A decline in absolute Mg^{2+} can indicate mixing with saline waters (Al Bassam et al, 1997).

It is possible that groundwaters within the monitoring zone of the southern Upper UER did not gain Mg^{2+} and loose Ca^{2+} . Horizontal flow dominates, with limited upward flow within the southern aquifer that was sampled, as such the deeper waters may not be the source of the southern UER shallower waters. Rather, the deeper waters are enriched in Ca^{2+} and depleted in Mg^{2+} as a result of less stoichiometric poorly ordered Ca-rich dolomites found in the southern core recrystallizing to more stoichiometric well-ordered (Ca=Mg) dolomites with palygorskite (Ryan et al., 2019).

Figure 6-3 Mineralogy of the southern well showing dolomite, crystal size and palygorskite content relative to geochemical groundwater excess. Crystal size increases with depth, and decreases in palygorskite below -79.4m (123.0mblg) (Rivers et al., 2019a, Ryan et al., 2019). At depth, groundwater Mg_{XS} is depleted and enriched in $\Delta\text{Ca}_{\text{XS}}$. Moving

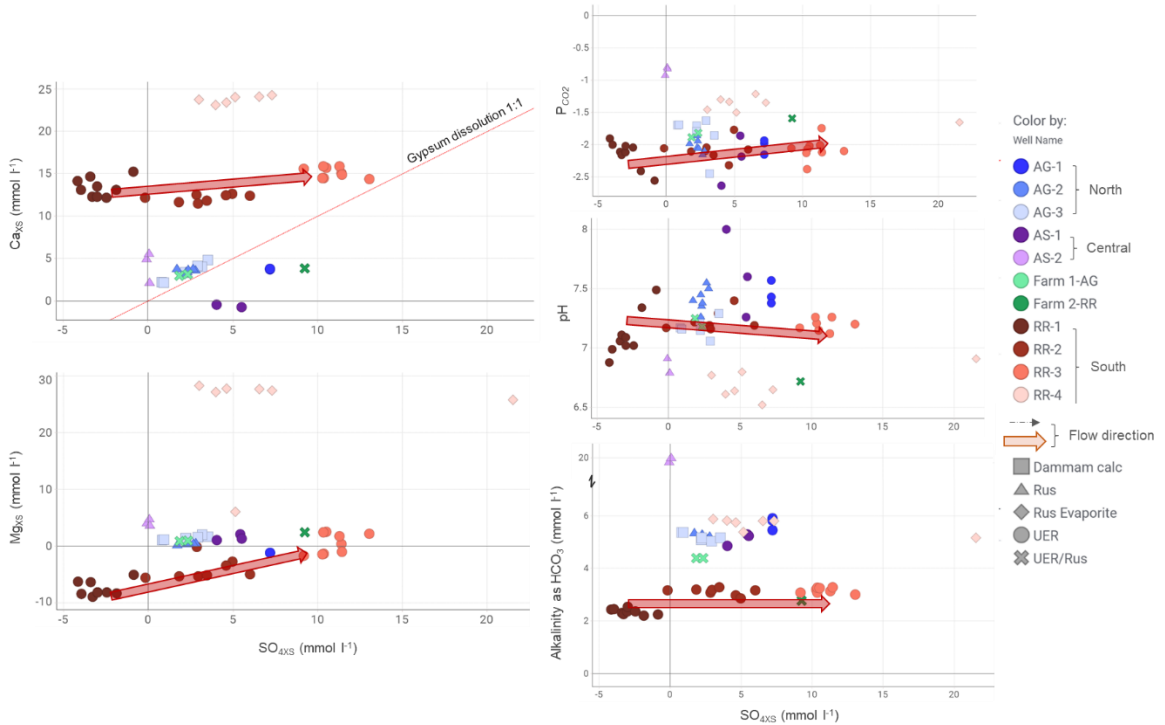
up the profile towards the top of the UER, Mg_{XS} increases and ΔCa_{XS} decreases. This trends could represent de-dolomitization or the recrystallization of poorly ordered Ca-rich dolomites to more stoichiometric well-ordered (Ca=Mg) dolomites.



To further understand water-rock interactions of the Lower Domain, sequential chemical processes associated with de-dolomitization, as documented in Plummer et al., 1990, were analysed. Plummer documents groundwaters systematically increase in both calcium and magnesium and sulfate due to gypsum dissolution, such that waters become saturated with respect to calcite leading to calcite precipitation. This in-turn decreases pH and increases P_{CO_2} causing dolomite undersaturation, subsequent dissolution and an increase in dissolved magnesium (Figure 6-4). As part of the de-dolomitization process, which includes the dissolution of gypsum and dolomite, their combined mass of which exceeds the mass of calcite precipitated, results in a net increase of dissolved calcium and a decrease in alkalinity. Many of these trends are typical of the Lower Domain groundwaters, although not definitively as alkalinity remains relatively similar irrespective of depth.

Dedolomitization can lead to the precipitation/replacement of calcite crystals in the bedrock, however no calcite was recorded in any of the rock core, nor as calcite cement or micrite (Rivers et al., 2019a). This lack of calcitization could be due to the current regional and local groundwater flows being a relatively young (+7000 years, Puls et al, 2016) and established in response to the Holocene rise in relative sea-level leading to the development of a freshwater body within rock that had formerly been within the vadose zone for an extended period of time (Eccleston et al., 1981). Alternatively, and possibly in addition to, the lack of alteration seen in the cores results from alteration occurring as a result of flow of groundwater that was focused by secondary permeability (Sharaf, 2001).

Figure 6-4 Possible dedolomitization trends comparing SO_{4XS} with Ca_{XS} , Mg_{XS} , pH, P_{CO_2} and alkalinity. There is increase in Ca_{XS} , Mg_{XS} and P_{CO_2} in the southern wells (red arrow) accompanied by a minor decrease in pH (red arrow), as gypsum dissolution progresses.

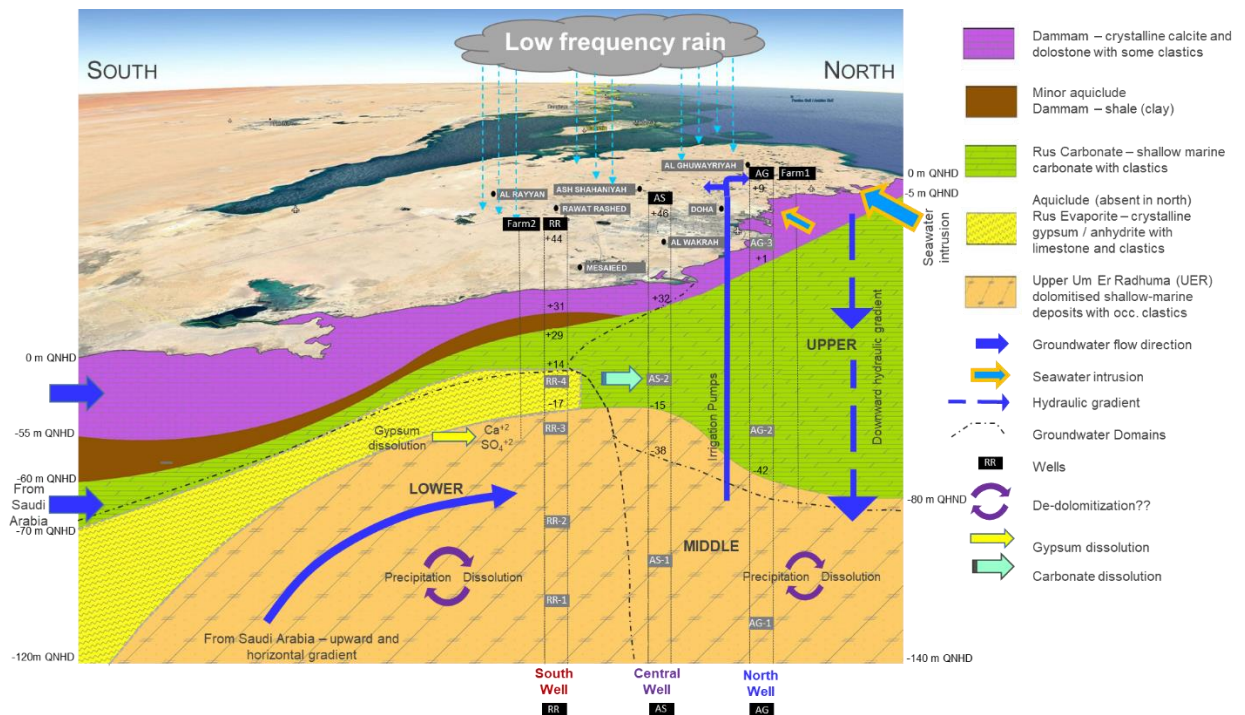


Clays have been recorded in all of the cores including illite, smectite and importantly palygorskite which can comprise up to 66% by volume of the clay recorded in UER, 47% in the Rus and as 100% in the Dammam (Rivers et al., 2019a, Ryan et al., 2019). Clays can have a profound role in groundwater geochemical processes due to their ion exchange capacity, for instance permitting uptake of Ca^{2+} and Mg^{2+} and subsequent release of Na^+ leading to carbonate dissolution (Drever, 1997; Plummer et al., 1990). The clay mineral transformation from smectite to illite releases Mg^{2+} during deep burial (Tucker, 2009), however these shallow deposits are understood not to have yet experienced deep burial. The formation of palygorskite which is concurrent with the post-dolomitization dissolution stage, following the recrystallization process of non-stoichiometric poorly-ordered dolomite into relatively well-ordered dolomite (Ryan et al., 2019) can lead to an enrichment of Ca^{2+} . Quantifying clays importance has not been established in this project however their impact must be included in conceptual analyses of groundwater characterisation.

6.5 Conceptual Model

A conceptual groundwater model is composed of “two systems, both physical and chemical, to aid in the description, explanation, prediction and control of hydrogeological conditions” (Tóth, 1970). The conceptual model that has been developed by this project for Qatar (Figure 6-5) shows the complexity of the shallow aquifers, their (approximate) geometric distribution and subsequent movement, and their chemical composition. Although not all parameters have been included, such as regional and local fluid flow velocity and this model is developed from a limited number of sites at which information has been gathered on the vertical distribution of groundwater, a conceptual model can aid in understanding the current hydrogeological regime and how it might change.

Figure 6-5 The Conceptual groundwater model comprises a lithological cross section, groundwater Domains (Upper, Middle and Lower), groundwater flow direction and the main geochemical processes affecting the waters sampled from the project wells (RR, AS, AG and both farms), as well as historical wells C14 (AM3A) and AMA1 (Eccleston et al., 1981). The Upper Domain is distinguishable as being the least saline, near-fresh waters in the central and north of the country. These waters sit, or float, on top of the Middle Domain which represents the top of increasing saline conditions. The Lower Domain records the highest salinity, is a semi to confined aquifer due to the presence of both the Rus Evaporite (yellow) and Midra Shale (brown) which extends only over the southern half of the country. The Lower Domain is fed by sulfate-rich north-easterly flowing waters from Saudi Arabia. Seawater confines all aquifers to the north, east and west (Eccleston et al., 1981).



6.6 Conclusion

- Gypsum dissolution and resulting sulfate-rich groundwaters appear to drive most geochemical processes in all Domains, including dedolomitization in the mixed carbonate-evaporite Tertiary sequence of modern Qatar, despite the aridity of the climate.
- Carbonate dissolution appears to be occurring in the central Rus well, and possibly in the other well of the Upper and Middle Domains, albeit to a lesser degree.
- Given the relatively brief duration of this flow system (established since the Holocene sea-level rise) and low rates of flow fluid flux, the impact of these diagenetic processes on the rock may be subtle. This could be investigated using mass balance calculations or process-based modelling.
- Anthropogenic abstraction and injection is extensive and most likely influencing diagenetic processes however its true extent and subsequent influence on groundwater has not been established and should be in important focus for future work.

Suggestions for further work include:

- Further investigation using sulphur and C₁₄ isotopes to understand distinct geological variations and rate of change through time, correlating stratigraphic sections and sequences plus dating (Payton, 2012),

- Further analyse the organic content of the groundwater using fluorescence techniques, noting its local, regional and seasonal variability, with a focus on quantifying sulfate reduction and carbonate dissolution,
- Undertake a geochemical mass balance to understand changes in groundwater composition by calculating the dissolved constituents in groundwater relative to where they are sourced (Drever, 1997),
- Quantify anthropogenic influences on recharge and abstraction, specifically water quality and quantity of injected TSE waters from the nearby sewage treatment plant to the south, and the quantity and fate of water abstracted from domestic and irrigation wells across the country.

REFERENCES

- Abu-Zeid, M., & Boukhary, M. (1984). Stratigraphy, facies and environment of sedimentation of Eocene rocks in Fhailil (Gebel Dukhan) section, Qatar, Arabian Gulf. *Review De Paleobiologie*, 3(No.2), 159–173.
- Afifi, A. M., & ExxonMobil. (2004). *Ghawar: The anatomy of the world's largest oil field*. Retrieved from <http://www.searchanddiscovery.com/documents/2004/afifi01/images/afifi01.pdf>
- Ahm, A. S. C., Bjerrum, C. J., Blättler, C. L., Swart, P. K., & Higgins, J. A. (2018). Quantifying early marine diagenesis in shallow-water carbonate sediments. *Geochimica et Cosmochimica Acta*, 236, 140–159. <https://doi.org/10.1016/j.gca.2018.02.042>
- Al Bassam, A.M., Hussein, M.T., Sharaf, M. A. (1997). Hydrochemical evaluation of the Umm-er-Radhuma aquifer system, Saudi Arabia. *Hydrochemistry, Proceedings of the Rabat Symposium*.
- Al Siddiqi, A., & Dawe, R. A. (1998). A Review Of Petroleum Engineering Aspects Of Qatar's Oil And Gas. *Engineering Journal of the University of Qatar*, 11, 11–45. Retrieved from <http://qspace.qu.edu.qa/handle/10576/7980>
- Al-Fahmi, M. M., Plesch, A., Shaw, J. H., & Cole, J. C. (2016). Restorations of faulted domes. *AAPG Bulletin*. <https://doi.org/10.1306/08171514211>
- Al-Hajari, S. (1990). *Geology of the Tertiary and its influence of the aquifer systems of Qatar and Eastern Arabia*. University of South Carolina.
- Al-Saad, H. (2003). Facies analysis, cyclic sedimentation and paleoenvironment of the Middle Eocene Rus Formation in Qatar and adjoining areas. *Carbonates and Evaporites*, 18(1), 41–50. <https://doi.org/10.1007/BF03178386>
- Al-Saad, H. (2005). Lithostratigraphy of the Middle Eocene Dammam Formation in Qatar, Arabian Gulf: Effects of sea-level fluctuations along a tidal environment. *Journal of Asian Earth Sciences*, 25(5), 781–789. <https://doi.org/10.1016/j.jseaes.2004.07.009>
- Al-Saad, H., & Hewaidy, A. G. (n.d.). *A review of the Eocene formations of the Qatar peninsula, Arabian Gulf: Stratigraphy and paleoenvironment*. Retrieved from https://www.researchgate.net/profile/Bouchta_El_Moumni/publication/266678208_Quaternary_mass-transport_deposits_on_the_north-eastern_Alboran_seamounts_SW_Mediterranean_Sea_Submarine_Mass_Movements_and_Their_Consequences_37_Advances_in_Natural_and_Technolo
- Alsharhan, A. ., Rizk, Z. A., Nairn, A. E. M., Bakhit, D. W., & Alhajari, S. A. (2001). *Hydrogeology of an arid region: the Arabian Gulf and adjoining areas*. Elsevier Science B.V.
- APHA. (2012). Standard Methods for Examination of Water and Wastewater (Standard Methods for the Examination of Water and Wastewater). *American Public Health Association (APHA): Washington, DC, USA*. https://doi.org/ISBN_9780875532356
- Baalousha, H. M. (2016a). Using Monte Carlo simulation to estimate natural groundwater recharge in Qatar. *Modeling Earth Systems and Environment*, 2(87).

- Baalousha, H. M. (2016b). Development of a groundwater flow model for the highly parameterized Qatar aquifers. *Modeling Earth Systems and Environment*, 2(2). <https://doi.org/10.1007/s40808-016-0124-8>
- Baalousha, H. M. (2016c). Groundwater vulnerability mapping of Qatar aquifers. *Journal of African Earth Sciences*. <https://doi.org/10.1016/j.jafrearsci.2016.09.017>
- Baalousha, H. M., Barth, N., Ramasomanana, F. H., & Ahzi, S. (2018). Groundwater recharge estimation and its spatial distribution in arid regions using GIS: a case study from Qatar karst aquifer. *Modeling Earth Systems and Environment*, 4(4), 1319–1329. <https://doi.org/10.1007/s40808-018-0503-4>
- Bell, S. (1999). A Beginner ' s Guide to Uncertainty of. *Measurement*, 20(11), 586–587. <https://doi.org/10.1111/j.1468-3148.2007.00360.x>
- Boukhary, M., Hewaidy, A. G., Luterbacher, H., Bassiouni, M. E.-A., & Al-Hitmi, H. (2011). Foraminifera and ostracodes of early eocene umm er radhuma formation, dukhan oil field, Qatar. *Micropaleontology*.
- Braithwaite, C. J. R., Rizzi, G., & Darke, G. (2008). The geometry and petrogenesis of dolomite hydrocarbon reservoirs: introduction. *Geological Society, London, Special Publications*. <https://doi.org/10.1144/gsl.sp.2004.235.01.01>
- Brennan, S. T., Lowenstein, T. K., & Cendon, D. I. (2013). The major-ion composition of cenozoic seawater: the past 36 million years from fluid inclusions in marine halite. *American Journal of Science*, 313(8). <https://doi.org/10.2475/08.2013.01>
- British Standards Institution. (2012). BS EN ISO 22282-1:2012 Geotechnical Investigation and Testing - Geohydraulic Testing - Part 3: Water Pressure Tests in Rock. *BSI Standards Publication*, 1–26.
- British Standards Institution. (2015). *Code of practice for ground investigations*. The British Standards Institution.
- Brown, E., Colling, A., Park, D., Phillips, J., Rothery, D., & Wright, J. (1989). *Seawater: Its composition, properties and behaviour* (2nd ed.; G. Bearman, Ed.). Open University.
- Cavelier C., Salatt A., Heuze, Y. (1970). *Geological description of the Qatar Peninsula. Explanation of the 1/100 000 geological maps of Qatar*.
- Chidambaram, S., Prasanna, M. V., Karmegam, U., Singaraja, C., Pethaperumal, S., Manivannan, R., ... Tirumalesh, K. (2011). Significance of pCO₂ values in determining carbonate chemistry in groundwater of Pondicherry region, India. *Frontiers of Earth Science*, 5(2), 197–206. <https://doi.org/10.1007/s11707-011-0170-5>
- Di Sipio, E., Galgaro, A., Destro, E., Teza, G., Chiesa, S., Giaretta, A., & Manzella, A. (2014). Subsurface thermal conductivity assessment in Calabria (southern Italy): a regional case study. *Environmental Earth Sciences*, 72(5), 1383–1401. <https://doi.org/10.1007/s12665-014-3277-7>
- Dill, H. G., Nasir, S., & Al-Saad, H. (2003). Lithological and structural evolution of the northern sector of Dukhan anticline, Qatar, during the early Tertiary: With special reference to sequence stratigraphic bounding surfaces. *GeoArabia*.
- Domenico, P., & Schwartz, F. (1999). Physical and Chemical Hydrogeology. In *Environment Quality*. <https://doi.org/10.2134/jeq1999.00472425002800060047x>

- Drever, J. (1997). *The Geochemistry of Natural Waters: Surface and Groundwater Environments*. Prentice-Hall.
- Drever, J. (1997). The geochemistry of natural waters--Surface and groundwater environments (3rd). In *Eos, Transactions American Geophysical Union*.
- Driscoll, F. G. (1986). Groundwater and Wells. In *Groundwater*.
- Dunham, R. J. (1962). Classification of carbonate rocks according to depositional texture. In *Classification of carbonate rocks: American Association of Petroleum Geologists Memoir*.
- Eccleston, B.L., Harhash, I. (1982). *The hydrogeology of Qatar. Water Resources and Agricultural Development Project*.
- Eccleston, B. L., Pike, J. G., & Harhash, I. (1981). *The Water Resources of Qatar and Their Development: Volume 1, Technical Report 5*. Water Resources and Agricultural Development project, Ministry of Industry and Agriculture and FAO (Food and Agriculture Organization-UN).
- Emara, H. (1998). Total organic carbon content in the waters of the Arabian Gulf. *Environment International*, 24(1–2), 97–103.
- Escorcia, L. C., Gomez-Rivas, E., Daniele, L., & Corbella, M. (2013). Dedolomitization and reservoir quality: Insights from reactive transport modelling. *Geofluids*, 13(2), 221–231. <https://doi.org/10.1111/gfl.12023>
- FAO. (1979). *Survey and Evaluation of available data on shared water resources in the Gulf states and the Arabian Peninsula*. Rome.
- Hamm, S. Y., Kim, M. S., Cheong, J. Y., Kim, J. Y., Son, M., & Kim, T. W. (2007). Relationship between hydraulic conductivity and fracture properties estimated from packer tests and borehole data in a fractured granite. *Engineering Geology*, 92(1–2), 73–87. <https://doi.org/10.1016/j.enggeo.2007.03.010>
- Harhash, I., & Yousif, A. M. (1985). *Groundwater recharge estimates for the period 1972-1983. Water Resources and Agricultural Development Project. Qatar*.
- Harmon, R. S., & Wicks, C. M. (2006). *Perspectives on karst geomorphology, hydrogeology, and geochemistry - A tribute volume to Derek C. Ford and William B. White*. Geological Society of America.
- Hem, J. . (1985). *Study and Interpretation of the Chemical Characteristics of Natural Water* (U.S. Department of Interior & U.S. Geological Survey, Eds.).
- Hydrocarbons Technology. (2019). The world's biggest natural gas reserves.
- James, N.P., Jones, B. (2016). *Origin of carbonate sedimentary rocks* (1st ed.). John Wiley & Sons Ltd.
- Javed, W., Wubuliksimu, Y., Figgs, B., & Guo, B. (2017). Characterization of dust accumulated on photovoltaic panels in Doha, Qatar. *Solar Energy*, 142, 123–135.

- Kalbus, E., Oswalk, S., Wang, W., Kolditz, O., Engelhardt, I., Al-Saud, M. I., & Rausch, R. (2011). Large-scale modeling of the groundwater resources on the Arabian Platform. *International Journal of Water Resources and Arid Environments*, 1(1), 38–47.
- Keys, W. S. (1990). Borehole geophysics applied to ground-water investigations. *Techniques of Water-Resources Investigations of the United States Geological Survey Book 2 Collection of Environmental Data*, 165.
- Kimrey, J. (1985). *Proposed artificial recharge studies in Northern Qatar*.
- Kuiper, N., Rowell, C., & Shomar, B. (2015). High levels of molybdenum in Qatar's groundwater and potential impacts. *Journal of Geochemical Exploration*, 150, 16–24.
- Le Blanc, J. (2017a). *A revised guide to the Cenozoic surface of Qatar, Middle East (not including the islands)*. Retrieved from <https://sites.google.com/site/leblancjacques/fossilhome>
- Le Blanc, J. (2017b). *Origin and types of silica in the Lower Eocene carbonates of the Rus Formation, Middle East*. Retrieved from <https://sites.google.com/site/leblancjacques/fossilhome>
- Lloyd, J., Pike, J., Eccleston, B., & Chidley, T. R. . (1987). The hydrogeology of complex lens conditions in Qatar. *Journal of Hydrology*, 89, 239–258.
- Machel, H. G. (2004). Concepts and models of dolomitization: a critical reappraisal. *Geological Society, London, Special Publications*. <https://doi.org/10.1144/gsl.sp.2004.235.01.02>
- Macumber, P. (2015). *Water heritage in Qatar* (I. C. on M. and Sites, Ed.). UNESCO World Heritage Convention.
- Ministry of Development Planning and Statistics. (2014). Water statistics in the State of Qatar 2017. Doha - Qatar. In *Quarterly Journal of Economic Research*.
- Ministry of Development Planning and Statistics, Q. (2014). *Environment Statistics Annual Report 2013*.
- Ministry of Development Planning and Statistics, Q. (2017). *Water Statistics In the state of Qatar 2015*.
- Moore, P. J., Martin, J. B., & Screamon, E. J. (2009). Geochemical and statistical evidence of recharge, mixing, and controls on spring discharge in an eogenetic karst aquifer. *Journal of Hydrology*, 376(3–4), 443–455. <https://doi.org/10.1016/j.jhydrol.2009.07.052>
- Moore, P. J., Martin, J. B., Screamon, E. J., & Neuhoff, P. S. (2010). Conduit enlargement in an eogenetic karst aquifer. *Journal of Hydrology*, 393(3–4), 143–155. <https://doi.org/10.1016/j.jhydrol.2010.08.008>
- Morse, J. W., & Mackenzie, F. T. (1990). *Geochemistry of sedimentary carbonates. Developments in sedimentology, Volume 48*. Elsevier Science B.V.
- MUKHOPADHYAY, A., ALSULAIMI, J., ALAWADI, E., & ALRUWAIH, F. (2002). An overview of the Tertiary geology and hydrogeology of the northern part of the Arabian Gulf region with special reference to Kuwait. *Earth-Science Reviews*. [https://doi.org/10.1016/0012-8252\(95\)00068-2](https://doi.org/10.1016/0012-8252(95)00068-2)
- Mukhopadhyay, A., Alsulaimi, J., Alawadi, E., & Alruwaih, F. (2002). An overview of the Tertiary geology and hydrogeology of the northern part of the Arabian Gulf region with special reference to Kuwait. *Earth-Science Reviews*, 40(3–4), 259–295. [https://doi.org/10.1016/0012-8252\(95\)00068-2](https://doi.org/10.1016/0012-8252(95)00068-2)

- Mwango, F. K. (2009). Shared Water Resources. In *Shared Water Resources – Kenyan Case*.
- Ooi, D. (2018). *Origin and Diagenesis of Evaporites in Coastal Sabkha*.
- Parkhurst, D. L., & Appelo, C. a. J. (2013). Description of Input and Examples for PHREEQC Version 3 — A Computer Program for Speciation , Batch-Reaction , One-Dimensional Transport , and Inverse Geochemical Calculations. In *U.S. Geological Survey Techniques and Methods, book 6, chapter A43*.
- Payton, A., Gray, E. T., Authors: Gradstein, F. M., Ogg, J. G., Schmitz, M. D., & Ogg, G. M. (2012). Chapter 9 - Sulfur Isotope Stratigraph, in The Geologic Time Scale 2012. In *The Geologic Time Scale 2012*. <https://doi.org/10.1016/C2011-1-08249-8>
- Pelizardi, F., Bea, S. A., Carrera, J., & Vives, L. (2017). Identifying geochemical processes using End Member Mixing Analysis to decouple chemical components for mixing ratio calculations. *Journal of Hydrology*. <https://doi.org/10.1016/j.jhydrol.2017.04.010>
- Perotti, C. R., Carruba, S., Rinaldi, M., Bertozzi, G., Feltre, L., & Rahimi, M. (2012). The Qatar–South Fars Arch Development (Arabian Platform, Persian Gulf): Insights from Seismic Interpretation and Analogue Modelling. In *New Frontiers in Tectonic Research - At the Midst of Plate Convergence*. <https://doi.org/10.5772/20299>
- Pike, J. G. (1985). Groundwater Resources and Development in the Central Region of the Arabian Gulf. *Hydrogeology in the Service of Man*, 46–55.
- Plummer, L. N., Vacher, H. L., Mackenzie, F. T., Bricker, O. P., & Land, L. S. (1976). Hydrogeochemistry of Bermuda: A case history of ground-water diagenesis of biocalcarenes. *Bulletin of the Geological Society of America*, 87(9). [https://doi.org/10.1130/0016-7606\(1976\)87<1301:HOBACH>2.0.CO;2](https://doi.org/10.1130/0016-7606(1976)87<1301:HOBACH>2.0.CO;2)
- Plummer, L. N., Busby, J. F., Lee, R. W., & Hanshaw, B. B. (1990). Geochemical Modeling of the Madison Aquifer in Parts of Montana, Wyoming, and South Dakota. *Water Resources Research*, 26, No.9. <https://doi.org/10.1029/WR026i009p01981>
- Puls, D., Jameson, J., Kozar, M., Al-Ansi, H., & LeBlanc, J. (2016). *The Dukhan Sabkha: A Modern Analogue for the Arab C Carbonate Reservoir, Dukhan Field, Qatar*. (January). <https://doi.org/10.2523/iptc-13629-ms>
- Rahimpour-Bonab, H., Asadi-Eskandar, A., & Sonei, R. (2009). Effects of the Permian-Triassic boundary on reservoir characteristics of the South Pars gas field, Persian Gulf. *Geological Journal*. <https://doi.org/10.1002/gj.1148>
- Rivers, J. M., & Larson, K. P. (2018). The Cenozoic kinematics of Qatar: Evidence for high-angle faulting along the Dukhan 'anticline.' *Marine and Petroleum Geology*, 92(November 2017), 953–961. <https://doi.org/10.1016/j.marpetgeo.2018.03.034>
- Rivers, J. M., Skeat, S. L., Yousif, R., Liu, C., Stanmore, E. S., Tai, P., & Al-Marri, S. M. (2019a). The depositional history of near-surface Qatar aquifer rocks, and its impact on the flow and storage properties. In *Arabian Journal of Geosciences*.
- Rivers, J. M., Varghese, L., Yousif, R., Whitaker, F. F., Skeat, S. L., & Al-Shaikh, I. (2019b). The geochemistry of Qatar coastal waters and its impact on carbonate sediment chemistry and early marine diagenesis. *Journal of Sedimentary Research*, 89, 1–18.

- Ryan, B. H., Kaczmarek, S. E., & Rivers, J. M. (2019). Dolomite dissolution: An alternative diagenetic pathway for the formation of palygorskite clay. *Sedimentology*. <https://doi.org/10.1111/sed.12559>
- Sadiq, A. M., & Nasir, S. J. (2002). Middle Pleistocene karst evolution in the state of Qatar, Arabian Gulf. *Journal of Cave and Karst Studies*.
- Seltrust Engineering Ltd. (1980). *Qatar Geological Map. Explanatory booklet*. Industrial Development Technical Centre.
- Shamrukh, M., Al-Muraikhi, A. A., & Al-Hamar, Y. I. (2012). Exploring of deep groundwater in the Southwest aquifer of Qatar. *The 10th Gulf Water Conference*.
- Sharaf, M. A. M. (2001). Review of the hydrogeological and hydrochemical aspects of groundwater in the Umm-Er-Radhuma aquifer system, Arabian Peninsula. *Journal of African Earth Sciences*. [https://doi.org/10.1016/S0899-5362\(01\)80068-3](https://doi.org/10.1016/S0899-5362(01)80068-3)
- Sharland, P. R., Archer, D. M., Casey, R. B., Davies, S. H., Hall, A. P., Heward, A. D., ... Simmons, M. D. (2001). Arabian Plate Sequence Stratigraphy. In *GeoArabia Special Publications 2*.
- Simmonds, J. (2014). *Characterising scale dependence of permeability in Holocene sabkhas and karstified Eocene carbonates of Qatar*. University of Bristol.
- Singurindy, O., & Berkowitz, B. (2003). Flow, dissolution, and precipitation in dolomite. *Water Resources Research*, 39(6), 1–13. <https://doi.org/10.1029/2002WR001624>
- Stoessell, R. K. (1992). Effects of sulfate reduction on CaCO₃ dissolution and precipitation in mixing-zone fluids. *Journal of Sedimentary Petrology*, 62(5).
- Stoessell, R. K., Moore, Y. H., & Coke, J. G. (1993a). The occurrence and effect of sulfate reduction and sulfide oxidation on coastal limestone dissolution in Yucatan Cenotes. *Groundwater*, 31(4), 566–575.
- Stoessell, R. K., Moore, Y. H., & Coke, J. G. (1993b). The Occurrence and Effect of Sulfate Reduction and Sulfide Oxidation on Coastal Limestone Dissolution in Yucatan Cenotes. *Groundwater*. <https://doi.org/10.1111/j.1745-6584.1993.tb00589.x>
- Streetly, M. J., & Kotoub, S. (1998). Determination of aquifer properties in northern Qatar for application of artificial recharge. *Quarterly Journal of Engineering Geology and Hydrogeology*, 31, 199–209.
- The World Bank Group. (2017). Average monthly temperature and rainfall for Qatar from 1901 to 2015. Retrieved from http://sdwebx.worldbank.org/climateportal/index.cfm?page=country_historical_climate&ThisCCCode=QAT
- Tibco Spotfire. (2018). *Tibco Spotfire (R)! 7.8.0 - User's Manual*.
- Tóth, J. (1970). A conceptual model of the groundwater regime and the hydrogeologic environment. *Journal of Hydrology*. [https://doi.org/10.1016/0022-1694\(70\)90186-1](https://doi.org/10.1016/0022-1694(70)90186-1)
- Tucker, M. E., Wright, V. P., & Dickson, J. A. D. (2009). Carbonate Sedimentology. In *Carbonate Sedimentology*. <https://doi.org/10.1002/9781444314175>

- Tyson, R. V., & Pearson, T. H. (1991). Modern and ancient continental shelf anoxia: an overview. *Geological Society, London, Special Publications*. <https://doi.org/10.1144/GSL.SP.1991.058.01.01>
- U.S. Department of Interior, & U.S. Geological Survey. (2016). Vertical flowmeter logging.
- UNESCWA and BGR. (2013). *Inventory of shared water resources in Western Asia*. New York.
- Wang, X. (2019). Uncertainty quantification and reduction in the characterization of subsurface stratigraphy using limited geotechnical investigation data. *Underground Space*. <https://doi.org/10.1016/j.undsp.2018.10.008>
- Warren, J. (1999). *Evaporites. Their evolution and economics* (1st ed.). Wiley-Blackwell.
- Weatheronline. (2019). Qatar weather. Retrieved from weatheronline.co.uk
- Whitaker, F. F., & Smart, P. L. (2000). Characterising scale-dependence of hydraulic conductivity in carbonates: Evidence from the Bahamas. *Journal of Geochemical Exploration*. [https://doi.org/10.1016/S0375-6742\(00\)00016-9](https://doi.org/10.1016/S0375-6742(00)00016-9)
- Whitaker, F. F., & Smart, P. L. (2007a). Geochemistry of meteoric diagenesis in carbonate islands of the northern Bahamas: 1. Evidence from field studies. *Hydrological Processes*. <https://doi.org/10.1002/hyp.6532>
- Whitaker, F. F., & Smart, P. L. (2007b). Geochemistry of meteoric diagenesis in carbonate islands of the northern Bahamas: 2. Geochemical modelling and budgeting of diagenesis. *Hydrological Processes*, 21(February), 967–982. <https://doi.org/10.1002/hyp>
- Whitaker, F. F., Smart, P. L., & Jones, G. D. (2008). Dolomitization: from conceptual to numerical models. *Geological Society, London, Special Publications*. <https://doi.org/10.1144/gsl.sp.2004.235.01.05>
- Whitaker, F. F., Didi-Ooi S.M., Jameson J., Strogmenger C.J., (2014). Origins of evaporites in a holocene mixed clastic and carbonate coastal sabka: Preliminary hydrogeological data from Mesaieed Sabka, Qatar. International Petroleum Technology Conference. IPTC17567.

Appendix A1 Drilling of cored boreholes and monitoring wells

The boreholes were initially located using a hand-held Garmin III GPS. On completion of drilling, as-built coordinates and elevations were established using a qualified land surveyor to an accuracy of +/-50mm using the Qatar National Grid 'QNG' co-ordinate system and the levels were referred to in m QNHD. All site works were carried out in accordance with BS 5930:2015 and BS EN ISO 14689:2018.

Continuous rock samples were obtained using a multipurpose rotary core drilling rig (Desco SP550OS) and a triple tube core barrel system (Geobore S) with semi-rigid plastic inner liner and diamond / tungsten drill bits. Rock cores were of 102mm minimum diameter and once retrieved, were stored in wooden boxes for transport, then photographed and logged.

In the southern (RR) and central (AS) boreholes, the initial cored boreholes were enlarged in diameter to allow for in-situ permeability testing, specifically flow meter logging and packer (lugeon) tests. Geophysical logging of the boreholes was also undertaken in all of the cored holes as part of the larger Exxon project and not available for this project.

Appendix A2 Packer (or Lugeon) Testing

Testing was undertaken in accordance with the British Standard BS5930:2015 and BS EN ISO 22282-3:2012. Methodology involved a single expandable packer - 'petrometallic' type - with nominal diameter of 72mm, lowered to the top of the test depth and inflated using compressed air. Test sections were from the base of the borehole to the base of the inflated packer, varying in length from 1.5m to 3.0m.

The test began by measuring the natural groundwater level using a dip meter. A water injection line from the packer water was connected via a flowmeter / pressure gauge group to the water supply pump (tanker). Water was pumped into the test zone at 3 increment pressure stages followed by two decreasing stages. Each pressure was maintained for 15 minutes and water flow rate into the test sections was recorded at 5, 10 and 15 minutes.

The maximum pressure was dependent on the rock fracturing records and test elevation as per the formula mentioned below (Equation 9) from the British Standard BS5930:2015 and BS EN ISO 22282-3:2012 (British Standards Institution, 2012, and British Standards Institution, 2015). Test pressures were selected such that the maximum test pressure (P_{Max}) did not exceed the overburden pressure at the centre of the test section to avoid hydraulic fracturing. Test results were interpreted and hydraulic conductivity ($m\ s^{-1}$) was ascertained using Equation 7 in (Hamm et al., 2007) and converted to Darcies (Section 4).

Equation A1 Pressure (bar) = Depth of the borehole during test x (1psi/feet)/100

Appendix A3 Methodology of groundwater monitoring

The monitoring event typically involved dipping the borehole to establish groundwater level. Groundwater measurements were taken from a specified monitoring point on each well casing which had been formally established by the survey team. Depths to groundwater were subsequently adjusted to absolute depths using the elevations provided by the survey team, including the difference between the monitoring point and ground elevation. All depths to groundwater in this report have been adjusted and are from ground level.

The borehole was purged however only 2 to 3 litres of groundwater were removed prior to sampling, as purging was limited due to concentrations of hydrogen sulphide in bedrock and groundwater and the potential for purging to induce oxidation.

Groundwater samples were taken using either a 1-litre hydrasleeve sampler or 1-litre Teflon bailer with a one-way valve that shut off as soon as the sampler was full, enabling a 'core' of water to be removed. Galvanised steel weights were added to the sampler to aid sinking the sampling equipment to the required depth. The samplers were placed (lowered) into the borehole, below the water table to the respective response zones, and returned to surface for field analyses and placement into amber glass bottles retrieved from the laboratory for chemical analysis. Bottles had been cleaned to inhouse standards, which involved soaking them in hot water with liquid laboratory detergent for two hours, rinsing four times with hot tap water, and then three times with Milli-Q water and inverting to drip dry. They were then placed in an oven maintained at 130°C over night and provided for sampling with a Teflon-lined septa screw cap.

All clean glass sample bottles were issued by the respective laboratories and following sampling were filled to the very top of the bottle to reduce any interaction with the atmosphere. All sample bottles were labelled detailing sample number, date & time of collection, well number, and name of sample collector. The sample bottles were placed in ice-filled cool boxes and transported to the respective laboratory for analysis. Chain of custody forms accompanied the samples and on receipt of the samples to the laboratory, the chain of custody was signed and stamped by the Laboratory. Samples were kept in ice-cooled boxes at 4°C till the sample reached the laboratory, after which the samples were kept in a refrigerator at 4°C until testing within the limits specified in ASTM. No filtration or preservatives were used in the field, and the respective laboratories undertook the necessary procedures prior to analyses.

Appendix A4 Laboratory details

Table A4-1 Laboratory standards, detection limit (DL) and uncertainty of measurement (UoM)

Tests	Standard	Unit	Gulf Labs		Fugro		Exxon	
			DL	UoM	DL	UoM	DL	UoM
pH H ⁺	APHA 4500 H ⁺ B	units	0.1	0.00950	0.1	0.00950	0.01	0.50
Electrical Conductivity @25 °C	APHA 2510 B	µS/cm	1	2.3	1	-	1	2.782
Total Dissolved Solids (TDS)	APHA 2540 C	mg/l	5.0	2	5.0	-	5.0	2.167
Total Alkalinity (CaCO ₃) @ endpoint pH-4.5	APHA 2320 B	mg/l	1.0	5.9	1.0	-	5.34	1.86
Sulphate (SO ₄ ²⁻)	APHA 4500 SO ₄ C	mg/l	2.0	0.04613	5.0	0.04771	5.0	12.45
Chloride (Cl ⁻)	APHA 4500 Cl ⁻ B	mg/l	1.0	0.1	1.0	0.54274	2.75	0.582
Calcium (Ca ²⁺)	APHA 3120 B / 3030 F	mg/l	0.005	0.004	0.04	0.06111	0.003	0.048
Magnesium (Mg ²⁺)	APHA 3120 B / 3030 F	mg/l	0.003	0.002	0.01	0.03816	0.002	0.046
Aluminum (Al ³⁺)	APHA 3120 B / 3030 F	mg/l	0.005	0.002	0.04	0.05272	0.003	0.036
Iron (Fe ³⁺)	APHA 3120 B / 3030 F	mg/l	0.003	0.003	0.008	0.03742	0.002	0.036
Potassium (K ⁺)	APHA 3120 B / 3030 F	mg/l	0.108	0.033	0.02	0.11117	0.002	0.049
Silicon (Si ²⁺)	APHA 3120 B / 3030 F	mg/l	0.008	0.006	0.02	0.05988	0.003	0.036
Sodium (Na ⁺)	APHA 3120 B / 3030 F	mg/l	0.052	0.120	0.09	0.13415	0.002	0.049

DL = Detection Limit

UoM = Uncertainty of measurement

APHA = American Public Health Association (APHA, 2012)

Appendix A4-2 Laboratory methods and machines used

Tests	Gulf Labs		Fugro		Exxon	
	Instrument	Brand / Model	Instrument	Brand / Model	Instrument	Brand / Model
pH H ⁺	Portable meter	Thermo Scientific Orion ROSS Ultra pH/ATC Triode Model: 8157BNUMD	Portable meter	HACH HQ 40	Portable meter	HACH HQ 40
Electrical Conductivity @25 °C	Portable meter	Thermo Scientific Orion Conductivity Cell Model: 013005MD	Portable meter	HACH HQ 40	Portable meter	HACH HQ 40
Total Dissolved Solids (TDS)	Filtration Assembly / Oven	Analytical Balance – Shimadzu; Model: ATX224 Oven – Dahin Scientific; Model: WOF-50	Filtration Assembly / Oven	Pyrex / Memert UN 55	Filtration Assembly / Oven	Shellab oven, VWR analytical balance
Total Alkalinty (CaCO3) @ endpoint pH-4.5	Burette	-	Burette	-	Burette	-
Sulphate (SO ₄ ²⁻)	Electronic Balance / Muffle Furnace	Analytical Balance – Shimadzu; Model: ATX224 M. Furnace – Hobersal; Model: 12PR/300	Electronic Balance / Muffle Furnace	Citizen / Carbolite	Electronic Balance / Muffle Furnace	Hach DR 2800 spectrophotometer
Chloride (Cl ⁻)	Pipette / Burette	-	Pipette / Burette	-	Pipette / Burette	-
Calcium (Ca ²⁺)	Inductively Coupled Plasma – Optical Emission Spectrometer	Perkin Elmer; Model: Optima 2000 DV	Inductively Coupled Plasma – Optical Emission Spectrometer	Shimadzu ICPE 9820	Inductively Coupled Plasma – Optical Emission Spectrometer	Agilent 5110 SVDV ICP_OES
Magnesium (Mg ²⁺)						
Aluminum (Al ³⁺)						
Iron (Fe ³⁺)						
Potassium (K ⁺)						
Silicon (Si ²⁺)						
Sodium (Na ⁺)						



















Appendix A5 Physical rock logging methodology based on BSI (2015) and geological logging methodology

Table A5-1 Physical methodology based on BSI (2015)

Characteristic	Methodology
Material	<ul style="list-style-type: none"> ▪ strength defined using thumb, knife and rock hammer and categorised according to Table 25 in BSI (2015) ▪ large scale structure of the core such as bedding, foliation including thickness and spacing ▪ colour including discolouration due to leaching or weathering, and on discontinuity faces ▪ texture regarding geometric aspects of grains such as size, angularity, and the fabric or arrangement of grains such as preferred orientation
Rock mass characteristics	<ul style="list-style-type: none"> ▪ weathering status using Section 36.4.2.2 and Figure 9 (BSI, 2015), state of alteration ▪ describe discontinuities ie fault, joint, bedding, induced or incipient, spacing, persistence, aperture, wall strength, face characteristics ie rough, undulating, any infill, and number of sets ▪ mass characteristics using total core recovery (TCR) a percentage of core recovered per drilling run, solid core recovery (SCR) indicating competent rock, rock quality description (RQD), and fracture index (FI) as defined in Table 31 (BSI, 2015).
General information	Stability of rock core, note of any minor constituents such as voids or vugs, soils, infill

Table A5-2 Geological logging methodology as per ExxonMobil

Characteristic	Methods
Texture	<p>Establish depositional texture from Dunham (1962) to differentiate between a mud or grain supported rock as 1) <i>the presence or absences of carbonate mud which differentiates muddy carbonate from grainstone</i> 2) <i>abundance of grains, which allows muddy carbonates to be subdivided into mudstone, wackestone, and packstone; and 3) presence of signs of binding during deposition which characterizes boundstone, or 4) crystalline.</i></p> <p>Practically this required observing grains such as fossils, oolites, pellets and carbonate intraclasts, interstitial material such as clay or cements, and allochems (anything not carbonate) using a hand lens. Also noted:</p> <ul style="list-style-type: none"> ▪ Strength and integrity of core ▪ maturity such as sorting and grain / crystal arrangements ▪ structure ie brecciated, laminated or bedded and its shape ie flat or wavy, thickness and spacing, ▪ colour ▪ porosity by observing size of grain / crystal relative to interparticle spacing and pore connectivity (distinguishing between micro porosity, touching vugs and between vugs) ▪ other features such as ripups, drop stones

Characteristic	Methods																																																		
	<p data-bbox="602 226 1040 258">Texture classification Dunham (1962)</p> <table border="1" data-bbox="613 264 1330 745"> <thead> <tr> <th colspan="4" data-bbox="613 264 1208 296">Depositional texture recognisable</th> <th colspan="2" data-bbox="1208 264 1330 296">Depositional texture not recognisable</th> </tr> <tr> <th colspan="3" data-bbox="613 296 1089 359">Original components not bound together during deposition</th> <th colspan="3" data-bbox="1089 296 1330 359">Original components were bound together</th> </tr> <tr> <th colspan="2" data-bbox="613 359 854 411">Contains mud (clay & fine silt-sized carbonate)</th> <th colspan="2" data-bbox="854 359 1089 411">Lacks mud and is grain supported</th> <th colspan="2" data-bbox="1089 359 1330 411"></th> </tr> <tr> <th colspan="2" data-bbox="613 411 854 453">Mud-supported</th> <th colspan="2" data-bbox="854 411 1089 453">Grain-supported</th> <th colspan="2" data-bbox="1089 411 1330 453"></th> </tr> <tr> <th data-bbox="613 453 735 569">Less than 10% grains</th> <th data-bbox="735 453 854 569">More than 10% grains</th> <th colspan="2" data-bbox="854 453 1089 569"></th> <th colspan="2" data-bbox="1089 453 1330 569"></th> </tr> <tr> <th data-bbox="613 569 735 600">Mudstone</th> <th data-bbox="735 569 854 600">Wackestone</th> <th data-bbox="854 569 976 600">Packstone</th> <th data-bbox="976 569 1089 600">Grainstone</th> <th data-bbox="1089 569 1208 600">Boundstone</th> <th data-bbox="1208 569 1330 600">Crystalline</th> </tr> <tr> <td data-bbox="613 600 735 745"></td> <td data-bbox="735 600 854 745"></td> <td data-bbox="854 600 976 745"></td> <td data-bbox="976 600 1089 745"></td> <td data-bbox="1089 600 1208 745"></td> <td data-bbox="1208 600 1330 745"></td> </tr> </thead> <tbody> <tr> <td data-bbox="266 751 586 846">Mineralogy</td> <td data-bbox="586 751 1433 846">Primarily using XRD analyses integrated with thin sections to determine material type by observing shape, colour including cross polars, cleavage or lack of, strength ie scratch test</td> </tr> <tr> <td data-bbox="266 846 586 877">Biota</td> <td data-bbox="586 846 1433 877">Classify biota to provide information about depositional environment</td> </tr> <tr> <td data-bbox="266 877 586 972">Grain / Crystals</td> <td data-bbox="586 877 1433 972">Observe grain or crystal size, grain or crystal shape, material type either carbonate or siliceous etc, if is it original or replaced, empty or infilled</td> </tr> <tr> <td data-bbox="266 972 586 1064">Laboratory XRD, pore, porosity and isotope analyses</td> <td data-bbox="586 972 1433 1064">Compare laboratory results with relevant core section</td> </tr> </tbody> </table>	Depositional texture recognisable				Depositional texture not recognisable		Original components not bound together during deposition			Original components were bound together			Contains mud (clay & fine silt-sized carbonate)		Lacks mud and is grain supported				Mud-supported		Grain-supported				Less than 10% grains	More than 10% grains					Mudstone	Wackestone	Packstone	Grainstone	Boundstone	Crystalline							Mineralogy	Primarily using XRD analyses integrated with thin sections to determine material type by observing shape, colour including cross polars, cleavage or lack of, strength ie scratch test	Biota	Classify biota to provide information about depositional environment	Grain / Crystals	Observe grain or crystal size, grain or crystal shape, material type either carbonate or siliceous etc, if is it original or replaced, empty or infilled	Laboratory XRD, pore, porosity and isotope analyses	Compare laboratory results with relevant core section
Depositional texture recognisable				Depositional texture not recognisable																																															
Original components not bound together during deposition			Original components were bound together																																																
Contains mud (clay & fine silt-sized carbonate)		Lacks mud and is grain supported																																																	
Mud-supported		Grain-supported																																																	
Less than 10% grains	More than 10% grains																																																		
Mudstone	Wackestone	Packstone	Grainstone	Boundstone	Crystalline																																														
																																																			
Mineralogy	Primarily using XRD analyses integrated with thin sections to determine material type by observing shape, colour including cross polars, cleavage or lack of, strength ie scratch test																																																		
Biota	Classify biota to provide information about depositional environment																																																		
Grain / Crystals	Observe grain or crystal size, grain or crystal shape, material type either carbonate or siliceous etc, if is it original or replaced, empty or infilled																																																		
Laboratory XRD, pore, porosity and isotope analyses	Compare laboratory results with relevant core section																																																		

Appendix A6 Conversion to effective permeability (D)

Conversion used Darcys' law

$$\text{Equation A2} \quad K = v \left(\frac{L}{\Delta P} \right) \quad (\text{Darcys Law})$$

$$\text{Equation A3} \quad \text{and } \Delta P \text{ (pressure gradient) = density x gravity x height (Pa)}$$

Density of seawater @ 20°C = 1.03 g/ml (Brown et al., 1989)

One standard atmosphere = 101,300Pa (www.unitconverters.net)

Gravity = 9.81 m/s²

v (flow velocity) = 1 cm/s or 0.01 m/s

L (length) = 0.01m

Therefore, 1 Darcy is the equal to a hydraulic conductivity (K) of 10⁻⁵m/s, or 1m/d ≈ 1.16 D.

Slug test data from Simmonds (2014), were averaged to provide one results, where each test measured both an 'in' and 'out' displacement value.

Appendix B1 Field Results

Well	DATE	TIME	pH	pH temp °C	EC ms/cm	DO mg/l	DO sa% %	DO temp °C	TDS g/L	Turbidity NTU	Observations
RR-4	22.02.17	11:15	6.63	29.7	27.50						clear, no odour
RR-4	02.05.17	14:00	6.55	33.1	23.18	2.90		33.1	15.00	-	very cloudy
RR-4	07.06.17	8:50	6.90	35.1	24.16	2.20		35.1	15.82	-	very cloudy
RR-4	26.07.17	8:00	7.14	33.2	22.24	0.17		33.2	14.44	-	very cloudy
RR-4	28.08.17	8:00	7.25	37.1	27.90			37.1		536	very cloudy
RR-4	31.10.17	10:35	6.91	31.7	32.16	0.17	3.00	31.7	22.18	289	cloudy, no odour
RR-4	18.01.18	11:35	7.20	25.6		0.15	2.22	25.6	22.69	-	turbid cloudy, no odour
RR-4	31.01.18	16:00	6.58	26.3		0.40	4.40	26.3	41.56	539	cloudy, no odour
RR-4	18.02.18	17:29	7.11	28.5		0.32	5.30	28.5	53.50	-	cloudy, no odour
RR-4	22.04.18	10:36	6.44	30.2		0.98	0.25	30.2	9.39	-	cloudy, no odour
RR-4	27.05.18	9:00	7.16	30.2		0.19	3.10	30.2	78.22	396	cloudy, no odour
RR-4	19.09.18	17:30	7.37	31.7		0.24	4.30	31.7	29.30	-	cloudy, no odour
RR-3	22.02.17	11:00	7.15	28.8	15.29						clear. Mild H2S odour
RR-3	02.05.17	13:00	7.07	32.0	13.52	1.20		32.0	8.79	66	clear, mild H2S odour
RR-3	07.06.17	6:43	6.80	29.8	15.07	1.10		29.8	9.97	113	clear. Mild H2S odour
RR-3	26.07.17	8:00	6.99	31.8	12.97	0.18		31.8	9.09	140	clear, mild H2S odour
RR-3	28.08.17	8:30	7.12	31.2	14.64	1.19		31.2	7.92	7	clear. Mild H2S odour
RR-3	31.10.17	9:15	7.13	30.6	16.97	0.35	5.30	30.6	11.38	225	clear, mild H2S odour
RR-3	18.01.18	10:55	7.66	23.3	15.50	0.45	6.20	23.3	14.81	34	cloudy, no odour
RR-3	31.01.18	16:00	7.36	27.1	16.28	0.38	4.00	27.1	19.45	56	clear, no odour
RR-3	18.02.18	16:50	7.46	29.1		0.35	5.10	29.1	25.70	25	clear, no odour
RR-3	22.04.18	9:40	7.30	29.2		0.45	0.45	29.2	9.79	22	clear, no odour
RR-3	27.05.18	10:30	7.40	29.3		0.42	4.30	29.3	3.74	48	clear, no odour
RR-3	19.09.18	15:00	7.45	31.2		0.29	7.30	31.2	21.60	2	clear, no odour
RR-2	02.05.17	12:00	7.22	33.2	18.38	0.05	0.80	33.2	11.97		clear, mild H2S odour
RR-2	07.06.17	8:10	6.84	31.6	20.13	1.80		31.6	13.40	280	clear. Mild H2S odour
RR-2	26.07.17	8:00	6.94	32.4	18.44	0.24		32.4	11.96	199	clear, mild H2S odour
RR-2	28.08.17	9:00	7.19	31.4	19.51	2.57		31.4	10.23	37	clear. Mild H2S odour
RR-2	31.10.17	9:50	7.33	30.8	22.09	1.48	23.10	30.8	14.95	4	clear, mild H2S odour
RR-2	18.01.18	10:20	7.73	27.0	20.91	0.16	2.20	27.0	29.48	58	clear, no odour
RR-2	31.01.18	16:00	7.30	25.3	22.43	0.32	4.80	25.3	26.14	66	clear, with clay no odour
RR-2	18.02.18	15:33	7.63	29.3		0.39	6.10	29.3	38.45	78	clear, no odour
RR-2	22.04.18	9:00	7.22	31.2		0.18	0.85	31.2	22.67	13	clear, no odour
RR-2	27.05.18	9:30	7.71	30.3		0.50	8.40	30.3	28.37	6	clear, no odour
RR-2	19.09.18	15:56	7.51	31.7		0.48	0.61	31.7	53.16	59	
RR-1	22.02.17	10:00	7.23	28.8	28.30						clear. Mild H2S odour
RR-1	02.05.17	10:56	7.10	32.1	27.21	0.00	0.00	32.1	17.64	116	clear, mild H2S odour
RR-1	07.06.17	9:50	6.88	31.3	26.69	0.30		31.3	17.90	109	clear, mild H2S odour
RR-1	26.07.17	8:00	6.95	28.5	27.66	0.22		28.5	17.93	125	clear. Mild H2S odour
RR-1	28.08.17	9:30	7.49	32.1	28.43	2.71		32.1	12.90		clear, mild H2S odour
RR-1	31.10.17	11:20	7.02	32.6	29.61	0.39	6.20	32.6	20.13	67	clear, mild H2S odour
RR-1	18.01.18	9:30	7.85	24.2		0.12	2.40	24.2	24.85	42	cloudy, mild H2S odour
RR-1	31.01.18	13:00	7.28	24.4		0.31	3.10	24.4	29.56	134	cloudy, mild H2S odour
RR-1	18.02.18	14:31	7.61	30.0		0.36	5.70	30.0	38.48	26	clear, mild H2S odour
RR-1	22.04.18	8:00	7.57	30.1		0.70	0.48	30.1	26.21	19	clear, mild H2S odour
RR-1	27.05.18	8:15	7.25	27.7		0.00	0.00	27.7	35.31	40	clear, mild H2S odour
RR-1	19.09.18	16:45	7.19	33.2		0.00	0.00	33.2	43.48	33	clear, mild H2S odour
AG-3	10.08.17	6:45	7.19	29.2	2.03	0.12		29.2	1.30	661	cloudy, no odour
AG-3	28.08.17	7:00	7.29	28.6	1.31	2.90		28.6	0.86	577	cloudy, no odour
AG-3	31.10.17	14:35	7.81	29.3	1.46	0.56	7.30	29.3	0.91	92	cloudy, no odour
AG-3	18.01.18	13:55	7.74	26.5	1.71	0.58	6.80	26.5	1.92	596	cloudy, no odour
AG-3	31.01.18	12:00	7.24	24.2		0.29	2.80	24.2	1.98	611	cloudy, no odour
AG-3	19.02.18	12:45	8.05	27.5		0.00	0.00	27.5	2.01	-	cloudy, no odour
AG-3	22.04.18	14:00	7.16	30.9		0.00	0.00	30.9	9.78	-	cloudy, no odour
AG-3	27.05.18	15:50	7.93	29.8		0.08	0.10	29.8	5.81	735	cloudy, no odour
AG-3	20.09.18	12:40	8.15	33.2		0.00	0.00	33.2	5.31	471	cloudy, no odour
AG-2	10.08.17	7:00	7.46	29.9	4.05	0.85		29.9	2.64	9	clear, mild H2S odour

Well	DATE	TIME	pH	pH temp °C	EC ms/cm	DO mg/l	DO sa% %	DO temp °C	TDS g/L	Turbidity NTU	Observations
AG-2	28.08.17	7:30	7.41	28.9	3.54	1.13		28.9	1.91	5	clear, mild H2S odour
AG-2	31.10.17	13:10	7.89	28.1	3.85	0.74	8.10	28.1	2.45	12	clear, mild H2S odour
AG-2	18.01.18	13:20	8.03	28.6	3.64	0.53	6.30	28.6	2.85	7	clear, no odour
AG-2	31.01.18	12:30	7.70	23.9			4.80	23.9	5.60	68	cloudy, mild H2S odour
AG-2	19.02.18	12:20	7.91	27.8		0.00	0.00	27.8	5.49	15	clear, mild H2S odour
AG-2	22.04.18	13:50	7.47	30.4		0.46	0.10	30.4	4.32	4	clear, no odour
AG-2	27.05.18	16:25	7.74	30.3		0.00	0.00	30.3	2.00	11	clear, mild H2S odour
AG-2	20.09.18	11:25	7.87	32.5		0.00	0.00	32.5	15.51	30	no odour, slightly turbid
AG-1	10.08.17	7:15	7.39	29.0	5.96	0.76		29.0	3.89	13	clear, mild H2S odour
AG-1	28.08.17	8:00	7.34	29.1	5.66	2.50		29.1	2.92	9	clear, mild H2S odour
AG-1	31.10.17	13:40	6.93	24.1	5.99	0.55	7.30	24.1	3.91	16	clear, mild H2S odour
AG-1	18.01.18	12:45	7.34	26.2	5.59	0.52	5.90	26.2	4.97	26	clear, mild H2S odour
AG-1	31.01.18	16:00	7.49	26.6		0.48	4.50	26.6	6.18	121	cloudy, mild H2S odour
AG-1	19.02.18	13:00	7.48	27.9		0.00	0.00	27.9	8.07	12	clear, mild H2S odour
AG-1	22.04.18	12:45	7.22	32.2		0.02	0.03	32.2	4.77	18	clear, mild H2S odour
AG-1	27.05.18	15:50	7.37	29.3		0.00	0.00	29.3	5.19	23	clear, mild H2S odour
AG-1	20.09.18	12:05	7.63	31.8		0.00	0.00	31.8	61.64	46	clear, mild H2S odour
AS-2	06.06.18		6.9	33.7	1.81	1.64		33.7	932.00		clear, H2S odour
AS-2	08.07.18	10:35	6.77	32.9	1.80	2.19		32.9	926.00		clear, H2S odour
AS-2	12.08.18		6.81	31.4	1.80	2.60		31.4	913.00		clear, H2S odour
AS-2	19.09.18	12:25	7.81	32.3	1.40	0.00		32.3	199.00	1	clear, H2S odour
AS-1	06.06.18		7.85	39.3	4.90	1.92		39.3	2700.00		clear, H2S odour
AS-1	08.07.18	10:30	8.01	32.3	5.20	0.44		32.3	2690.00		clear, H2S odour
AS-1	12.08.18		7.61	31.3	5.10	0.47		31.3	2660.00		clear, H2S odour
AS-1	19.09.18	11:20	7.66	33.4	3.13	0.00		33.4	1947.00	19	H2S odour, turbid
Farm 1	22.04.18	14:40	7.21	27.3	4.92	0.08	0.17	27.3	3.02	2	clear, no odour
Farm 1	27.05.18	10:40	7.61	28.7	4.34	1.36	35.30	28.7	0.02	1	clear, no odour
Farm 1	19.09.18	10:45	8.29	28.2	4.78	0.61	0.19	28.2	79.65	7	clear, no odour
Farm 2	07.10.18	10:59	6.72		5.63				3.84		clear, slight H2S odour

Appendix B2 Laboratory Results

Well	Date	EC	pH	Ca	Cl	Mg	SO4	Alkalinity (CaCO3)	Al	Fe	K	Si	Na	TDS	LAB
		mS cm-1		mm l-1	mm l-1	mm l-1	mm l-1	mm l-1	mm l-1	mm l-1	mm l-1	mm l-1	mm l-1	mg l-1	
RR-4	22.02.17		6.77	32.4	239.2	25.3	25.5	2.8	<0.001	<0.001	2.7	0.8	203.2	18060	GL
RR-4	02.05.17		6.63	30.9	226.5	31.7	24.0	3.0	<0.001	<0.001	1.8	0.9	244.2	17484	GL
RR-4	07.06.17		6.90	22.8	261.9	17.7	10.4	1.1	<0.001	<0.001	4.7	0.3	224.0	17950	GL
RR-4	26.07.17		6.80	32.5	264.7	31.2	19.8	2.7	<0.001	<0.001	1.9	0.6	204.7	18350	GL
RR-4	28.08.17		7.25												GL
RR-4	31.10.17		6.91	34.9	273.2	51.7	36.5	2.6	<0.001	<0.001	2.0	0.7	208.7		GL
RR-4	18.01.18	29.7	6.77	32.1	266.2	53.6	17.7	2.9	0.002	<0.001	2.4	0.5	190.3		Exxon
RR-4	31.01.18	29.4	6.64	31.8	265.2	53.0	19.3	2.9	0.001	<0.001	2.5	0.5	191.1		Exxon
RR-4	18.02.18	28.8	6.61	31.5	268.1	52.6	18.8	2.9	0.002	<0.001	2.5	0.5	194.3		Exxon
RR-4	23.04.18	30.5	6.52	32.7	284.7	54.6	21.9	2.9	0.001	<0.001	2.4	0.5	210.7		Exxon
RR-4	28.05.18	31.2	6.65	33.0	292.6	55.0	22.9	2.9	0.002	<0.001	2.5	0.5	216.7		Exxon
RR-3	22.02.17		7.20	21.0	112.1	14.0	22.4	1.5	<0.001	<0.001	3.3	0.4	95.8	9905	GL
RR-3	02.05.17		7.15	22.3	109.7	14.1	19.8	1.6	<0.001	<0.001	2.4	0.5	120.8	10056	GL
RR-3	07.06.17		6.80	21.8	114.1	12.4	20.8	1.3	<0.001	<0.001	2.3	0.4	99.0	9970	GL
RR-3	26.07.17		7.48	22.5	114.6	14.5	19.8	1.5	<0.001	<0.001	2.6	0.4	92.4	9590	GL
RR-3	28.08.17		7.12	22.6	118.0	14.1	20.8	1.6	<0.001	<0.001	2.4	0.4	102.2		GL
RR-3	31.10.17		7.13	22.9	123.1	10.9	28.1	1.5	<0.001	<0.001	2.6	0.4	125.4		GL
RR-3	18.01.18	15.02	7.21	21.2	114.5	10.7	19.8	1.6	0.001	<0.001	2.9	0.3	93.5		Exxon
RR-3	31.01.18	15.01	7.26	21.2	116.5	10.7	19.8	1.6	0.001	<0.001	3.0	0.3	93.9		Exxon
RR-3	18.02.18	14.98	7.26	21.6	113.5	10.9	20.8	1.6	0.001	<0.001	3.1	0.3	94.3		Exxon
RR-3	23.04.18	15.77	7.17	22.3	118.6	10.7	18.8	1.5	0.002	<0.001	3.0	0.3	92.4		Exxon
RR-3	28.05.18	16.96	7.21	24.8	134.5	11.3	18.8	1.6	0.001	<0.001	3.1	0.3	102.8		Exxon
RR-2	22.02.17		7.44	19.6	169.9	12.9	20.8	1.4	<0.001	<0.001	4.5	0.4	148.4	13010	GL
RR-2	02.05.17		7.14	19.0	170.4	16.6	15.6	1.5	<0.001	<0.001	3.2	0.5	171.0	12980	GL
RR-2	07.06.17		6.84	20.1	179.5	14.9	16.7	1.4	<0.001	<0.001	3.2	0.3	161.3	13410	GL
RR-2	26.07.17		7.40	19.8	175.2	13.9	16.1	1.5	<0.001	<0.001	3.2	0.3	149.5	12610	GL
RR-2	28.08.17		7.19	20.0	180.8	17.7	14.6	1.5	<0.001	<0.001	3.4	0.4	155.7		GL
RR-2	31.10.17		7.33	25.3	198.5	20.7	19.8	1.4	<0.001	<0.001	3.4	0.4	166.5		GL
RR-2	18.01.18	20.05	7.16	18.9	178.1	12.2	14.6	1.6	0.001	<0.001	3.8	0.3	145.4		Exxon
RR-2	31.01.18	20.24	7.29	19.2	178.1	12.4	15.1	1.6	0.001	<0.001	3.9	0.3	145.8		Exxon
RR-2	18.02.18	20.05	7.22	19.1	180.1	12.4	13.5	1.6	0.001	<0.001	4.0	0.3	144.1		Exxon
RR-2	23.04.18	20.80	7.17	19.6	177.9	12.0	11.5	1.6	0.001	<0.001	3.9	0.3	148.8		Exxon
RR-2	28.05.18	20.83	7.19	19.8	179.9	12.8	17.7	1.6	0.001	<0.001	3.9	0.3	150.9		Exxon
RR-1	22.02.17		7.36	22.5	253.6	17.2	18.8	1.1	<0.001	<0.001	6.5	0.4	219.7	17820	GL
RR-1	02.05.17		7.06	23.0	255.8	18.0	10.9	1.2	<0.001	<0.001	4.2	0.4	240.3	17404	GL
RR-1	07.06.17		6.88	22.5	262.6	18.7	10.4	1.2	<0.001	<0.001	4.4	0.3	224.1	17910	GL
RR-1	26.07.17		7.34	21.4	256.8	16.1	12.5	1.1	<0.001	<0.001	4.4	0.3	219.0	16910	GL
RR-1	28.08.17		7.49	23.4	242.7	18.1	13.0	1.1	<0.001	<0.001	4.9	0.3	211.8		GL
RR-1	31.10.17		7.02	27.7	280.2		20.8	1.0	<0.001	<0.001	3.3	0.4	219.6		GL
RR-1	18.01.18	26.8	7.11	20.5	252.5	15.1	10.9	1.1	0.002	<0.001	5.1	0.2	201.0		Exxon
RR-1	31.01.18	26.9	7.02	20.3	243.7	15.1	11.5	1.2	0.001	<0.001	5.1	0.2	194.1		Exxon
RR-1	18.02.18	26.8	7.09	20.5	244.7	15.2	10.9	1.2	0.001	<0.001	5.3	0.2	193.3		Exxon
RR-1	23.04.18	28.1	7.02	21.9	259.0	16.4	11.5	1.3	0.001	<0.001	5.6	0.3	203.7		Exxon
RR-1	28.05.18	27.8	6.99	21.4	257.0	16.0	10.4	1.2	0.001	<0.001	5.6	0.3	202.0		Exxon
AG-3	10.08.17		7.19	6.5	3.0	2.3	6.3	2.4	<0.001	<0.001	0.4	0.5	3.0	1303	GL
AG-3	28.08.17		7.29	4.9	2.9	2.0	3.6	2.6	<0.001	<0.001	0.3	0.5	2.5	858	GL
AG-3	31.10.17		7.81	4.1	3.7	2.4	3.3	2.2	<0.0021	<0.001	0.3	0.5	3.1	912	GL
AG-3	18.01.18	1.56	7.06	4.2	5.0	2.0	3.1	2.5	0.001	<0.001	0.4	0.4	4.0	1924	Exxon
AG-3	31.01.18	1.398	7.15	3.5	4.5	1.9	2.4	2.6	0.001	<0.001	0.4	0.4	3.8	1978	Exxon
AG-3	19.02.18	1.416	7.23	3.5	5.0	1.9	2.4	2.5	0.001	<0.001	0.4	0.4	3.8	2005	Exxon
AG-3	23.04.18	1.127	7.17	2.3	3.2	1.4	0.9	2.7	0.001	<0.001	0.3	0.4	2.7		Exxon
AG-3	28.05.18	1.079	7.16	2.3	3.0	1.5	1.0	2.7	0.001	<0.001	0.3	0.4	3.0		Exxon
AG-2	10.08.17		7.46	4.0	20.9	3.4	3.1	2.7	<0.001	<0.001	0.7	0.3	20.6	2635	GL
AG-2	28.08.17		7.41	4.3	21.5	2.3	2.6	2.7	<0.001	<0.001	0.7	0.3	18.3	1914	GL
AG-2	31.10.17		7.89	3.8	23.9	5.2	5.7	2.4	<0.001	<0.001	0.7	0.3	23.8	2454	GL
AG-2	18.01.18	3.64	7.36	4.0	22.3	2.6	3.2	2.6	0.001	<0.001	0.9	0.3	20.1	2853	Exxon
AG-2	31.01.18	3.37	7.51	4.2	23.0	2.8	3.8	2.6	0.001	<0.001	1.0	0.3	21.0	5597	Exxon
AG-2	19.02.18	3.874	7.56	4.3	24.0	2.8	3.6	2.6	0.001	<0.001	1.0	0.3	21.2	5489	Exxon
AG-2	23.04.18	3.56	7.27	3.7	20.8	2.5	3.1	2.6	0.001	<0.001	1.0	0.3	18.2		Exxon
AG-2	28.05.18	3.51	7.39	4.2	20.8	2.6	3.2	2.2	0.001	<0.001	1.0	0.3	18.0		Exxon
AG-1	10.08.17		7.39	9.3	23.8	3.3	13.5	1.2	<0.001	<0.001	0.7	0.2	27.6	3892	GL
AG-1	28.08.17		7.34	9.4	23.9	3.8	10.4	1.2	<0.001	<0.001	0.7	0.2	21.3	2915	GL
AG-1	31.10.17		6.93	9.7	28.2	2.9	13.5	2.7	<0.001	<0.001	0.7	0.2	36.1	3912	GL
AG-1	18.01.18	5.62	7.57	9.4	25.0	3.0	13.5	2.7	0.001	<0.001	0.9	0.2	34.2	6965	Exxon
AG-1	31.01.18	5.68	7.43	9.4	25.0	3.0	13.5	3.0	0.001	<0.001	0.9	0.2	34.1		Exxon
AG-1	19.02.18	5.61	7.38	9.5	24.9	3.0	13.5	2.9	0.001	<0.001	0.9	0.2	34.5		Exxon
AG-1	23.04.18	5.81	7.68	9.1	24.7	3.0	13.0	2.6	0.001	<0.001	0.9	0.1	31.3		Exxon
AG-1	28.05.18	5.78	7.33	9.1	24.7	3.1	14.1	2.6	0.001	<0.001	0.8	0.1	33.3		Exxon
AS-2	14.03.18	2.08	6.92	5.2	2.6	4.5	0.0	9.9	0.05	<0.001	0.5	1.1	3.3		Exxon
AS-2	06.06.18	1.81	6.9	3.4		3.5	0.3	9.9	0.010519	<0.001	0.4	0.8	2.2	932	Fugro

Well	Date	EC	pH	Ca	Cl	Mg	SO4	Alkalinity (CaCO3)	Al	Fe	K	Si	Na	TDS	LAB
		mS cm-1		mm l-1	mm l-1	mm l-1	mm l-1	mm l-1	mm l-1	mm l-1	mm l-1	mm l-1	mm l-1	mg l-1	
AS-2	08.07.18	1.81	6.8	5.8	2.4	5.2	0.2	10.1	<0.001	<0.001	0.5	0.4	2.1	1006	Fugro
AS-2	12.08.18	1.83	6.8	2.3	2.0	4.0	0.2	9.1	0.001	<0.001	0.5	0.2	2.0	1010	Fugro
AS-1	14.03.18	5.72	7.3	8.9	33.9	7.0	12.1	2.7	0.027	<0.001	2.5	0.3	32.7		Exxon
AS-1	06.06.18	4.90		3.7		3.6	10.0	1.5	0.004	<0.001	3.7	0.2	17.7	2700	Fugro
AS-1	08.07.18	5.20	8.0	5.2	28.7	5.6	10.5	2.4	<0.001	<0.001	3.6	0.1	16.1	2690	Fugro
AS-1	12.08.18	5.10	7.6	4.9	21.0	5.2	11.7	2.6	0.000815	<0.001	2.5	0.1	14.5	2810	Fugro
Farm 1 - AG	22.04.18	2.59	7.25	3.2	13.2	2.1	2.4	2.2	0.001	<0.001	0.6	0.3	11.3	3015	Exxon
Farm 1 - AG	27.05.18	2.67	7.18	3.5	14.0	2.3	2.9	2.2	0.001	<0.001	0.7	0.3	12.3	23	Exxon
Farm 2 - RR	07.10.18	5.63	6.72	9.5	26	6.8	16	1	0.034	0.002	1.9	0.3	30.2	3835	Exxon
UER Saudi	UER Saudi1		7.9	3.1	8.0	1.8	2.9				0.2		6.5		Unknown
UER Saudi	UER Saudi2			7.6	6.6	4.0	10.6						7.4		Unknown
UER Saudi	UER Saudi3		8.3	6.3	5.2	4.0	7.5				0.2		4.7		Unknown
UER Saudi	UER Saudi4			6.5	10.8	3.5	7.4						7.8		Unknown
UER Saudi	UER Saudi5			5.7	8.8	4.0	6.6						7.5		Unknown
UER Saudi	UER Saudi6			6.2	9.4	3.8	6.8						8.0		Unknown
UER Saudi	UER Saudi7			2.0	5.6	1.9	2.0						4.3		Unknown
UER Saudi	UER Saudi8			3.8	6.4	0.6	2.5						5.3		Unknown
UER Saudi	UER Saudi9			8.0	9.4	5.2	7.7						1.3		Unknown
UER Saudi	UER Saudi10			4.1	7.1	3.0	4.4						3.7		Unknown
UER Saudi	UER Saudi11			1.0	1.9	0.4	2.4						7.3		Unknown
UER Saudi	UER Saudi12			8.8	16.6	4.7	7.3						6.7		Unknown
UER Saudi	UER Saudi13			4.5	7.2	2.6	5.2						6.5		Unknown
UER Saudi	UER Saudi14			7.6	21.0	4.5	7.6						15.4		Unknown
UER Saudi	UER Saudi15		7.6	5.3	7.3	4.1	5.9						3.3		Unknown
UER Saudi	UER Saudi16			6.2	15.6	4.5	8.5						13.8		Unknown
UER Saudi	UER Saudi17			1.1	5.3	2.8	2.7						5.1		Unknown
UER Saudi	UER Saudi18			2.3	11.8	3.6	6.0						14.6		Unknown
UER Saudi	UER Saudi19			4.0	13.1	2.5	4.2						10.0		Unknown
UER Saudi	UER Saudi20			3.2	8.0	2.0	4.6						10.5		Unknown
UER Saudi	UER Saudi21			12.8	26.0	8.6	17.4						22.0		Unknown
UER Saudi	UER Saudi22			3.5	9.4	2.1	2.4						6.5		Unknown
UER Saudi	UER Saudi23			1.7	3.4	1.9	2.1						3.4		Unknown
UER Saudi	UER Saudi24			3.1	6.2	2.2	2.7						4.3		Unknown
UER Saudi	UER Saudi25			1.9	5.2	2.1	2.1						3.8		Unknown
UER Saudi	UER Saudi26			1.2	2.8	0.9	0.8						2.1		Unknown
UER Saudi	UER Saudi27			5.4	7.0	3.7	7.4						5.6		Unknown
UER Saudi	UER Saudi28			4.5	4.6	2.4	4.1						2.5		Unknown
UER Saudi	UER Saudi29			5.8	13.0	4.8	5.7						9.6		Unknown
UER Saudi	UER Saudi30			5.8	25.1	3.5	6.2						13.4		Unknown
UER Saudi	UER Saudi31			5.6	20.0	5.0	6.6						15.3		Unknown
UER Saudi	UER Saudi32			6.3	21.2	6.3	6.4						14.4		Unknown
UER Saudi	UER Saudi33			6.1	26.0	4.1	8.6						24.6		Unknown
UER Saudi	UER Saudi34			4.9	23.0	3.5	6.0						20.0		Unknown
UER Saudi	UER Saudi35			6.0	22.8	5.3	9.2						20.3		Unknown
UER Saudi	UER Saudi36			3.2	10.8	2.3	3.2						8.1		Unknown
UER Saudi	UER Saudi37		7.8	4.2	14.3	2.8	4.4				0.4		11.7		Unknown
UER Saudi	UER Saudi38		7.9	5.4	22.8	3.7	5.8				0.5		18.9		Unknown
UER Saudi	UER Saudi39		7.9	6.0	10.7	3.1	7.5				0.2		10.3		Unknown
UER Saudi	UER Saudi40		7.9	6.8	9.5	3.7	8.5				0.3		9.0		Unknown
UER Saudi	UER Saudi41		8.0	7.2	17.6	4.0	8.8				0.3		15.3		Unknown
UER Saudi	UER Saudi42		7.8	3.2	5.7	1.9	3.3				0.2		4.9		Unknown
UER Saudi	UER Saudi43		7.9	3.5	8.7	2.0	3.1				0.2		6.6		Unknown
UER Saudi	UER Saudi44		7.8	3.8	9.1	2.2	3.5				0.3		7.1		Unknown
UER Saudi	UER Saudi45		7.9	4.1	7.0	2.3	4.6				0.2		6.0		Unknown
UER Saudi	UER Saudi46		7.8	3.7	7.2	2.2	3.3				0.2		5.7		Unknown
UER Saudi	UER Saudi47		7.8	8.7	15.3	5.0	11.5				0.4		12.1		Unknown
UER Saudi	UER Saudi48		7.9	4.2	15.7	2.1	3.5				0.6		13.0		Unknown
UER Saudi	UER Saudi49		7.8	4.3	18.4	2.3	4.6				0.8		15.7		Unknown
UER Saudi	UER Saudi50		8.1	9.4	8.2	3.2	10.4				0.4		7.8		Unknown
UER Saudi	UER Saudi51		8.1	4.6	8.3	3.5	6.7				0.4		7.3		Unknown
UER Saudi	UER Saudi52		7.8	7.8	13.5	5.3	14.2				0.6		20.0		Unknown
UER Saudi	UER Saudi53		7.9	5.3	24.3	3.0	4.6				0.6		18.8		Unknown
UER Saudi	UER Saudi54		7.9	4.6	14.7	2.5	4.4				0.5		12.0		Unknown
UER Saudi	UER Saudi55		7.9	1.3	0.6	0.7	0.2				0.3		0.4		Unknown
UER Saudi	UER Saudi56		7.6	1.9	1.0	0.4	0.3				0.2		0.4		Unknown
UER Saudi	UER Saudi57		6.7	0.9	0.3	0.3	0.1				1.2		0.4		Unknown
UER Saudi	UER Saudi58		7.7	2.0	5.9	2.8	2.5				2.2		5.8		Unknown
UER Saudi	UER Saudi59		7.8	3.1	2.2	0.7	1.3				0.2		2.4		Unknown
UER Saudi	UER Saudi60			4.3	8.6	3.0	5.2						7.8		Unknown
UER Saudi	UER Saudi61			3.7	6.1	2.0	4.4						6.4		Unknown
UER Saudi	UER Saudi62		7.8	3.2	11.5	2.8	5.1				0.4		14.1		Unknown
UER Saudi	UER Saudi63		7.7	3.7	11.5	2.3	3.1				0.3		8.9		Unknown

Well	Date	EC	pH	Ca	Cl	Mg	SO4	Alkalinity (CaCO3)	Al	Fe	K	Si	Na	TDS	LAB
		mS cm-1		mm l-1	mm l-1	mm l-1	mm l-1	mm l-1	mm l-1	mm l-1	mm l-1	mm l-1	mm l-1	mg l-1	
UER Saudi	UER Saudi64		7.7	7.4	9.0	4.4	9.0				0.4		9.6		Unknown
UER Saudi	UER Saudi65		7.2	4.8	16.0	1.2	4.3				0.0		14.6		Unknown
UER Saudi	UER Saudi66		6.8	35.9	222.3	18.8	22.7				0.0		158.8		Unknown
UER Saudi	UER Saudi67		7.3	24.9	120.0	17.1	28.1				0.0		95.5		Unknown
UER Saudi	UER Saudi68			17.6	65.6	10.8	15.9				0.0		46.3		Unknown
UER Saudi	UER Saudi69		7.6	4.4	15.7	1.9	4.0				0.9		12.7		Unknown
UER Saudi	UER Saudi70		8.0	14.1	105.0	11.5	10.0				1.4		82.2		Unknown
UER Saudi	UER Saudi71														Unknown
UER Saudi	UER Saudi72														Unknown
UER Saudi	UER Saudi73														Unknown
UER Saudi	UER Saudi74														Unknown
UER Saudi	UER Saudi75														Unknown
UER Saudi	UER Saudi76														Unknown
UER Saudi	UER Saudi77		7.6	6.1	30.8	3.4	4.9				0.8		26.3		Unknown
UER Saudi	UER Saudi78			5.8	11.0	3.5	6.9				0.0		9.5		Unknown
UER Saudi	UER Saudi79			8.2	20.0	0.9	7.3				0.0		19.2		Unknown
UER Saudi	UER Saudi80		7.9	1.9	9.4	2.1	2.4				0.6		9.3		Unknown
UER Saudi	UER Saudi81			3.2	9.4	2.1	2.7						7.4		Unknown
UER Saudi	UER Saudi82		7.3	2.9	7.9	2.0	2.2						5.5		Unknown
UER Saudi	UER Saudi83		6.9	3.7	11.2	2.2	2.7						8.7		Unknown
UER Saudi	UER Saudi84		7.7	2.8	7.2	2.8	2.5						4.0		Unknown
UER Saudi	UER Saudi85		7.3	3.6	10.8	2.1	3.5						9.3		Unknown
UER Saudi	UER Saudi86		7.3	3.2	8.9	2.0	2.7						7.0		Unknown
UER Saudi	UER Saudi87		7.3	3.4	10.7	2.2	2.7						8.0		Unknown
UER Saudi	UER Saudi88		7.1	3.5	10.6	2.1	3.0						8.5		Unknown
UER Saudi	UER Saudi89		7.4	3.6	10.8	2.3	3.3						8.9		Unknown
UER Saudi	UER Saudi90		7.4	3.0	9.1	1.9	2.1						6.6		Unknown
UER Saudi	UER Saudi91		8.1	3.6	11.9	2.4	2.8				0.2		8.0		Unknown
UER Saudi	UER Saudi92		8.0	3.6	10.9	2.3	2.9				0.2		7.5		Unknown
UER Saudi	UER Saudi93		8.0	3.0	9.0	2.0	2.3				0.2		6.9		Unknown
UER Saudi	UER Saudi94		8.0	2.7	7.5	1.8	2.0				0.2		5.8		Unknown
UER Saudi	UER Saudi95		8.1	2.6	6.8	1.8	2.2				0.2		5.6		Unknown
UER Saudi	UER Saudi96		8.0	2.0	6.8	1.4	3.1				0.5		7.9		Unknown
UER Saudi	UER Saudi97		7.7	2.0	7.2	2.1	2.5						7.0		Unknown
UER Saudi	UER Saudi98		7.7	2.8	7.4	1.9	2.4						5.8		Unknown
UER Saudi	UER Saudi99		6.6	3.9	39.2	3.3	1.7				0.8		32.0		Unknown
UER Saudi	UER Saudi100			3.7	11.8	2.4	2.8						7.8		Unknown
UER Saudi	UER Saudi101			3.1	11.0	2.1	3.2						9.7		Unknown
UER Saudi	UER Saudi102			3.0	11.0	2.4	2.4						7.0		Unknown
UER Saudi	UER Saudi103			1.7	4.7	1.4	1.3						3.3		Unknown
UER Saudi	UER Saudi104			1.7	7.0	2.1	2.0						5.4		Unknown
UER Saudi	UER Saudi105			2.3	7.2	1.9	2.3						5.5		Unknown
UER Saudi	UER Saudi106			2.8	11.0	2.8	3.3						8.6		Unknown
UER Saudi	UER Saudi107			3.7	11.6	2.7	2.9						8.0		Unknown
UER Saudi	UER Saudi108			6.8	7.6	3.3	7.0						6.7		Unknown
UER Saudi	UER Saudi109			3.8	12.8	2.9	3.1						8.0		Unknown
UER Saudi	UER Saudi110			3.6	6.5	3.0	4.4						0.7		Unknown
UER Saudi	UER Saudi111			2.8	10.0	2.5	3.7						9.1		Unknown
UER Saudi	UER Saudi112			3.4	11.6	2.5	2.8						8.3		Unknown
UER Saudi	UER Saudi113			3.7	11.0	2.5	2.6						8.7		Unknown
UER Saudi	UER Saudi114		7.9	14.5	14.2	7.4	20.1				0.5		12.7		Unknown
UER Saudi	UER Saudi115		7.4	2.4	15.2	1.8	3.6						18.5		Unknown
UER Saudi	UER Saudi116		7.6	5.0	4.5	2.8	5.8				0.2		6.7		Unknown
UER Saudi	UER Saudi117			3.1	19.0	2.3	4.4						20.2		Unknown
UER Saudi	UER Saudi118		8.1	2.9	5.3	2.6	3.5				0.2		4.1		Unknown
UER Saudi	UER Saudi119		7.6	9.8	60.9	8.2	9.6				0.6		44.4		Unknown
UER Saudi	UER Saudi120		8.0	1.9	0.8	0.8	0.7				1.1		1.1		Unknown
UER Saudi	UER Saudi121		8.0	3.0	6.8	1.6	2.2				0.2		5.6		Unknown
UER Saudi	UER Saudi122		7.1	3.9	12.3	2.3	3.5						9.7		Unknown
UER Saudi	UER Saudi123		8.1	7.7	6.5	4.2	10.8						6.3		Unknown
UER Saudi	UER Saudi124		8.1	9.2	8.1	4.8	12.1				0.3		6.8		Unknown
UER Saudi	UER Saudi125		8.1	7.2	8.0	5.1	12.1				0.3		6.4		Unknown
UER Saudi	UER Saudi126		7.9	5.3	6.4	3.0	5.6				0.3		7.9		Unknown
UER Saudi	UER Saudi127		8.1	5.8	10.0	3.2	6.7				0.3		8.0		Unknown
UER Saudi	UER Saudi128		7.7	4.8	18.1	3.2	5.0				0.5		15.2		Unknown
UER Saudi	UER Saudi129		7.7	4.5	16.1	3.4	5.0				0.5		14.0		Unknown
UER Saudi	UER Saudi130		7.6	4.5	13.7	2.7	4.6				0.3		10.2		Unknown
UER Saudi	UER Saudi131		7.9	5.3	9.0	3.4	7.1				0.3		7.8		Unknown
UER Saudi	UER Saudi132		8.0	6.2	9.0	3.5	7.3				0.3		7.5		Unknown
UER Saudi	UER Saudi133		7.9	16.5	4.9	7.0	22.5				0.3		4.5		Unknown
UER Saudi	UER Saudi134		7.7	17.2	6.8	4.9	22.5				0.4		8.4		Unknown
UER Saudi	UER Saudi135		7.9	8.2	4.8	6.0	15.6				0.8		9.7		Unknown

Well	Date	EC	pH	Ca	Cl	Mg	SO4	Alkalinity (CaCO3)	Al	Fe	K	Si	Na	TDS	LAB
		mS cm-1		mm l-1	mm l-1	mm l-1	mm l-1	mm l-1	mm l-1	mm l-1	mm l-1	mm l-1	mm l-1	mg l-1	
UER Saudi	UER Saudi136		7.9	5.4	4.6	3.5	8.0				0.6		4.8		Unknown
UER Saudi	UER Saudi137		8.2	5.6	30.4	3.2	4.8				0.8		24.2		Unknown
UER Saudi	UER Saudi138			7.1	35.4	4.0	5.8						27.7		Unknown
UER Saudi	UER Saudi139			3.3	8.0	1.8	1.2						3.6		Unknown
UER Saudi	UER Saudi140			2.9	9.0	2.1	2.2						6.0		Unknown
UER Saudi	UER Saudi141		8.1	11.2	4.4	4.2	13.1				0.4		4.7		Unknown
UER Saudi	UER Saudi142			7.8	6.4	6.4	15.5						10.6		Unknown
UER Saudi	UER Saudi143			9.4	14.7	7.2	17.6						17.5		Unknown
UER Saudi	UER Saudi144		7.5	15.2	71.9	10.2	19.4				1.6		62.5		Unknown
UER Saudi	UER Saudi145		7.9	5.8	9.3	3.5	6.9				0.3		8.0		Unknown
UER Saudi	UER Saudi146			3.2	10.8	1.6	3.5						12.4		Unknown
UER Saudi	UER Saudi147			1.5	7.4	1.3	3.2						9.0		Unknown
UER Saudi	UER Saudi148			10.0	8.0	6.5	15.9						8.4		Unknown
UER Saudi	UER Saudi149			14.2	7.6	7.0	20.8						7.8		Unknown
UER Saudi	UER Saudi150			3.1	7.2	2.1	7.1						13.3		Unknown
UER Saudi	UER Saudi151			3.3	14.0	2.4	4.8						14.8		Unknown
UER Saudi	UER Saudi152			0.9	2.6	0.7	1.0						4.1		Unknown
UER Saudi	UER Saudi153			2.2	9.6	2.2	5.1						14.7		Unknown
UER Saudi	UER Saudi154			2.2	3.2	0.4	1.9						4.4		Unknown
UER Saudi	UER Saudi155			1.5	2.0	0.5	0.9						2.7		Unknown
UER Saudi	UER Saudi156		7.8	6.5	5.7	3.8	9.2				0.2		4.6		Unknown
Seawater	Seawater 1		8.1	13.5	739.6	63.9	31.3	1.5					627.4		Exxon
Seawater	Seawater 2		8.2	13.3	711.8	62.3	31.3	1.5					631.4		Exxon
Seawater	Seawater 3		8.5	14.0	721.7	66.9	29.2	1.3					620.5		Exxon
Seawater	Seawater 4		8.2	12.0	674.0	68.0	35.4		0.0	0.1	11.9		587.0		Unknown
Seawater	Seawater 5		8.2	12.8	631.0	63.0	36.3				10.8		531.0		Unknown
Rain	Rain		4.6	0.1	0.2	0.1	0.1				0.0		0.1		Unknown

Appendix B3 Scale Permeability Results

Scale Permeability

	Formation	Test Type	k (D)		Formatic	Test Type	k (D)		Formation	Test Type	k (D)
1	Dammam	core	1.00E-05	67	Rus	core	2.90E-03	133	Rus	core	2.68E-01
2	Dammam	core	1.00E-05	68	Rus	core	3.09E-03	134	Rus	core	2.81E-01
3	Dammam	core	1.00E-05	69	Rus	core	3.16E-03	135	Rus	core	3.04E-01
4	Dammam	core	1.00E-05	70	Rus	core	3.70E-03	136	Rus	core	3.18E-01
5	Dammam	core	1.00E-05	71	Rus	core	4.50E-03	137	Rus	core	3.42E-01
6	Dammam	core	1.00E-05	72	Rus	core	5.00E-03	138	Rus	core	3.79E-01
7	Dammam	core	1.00E-05	73	Rus	core	5.79E-03	139	Rus	core	4.49E-01
8	Dammam	core	1.00E-05	74	Rus	core	5.86E-03	140	Rus	core	4.85E-01
9	Dammam	core	1.00E-05	75	Rus	core	6.10E-03	141	Rus	core	5.02E-01
10	Dammam	core	1.00E-05	76	Rus	core	6.20E-03	142	Rus	core	5.15E-01
11	Dammam	core	1.00E-05	77	Rus	core	6.25E-03	143	Rus	core	5.65E-01
12	Dammam	core	1.00E-05	78	Rus	core	7.40E-03	144	Rus	core	6.35E-01
13	Dammam	core	1.00E-05	79	Rus	core	7.46E-03	145	Rus	core	6.49E-01
14	Dammam	core	1.00E-05	80	Rus	core	9.20E-03	146	Rus	core	7.44E-01
15	Dammam	core	1.00E-05	81	Rus	core	9.33E-03	147	Rus	core	7.80E-01
16	Dammam	core	1.00E-05	82	Rus	core	9.37E-03	148	Rus	core	8.23E-01
17	Dammam	core	1.00E-05	83	Rus	core	1.10E-02	149	Rus	core	9.82E-01
18	Dammam	core	1.00E-05	84	Rus	core	1.10E-02	150	Rus	core	1.05E+00
19	Dammam	core	1.00E-05	85	Rus	core	1.20E-02	151	Rus	core	1.15E+00
20	Dammam	core	1.00E-05	86	Rus	core	1.30E-02	152	Rus	core	2.24E+00
21	Dammam	core	1.00E-05	87	Rus	core	1.30E-02	153	UER	core	1.00E-05
22	Dammam	core	1.00E-05	88	Rus	core	1.39E-02	154	UER	core	1.00E-05
23	Dammam	core	1.00E-05	89	Rus	core	1.40E-02	155	UER	core	1.00E-05
24	Dammam	core	1.00E-05	90	Rus	core	1.75E-02	156	UER	core	2.57E-05
25	Dammam	core	1.00E-05	91	Rus	core	1.81E-02	157	UER	core	3.00E-05
26	Dammam	core	1.00E-05	92	Rus	core	2.10E-02	158	UER	core	4.89E-05
27	Dammam	core	1.00E-05	93	Rus	core	2.10E-02	159	UER	core	5.00E-05
28	Dammam	core	1.45E-05	94	Rus	core	2.23E-02	160	UER	core	8.00E-05
29	Dammam	core	3.00E-05	95	Rus	core	2.59E-02	161	UER	core	1.00E-04
30	Dammam	core	4.29E-05	96	Rus	core	2.60E-02	162	UER	core	1.03E-04
31	Dammam	core	5.84E-05	97	Rus	core	2.65E-02	163	UER	core	1.50E-04
32	Dammam	core	5.90E-04	98	Rus	core	2.71E-02	164	UER	core	2.63E-04
33	Dammam	core	1.25E-03	99	Rus	core	2.77E-02	165	UER	core	3.80E-04
34	Dammam	core	1.29E-03	100	Rus	core	3.82E-02	166	UER	core	4.19E-04
35	Dammam	core	1.50E-03	101	Rus	core	4.10E-02	167	UER	core	5.60E-04
36	Dammam	core	1.50E-03	102	Rus	core	4.15E-02	168	UER	core	6.90E-04
37	Dammam	core	4.03E-02	103	Rus	core	5.28E-02	169	UER	core	8.10E-04
38	Dammam	core	5.19E-02	104	Rus	core	5.70E-02	170	UER	core	9.70E-04
39	Dammam	core	1.16E-01	105	Rus	core	5.94E-02	171	UER	core	9.70E-04
40	Dammam	core	1.54E-01	106	Rus	core	6.21E-02	172	UER	core	1.30E-03
41	Rus	core	2.00E-06	107	Rus	core	8.27E-02	173	UER	core	1.30E-03
42	Rus	core	8.05E-06	108	Rus	core	8.45E-02	174	UER	core	1.31E-03
43	Rus	core	1.00E-05	109	Rus	core	8.45E-02	175	UER	core	1.40E-03
44	Rus	core	1.00E-05	110	Rus	core	8.81E-02	176	UER	core	1.40E-03
45	Rus	core	1.00E-05	111	Rus	core	9.62E-02	177	UER	core	1.50E-03
46	Rus	core	1.00E-05	112	Rus	core	1.01E-01	178	UER	core	1.50E-03
47	Rus	core	1.00E-05	113	Rus	core	1.11E-01	179	UER	core	1.52E-03
48	Rus	core	1.85E-05	114	Rus	core	1.12E-01	180	UER	core	2.10E-03
49	Rus	core	2.00E-05	115	Rus	core	1.17E-01	181	UER	core	2.30E-03
50	Rus	core	2.00E-05	116	Rus	core	1.17E-01	182	UER	core	2.40E-03
51	Rus	core	2.05E-05	117	Rus	core	1.22E-01	183	UER	core	2.51E-03
52	Rus	core	4.00E-05	118	Rus	core	1.26E-01	184	UER	core	2.71E-03
53	Rus	core	6.04E-05	119	Rus	core	1.28E-01	185	UER	core	2.80E-03
54	Rus	core	1.00E-04	120	Rus	core	1.30E-01	186	UER	core	3.10E-03
55	Rus	core	1.20E-04	121	Rus	core	1.51E-01	187	UER	core	4.50E-03
56	Rus	core	3.20E-04	122	Rus	core	1.53E-01	188	UER	core	4.95E-03
57	Rus	core	5.52E-04	123	Rus	core	1.55E-01	189	UER	core	5.00E-03
58	Rus	core	6.00E-04	124	Rus	core	1.66E-01	190	UER	core	5.20E-03
59	Rus	core	6.10E-04	125	Rus	core	1.84E-01	191	UER	core	5.44E-03
60	Rus	core	8.90E-04	126	Rus	core	1.99E-01	192	UER	core	5.50E-03
61	Rus	core	1.36E-03	127	Rus	core	2.06E-01	193	UER	core	5.70E-03
62	Rus	core	1.40E-03	128	Rus	core	2.28E-01	194	UER	core	6.39E-03
63	Rus	core	1.50E-03	129	Rus	core	2.47E-01	195	UER	core	6.44E-03
64	Rus	core	1.60E-03	130	Rus	core	2.55E-01	196	UER	core	6.72E-03
65	Rus	core	1.85E-03	131	Rus	core	2.61E-01	197	UER	core	7.10E-03
66	Rus	core	2.82E-03	132	Rus	core	2.61E-01	198	UER	core	8.60E-03

Scale Permeability

Formation	Test Type	k (D)	Formation	Test Type	k (D)	Formation	Test Type	k (D)
199 UER	core	9.00E-03	265 UER	core	1.23E-01	331 Dammam	pump	1.46E+01
200 UER	core	9.30E-03	266 UER	core	1.25E-01	332 Dammam	pump	3.89E+01
201 UER	core	9.90E-03	267 UER	core	1.26E-01	333 Rus	pump	1.53E-02
202 UER	core	1.00E-02	268 UER	core	1.29E-01	334 Rus	pump	7.39E-01
203 UER	core	1.10E-02	269 UER	core	1.29E-01	335 Rus	pump	9.66E-01
204 UER	core	1.11E-02	270 UER	core	1.44E-01	336 Rus	pump	9.84E-01
205 UER	core	1.14E-02	271 UER	core	1.45E-01	337 Rus	pump	1.67E+00
206 UER	core	1.20E-02	272 UER	core	1.47E-01	338 Rus	pump	2.76E+00
207 UER	core	1.35E-02	273 UER	core	1.59E-01	339 Rus	pump	2.94E+00
208 UER	core	1.40E-02	274 UER	core	1.60E-01	340 Rus	pump	3.99E+00
209 UER	core	1.40E-02	275 UER	core	1.62E-01	341 Rus	pump	4.60E+00
210 UER	core	1.40E-02	276 UER	core	1.70E-01	342 Rus	pump	6.94E+00
211 UER	core	1.50E-02	277 UER	core	1.74E-01	343 Rus	pump	2.31E+01
212 UER	core	1.63E-02	278 UER	core	1.84E-01	344 Rus	pump	2.43E+01
213 UER	core	1.90E-02	279 UER	core	1.96E-01	345 Rus	pump	3.47E+01
214 UER	core	2.00E-02	280 UER	core	1.98E-01	346 Rus	pump	4.80E+01
215 UER	core	2.10E-02	281 UER	core	2.10E-01	347 Rus	pump	8.10E+01
216 UER	core	2.20E-02	282 UER	core	2.43E-01	348 UER	pump	4.50E+00
217 UER	core	2.22E-02	283 UER	core	2.47E-01	349 UER	pump	5.09E+00
218 UER	core	2.31E-02	284 UER	core	2.52E-01	350 UER	pump	1.30E+01
219 UER	core	2.50E-02	285 UER	core	2.61E-01	351 UER	pump	2.20E+01
220 UER	core	2.67E-02	286 UER	core	2.64E-01	352 UER	pump	5.07E+01
221 UER	core	2.90E-02	287 UER	core	2.66E-01	353 UER	pump	5.67E+01
222 UER	core	3.00E-02	288 UER	core	2.85E-01	354 UER	pump	1.56E+02
223 UER	core	3.20E-02	289 UER	core	2.97E-01	355 UER	pump	1.67E+02
224 UER	core	3.50E-02	290 UER	core	3.00E-01	356 UER	pump	2.92E+02
225 UER	core	3.70E-02	291 UER	core	3.25E-01	357 UER	pump	4.34E+02
226 UER	core	3.90E-02	292 UER	core	3.30E-01	358 UER	pump	1.10E+03
227 UER	core	4.00E-02	293 UER	core	3.31E-01	359 UER	pump	1.62E+03
228 UER	core	4.20E-02	294 UER	core	3.37E-01	360 Dammam	slug	8.81E-01
229 UER	core	4.52E-02	295 UER	core	3.57E-01	361 Dammam	slug	1.24E+00
230 UER	core	4.81E-02	296 UER	core	3.58E-01	362 Dammam	slug	3.29E+00
231 UER	core	5.40E-02	297 UER	core	5.12E-01	363 Dammam	slug	4.34E+00
232 UER	core	5.40E-02	298 UER	core	5.71E-01	364 Dammam	slug	5.05E+00
233 UER	core	5.40E-02	299 UER	core	5.76E-01	365 Dammam	slug	8.67E+00
234 UER	core	5.57E-02	300 UER	core	6.64E-01	366 Dammam	slug	9.39E+00
235 UER	core	5.60E-02	301 UER	core	6.80E-01	367 Dammam	slug	9.53E+00
236 UER	core	5.71E-02	302 UER	core	7.76E-01	368 Dammam	slug	9.92E+00
237 UER	core	5.73E-02	303 UER	core	7.78E-01	369 Dammam	slug	1.30E+01
238 UER	core	5.80E-02	304 UER	core	8.09E-01	370 Dammam	slug	1.63E+01
239 UER	core	6.10E-02	305 UER	core	8.27E-01	371 Dammam	slug	1.86E+01
240 UER	core	6.20E-02	306 UER	core	1.04E+00	372 Dammam	slug	2.52E+01
241 UER	core	6.60E-02	307 UER	core	1.07E+00	373 Dammam	slug	2.72E+01
242 UER	core	6.70E-02	308 UER	core	1.31E+00	374 Dammam	slug	4.00E+01
243 UER	core	6.92E-02	309 UER	core	1.33E+00	375 Dammam	slug	4.33E+01
244 UER	core	7.20E-02	310 UER	core	1.47E+00	376 Dammam	slug	4.66E+01
245 UER	core	7.36E-02	311 UER	core	1.68E+00	377 Dammam	slug	4.98E+01
246 UER	core	7.37E-02	312 UER	core	1.91E+00	378 Dammam	slug	5.44E+01
247 UER	core	7.70E-02	313 UER	core	2.54E+00	379 Dammam	slug	5.66E+01
248 UER	core	8.05E-02	314 UER	core	2.91E+00	380 Dammam	slug	6.47E+01
249 UER	core	9.00E-02	315 UER	core	3.16E+00	381 Dammam	slug	7.95E+01
250 UER	core	9.20E-02	316 UER	core	3.18E+00	382 Dammam	slug	8.73E+01
251 UER	core	9.20E-02	317 UER	core	7.42E+00	383 Dammam	slug	8.75E+01
252 UER	core	9.30E-02	318 Rus	packer	1.80E-02	384 Dammam	slug	1.08E+02
253 UER	core	9.30E-02	319 Rus	packer	5.00E-02	385 Dammam	slug	1.47E+02
254 UER	core	9.40E-02	320 UER	packer	8.00E-05	386 Dammam	slug	1.79E+02
255 UER	core	9.70E-02	321 UER	packer	6.00E-03	387 Dammam	slug	1.95E+02
256 UER	core	1.02E-01	322 UER	packer	2.84E-01	388 Dammam	slug	2.04E+02
257 UER	core	1.02E-01	323 UER	packer	3.21E-01	389 Dammam	slug	2.61E+02
258 UER	core	1.06E-01	324 Damman	pump	2.56E-01	390 Dammam	slug	2.88E+02
259 UER	core	1.07E-01	325 Damman	pump	8.17E-01	391 Dammam	slug	5.41E+02
260 UER	core	1.09E-01	326 Damman	pump	1.98E+00	392 Rus	slug	6.08E-02
261 UER	core	1.11E-01	327 Damman	pump	2.49E+00			
262 UER	core	1.14E-01	328 Damman	pump	2.57E+00			
263 UER	core	1.17E-01	329 Damman	pump	3.50E+00			
264 UER	core	1.21E-01	330 Damman	pump	8.58E+00			

Appendix C Geotechnical Logs



GULF LABORATORIES Co.

Doha - State of Qatar

Project:
Geological Survey

Borehole
EMRQ_RR_01

Machine: DESCO-02 Flush: Water Core Dia (mm): 102 Method: Hand Excavation & Rotary coring	Borehole Diameter (mm): 146/150 Casing Diameter (mm): 146/150 Location: Rawdat Rashid Coordinates: 201246.1 mE 387180.6 mN	Ground Level (m QNHD): 43.55 Start Date: 10/4/16 End Date: 10/27/16	Client: EXXON MOBILE RESEARCH QATAR Engineer:	Project No. SI1998 Sheet 1 of 14
--	--	--	---	---

Borehole Progress			Rock Core Quality				Sample Type	Sample Depth	Field Records	Level	Depth (m) (Thickness)	Description	Legend	Water
Date	Casing Depth (m)	Depth to Water (m) Flush Return	TCR	SCR	RQD	FI								
04/10	0.70											Light brown silty sandy GRAVEL of fine to coarse limestone. (RESIDUAL SOIL)		
05/10			100	100	100			SPT (c) 25/35mm, 100/55mm N=100/55mm	42.85	0.70	Very weak to weak white occasionally pinkish white, crystalline rinded LIMESTONE within matrix (15-20%) of extremely to very weak white, off-white, light brownish white and greenish grey, locally red, SILTSTONE. Occasional vugs (<2mm diameter) within crystalline limestone. Slightly weathered. Discontinuities are medium spaced and sub-vertical. (SIMSIMA LIMESTONE)			
			100	100	100					1.30				
			100	100	100					2.30				
			100	100	100				40.62	2.93	Very weak to weak white and light pinkish red crystalline LIMESTONE within matrix (15-20%) of extremely to very weak white, light greyish green and red SILTSTONE. Partially weathered. Occasional vugs (<2mm diameter) within crystalline limestone. Slightly weathered. Discontinuities are medium spaced and sub-vertical. (SIMSIMA LIMESTONE)			
			100	100	100	15				3.80				
			100	100	100					5.30				
			100	100	100					6.80				
			100	93	89					7.86		Weak white locally light yellowish brown crystalline LIMESTONE. Fresh. Widely spaced and sub-vertical. (SIMSIMA LIMESTONE)		
			100	100	100	3				8.30				
			100	100	100					9.80				
			100	100	100	12								

Remarks : 1. Hand excavation up to 0.70m bgl. 2. Groundwater was encountered at 6.80m bgl during drilling. 3. Logged in accordance with BS 5930: 1999+A2:2010.	Logged By :	Checked by :
		E.Stanmore
	Appendix No. :	
	1	

GL LIB 06.GLB Log GI CORE LOG-2 EXXON MOBILE.GPJ <<DrawingFiles>> 11/06/2017 08:13 Produced by gINT Professional



GULF LABORATORIES Co.

Doha - State of Qatar

Project:
Geological Survey

Borehole
EMRQ_RR_01

Machine: DESCO-02 Flush: Water Core Dia (mm): 102 Method: Hand Excavation & Rotary coring	Borehole Diameter (mm): 146/150 Casing Diameter (mm): 146/150	Ground Level (m QNHD): 43.55	Client: EXXON MOBILE RESEARCH QATAR	Project No. SI1998
	Location: Rawdat Rashid Coordinates: 201246.1 mE 387180.6 mN	Start Date: 10/4/16 End Date: 10/27/16	Engineer:	Sheet 2 of 14

Borehole Progress			Rock Core Quality				Sample Type	Sample Depth	Field Records	Level	Depth (m) (Thickness)	Description	Legend	Water
Date	Casing Depth (m)	Depth to Water (m) Flush Return	TCR	SCR	RQD	FI								
			100	100	100		C			32.83	(2.86) 10.72	Weak white locally light yellowish brown crystalline LIMESTONE. Fresh. Widely spaced and sub-vertical. (SIMSIMA LIMESTONE)		
			100	100	100		C			11.30	11.0	Very weak locally weak white and light yellowish brown fine grained LIMESTONE interbedded with very weak brown SHALE and very weak white mottled yellowish brown SILTSTONE. Slightly weathered. Discontinuities are medium spaced and sub-vertical. (SIMSIMA LIMESTONE) ...from 10.85m to 11.03m very weak brown shale thickly laminated to very thinly interbedded with very weak off-white and yellowish white siltstone		
			100	100	100		C			12.80	12.0	...from 11.27m to 11.29m extremely weak brown shale ...from 11.59m to 11.65m extremely weak white siltstone very thinly to thickly interbedded with very weak brown shale and very weak white limestone ...between 11.89m and 12.28m extremely weak with two vertical discontinuities - healed		
			100	87	87	12	C			14.30	13.0	...between 12.78m and 12.94m very weak brown shale and very weak reddish brown siltstone with vertical discontinuity		
			100	87	87	12	C			29.78	13.77below 13.54 extremely to very weak brown shale with light greyish green siltstone with vertical discontinuity		
			100	100	100		C			14.30	14.0	Very weak and weak white crystalline LIMESTONE. Slightly weathered. Discontinuities are medium spaced and sub-horizontal and sub-vertical. (SIMSIMA LIMESTONE)		
			100	100	100		C			28.97	14.58	Very weak white and yellow brown Siltstone. Slightly weathered. (SIMSIMA LIMESTONE)		
			100	100	100		C			28.60	15.0between 14.84m and 14.95m very weak brown shale		
			100	100	100		C			15.80	15.80	Very weak and weak white crystalline and fine grained LIMESTONE with occasional vugs (<20mm diameter) interbedded with very weak white, greyish green and locally orangish brown SILTSTONE. Slightly weathered. Discontinuities are medium spaced and sub-vertical. (RUS FORMATION)		
			100	100	100		C			16.0	16.0	...from 15.60m to 16.05m with frequent vugs (<30mm diameter)		
			100	100	100		C			26.87	16.68	...from 16.20m to 16.68m very weak light greyish green siltstone		
			0				C			17.30	17.0	Very weak off-white pitted LIMESTONE. Slightly weathered. Discontinuities are widely spaced and sub-horizontal. (RUS FORMATION)		
			100	100	100	4	C			18.0	18.0			
			100	100	100		C			(3.83)	18.0			
05/10	18.80	6.80					C			18.80	18.80			
06/10			0	100	100		C				19.0			

Remarks : 1.Hand excavation up to 0.70m bgl. 2. Groundwater was encountered at 6.80m bgl during drilling. 3. Logged in accordance with BS 5930: 1999+A2:2010.	Logged By :	Checked by : E.Stanmore
	Appendix No. :	
	2	

GL LIB 06.GLB Log_GI_CORE LOG-2 EXXON MOBILE.GPJ <-DrawingFiles>> 11/06/2017 08:13 Produced by gINT Professional



GULF LABORATORIES Co.

Doha - State of Qatar

Project:
Geological Survey

Borehole
EMRQ_RR_01

Machine: DESCO-02 Flush: Water Core Dia (mm): 102 Method: Hand Excavation & Rotary coring	Borehole Diameter (mm): 146/150 Casing Diameter (mm): 146/150 Location: Rawdat Rashid Coordinates: 201246.1 mE 387180.6 mN	Ground Level (m QNHD): 43.55 Start Date: 10/4/16 End Date: 10/27/16	Client: EXXON MOBILE RESEARCH QATAR Engineer:	Project No. SI1998 Sheet 3 of 14
--	--	--	---	---

Borehole Progress			Rock Core Quality				Sample Type	Sample Depth	Field Records	Level	Depth (m) (Thickness)	Description	Legend	Water
Date	Casing Depth (m)	Depth to Water (m) Flush Return	TCR	SCR	RQD	FI								
			100	100	100		C			20.30	Very weak off-white pitted LIMESTONE. Slightly weathered. Discontinuities are widely spaced and sub-horizontal. (RUS FORMATION)			
						4	C			20.51				
			100	100	100		C			21.0 (1.19)	Very weak off-white chalky LIMESTONE. Slightly weathered. (RUS FORMATION)			
							C			21.70	Very weak and weak crystalline LIMESTONE with occasional vugs (1-30mm diameter, max. 70mm diameter) thinly to interbedded with very weak green SILTSTONE. Slightly weathered. Discontinuities are medium locally closely spaced and sub-vertical. (RUS FORMATION)			
			100	100	100		C			21.80				
							C			22.0	...between 23.40m to 23.86m pinkish red, very closely spaced with subvertical discontinuity			
			100	90	87		C			23.0				
							C			23.30				
		0					C			24.0	...from 24.90m to 25.00m open discontinuity infilled with small to medium sized gravel crystals and stained orange-brown			
			93	94	94	25	C			24.80				
							C			25.0 (6.74)	Very weak locally extremely weak light green and light brown occasionally pinkish red SILTSTONE interbedded with very weak off-white and orangish brown chalky LIMESTONE and extremely weak greyish green CLAYSTONE. Slightly weathered. Discontinuities are medium spaced and sub-horizontal. (RUS FORMATION)			
			100	100	100		C			26.0				
			100	100	100		C			26.30				
							C			27.0	Very weak locally extremely weak light green and light brown occasionally pinkish red SILTSTONE interbedded with very weak off-white and orangish brown chalky LIMESTONE and extremely weak greyish green CLAYSTONE. Slightly weathered. Discontinuities are medium spaced and sub-horizontal. (RUS FORMATION)			
			100	93	91		C			27.70				
							C			28.0	Very weak locally extremely weak light green and light brown occasionally pinkish red SILTSTONE interbedded with very weak off-white and orangish brown chalky LIMESTONE and extremely weak greyish green CLAYSTONE. Slightly weathered. Discontinuities are medium spaced and sub-horizontal. (RUS FORMATION)			
			100	93	91		C			28.44				
							C			29.0	Very weak locally extremely weak light green and light brown occasionally pinkish red SILTSTONE interbedded with very weak off-white and orangish brown chalky LIMESTONE and extremely weak greyish green CLAYSTONE. Slightly weathered. Discontinuities are medium spaced and sub-horizontal. (RUS FORMATION)			
			100	100	100	10	C			29.20 (3.71)				

Remarks : 1. Hand excavation up to 0.70m bgl. 2. Groundwater was encountered at 6.80m bgl during drilling. 3. Logged in accordance with BS 5930: 1999+A2:2010.	Logged By : Checked by : E.Stanmore	Appendix No. : 3
---	---	----------------------------

GL LIB 06.GLB Log GI CORE LOG-2 EXXON MOBILE.GPJ <-DrawingFiles> 11/06/2017 08:13 Produced by gINT Professional



GULF LABORATORIES Co.

Doha - State of Qatar

Project:
Geological Survey

Borehole
EMRQ_RR_01

Machine: DESCO-02 Flush: Water Core Dia (mm): 102 Method: Hand Excavation & Rotary coring	Borehole Diameter (mm): 146/150 Casing Diameter (mm): 146/150 Location: Rawdat Rashid Coordinates: 201246.1 mE 387180.6 mN	Ground Level (m QNHD): 43.55 Start Date: 10/4/16 End Date: 10/27/16	Client: EXXON MOBILE RESEARCH QATAR Engineer:	Project No. SI1998 Sheet 4 of 14
--	--	--	---	---

Borehole Progress			Rock Core Quality				Field Records		Level	Depth (m) (Thickness)	Description	Legend	Water
Date	Casing Depth (m)	Depth to Water (m) Flush Return	TCR	SCR	RQD	FI	Sample Type	Sample Depth					
			100	100	100								
						10		30.70					
			93	93	93								
								32.20	11.40	32.15			
		0	100	100	100								
								33.70					
			93	93	93				9.52	34.03 (0.40)			
06/10	35.20	34.20						35.20	8.49	35.06 (0.63)			
08/10		35.00											
			100	100	100	15			7.67	35.88 (0.34)			
								36.70	7.33	36.22 (0.48)			
			100	100	100								
								38.20					
			100	100	100								
								39.70					
			53	53	53					39.85 (1.52)			

GL LIB 06.GLB Log GI CORE LOG-2 EXXON MOBILE.GPJ <-DrawingFiles> 11/06/2017 08:13 Produced by gINT Professional

Remarks : 1. Hand excavation up to 0.70m bgl. 2. Groundwater was encountered at 6.80m bgl during drilling. 3. Logged in accordance with BS 5930: 1999+A2:2010.	Logged By :	Checked by : E.Stanmore
	Appendix No. :	
	4	



GULF LABORATORIES Co.

Doha - State of Qatar

Project:
Geological Survey

Borehole
EMRQ_RR_01

Machine: DESCO-02 Flush: Water Core Dia (mm): 102 Method: Hand Excavation & Rotary coring	Borehole Diameter (mm): 146/150 Casing Diameter (mm): 146/150	Ground Level (m QNHD): 43.55	Client: EXXON MOBILE RESEARCH QATAR	Project No. SI1998
	Location: Rawdat Rashid Coordinates: 201246.1 mE 387180.6 mN	Start Date: 10/4/16 End Date: 10/27/16	Engineer:	Sheet 6 of 14

Borehole Progress			Rock Core Quality				Field Records		Level	Depth (m) (Thickness)	Description	Legend	Water
Date	Casing Depth (m)	Depth to Water (m) Flush Return	TCR	SCR	RQD	FI	Sample Type	Sample Depth					
			100	100	100					green siltstone Very weak to weak light greyish white GYPSUM. Slightly weathered. Discontinuities are widely spaced and horizontal to sub-horizontal. (RUS FORMATION)	◇		
								51.30					
			100	100	100	15			52.0 (9.05)				
								52.80					
		0	68	68	68				53.0				
								54.30	-10.62	...from 54.1m to 55.60m packer test taken with seal from 53.1m to 54.1m			
			0	0	0			54.80	-10.75	Weak light brownish grey fine to medium grained LIMESTONE. Slightly weathered. Discontinuities are horizontal. (RUS FORMATION)			
			0	0	0	0		55.0 (1.30)		No recovery			
								55.30					
09/10	55.60	41.39						55.60					
11/10		43.73	82	70	70			56.0	-12.05	Very weak light brown and light greyish green SILTSTONE. Slightly weathered. Discontinuities are widely spaced and sub-vertical. (RUS FORMATION)	×		
								56.10					
			100	100	100			56.60					
								57.0 (2.85)					
			95	95	95			57.60					
								58.0					
		0	100	100	100	4		58.45	-14.90	Very weak to weak light greyish white GYPSUM. Slightly weathered. Discontinuities are widely spaced and sub-horizontal. (RUS FORMATION)	◇		
								58.80					
			82	82	82			59.0 (1.67)					

Remarks : 1.Hand excavation up to 0.70m bgl. 2. Groundwater was encountered at 6.80m bgl during drilling. 3. Logged in accordance with BS 5930: 1999+A2:2010.	Logged By :	Checked by : E.Stanmore
	Appendix No. : 6	

GL LIB 06.GLB Log GI CORE LOG-2 EXXON MOBILE.GPJ <-DrawingFiles>> 11/06/2017 08:13 Produced by gINT Professional



GULF LABORATORIES Co.

Doha - State of Qatar

Project:
Geological Survey

Borehole
EMRQ_RR_01

Machine: DESCO-02 Flush: Water Core Dia (mm): 102 Method: Hand Excavation & Rotary coring	Borehole Diameter (mm): 146/150 Casing Diameter (mm): 146/150 Location: Rawdat Rashid Coordinates: 201246.1 mE 387180.6 mN	Ground Level (m QNHD): 43.55 Start Date: 10/4/16 End Date: 10/27/16	Client: EXXON MOBILE RESEARCH QATAR Engineer:	Project No. SI1998 Sheet 7 of 14
--	--	--	---	---

Borehole Progress			Rock Core Quality				Sample Type	Sample Depth	Field Records	Level	Depth (m) (Thickness)	Description	Legend	Water
Date	Casing Depth (m)	Depth to Water (m) Flush Return	TCR	SCR	RQD	FI								
11/10	61.80	43.65	82	82	82	4	C		-16.57	60.72	...from 60.0m to 61.80m packer test undertaken with seal from 59m to 60m	△		
		0	54	54	54		C			(1.08)	Very weak locally extremely weak brown fine grained SILTSTONE occasionally horizontally interbedded with weak gypsum. Slightly weathered. Discontinuities are closely to medium spaced and horizontal. (Loss of recovery during drilling, most likely due to extremely weak siltstone. (UMM ER RADHUMA FORMATION)	x		
			100	100	100		C		-17.65	61.20	Very weak pseudo-brecciated brownish grey fine grained SILTSTONE with occasional vugs, and frequent gravel and cobble sized nodules of gypsum and chert. Slightly weathered. Discontinuities are medium spaced and horizontal. (UMM ER RADHUMA FORMATION)	x		
12/10	61.80	38.89					C			61.80	...from 61.28m to 61.30m very thinly bedded ...from 61.33 to 61.38m very thinly bedded	x		
12/10	66.30	38.85	100	100	100	12	C			62.0		x		
13/10		40.93					C			63.0		x		
		0	100	100	100		C			63.30		x		
							C			(5.35)	...from 65.02m to 65.06m very thinly bedded ...from 65.80m to 66.04m very thinly bedded	x		
			100	100	100		C			64.0		x		
							C			64.80		x		
							C			65.0		x		
							C			66.0		x		
12/10	66.30	38.85					C			66.30		x		
13/10		40.93					C			66.55	Very weak to weak brown occasionally grey SILTSTONE interbedded with very weak locally extremely weak brown argillaceous LIMESTONE and very weak brown fine to medium grained SANDSTONE and frequent gravel and cobble sized nodules of gypsum and chert. Slightly weathered. Discontinuities are widely spaced and horizontal. (UMM ER RADHUMA FORMATION)	x		
		0	100	100	100	22	C			67.0		x		
							C			67.80		x		
							C			(22.00)		x		
							C			68.0		x		
							C			69.0		x		
							C			69.30		x		
			100	100	100		C					x		

GL LIB 06.GLB Log_GI_CORE LOG-2 EXXON MOBILE.GPJ <-DrawingFiles> 11/06/2017 08:13 Produced by gINT Professional

Remarks : 1. Hand excavation up to 0.70m bgl. 2. Groundwater was encountered at 6.80m bgl during drilling. 3. Logged in accordance with BS 5930: 1999+A2:2010.	Logged By : Checked by : E.Stanmore	Appendix No. : 7
---	---	----------------------------



GULF LABORATORIES Co.

Doha - State of Qatar

Project:
Geological Survey

Borehole
EMRQ_RR_01

Machine: DESCO-02 Flush: Water Core Dia (mm): 102 Method: Hand Excavation & Rotary coring	Borehole Diameter (mm): 146/150 Casing Diameter (mm): 146/150 Location: Rawdat Rashid Coordinates: 201246.1 mE 387180.6 mN	Ground Level (m QNHD): 43.55 Start Date: 10/4/16 End Date: 10/27/16	Client: EXXON MOBILE RESEARCH QATAR Engineer:	Project No. SI1998 Sheet 10 of 14
--	--	---	---	--

Borehole Progress			Rock Core Quality				Field Records		Level	Depth (m) (Thickness)	Description	Legend	Water
Date	Casing Depth (m)	Depth to Water (m) Flush Return	TCR	SCR	RQD	FI	Sample Type	Sample Depth					
			100	100	100					Very weak brown and light grey LIMESTONE and SILTSTONE interbedded with very weak brown fine grained SANDSTONE with occasional gravel and cobble sized gypsum and chert. Slightly weathered. Discontinuities are widely spaced and sub-horizontal. (UMM ER RADHUMA FORMATION)			
									90.70				
			100	100	100	5				(4.61)			
										92.0			
		0	100	100	100					92.20			
			100	100	100					93.0	...from 92.76 to 93.00m vertical discontinuity thickly to very closely spaced ...from 93.00m to 95.0m packer test undertaken with seal from 92m to 93m		
										-49.61			
			100	100	100					93.16	Weak brown LIMESTONE and very weak locally weak brown SILTSTONE interbedded with very weak brown fine to medium grained SANDSTONE with occasional fine gravel sized nodules of chert, gypsum and calcite. Slightly weathered. Discontinuities are widely spaced, sub-horizontal to sub-vertical. (UMM ER RADHUMA FORMATION)		
			100	100	100					93.70			
										94.0			
			100	100	100					95.0			
18/10	95.00	39.95								95.00			
20/10		44.35											
			100	100	100					96.0			
						12				96.50	(14.94)		
			100	100	100					97.0			
		0											
										98.0			
			91	91	67					99.0			
			93	93	93					99.50			

Remarks : 1. Hand excavation up to 0.70m bgl. 2. Groundwater was encountered at 6.80m bgl during drilling. 3. Logged in accordance with BS 5930: 1999+A2:2010.	Logged By :	Checked by :
		E.Stanmore
Appendix No. :		
10		

GL LIB 06.GLB Log GI CORE LOG-2 EXXON MOBILE.GPJ <<DrawingFiles>> 11/06/2017 08:13 Produced by gINT Professional



GULF LABORATORIES Co.

Doha - State of Qatar

Project:
Geological Survey

Borehole
EMRQ_RR_01

Machine: DESCO-02 Flush: Water Core Dia (mm): 102 Method: Hand Excavation & Rotary coring	Borehole Diameter (mm): 146/150 Casing Diameter (mm): 146/150 Location: Rawdat Rashid Coordinates: 201246.1 mE 387180.6 mN	Ground Level (m QNHD): 43.55 Start Date: 10/4/16 End Date: 10/27/16	Client: EXXON MOBILE RESEARCH QATAR Engineer:	Project No. SI1998 Sheet 11 of 14
--	--	---	---	--

Borehole Progress			Rock Core Quality				Field Records		Level	Depth (m) (Thickness)	Description	Legend	Water
Date	Casing Depth (m)	Depth to Water (m) Flush Return	TCR	SCR	RQD	FI	Sample Type	Sample Depth					
			93	93	93						Weak brown LIMESTONE and very weak locally weak brown SILTSTONE interbedded with very weak brown fine to medium grained SANDSTONE with occasional fine gravel sized nodules of chert, gypsum and calcite. Slightly weathered. Discontinuities are widely spaced, sub-horizontal to sub-vertical. (UMM ER RADHUMA FORMATION)		
								101.00	101.0				
			100	100	100								
								102.50	102.0				
			97	97	97								
								104.00	104.0 (14.94)				
		0	100	97	93	12							
								105.50	105.0				
			100	100	100								
								107.00	107.0				
			100	100	100								
								108.50	108.0				
			97	97	97	10			109.0 (16.50)				
20/10	110.00	43.65											

Remarks : 1. Hand excavation up to 0.70m bgl. 2. Groundwater was encountered at 6.80m bgl during drilling. 3. Logged in accordance with BS 5930: 1999+A2:2010.	Logged By : Appendix No. : 11	Checked by : E.Stanmore
---	---	-----------------------------------

GL LIB 06.GLB Log GI CORE LOG-2 EXXON MOBILE.GPJ <-DrawingFiles>> 11/06/2017 08:13 Produced by gINT Professional



GULF LABORATORIES Co.

Doha - State of Qatar

Project:
Geological Survey

Borehole
EMRQ-AG-BH001

Machine: DESCO-03 Flush: Water Core Dia (mm): 102 Method: Hand excavation and rotary coring	Borehole Diameter (mm): 146/150 Casing Diameter (mm): 146/150 Location: Coordinates: 204618.9 mE 456320.0 mN	Ground Level (m QNHD): 9.11 Start Date: 5/11/17 End Date: 6/21/17	Client: EXXON Engineer: EXXON	Project No. GD/2065/SI Sheet 1 of 13
--	--	--	--	---

Borehole Progress			Rock Core Quality				Field Records		Level	Depth (m) (Thickness)	Description	Legend	Water
Date	Casing Depth (m)	Depth to Water (m) Flush Return	TCR	SCR	RQD	FI	Sample Type	Sample Depth					
										0.80	Brown slightly sandy SILT/CLAY. (Topsoil)		
									8.31	0.80	Light greyish brown silty sandy very angular to subangular fine to coarse GRAVEL and occasional cobbles of limestone. (RESIDUAL SOIL)		
									7.91	1.20			
			91	34	23					2.20	Weak grey, light grey and light brown crystalline LIMESTONE with pockets of very brown locally red brown calcareous siltstone. Partially weathered. Occasional vugs. Discontinuities closely to medium spaced, sub-horizontal. (DAMMAM FORMATION)		
										3.0 (3.60)			
			100	71	65					3.70			
										4.0			
			100	87	77					4.31	Weak to medium strong light grey, light brown and light pink crystalline LIMESTONE with pockets of very weak light brown and light grey calcareous siltstone. Partially weathered. Occasional vugs. Discontinuities are medium spaced and horizontal to sub-horizontal. (DAMMAM FORMATION)		
										5.20			
			99	71	64					6.70			
										7.0 (4.20)			
			100	78	78					8.20			
										9.0			
			100	86	71				0.11	9.00	Weak light pinkish grey to light brownish grey crystalline LIMESTONE with pockets of extremely to very weak light greyish green, yellow brown and reddish brown siltstone. Partially weathered. Discontinuities are medium spaced and subhorizontal. (DAMMAM FORMATION)		
										(2.20)			
			100	100	100					9.70			

Remarks : 1. Hand dug inspection pit dug to 1.25m bgl. 2. Groundwater was encountered at 7.09m bgl. 3. Potable water was used as drilling flush and recirculated 4. Logged in accordance with BS 5930:1999+A2:2010	Logged By :	Checked by :
	Liz	Liz
	Appendix No. :	
	1	

GL_LIB_06.GLB.Log_GI_CORE LOG-2 EXXON.GPJ <-DrawingFile> 07/08/2017 15:29 Produced by gINT Professional



GULF LABORATORIES Co.

Doha - State of Qatar

Project:
Geological Survey

Borehole
EMRQ-AG-BH001

Machine: DESCO-03 Flush: Water Core Dia (mm): 102 Method: Hand excavation and rotary coring	Borehole Diameter (mm): 146/150 Casing Diameter (mm): 146/150	Ground Level (m QNHD): 9.11	Client: EXXON	Project No. GD/2065/SI
	Location: Coordinates: 204618.9 mE 456320.0 mN	Start Date: 5/11/17 End Date: 6/21/17	Engineer: EXXON	Sheet 2 of 13

Borehole Progress			Rock Core Quality				Field Records		Level	Depth (m) (Thickness)	Description	Legend	Water
Date	Casing Depth (m)	Depth to Water (m) Flush Return	TCR	SCR	RQD	FI	Sample Type	Sample Depth					
			100	100	100					Weak light pinkish grey to light brownish grey crystalline LIMESTONE with pockets of extremely to very weak light greyish green, yellow brown and reddish brown siltstone. Partially weathered. Discontinuities are medium spaced and subhorizontal. (DAMMAM FORMATION)			
									11.20				
			100	100	100				-2.09	11.20	Weak light grey chalky LIMESTONE. Partially weathered. Discontinuities medium spaced and horizontal. (RUS FORMATION)		
										12.0			
										(2.70)			
			100	100	100					13.0			
										13.90			
									-4.79	14.0	Very weak to weak light green to yellowish brown SILTSTONE/CLAYSTONE with occasional inclusions of very weak limestone, interbedded with weak light grey chalky LIMESTONE. Partially weathered. Discontinuities medium spaced and horizontal. (RUS FORMATION)	x x x x	
			100	100	100					15.0			
										(3.05)			
										15.70			
										16.0			
			100	100	100					17.0			
										17.20			
			67	80	80					18.0			
										(2.45)			
										18.70			
										19.0			
			100	100	100					19.40			
										(5.10)			

Remarks : 1. Hand dug inspection pit dug to 1.25m bgl. 2. Groundwater was encountered at 7.09m bgl. 3. Potable water was used as drilling flush and recirculated 4. Logged in accordance with BS 5930:1999+A2:2010	Logged By : Liz	Checked by : Liz
	Appendix No. : 2	

GL LIB 06.GLB.Log GL CORE LOG-2 EXXON.GPJ <<DrawingFile>> 07/08/2017 15:29 Produced by gINT Professional



GULF LABORATORIES Co.

Doha - State of Qatar

Project:
Geological Survey

Borehole
EMRQ-AG-BH001

Machine: DESCO-03 Flush: Water Core Dia (mm): 102 Method: Hand excavation and rotary coring	Borehole Diameter (mm): 146/150 Casing Diameter (mm): 146/150 Location: Coordinates: 204618.9 mE 456320.0 mN	Ground Level (m QNHD): 9.11 Start Date: 5/11/17 End Date: 6/21/17	Client: EXXON Engineer: EXXON	Project No. GD/2065/SI Sheet 4 of 13
--	--	--	--	---

Borehole Progress			Rock Core Quality				Field Records		Level	Depth (m) (Thickness)	Description	Legend	Water
Date	Casing Depth (m)	Depth to Water (m) Flush Return	TCR	SCR	RQD	FI	Sample Type	Sample Depth					
			100	82	82						Weak white localized orange brown chalky LIMESTONE with laminae and beds of very weak light brownish grey and light greyish green calcareous claystone. Occasional vugs. Partially weathered. Discontinuities are medium spaced horizontal to sub-horizontal. (RUS FORMATION)		
									30.70				
			100	87	87								
									32.20				
			97	97	87								
									33.70				
			92	92	92								
									35.20	(15.18)			
			89	69	69								
									36.70				
			93	37	37								
									38.20				
			94	72	65								
									39.70				
			89	57	34								
										-30.57			
										39.68			
										(13.52)			

Remarks : 1. Hand dug inspection pit dug to 1.25m bgl. 2. Groundwater was encountered at 7.09m bgl. 3. Potable water was used as drilling flush and recirculated 4. Logged in accordance with BS 5930:1999+A2:2010	Logged By :	Checked by :
	Liz	Liz
	Appendix No. :	
	4	

GL_LIB_06.GLB.Log GL_CORE LOG-2 EXXON.GPJ <<DrawingFile>> 07/08/2017 15:29 Produced by gINT Professional



GULF LABORATORIES Co.

Doha - State of Qatar

Project:
Geological Survey

Borehole
EMRQ-AG-BH001

Machine: DESCO-03 Flush: Water Core Dia (mm): 102 Method: Hand excavation and rotary coring	Borehole Diameter (mm): 146/150 Casing Diameter (mm): 146/150 Location: Coordinates: 204618.9 mE 456320.0 mN	Ground Level (m QNHD): 9.11 Start Date: 5/11/17 End Date: 6/21/17	Client: EXXON Engineer: EXXON	Project No. GD/2065/SI Sheet 5 of 13
--	--	---	--	---

Borehole Progress			Rock Core Quality				Sample		Field Records	Level	Depth (m) (Thickness)	Description	Legend	Water
Date	Casing Depth (m)	Depth to Water (m) Flush Return	TCR	SCR	RQD	FI	Type	Depth						
			89	57	34						Weak white to light yellowish brown chalky LIMESTONE. Partially weathered. Occasional vugs. Discontinuities are medium spaced, horizontal to sub-horizontal. (RUS FORMATION)			
										41.20				
			97	65	60					42.70				
										44.20				
			97	97	97					45.70				
										47.20				
			85	42	36					48.70				
										49.20				
			100	50	50									
			98	98	98									
			100	100	100									
			100	100	100									

Remarks : 1. Hand dug inspection pit dug to 1.25m bgl. 2. Groundwater was encountered at 7.09m bgl. 3. Potable water was used as drilling flush and recirculated 4. Logged in accordance with BS 5930:1999+A2:2010	Logged By : Liz	Checked by : Liz
Appendix No. : 5		

GL_LIB_06.GLB.Lib Log GL CORE LOG-2 EXXON.GPJ <<DrawingFile>> 07/08/2017 15:29 Produced by gINT Professional



GULF LABORATORIES Co.

Doha - State of Qatar

Project:
Geological Survey

Borehole
EMRQ-AG-BH001

Machine: DESCO-03 Flush: Water Core Dia (mm): 102 Method: Hand excavation and rotary coring	Borehole Diameter (mm): 146/150 Casing Diameter (mm): 146/150 Location: Coordinates: 204618.9 mE 456320.0 mN	Ground Level (m QNHD): 9.11 Start Date: 5/11/17 End Date: 6/21/17	Client: EXXON Engineer: EXXON	Project No. GD/2065/SI Sheet 6 of 13
--	--	--	--	---

Borehole Progress			Rock Core Quality				Field Records		Level	Depth (m) (Thickness)	Description	Legend	Water
Date	Casing Depth (m)	Depth to Water (m) Flush Return	TCR	SCR	RQD	FI	Sample Type	Sample Depth					
			100	100	100			C	50.20	Weak white to light yellowish brown chalky LIMESTONE. Partially weathered. Occasional vugs. Discontinuities are medium spaced, horizontal to sub-horizontal. (RUS FORMATION)			
			97	92	99			C	51.0				
								C	51.70 (13.52)				
			90	90	70			C	52.0				
								C	53.0				
			89	89	89			C	53.20 -44.09				
								C	54.0				
								C	54.70				
			93	83	83			C	55.0				
								C	56.0				
								C	56.20 (6.50)				
			97	90	90			C	57.0				
								C	57.70				
			100	90	74			C	58.0				
								C	58.20				
			100	67	67			C	58.65				
			96	96	96			C	59.0				
								C	59.20				
			96	96	96			C	59.70 -50.59				
								C	59.70 (15.00)				

Remarks : 1. Hand dug inspection pit dug to 1.25m bgl. 2. Groundwater was encountered at 7.09m bgl. 3. Potable water was used as drilling flush and recirculated 4. Logged in accordance with BS 5930:1999+A2:2010	Logged By :	Checked by :
	Liz	Liz
	Appendix No. :	
	6	

GL_LIB_06.GLB.Lib Log GL CORE LOG-2 EXXON.GPJ <<DrawingFile>> 07/08/2017 15:29 Produced by gINT Professional



GULF LABORATORIES Co.

Doha - State of Qatar

Project:
Geological Survey

Borehole
EMRQ-AG-BH001

Machine: DESCO-03 Flush: Water Core Dia (mm): 102 Method: Hand excavation and rotary coring	Borehole Diameter (mm): 146/150 Casing Diameter (mm): 146/150 Location: Coordinates: 204618.9 mE 456320.0 mN	Ground Level (m QNHD): 9.11 Start Date: 5/11/17 End Date: 6/21/17	Client: EXXON Engineer: EXXON	Project No. GD/2065/SI Sheet 7 of 13
--	--	--	--	---

Borehole Progress			Rock Core Quality				Field Records		Level	Depth (m) (Thickness)	Description	Legend	Water
Date	Casing Depth (m)	Depth to Water (m) Flush Return	TCR	SCR	RQD	FI	Sample Type	Sample Depth					
			96	96	96						Weak, locally very weak and medium strong, light brown and light grey vesicular LIMESTONE occasionally interbedded with very weak light brown fine grained calcareous sandstone. With Occasional thicknesses of chert and occasional vugs. Partially weathered. Discontinuities are medium locally closely spaced, sub-horizontal to sub-vertical. (UMM ER RADHUMA FORMATION)		
									60.70				
			100	100	0								
									62.20				
			100	100	100								
									63.70				
			95	95	95								
									65.20	65.0(15.00)			
			87	40	35								
									66.70				
			90	64	60								
									68.20				
			100	100	100								
									69.70				
			84	48	43								

Remarks : 1. Hand dug inspection pit dug to 1.25m bgl. 2. Groundwater was encountered at 7.09m bgl. 3. Potable water was used as drilling flush and recirculated 4. Logged in accordance with BS 5930:1999+A2:2010	Logged By : Liz	Checked by : Liz
Appendix No. : 7		

GL LIB 06.GLB Log GL CORE LOG-2 EXXON.GPJ <<DrawingFile>> 07/08/2017 15:29 Produced by gINT Professional



GULF LABORATORIES Co.

Doha - State of Qatar

Project:
Geological Survey

Borehole
EMRQ-AG-BH001

Machine: DESCO-03 Flush: Water Core Dia (mm): 102 Method: Hand excavation and rotary coring	Borehole Diameter (mm): 146/150 Casing Diameter (mm): 146/150 Location: Coordinates: 204618.9 mE 456320.0 mN	Ground Level (m QNHD): 9.11 Start Date: 5/11/17 End Date: 6/21/17	Client: EXXON Engineer: EXXON	Project No. GD/2065/SI Sheet 8 of 13
--	--	--	--	---

Borehole Progress			Rock Core Quality				Field Records		Level	Depth (m) (Thickness)	Description	Legend	Water		
Date	Casing Depth (m)	Depth to Water (m) Flush Return	TCR	SCR	RQD	FI	Sample Type	Sample Depth							
			84	48	43		C		71.20	Weak, locally very weak and medium strong, light brown and light grey vesicular LIMESTONE occasionally interbedded with very weak light brown fine grained calcareous sandstone. With Occasional thicknesses of chert and occasional vugs. Partially weathered. Discontinuities are medium locally closely spaced, sub-horizontal to sub-vertical. (UMM ER RADHUMA FORMATION)					
			90	90	90		C		72.00						
									(15.00)						
									72.70						
			57	30	30		C		73.00						
									74.00						
			64	64	64		C		74.20						
									74.70						
			52	0	0		C		-65.59 74.70				Recovered as brown fine sandy CLAY. (UMM ER RADHUMA FORMATION)		
									75.00				(1.00)		
			50	0	0		C		75.20						
									75.70						
			54	24	24		C		-66.59 75.70				Very weak to weak light greyish brown LIMESTONE. Partially weathered. Discontinuities are closely to medium spaced. (UMM ER RADHUMA FORMATION).		
									76.20				-67.09 76.20		
			92	0	0		C		76.70				Recovered as brown clayey fine SAND. (UMM ER RADHUMA FORMATION)		
									77.00	(0.90)					
			70	0	0		C		77.20	-67.99 77.10					
									77.70						
			100	0	0		C		78.00	Recovered as brown sandy CLAY / clayey fine SAND (UMM ER RADHUMA FORMATION) ...at 77.10m with chert band 30mm thick					
									78.20						
			100	0	0		C		78.70	(9.10)					
									79.00						
			100	0	0		C		79.20						

Remarks : 1. Hand dug inspection pit dug to 1.25m bgl. 2. Groundwater was encountered at 7.09m bgl. 3. Potable water was used as drilling flush and recirculated 4. Logged in accordance with BS 5930:1999+A2:2010	Logged By : Liz	Checked by : Liz
Appendix No. : 8		

GL_LIB_06.GLB.Log_GI_CORE LOG-2 EXXON.GPJ <-DrawingFile> 07/08/2017 15:29 Produced by gINT Professional



GULF LABORATORIES Co.

Doha - State of Qatar

Project:
Geological Survey

Borehole
EMRQ-AG-BH001

Machine: DESCO-03 Flush: Water Core Dia (mm): 102 Method: Hand excavation and rotary coring	Borehole Diameter (mm): 146/150 Casing Diameter (mm): 146/150 Location: Coordinates: 204618.9 mE 456320.0 mN	Ground Level (m QNHD): 9.11 Start Date: 5/11/17 End Date: 6/21/17	Client: EXXON Engineer: EXXON	Project No. GD/2065/SI Sheet 9 of 13
--	--	--	--	---

Borehole Progress			Rock Core Quality				Sample Type	Sample Depth	Field Records	Level	Depth (m) (Thickness)	Description	Legend	Water
Date	Casing Depth (m)	Depth to Water (m) Flush Return	TCR	SCR	RQD	FI								
			100	0	0		C					Recovered as brown sandy CLAY / clayey fine SAND (UMM ER RADHUMA FORMATION)		
			69	0	0		C							
			100	0	0		C			81.0				
			50	0	0		C							
			77	0	0		C			82.0				
			76	0	0		C							
			89	0	0		C			83.0 (9.10)				
			41	0	0		C			84.0				
			73	0	0		C			85.0				
			87	0	0		C							
			51	0	0		C			-77.09 86.20	Very weak to weak light greyish brown LIMESTONE. Partially weathered. Discontinuities are closely to medium spaced. (UMM ER RADHUMA FORMATION).			
			52	0	0		C			87.0 (1.50)				
			87	0	0		C			-78.59 87.70	Recovered as brown sandy CLAY / clayey fine SAND (UMM ER RADHUMA FORMATION)			
			63	0	0		C							
			73	0	0		C			89.0 (3.00)				
							C			89.95				

Remarks : 1. Hand dug inspection pit dug to 1.25m bgl. 2. Groundwater was encountered at 7.09m bgl. 3. Potable water was used as drilling flush and recirculated 4. Logged in accordance with BS 5930:1999+A2:2010	Logged By : Liz	Checked by : Liz	Appendix No. : 9
---	---------------------------	----------------------------	----------------------------

GL LIB 06.GLB.Log GL CORE LOG-2 EXXON.GPJ <<DrawingFile>> 07/08/2017 15:29 Produced by gINT Professional



GULF LABORATORIES Co.

Doha - State of Qatar

Project:
Geological Survey

Borehole
EMRQ-AG-BH001

Machine: DESCO-03 Flush: Water Core Dia (mm): 102 Method: Hand excavation and rotary coring	Borehole Diameter (mm): 146/150 Casing Diameter (mm): 146/150 Location: Coordinates: 204618.9 mE 456320.0 mN	Ground Level (m QNHD): 9.11 Start Date: 5/11/17 End Date: 6/21/17	Client: EXXON Engineer: EXXON	Project No. GD/2065/SI Sheet 10 of 13
--	--	--	--	--

Borehole Progress			Rock Core Quality				Sample Type	Sample Depth	Field Records	Level	Depth (m) (Thickness)	Description	Legend	Water
Date	Casing Depth (m)	Depth to Water (m) Flush Return	TCR	SCR	RQD	FI								
			63	0	0							Recovered as brown sandy CLAY / clayey fine SAND (UMM ER RADHUMA FORMATION)		
			63	0	0						(3.00)			
											90.70			
			63	0	0						91.0	Very weak to weak light greyish brown LIMESTONE. Partially weathered. Discontinuities are closely to medium spaced. (UMM ER RADHUMA FORMATION).		
											91.45			
			40	20	20						92.0			
											92.20			
											(3.10)			
			43	31	31						92.95			
											93.0			
			23	0	0						93.70			
											93.80			
			35	0	0						94.0	Very weak to weak light grey CALCARENITE. Partially weathered. Locally recovered as a gravel. (UMM ER RADHUMA FORMATION)		
											94.45			
			27	0	0						95.0			
											95.20			
			40	0	0						95.45			
											96.0			
			14	13	13						96.70			
											(5.70)			
			56	40	40						97.0			
											97.45			
			77	75	75						98.0			
											98.20			
			47	11	0						98.95			
											99.0			
			69	24	13						99.70			
											99.70			
			21	0	0						(15.00)	Recovered as brown clayey fine SAND (UMM ER RADHUMA FORMATION)		

Remarks : 1. Hand dug inspection pit dug to 1.25m bgl. 2. Groundwater was encountered at 7.09m bgl. 3. Potable water was used as drilling flush and recirculated 4. Logged in accordance with BS 5930:1999+A2:2010	Logged By :	Checked by :
	Liz	Liz
	Appendix No. :	
	10	

GL_LIB_06.GLB.Lib Log GL CORE LOG-2 EXXON.GPJ <<DrawingFile>> 07/08/2017 15:29 Produced by gINT Professional



GULF LABORATORIES Co.

Doha - State of Qatar

Project:
Geological Survey

Borehole
EMRQ-AG-BH001

Machine: DESCO-03 Flush: Water Core Dia (mm): 102 Method: Hand excavation and rotary coring	Borehole Diameter (mm): 146/150 Casing Diameter (mm): 146/150 Location: Coordinates: 204618.9 mE 456320.0 mN	Ground Level (m QNHD): 9.11 Start Date: 5/11/17 End Date: 6/21/17	Client: EXXON Engineer: EXXON	Project No. GD/2065/SI Sheet 11 of 13
--	--	--	--	--

Borehole Progress			Rock Core Quality				Field Records		Level	Depth (m) (Thickness)	Description	Legend	Water
Date	Casing Depth (m)	Depth to Water (m) Flush Return	TCR	SCR	RQD	FI	Sample Type	Sample Depth					
			21	0	0			C	100.45	Very weak to weak light greyish brown and light grey fossiliferous LIMESTONE. Partially weathered. Locally recovered as gravel. Discontinuities are closely spaced, and sub-vertical. (UMM ER RADHUMA FORMATION)			
			27	0	0			C	101.20				
			100	29	0			C	101.75				
			81	49	0			C	102.70				
			100	45	35			C	104.20				
			64	19	9			C	105.70				
			100	93	93			C	107.20				
			95	50	37			C	108.70				
			85	85	85			C	109.0				

Remarks : 1. Hand dug inspection pit dug to 1.25m bgl. 2. Groundwater was encountered at 7.09m bgl. 3. Potable water was used as drilling flush and recirculated 4. Logged in accordance with BS 5930:1999+A2:2010	Logged By : Liz	Checked by : Liz
Appendix No. : 11		

GL_LIB_06.GLB.Log_GI_CORE LOG-2 EXXON.GPJ <-DrawingFile>> 07/08/2017 15:29 Produced by gINT Professional



GULF LABORATORIES Co.

Doha - State of Qatar

Project:
Geological Survey

Borehole
EMRQ-AG-BH001

Machine: DESCO-03 Flush: Water Core Dia (mm): 102 Method: Hand excavation and rotary coring	Borehole Diameter (mm): 146/150 Casing Diameter (mm): 146/150 Location: Coordinates: 204618.9 mE 456320.0 mN	Ground Level (m QNHD): 9.11 Start Date: 5/11/17 End Date: 6/21/17	Client: EXXON Engineer: EXXON	Project No. GD/2065/SI Sheet 12 of 13
--	--	--	--	--

Borehole Progress			Rock Core Quality				Sample Type	Sample Depth	Field Records	Level	Depth (m) (Thickness)	Description	Legend	Water
Date	Casing Depth (m)	Depth to Water (m) Flush Return	TCR	SCR	RQD	FI								
			85	85	85		C				110.20	Very weak to weak light greyish brown and light grey fossiliferous LIMESTONE. Partially weathered. Locally recovered as gravel. Discontinuities are closely spaced, and sub-vertical. (UMM ER RADHUMA FORMATION)		
			77	63	58		C			111.0				
			61	53	53		C			111.70 112.0 (15.00)				
			43	35	35		C			113.0 113.20				
			93	77	77		C			114.0 114.70 -105.59 114.70	Weak light grey fossiliferous LIMESTONE. Partially weathered. Discontinuities are medium spaced and horizontal. (UM ER RADHUMA FORMATION)			
			17	5	0		C			115.0 116.0 116.20				
			77	67	67		C			117.0 117.70 (7.50)				
			28	4	0		C			118.0 119.0 119.20				

Remarks : 1. Hand dug inspection pit dug to 1.25m bgl. 2. Groundwater was encountered at 7.09m bgl. 3. Potable water was used as drilling flush and recirculated 4. Logged in accordance with BS 5930:1999+A2:2010	Logged By : Liz	Checked by : Liz
Appendix No. : 12		

GL_LIB_06.GLB.Lib Log GL CORE LOG-2 EXXON.GPJ <<DrawingFile>> 07/08/2017 15:29 Produced by gINT Professional



GULF LABORATORIES Co.

Doha - State of Qatar

Project:
Geological Survey

Borehole
EMRQ-AG-BH001

Machine: DESCO-03 Flush: Water Core Dia (mm): 102 Method: Hand excavation and rotary coring	Borehole Diameter (mm): 146/150 Casing Diameter (mm): 146/150 Location: Coordinates: 204618.9 mE 456320.0 mN	Ground Level (m QNHD): 9.11 Start Date: 5/11/17 End Date: 6/21/17	Client: EXXON Engineer: EXXON	Project No. GD/2065/SI Sheet 13 of 13
--	--	--	--	--

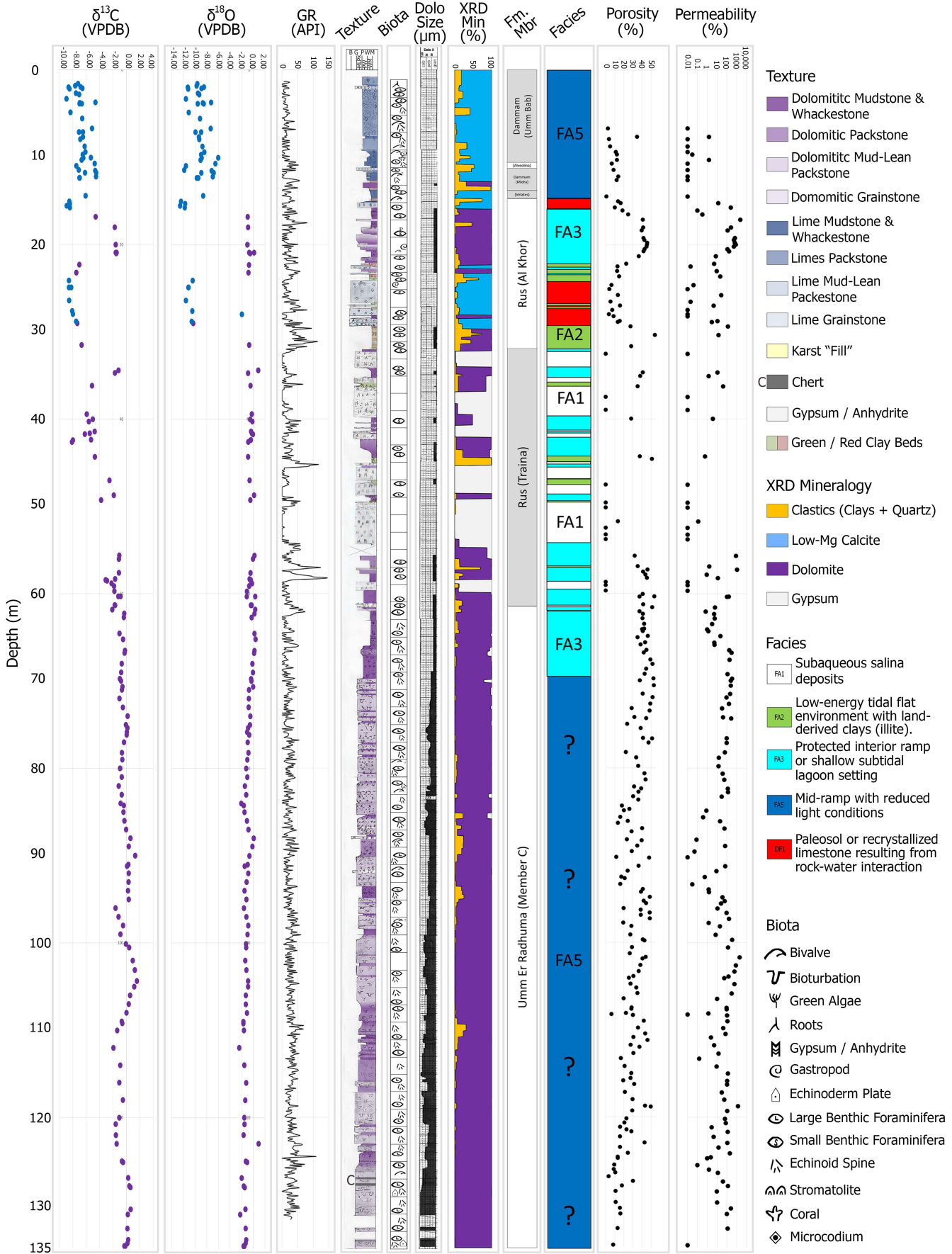
Borehole Progress			Rock Core Quality				Field Records		Level	Depth (m) (Thickness)	Description	Legend	Water
Date	Casing Depth (m)	Depth to Water (m) Flush Return	TCR	SCR	RQD	FI	Sample Type	Sample Depth					
			28	4	0			C	120.70	Weak light grey fossiliferous LIMESTONE. Partially weathered. Discontinuities are medium spaced and horizontal. (UM ER RADHUMA FORMATION)			
			97	83	83		C	122.20					
									-113.09	Completed at 122.20 m			

Remarks : 1. Hand dug inspection pit dug to 1.25m bgl. 2. Groundwater was encountered at 7.09m bgl. 3. Potable water was used as drilling flush and recirculated 4. Logged in accordance with BS 5930:1999+A2:2010	Logged By : Liz	Checked by : Liz	
			Appendix No. : 13

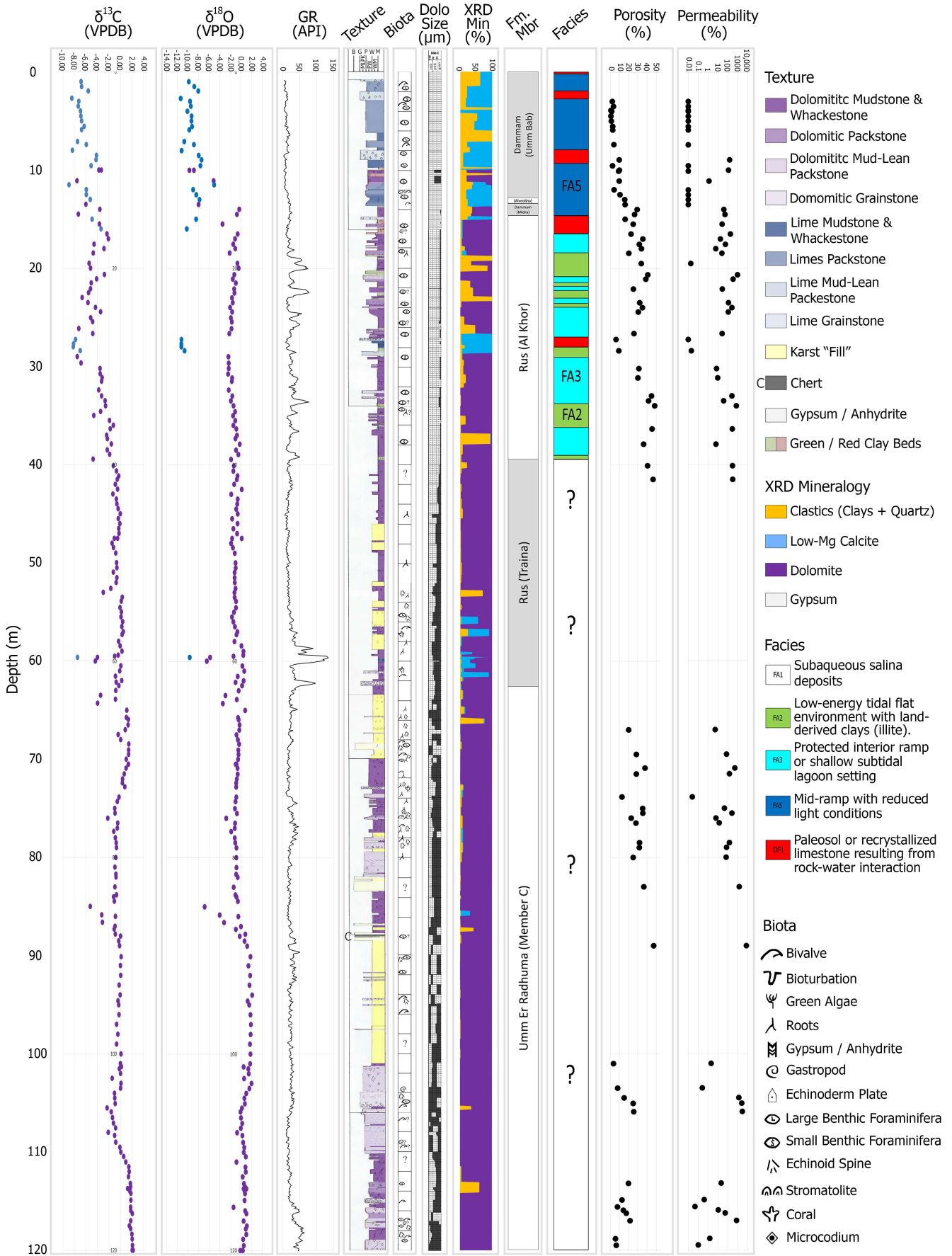
GL_LIB_06.GLB.Log GL_CORE LOG-2 EXXON.GPJ <<DrawingFile>> 07/08/2017 15:29 Produced by gINT Professional

Appendix D Composite Geology Logs (Rivers et al., 2019a)

Southern Well (RR)



Central Well (AS)



North Well (AG)

